MISSOURI S&T

CENTER FOR TRANSPORTATION INFRASTRUCTURE AND SAFETY

Coated Steel Rebar for Enhanced Concrete-Steel Bond Strength and Corrosion Resistance

by

Genda Chen, Jeffery Volz, Richard Brow,
Dongming Yan, Signo Reis, Chenglin Wu,
Fujian Tang, Charles Werner, and Xing Tao

A National University Transportation Center
at Missouri University of Science and Technology

Disclaimer

The contents of this report reflect the views of the author(s), who are responsible for the facts and the accuracy of information presented herein. This document is disseminated under the sponsorship of the Department of Transportation, University Transportation Centers Program and the Center for Transportation Infrastructure and Safety NUTC program at the Missouri University of Science and Technology, in the interest of information exchange. The U.S. Government and Center for Transportation Infrastructure and Safety assumes no liability for the contents or use thereof.

Technical Report Documentation Page

1. Report No.	2. Government Accession No.	3. Recipient's Catalog No.
NUTC R236		

4. Title and Subtitle	5. Report Date
Coated Steel Rebar for Enhanced Concrete-Steel Bond Strength and Corrosion Resistance	October 2010
	6. Performing Organization Code

7. Author/s	8. Performing Organization Report No.
Genda Chen, Jeffery Volz, Richard Brow, Dongming Yan, Signo Reis, Chenglin Wu, Fujian Tang, Charles Werner, and Xing Tao	00022976

9. Performing Organization Name and Address	10. Work Unit No. (TRAIS)
Center for Transportation Infrastructure and Safety/NUTC program Missouri University of Science and Technology 220 Engineering Research Lab Rolla, MO 65409	11. Contract or Grant No. DTRT06-G-0014

12. Sponsoring Organization Name and Address	13. Type of Report and Period Covered
U.S. Department of Transportation Research and Innovative Technology Administration 1200 New Jersey Avenue, SE Washington, DC 20590	Final
	14. Sponsoring Agency Code

15. Supplementary Notes

16. Abstract

This report summarizes the findings and recommendations on the use of enamel coating in reinforced concrete structures both for bond strength and corrosion resistance of steel rebar. Extensive laboratory tests were conducted to characterize the properties of one- and two-layer enamel coatings. Pseudostatic tests were performed with pullout, beam and column specimens to characterize mechanical properties and develop design equations for the development length of steel rebar in lap splice and anchorage areas. The splice length equation was validated with the testing of large-scale columns under cyclic loading. For corrosion properties, ponding, salt spray, accelerated corrosion, potentiodynamic and electrochemical impedance spectroscopy (EIS) tests were conducted to evaluate the corrosion resistance and performance of enamel-coated steel and rebar. Experimental procedures and observations from various laboratory tests are documented in detail. The corrosion performances of enamel and epoxy coatings were compared. It is concluded that a one-layer enamel coating doped with 50% calcium silicate has improved bond strengths with steel and concrete but its corrosion resistance is low due to porosity in the coating, allowing chloride ions to pass through. Based on limited laboratory tests, a two-layer enamel coating with an inner layer of pure enamel and an outer layer of enamel and calcium silicate mixture has been shown to be practical and effective for both corrosion resistance and bond strength. A coating factor of 0.85 is recommended to use with the current development length equations as specified in ACI318-08. The large-scale column tests indicated that the column-footing lap splice with enamel-coated dowel bars had higher load and energy dissipation capacities compared to uncoated dowel bars. When damaged unintentionally, chemically reactive enamel coatings limit corrosion to a very small area whereas epoxy coatings allow corrosion expansion in a wide area underneath the coating.

17. Key Words	18. Distribution Statement
Enamel coating, bond strength, pullout test, beam test, column test, large-scale test, development length, lap splice, anchorage length, optical fiber sensor, corrosion resistance, corrosion resistance, salt spray, accelerated corrosion test, ponding test, potentiodynamic test, electrochemical impedance spectroscopy	No restrictions. This document is available to the public through the National Technical Information Service, Springfield, Virginia 22161.

19. Security Classification (of this report)	20. Security Classification (of this page)	21. No. Of Pages	22. Price
unclassified	unclassified	226	

Form DOT F 1700.7 (8-72)

EXECUTIVE SUMMARY

Approximately $10 Billion is spent annually to directly remediate corrosion problems with our nation's bridges, and indirect costs push that annual expenditure up by a factor of ten. Epoxy coatings have been widely used for corrosion protection of steel rebar in reinforced concrete (RC) structures. However, epoxy coatings reduce the concrete-steel bond strengths, thus requiring longer development lengths for epoxy-coated rebar and causing extensive rebar congestions in the joint areas of structures.

In this study, enamel coating is introduced to enhance both corrosion resistance and bond strength of reinforcing steel. The overall goal of this study was to optimize this technology for the construction of RC structures in bridge applications, with the objective of reducing construction and maintenance costs and improving structural performance. The technical scope of work includes:

1) Characterize the bond strength between deformed steel rebar and concrete;
2) Characterize the corrosion resistant properties of coated rebar in alkaline environments, including reinforced concrete; and
3) Study the behavior of beam-column concrete structures reinforced with enamel-coated rebar, develop and validate new design equations for the tension *development lengths* of coated steel rebar in RC members.

This report summarizes the findings and recommendations on the use of various enamel coatings in RC structures. Pseudostatic tests with pullout, beam and column specimens were performed to establish the development length equations of enamel-coated steel rebar in lap splice and anchorage areas. The splice length equation was validated by testing large-scale columns under cyclic loading. Salt spray, accelerated corrosion, ponding, potentiodynamic and electrochemical impedance spectroscopy (EIS) tests were conducted to evaluate the corrosion resistance and performance of enamel-coated steel rebar.

Significant Findings

Steel-mortar cylinders failed in different modes from ductile steel pullouts to brittle concrete splitting and their bond strengths increased as the calcium silicate component of a reactive enamel coating was increased. For example, the steel rods coated with pure enamel were consistently pulled out of the mortar whereas the rods coated with 50/50 enamel coating consistently failed in splitting the mortar cylinder. As the mortar strength increased over time, the failure mode became less ductile and the slip before the steel-mortar bond stress reached at its maximum increased for specimens that failed in concrete splitting.

Enamel-coated steel provided greater adhesion and initial stiffness at steel-concrete interfaces than those uncoated and epoxy-coated steel, exhibiting less slippage at the same load level. At a steel-concrete slip of 0.002 in., the average bond force in enamel-coated rebar was 11% and 52% higher than that in uncoated and epoxy-coated bars, respectively. The ultimate bond strength of enamel-coated deformed rebar in concrete, when failed in rebar pullout, only increased 5% compared to uncoated deformed rebar since it is dominated by the concrete shear strength. The ultimate bond strength of epoxy-coated rebar *decreased* by 10% compared to uncoated deformed rebar. The post-peak portions of load-slip curves reflected the continual wearing condition at rebar-concrete interfaces as rebar is being pulled out of the concrete.

The coating effect on the bond strength of enamel-coated rebar in concrete can be well represented by a coating factor in the ACI 318-08 development length equation. Based on the results of 12 beam tests, a coating factor of 0.85 represented an average plus two standard deviations of the coating factor distribution for over-conservatively designed specimens. This coating factor is in contrast to 1.2 or 1.5 for epoxy-coated rebar as required by the ACI 318-08, depending on the concrete cover and rebar spacing. All rebar pullout specimens with #4 reinforcing bars, coated or uncoated, failed in rebar pullout. For specimens with #8 enamel-coated rebar, the failure mode was dominated by concrete splitting.

Based on the large-scale column tests with a column-footing lap splice of 70% the development length required by ACI 318-08, the secant stiffness of the concrete column reinforced with enamel-coated dowel bars was 23%-40% higher than that with uncoated dowel bars at various displacement levels. The overall tangential stiffness and energy dissipation capacity of the column with enamel-coated reinforcement also increased by approximately 35% and 30%, respectively, compared to uncoated dowel bars.

All short column tests consistently showed steel bar yielding and no concrete spalling even though 60% of the development length required by ACI318-08 for uncoated rebar was used for enamel-coated dowel bars. The severely cracked concrete pieces were still attached to the enamel-coated rebar, indicative of a strong bond between the enamel-coated rebar and concrete. With equal development lengths, the column specimen with enamel-coated dowel bars experienced less (or no) concrete cracks near the steel bars than that with uncoated dowel bars. With reduced development lengths, more flexural and shear cracks were observed on columns due mainly to their reduced cross sections.

The corrosion performance of three different enamel coatings (pure, 50/50 with 50% calcium silicate, and double-coat with a layer of pure and a layer of 50/50 enamel) largely depended upon the coating's thickness and the concentration of calcium silicate within the coating. Overall, the uniformly coated smooth specimens outperformed the inconsistently coated deformed specimens that often possessed thinly coated areas along their transverse and longitudinal ribs. The double enamel coating and pure enamel coating had higher corrosion resistances than the 50/50 enamel coating due to high porosity associated with the reactive calcium silicate component. However, the double coating applied on deformed rebar showed areas of weakness along a portion of their transverse ribs. These areas of weakness were again thinly coated with what appeared to be an amalgamation of the two applied coatings. This mixing of the two coatings would, at times, lead to large concentrations of calcium silicate within the thinly coated sections of the coating. As a result, the coating along these sections exhibited similar corrosion-resistance properties to that of the 50/50 enamel. The wide variation of corrosion performances of various enamel coatings was mainly due to raw material selection and inconsistent manufacture processes. For example, the thickness of enamel coatings tested in this study ranged from 2 to 39.4 mils. Based on the test results, a minimum coating thickness of 8 mils seemed necessary.

When damaged, chemically reactive enamel coating maintained its bond with the steel and no corrosion undercutting was observed. As a result, corrosion in enamel coating was not spread around the damaged area. On the other hand, epoxy coating is a physical layer applied on steel rebar. When corroded at one point, epoxy coating was observed to experience significant undercutting and steel corrosion beneath the epoxy was spread in a wide area at an accelerated rate due to the moisture trapped underneath the epoxy coating. For example, ponding tests

indicated that a 28% decrease in corrosion resistance was observed due to damage in epoxy coating and only a 4% variation in corrosion resistance was seen due likely to damage in 50/50 enamel coating. However, epoxy coating can significantly delay the onset of corrosion in comparison with pure enamel coating or even the double coating. For example, the accelerated corrosion tests indicated that the times to corrosion are approximately 170 hours, 190 hours, 410 hours, 660 hours, and over 1300 hours for uncoated, 50/50 enamel-coated, pure enamel-coated, double enamel-coated, and epoxy-coated rebar in mortar, respectively.

Both polarization curves and chloride analyses on 1.5-in.-diameter mortar cylinders with one #4 deformed rebar confirmed that the coated and uncoated mortar cylinder rebar started corrosion after three months of immersion in the 3.5% NaCl solution. The coated rebar likely experienced moderate corrosion between three and six months. The uncoated rebar, however, was subjected to a high probability of corrosion after four to five months of immersion. At the end of six months, the probability of corrosion in the uncoated rebar became very high. Therefore, the enamel coating slows down the corrosion process limiting the diffusion of chloride ions through the coating.

The modulus of impedance for mortar cylinder samples rapidly drops until an excitation frequency of approximately 0.1 Hz is reached and then decreases slowly. Both the modulus and phase angle of uncoated and coated rebar samples become much smaller above 1.0 Hz. For mortar cylinder samples, the impedance magnitude of enamel-coated rebar is generally higher than that of uncoated rebar. In comparison with uncoated rebar samples, the enamel-coated rebar samples have a more significant capacitive behavior that is closely related to steel passivity.

Recommendations

A mixture of 50% enamel and 50% calcium silicate or 50/50 enamel coating is recommended for a maximum increase of the bond strength between steel rebar and concrete. Pure enamel is recommended for a moderate protection of steel rebar in corrosive environments. When both corrosion resistance and bond strength are a concern in designs, a double enamel coating consisting of an inner layer of pure enamel and an outer layer of 50/50 enamel coating is recommended based on the limited laboratory tests of deformed rebar in mortar. Furthermore, a manufacturing technique that consistently provides uniform coating thicknesses, such as electrostatic applications, will significantly improve the corrosion performance of the enamel coatings.

For the 50/50 enamel coatings with enhanced bond strengths, a coating factor of 0.85 is recommended for lap splice designs according to the development length equation in ACI318-08. The recommended anchorage length for enamel-coated rebar is 85% of what is required for uncoated rebar by ACI 318-08.

Future studies on double enamel coatings are needed to further characterize their bond strength and corrosion resistance for deformed rebar in concrete and to improve the manufacturing process for more consistent performance. In addition, case studies with actual bridges are required to validate and document the field performance of enamel coating technologies.

ACKNOWLEDGEMENTS

Financial supports to complete this study by Missouri Department of Transportation (MoDOT) and Missouri S&T Center for Transportation Infrastructure and Safety are greatly appreciated. The authors are grateful to Jennifer Harper for her continuing efforts to seek and provide inputs from MoDOT engineers and coordinate various project meetings over the duration of this project. Special thanks are due to Julie W. Lamberson, John D. Wenzlick, and Ken Shamet for their service as the Technical Advisory Panel (TAP) members of this project. Thanks are also due to MoDOT and Federal Highway Administration (FHWA) Missouri Division engineers for their valuable comments during various project meetings and review of the final report.

The authors are also grateful to Mike Koenigstein from ProPerma Engineered Coatings, who has supported the research team free-of-charge since the beginning of this study and prepared all enamel-coated samples for material, mechanical, and corrosion characterizations in the laboratory. Without his support, this study would not be completed in time.

Table of Contents

LIST OF FIGURES

Page

LIST OF TABLES

Page

1. INTRODUCTION

Approximately $10B is spent annually to directly remediate corrosion problems with our nation's bridges, and indirect costs push that annual expenditure up by a factor of ten [Hartt et al., 2004]. Epoxy coated rebar has been the most widely used method for corrosion protection. The epoxy coating is intended to isolate the steel from any corrosive environment associated with the service condition of the concrete, such as road salts, acids, or carbonation. However, under certain conditions, the epoxy coating can actually accelerate the corrosion of the steel [Sagues et al., 1994; Brown and Weyers, 2003]. The relatively weak physical bond between the epoxy and steel is not a sufficient barrier to attack by moisture. Furthermore, use of the epoxy coating reduces the concrete-steel bond strength, thus requiring longer development lengths for epoxy coated rebar [ACI, 2008]. Other types of rebar such as zbar, stainless steel, stainless steel clad, and fiberglass have been evaluated for reinforcement in RC bridge structures. Most of these alternative reinforcing systems do not form chemical bonds with the surrounding concrete matrix, and so offer no opportunity to enhance the overall strength of the RC structure.

Approximately 90% of the bridges in the MoDOT inventory are reinforced concrete (RC) structures in super- and/or substructures. Their construction and maintenance constitute a major portion of the up-front costs in the MoDOT's budget for bridges. Therefore, the development and utilization of new technologies that can reduce the amount of steel needed for safe RC structures, and that can prolong the useful life span of RC members, beam-column joints, and column-footing connections could have a significant impact on MoDOT operations, especially as the steel price continues to increase in recent years. More importantly, using less reinforcement in joint and connection areas will alleviate the congestion of reinforcing bars, and reduce the time-consuming construction process from rebar caging to concrete casting, and will ultimately improve the quality and thus structural safety of a constructed RC bridge.

In this study, steel bars coated with a recently developed chemically-bonded enamel coating are investigated as a means for improving performance and reducing the cost of bridge construction. Chemically-active enamels have been developed for steel to improve the bond strength with concrete. Tests with smooth steel rods at Missouri S&T indicated that, after 28 days in concrete, the bond strengths of coated rods are at least twice those for uncoated or epoxy-coated rods [Chen et al., 2009; 2010]. Similar results were reported by the Army Corp of Engineers [Day et al., 2006; Hackler et al., 2006]. The combination of enhanced bond-strength between the steel and concrete, and the potential for improved corrosion resistance, indicates that the *development length* in the design of RC bridge structures can be reduced with the use of the new coating, thus reducing the construction and maintenance costs of RC structures.

2. OBJECTIVES

The conventional approach to improve the corrosion resistance of steel rebar is to apply a coating, like epoxy, that provides a physical barrier to the corroding environment. These coatings do not improve the bond strengths between the steel and the surrounding concrete environment. The chemically bonded reactive enamel coatings increase that bond strength while providing corrosion protection. The overall goal of this study is to optimize this technology for the construction of RC structures in bridge applications, with the objective of reducing construction and maintenance costs and improving structural performance. The scope of work or main research tasks includes:

1) Characterize the bond strength between deformed steel rebar and concrete;
2) Characterize the corrosion resistant properties of coated rebar in alkaline environments, including reinforced concrete;
3) Study the behavior of beam-column concrete structures reinforced with enamel-coated rebar, develop and validate new design equations for the tension *development lengths* of coated steel rebar in RC members;
4) Develop design specifications for RC members using coated rebar and provide design training for MoDOT engineers as well as compare costs with conventional RC members.

3. PRESENT CONDITIONS

MoDOT currently uses epoxy-coated rebar for corrosion sensitive applications. Although epoxy-coated rebar applied in MoDOT bridges seems to have thus far performed satisfactorily, studies of evaluating epoxy-coated rebar performance in field conditions by Virginia, Florida, and Oregon DOTs concluded that epoxy-coated rebar corroded at a faster rate than uncoated rebar due to moisture trapped underneath breached epoxy coatings [Sagues et al., 1994; Brown and Weyers, 2003]. More importantly, the use of epoxy coated rebar requires longer development length because of a reduction in the pullout strength of the rebar in concrete. As such, developing new coatings for both improved corrosion resistance and increased bond strength is highly desirable.

4. BOND BEHAVIOR AND STRENGTH

This section deals with the optimization of the formulation of the reactive enamel coating for bond enhancement and the characterization of bond strength of enamel-coated deformed bars in concrete. The effects of concrete compressive strength and rebar size on bond behavior are investigated. Attempt was also made to understand the mechanism of bond enhancement with enamel coating on deformed rebar.

4.1. Background

The previous studies by Chen et al. [2009, 2010] were focused on an enamel formulation that consists of 50% enamel (the glassy bonding phase) and 50% calcium silicate (the reactive component) or 50/50 enamel coating. In those studies, the bond behavior of 50/50 enamel-coated bars in mortar and concrete were determined. All pullout tests were done with small, smooth steel pins in mortar. How the 50/50 enamel coating performs on deformed rebar was not previously investigated in detail except for demonstration tests on slabs and walls to understand the implications of enamel coating in structural applications. In addition, the 50/50 enamel composition was initially selected mainly based on the simplicity of manufacture. How much bond improvement this composition may have was unknown. The present study was intended to address questions about the preferred enamel formulation and about enhanced bond strength on deformed rebar.

4.2. Technical Approach

Pin pullout tests were conducted to understand the optimal content of calcium silicate (CS) in enamel coating for bond performance. Rebar pullout tests were performed to characterize the bond strength of deformed rebar in concrete and understand the effects of various material parameters. Forensic studies were carried out to understand various failure modes and interfacial behavior among concrete, enamel coating, and steel.

4.2.1. Specimens, Material Properties, and Setup of Pin Pullout Tests

A total of 36 pin pullout specimens were prepared with mortar and mild steel rods (C1018). Each specimen has one steel rod embedded into the center of a mortar cylinder as shown in Figure 4.1. The steel rod is ¼ in. in diameter and 2.5 in. long. The mortar cylinder is 2.25 in. in diameter and 1.5 in. tall. Specimens were prepared in accordance with ASTM C109 guidelines [2007]. The steel rod that was ¼ in. in diameter and 1.5 in long was first placed into the center of a polypropylene container. Fresh mortar was then poured into the container around the steel rod to a height of 1.5 in. Next, each cylinder was tapped and vibrated to remove entrapped air from the mortar. Lastly, all samples were cured in a 100% humidity environment at room temperature for up to 60 days. After curing, each cylinder was removed from its container. The mortar used in this study had a mixture of 0.485: 1.0: 2.75 for water, Type I cement, and sand, respectively.

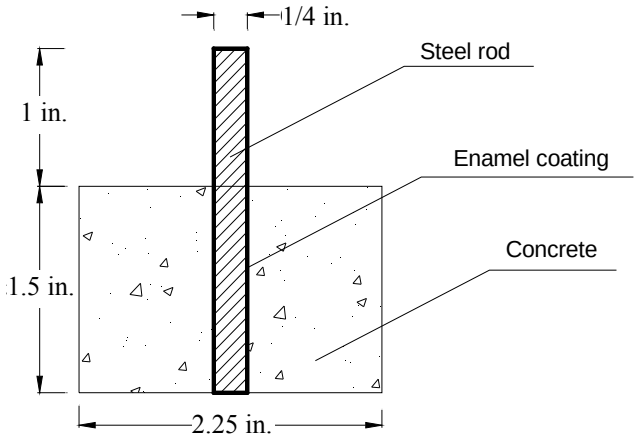

Figure 4.1 Specimen dimensions and schematic view of pin pullout specimens.

The 36 specimens were evenly divided into four groups with four types of enamel coating: 100/0 (pure enamel or 0% CS), 80/20, 65/35, and 50/50 (50% CS). Enamels are vitreous materials with a range of chemical compositions, depending on specific applications. The composition of glass frits for use on reinforcing steel can vary with the manufacturer and the exact compositions of most formulations are often proprietary. The composition of a typical glass frit used in an alkali-resistant ground-coat is given in *International Critical Tables* (1927). In the present study, similar glasses were made in platinum crucibles in air for several hours, at 1400-1450°F, using standard raw materials. A typical melt size was approximately 100 grams. Melts were quenched on steel plates to form glasses. The glasses have ZrO_2 as one component, which provides enhanced durability in alkaline environments [Fyles and Shorrock, 1982]. Glass powders were then mixed with commercially available calcium silicate powers to form the reactive enamels. The microstructures of enamel coating with various CS contents are shown in Figure 4.2. It can be clearly seen from Figure 4.2 that the thicknesses of various coatings were not uniform. As the CS content increases, the microstructure appears to be more porous.

Four types of enamel-coated steel rods are shown in Figure 4.3. The surface roughness of an uncoated smooth rod and each type of coating was measured at three locations according to ASME B46. Their average and standard deviation are presented in Table 4.1. It is clearly seen from Table 4.1 that the surface of coated rods becomes rougher as more CS is added into the coating. This is because, as indicated in Figure 4.2, the higher the CS content, the more porous the enamel coating. The more porous material means the rougher surface. The roughness of the 50/50 enamel coating is approximately 10 times that of uncoated smooth rods.

Each specimen was tested on an MTS loading machine as shown in Figure 4.4. The steel rod was pulled out of the mortar at a strain rate of 2 in. per minute in displacement control. The applied load was monitored with a built-in load cell. The relative displacement between the steel rod and mortar was measured with a built-in linear variable differential transformer (LVDT) in the loading machine.

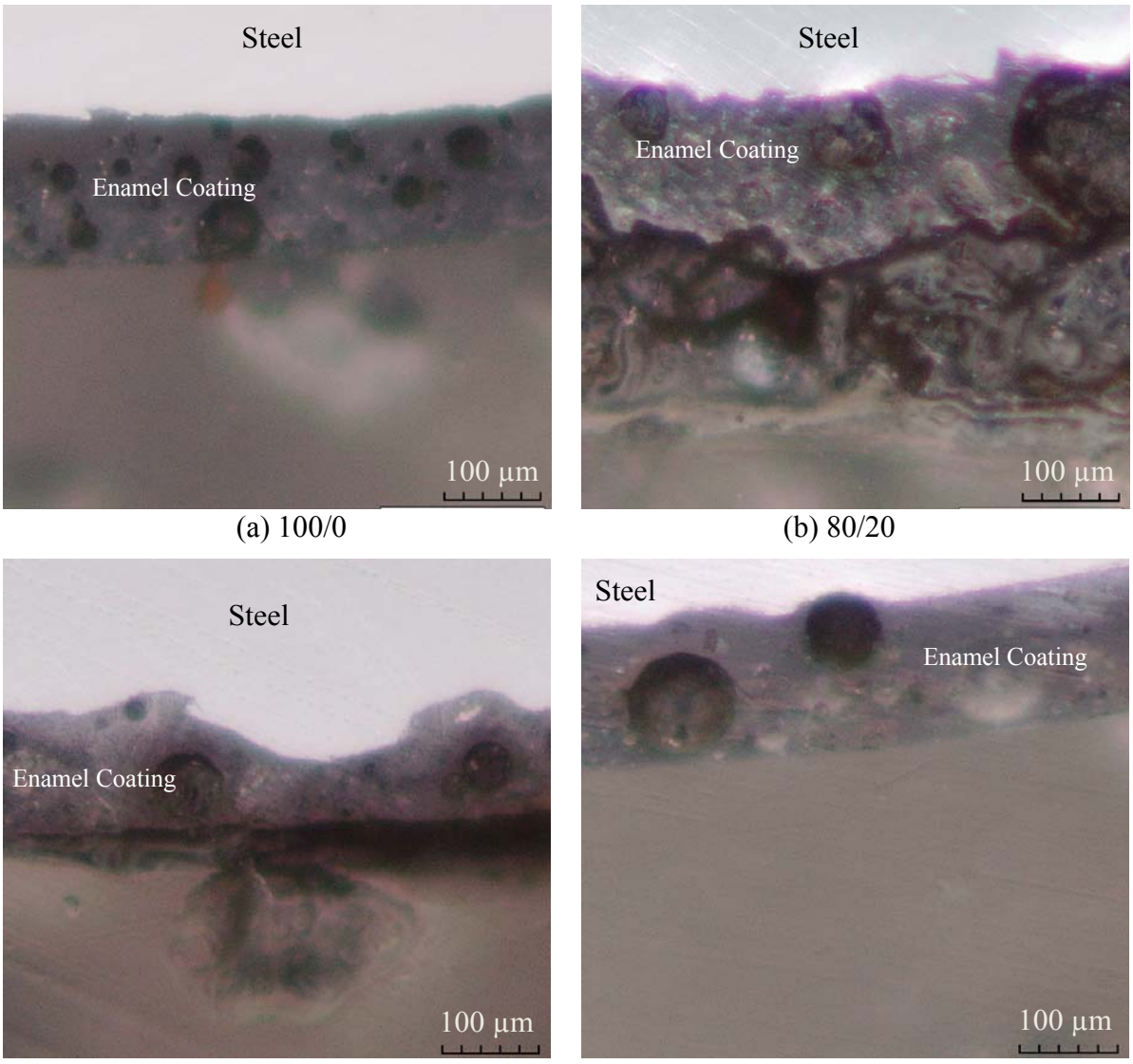

Figure 4.2 Microstructures of various enamel coatings.

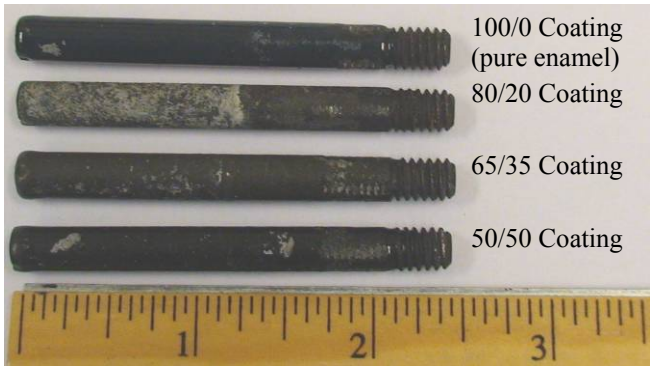

Figure 4.3 A snapshot of four types of enamel-coated steel rods.

Table 4.1 Surface roughness of steel rods with different types of coating

Coating	Surface Roughness (μm)	Standard Deviation (μm)
Uncoated smooth rod	1.2	0.2
100/0 (Pure enamel)	1.3	0.3
80/20	9.0	1.6
65/35	9.4	1.5
50/50	12.8	2.0

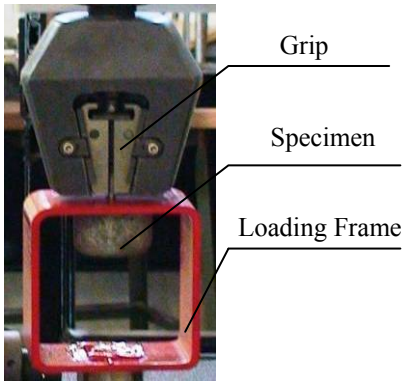

Figure 4.4 Test setup of a pin pullout specimen on MTS loading machine.

4.2.2. Specimens, Material Properties, and Setup of Rebar Pullout Tests

Rebar pullout specimens were designed to have one deformed rebar embedded in the center of a concrete cylinder as described by Abrams [1913]. Each concrete cylinder was 8 in. in diameter and 6.5 in. long. The deformed rebar was embedded in the 2.5 in. center portion of concrete with two bond breaks of 2 in. each at both ends of the embedded portion.

The pullout test program considered three experimental variables: rebar coating (uncoated, 50/50 enamel-coated, and epoxy-coated), rebar size (#4 and #8), and concrete mix designs (Rolla Ready Mix and MoDOT Bridge Mix - MB-2). Correspondingly, specimens were divided into three groups as shown in Table 4.2. For each group, new specimens were cast and tested at various curing ages (3, 7, 14, 28, and 60 days). Three specimens were tested for each condition. In Table 4.2, each specimen is designated by two capital letters and two numbers. The first letter represents the type of coating (U for uncoated, C for enamel-coated, or E for epoxy-coated) and the second letter represents the type of concrete mix designs (A for Rolla Ready Mix or B for MoDOT Bridge Mix specified in Table 4.3). The first single-digit number denotes the size of rebar expressed in 1/8 in. and the second two-digit number refers to the number of days of curing. For example, U4-A03 designates a 3-day specimen with an uncoated, #4 steel rebar in concrete cast using the Rolla Ready Mix design.

Table 4.2 Summary of rebar pullout specimens

Group	Specimen Designation	Type of Coating	Embedment Length	Rebar Size
Coating Effect (U=uncoated, C=enamel, E=epoxy)	U4-A28	Uncoated	2.5 in	#4
	C4-A28	Enamel	2.5 in	#4
	E4-A28	Epoxy	2.5 in	#4
Concrete Mix Effect (A=Rolla Ready Mix, B=MoDOT Bridge Mix)	U4-A03	Uncoated	2.5 in	#4
	U4-A07	Uncoated	2.5 in	#4
	U4-A14	Uncoated	2.5 in	#4
	U4-A28	Uncoated	2.5 in	#4
	U4-A60	Uncoated	2.5 in	#4
	U4-B03	Uncoated	2.5 in	#4
	U4-B07	Uncoated	2.5 in	#4
	U4-B14	Uncoated	2.5 in	#4
	U4-B28	Uncoated	2.5 in	#4
	U4-B60	Uncoated	2.5 in	#4
Rebar Size Effect (#4 or #8)	C4-A03	Enamel	2.5 in	#4
	C4-A07	Enamel	2.5 in	#4
	C4-A14	Enamel	2.5 in	#4
	C4-A28	Enamel	2.5 in	#4
	C4-A60	Enamel	2.5 in	#4
	C8-A03	Enamel	2.5 in	#8
	C8-A07	Enamel	2.5 in	#8
	C8-A14	Enamel	2.5 in	#8
	C8-A28	Enamel	2.5 in	#8
	C8-A60	Enamel	2.5 in	#8

Table 4.3 Specifications of MoDOT bridge mix design

Material	Quantity
Portland Cement Type I (lb/yd^3)	360
Water (lb/yd^3)	240
Fly Ash (Class C) (lb/yd^3)	90
GGBFS (lb/yd^3)	151
Coarse Aggregate (lb/yd^3)	1843
Fine Aggregate (lb/yd^3)	1138
Air Entraining Agent (Oz)	13.2
Low-range Water reducer (Oz)	18.6

Rebar pullout specimens were cast using 8 in. diameter Sonotubes and top and bottom plywood sheets, as illustrated in Figure 4.5. For each specimen, a circular groove was cut on the top and bottom plywood sheets to prevent both sheets from sliding against the Sonotube. Two 2-in.-long PVC pipes (0.5 in. and 1.0 in. in diameter for #4 and #8 rebar, respectively) were cut with a longitudinal groove. They were attached to the deformed rebar after the rebar was wrapped with Teflon tape in the bond break area. One PVC pipe was flush with the bottom end of rebar and the other PVC pipe was 2.5 in. (clear distance) away from the first one. The rebar and PVC pipes were then placed in the center of a Sonotube and passed through the hole at the center of the top plywood sheet after casting of concrete in order to hold the rebar in place during the curing process. The complete pullout specimens are shown in Figure 4.6(a).

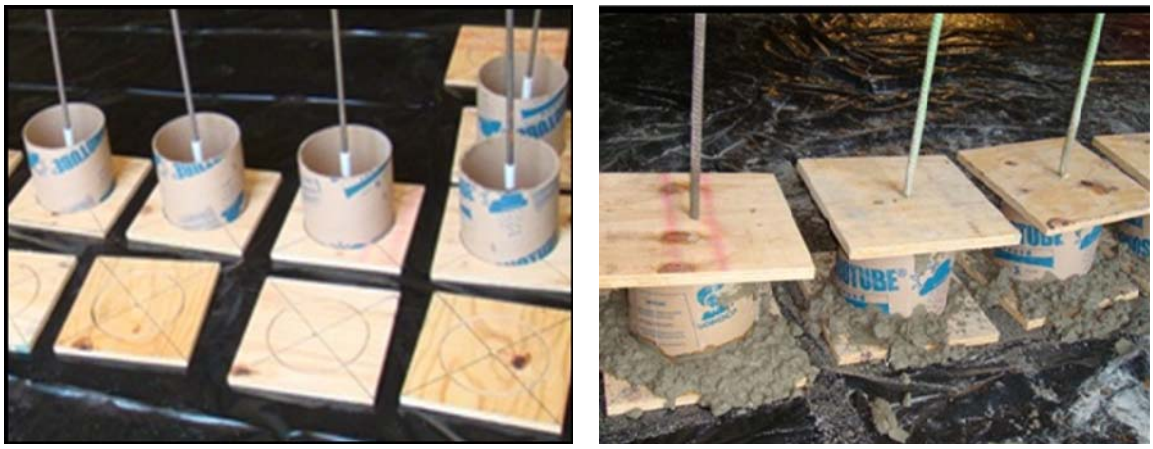

(a) Molds for specimen casting (b) Completion of casting

Figure 4.5 Specimen fabrications.

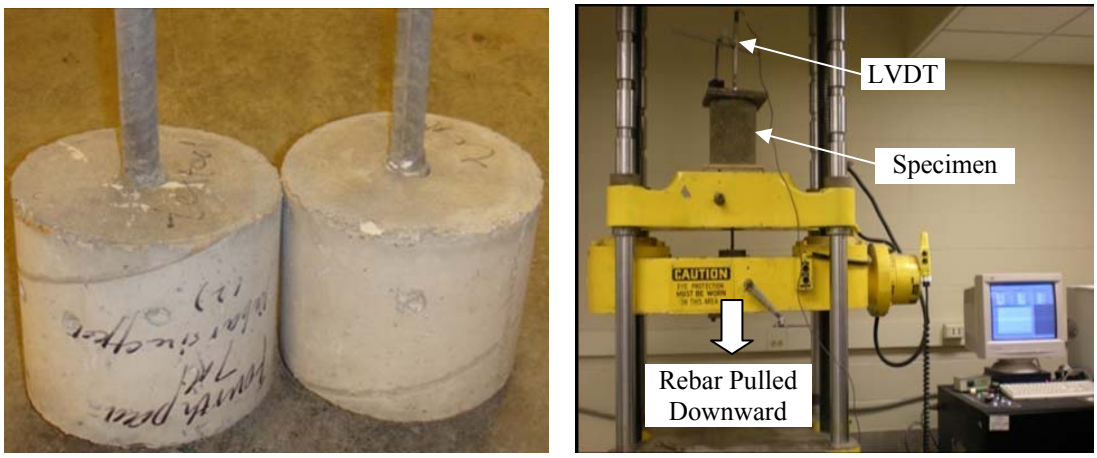

(a) Finished specimens (b) Test setup

Figure 4.6 Specimens and test setup.

Pullout tests were conducted on the Tinius Olson Loading Machine as shown in Figure 4.6(b). A specimen was placed on the upper crosshead in an upside down position with the rebar passed through the hole on the upper crosshead. The rebar further passed through the hole on the lower moving head and was anchored by a pair of hydraulic jaws. The rebar was drawn down monotonically at a displacement rate of 0.1 in/min. To minimize the eccentricity effect, a shim plate was placed between the concrete cylinder and the upper crosshead of the testing machine. The rebar slip was measured on top of the concrete cylinder with a LVDT. All measurements including the pullout load, moving head displacement, and the rebar slip were recorded by a computer-controlled data acquisition system at the rate of 250 values per minute.

4.3. Results and Discussion

The test results of both pin and rebar pullout specimens are reported and discussed in this section. For each type of specimen, the ultimate bond strength, the bond stress versus slip curves, and forensic analyses are presented.

4.3.1. Pin Pullout Specimen Tests

4.3.1.1. Bond strength

Three specimens were tested at each curing age. Both the average bond strength and the range of bond strength are presented in Figure 4.7. It can be seen from Figure 4.7 that the bond strength increases with increasing CS content at all three curing ages (14-day, 28-day and 60-day). This is partly due to the increasing roughness of the initial coating as more CS is added to the enamel coating as seen from Table 4.1. More importantly, the CS in the enamel coating is chemically reactive with the cement, forming a chemical as well as mechanical bond with the mortar.

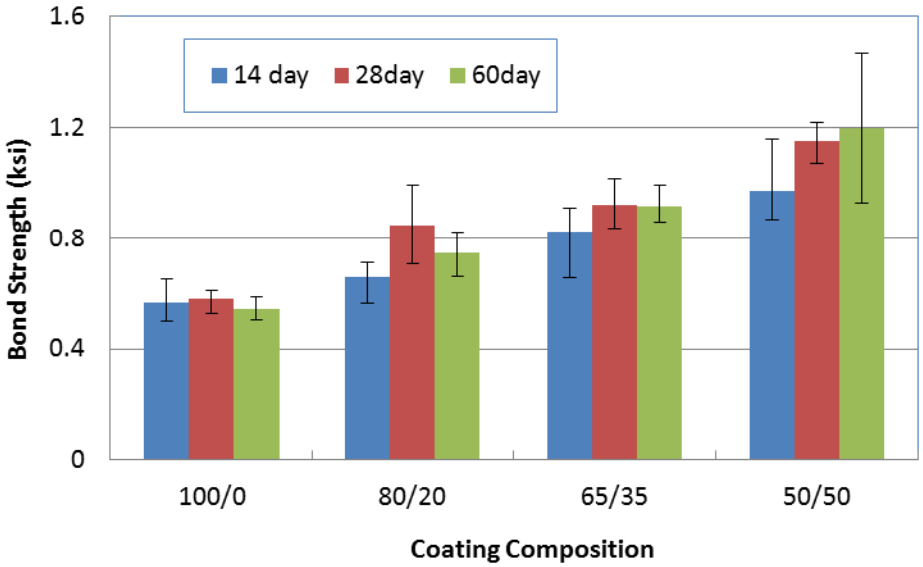

Figure 4.7 Concrete bonding to steel rods coated with various enamel coatings.

Figure 4.7 also indicates that the bond strength changed little between 28 days and 60 days of curing time. Therefore, the enamel coating is compatible with concrete materials used in civil engineering applications, as the 28-day material strength is commonly used in design practices. Note that, for 80/20 enamel coating, the 28-day bond strength is slightly higher than that in 60 days of curing. This difference is likely due to inconsistent mortar and casting conditions that may be involved during the preparation of various specimens.

4.3.1.2. Bond stress versus slip curves

The bond stress-slip curves are depicted in Figures 4.8 through 4.10. They indicated that the rods coated with pure enamel experienced much larger slippage and their corresponding specimens have a more ductile bond behavior than the remaining specimens. Rods coated with enamels with 20% calcium silicate also exhibited a greater degree of slipping, particularly at early curing ages. These results reflect the difference in failure modes between the samples. As shown in Figure 4.11, the steel rods coated with pure enamel were consistently pulled out of the mortar cylinders due to low surface roughness and no chemical reaction with the mortar. When rods coated with the reactive enamel were pulled out, the mortar cylinders often split. The slip between a rod and mortar before the applied load reached its peak decreased with increased curing age for the pure enamel coating and increased for the 65/35 enamel coating. This was also related to the switch in failure modes, but attributable to the fact that mortar becomes stronger with curing time. Stronger mortar becomes more brittle at the mortar-steel interface with pure enamel but delays the splitting failure that controls the slip in the 65/35 coating. The change from ductile to brittle bond behavior of mortar cylinders reinforced with the 80/20 coating was observed as the curing age increased, indicative of the switch from a rod pullout failure to concrete splitting failure. Although the specimens with 50/50 coating consistently failed by the concrete splitting mode, the level of slips before failure follows no consistent pattern, and is most likely due to inconsistent mortar and casting conditions for various specimens. At 28 days of curing, one 65/35 specimen and one 50/50 specimen were damaged during the tests.

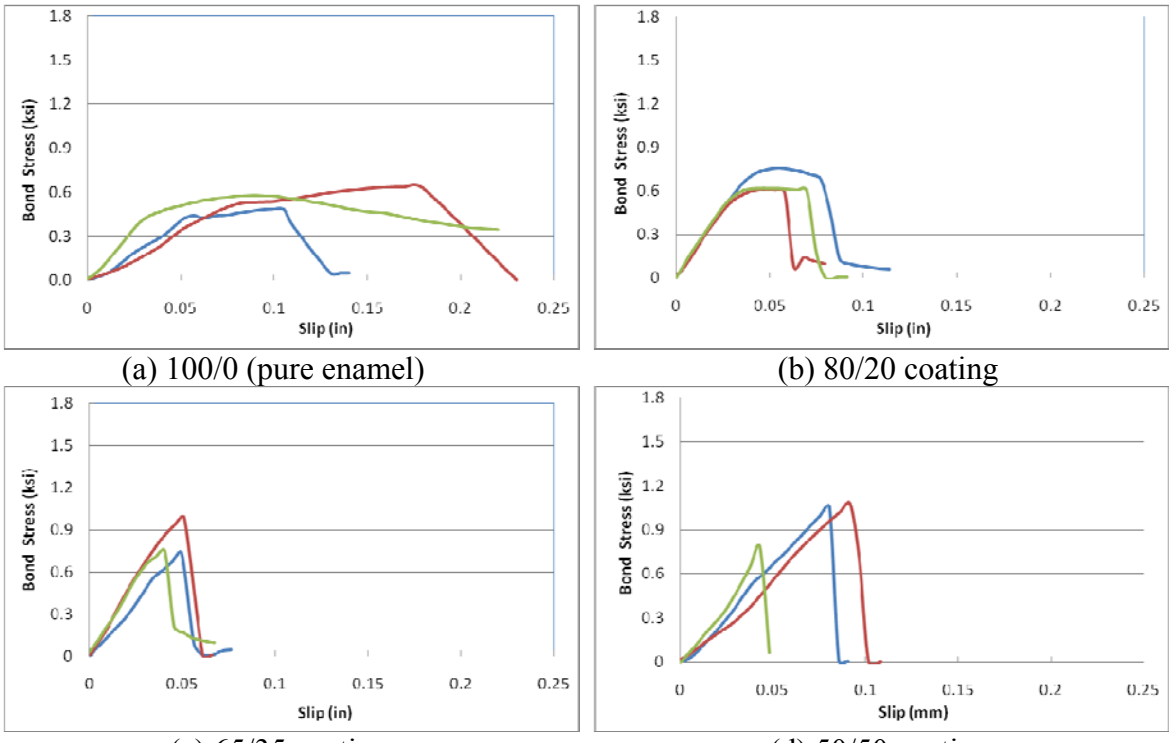

(a) 100/0 (pure enamel) (b) 80/20 coating

(c) 65/35 coating (d) 50/50 coating

Figure 4.8 Stress-slip curves of specimens with various coatings at curing age of 14 days.

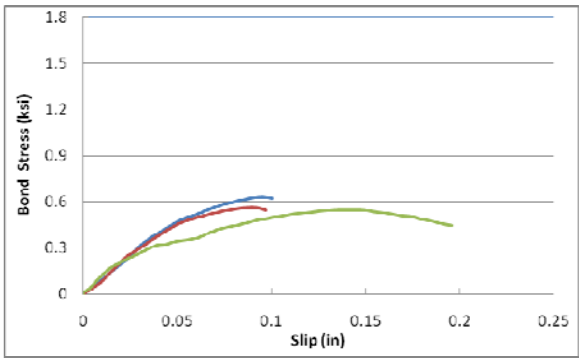

(a) 100/0 (pure enamel)

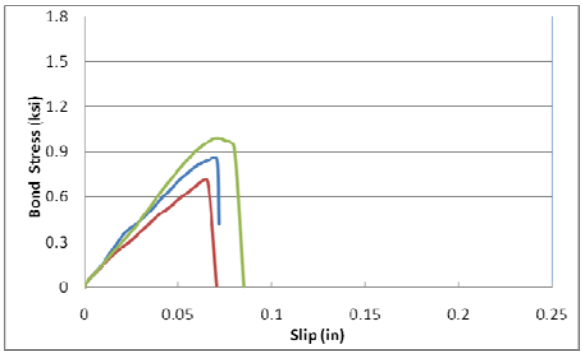

(b) 80/20 coating

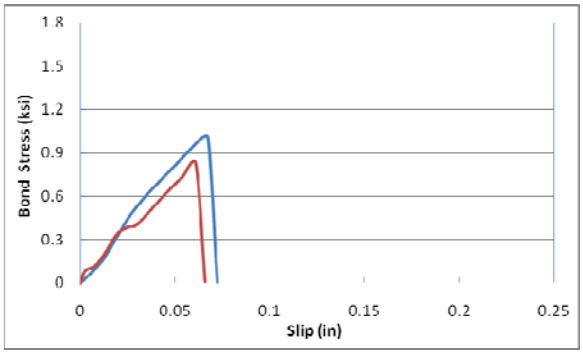

(c) 65/35 coating

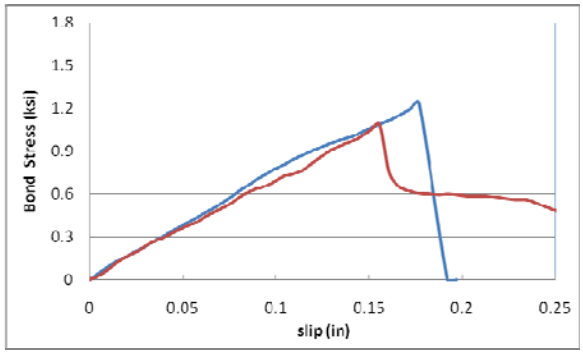

(d) 50/50 coating

Figure 4.9 Stress-slip curves of specimens with various coatings at curing age of 28 days.

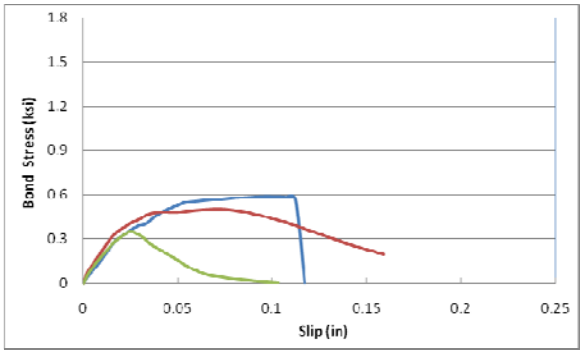

(a) 100/0 (pure enamel)

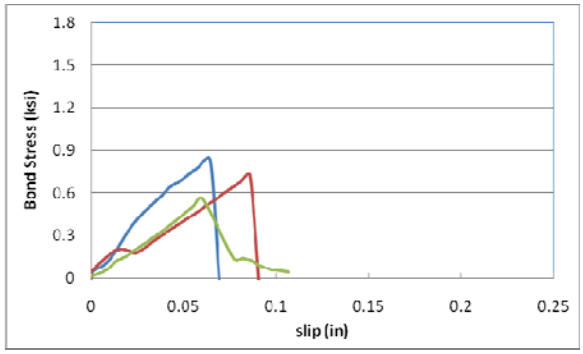

(b) 80/20 coating

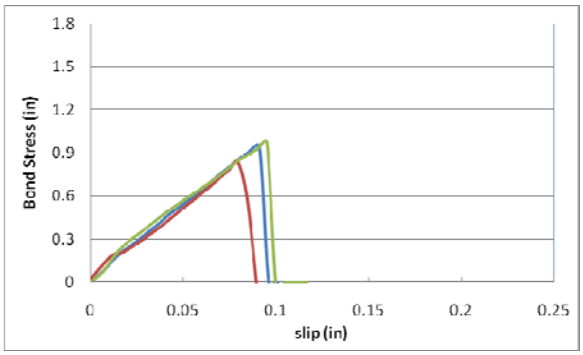

(c) 65/35 coating

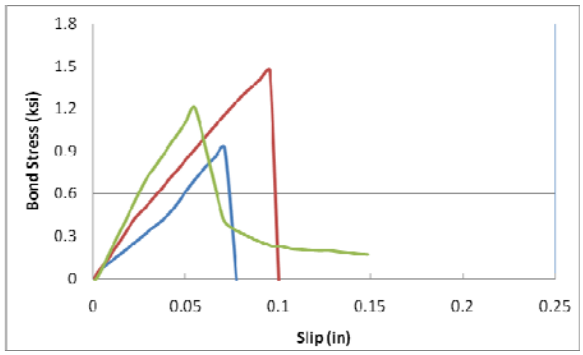

(d) 50/50 coating

Figure 4.10 Stress-slip curves of specimens with various coatings at curing age of 60 days.

4.3.1.3. Failure modes

Typical failure modes of various specimens coated with different coatings are presented in Figure 4.11. Rods with pure enamel coating were consistently pulled out of the mortar, leaving no crack in the mortar as shown in Figure 4.11(a). For rods with 65/35 and 50/50 coatings, specimens failed by concrete splitting as observed in Figure 4.11(c, d). The mortar cylinders reinforced with 80/20 enamel-coated rods represented a balanced steel pullout and concrete splitting at 28 days. As illustrated in Figure 4.11(b), a crack was observed in the mortar but did not extend across the entire cross section of the mortar cylinder. The failure modes shown in Figure 4.11 strongly support the bond stress versus slip curves as presented in Figure 4.10.

(a) 100/0 (b) 80/20 (c) 65/35 (d) 50/50

Figure 4.11 Typical failure modes of pin pullout specimens tested at 28 days.

4.3.2. Rebar Pullout Specimen Tests

4.3.2.1. Coating effect

The load-slip curves of nine specimens with 50/50 enamel-coated, epoxy coated and uncoated #4 steel bars are compared in Figure 4.12(a). The expanded view at small slips is presented in Figure 4.12(b). At small slips, the proportional points (linear portions) of the load-slip curves for enamel-coated rebar are significantly higher than those of epoxy-coated rebar and uncoated rebar, indicating a higher adhesion force for the enamel-coated rebar due to the chemically reactive nature of enamels containing calcium silicate. For example, at a slip of 0.002 in. marked with a solid vertical line in Figure 4.12(b), the average bond force with enamel-coated rebar was 11% and 52% higher than that with uncoated rebar and with epoxy-coated rebar, respectively. The slopes of the load-slip curves for enamel-coated rebar are also larger, which could lead to a stiffer structural system when enamel coating is used on steel rebar. As a result, the epoxy-coated specimens experienced a larger slip than those with enamel coatings and uncoated rebar under the same applied load. For example, at 8 kips, the average slip of three enamel-coated rebar was 0.0021 in. compared to 0.0023 in. and 0.0078 in. for uncoated and epoxy-coated rebar, respectively. It can also be seen from Figure 4.12(a) that the post-peak portions of the load-slip curves for all three types of specimens become parallel to each other and the applied loads linearly decrease toward the kinematic friction level. This phenomenon is an indication of similar pullout failures of the specimens that were all dominated by the shear strength of the concrete.

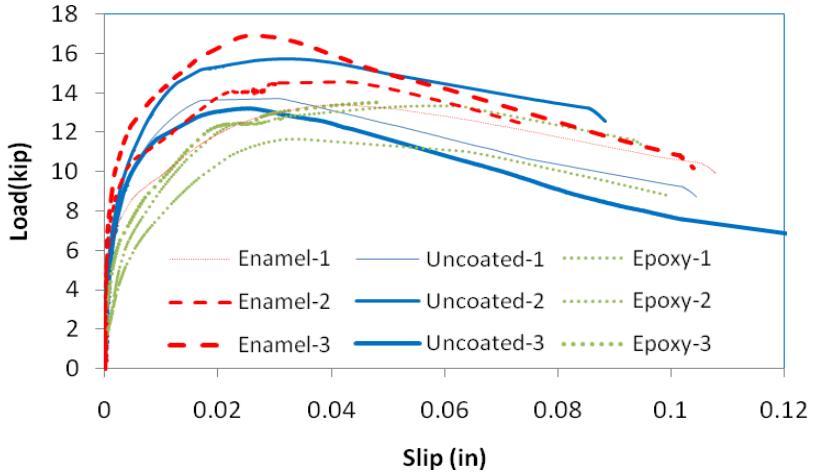

(a) Overall view

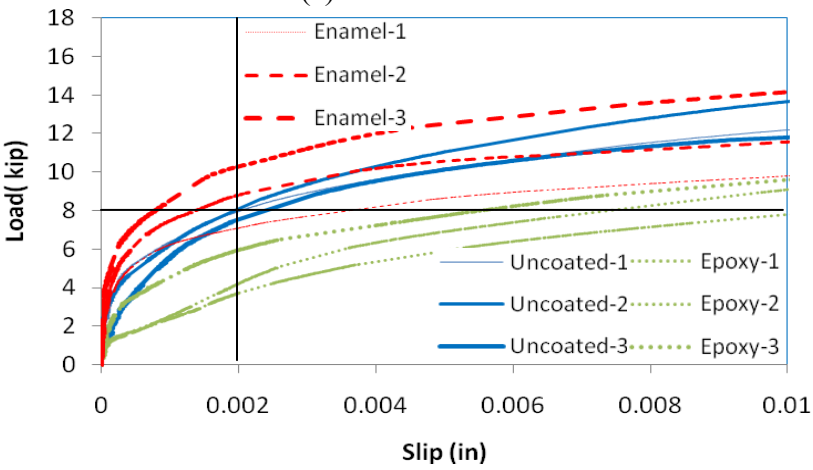

(b) Expanded view

Figure 4.12 Load-slip curves of specimens with various coatings.

The applied load in Figure 4.12 was divided by the shear area of 6.5-in. high cylinders to determine the bond strength of rebar pullout specimens. The average and the range of three ultimate bond strengths are presented in Figure 4.13 for each of the three types of samples. In comparison with the uncoated specimens, the enamel-coated specimens had a bond strength that was greater by 5% and the epoxy-coated specimens had a bond strength that was reduced by 10%. This can be explained based on the failure mechanism of the pullout specimens. The bond strength between rebar and concrete is generally a combination of adhesion, friction, and concrete bearing. The chemically reactive enamel coating can increase the adhesion effect. In addition, the rougher surfaces of the enamel coating also contributed to the friction effect between the concrete and steel rebar. The concrete bearing effect mainly depends upon the geometry of rebar deformations. In the cases with #4 rebar, pullout failures occurred along a cylindrical surface connecting the tips of rebar deformations, resulting in a bond strength that was dominated by the shear strength of concrete and insignificantly affected by coating through the small area at the tips of rebar deformations. The reduction in bond strength of epoxy-coated

rebar is likely due to the fact that the inert epoxy material does not interact with the concrete [Jalili et al., 2009]. The inorganic enamel coating is chemically reactive with the concrete.

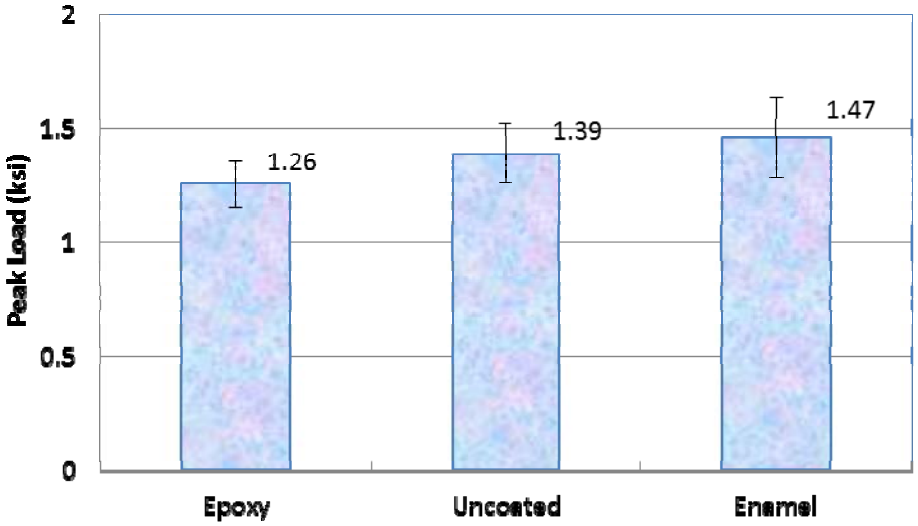

Figure 4.13 Ultimate bond strengths of specimens with various coatings.

4.3.2.2. Concrete mix effect

The Rolla Ready Mix and MoDOT Bridge Mix were used to investigate the effect of concrete mixtures on bond strengths. Their 28-day compressive strengths are 5.2 ksi and 3.95 ksi with standard deviations of 0.22 ksi and 0.21 ksi, respectively. Representative load-slip curves for specimens using the Rolla Ready Mix are presented in Figure 4.14(a). The expanded view is shown in Figure 4.14(b). It can be seen from Figure 4.14(a) that, at early curing ages of 3 and 7 days, the applied loads increased linearly and then gradually decreased with increasing slip, revealing a ductile behavior of the structure. At later curing ages of 14, 28, and 60 days, the applied loads increased and then decreased more rapidly than those of the early ages. However, all loads eventually approached similar levels as the slip increased beyond 0.015 in. The asymptotic values mainly represented the kinematic friction force between rebar and concrete. Up to a slip of 0.003 in., all the load-slip curves, except the one at 14 days, clearly revealed a plateau as illustrated in Figure 4.14(b).

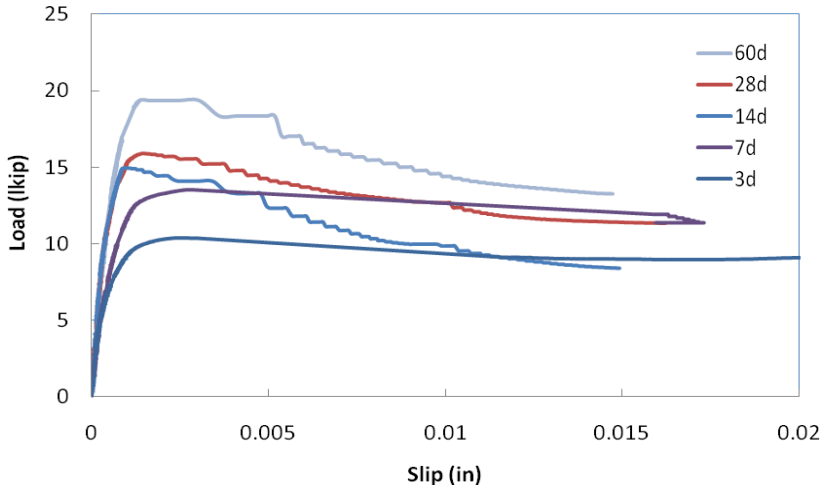

(a) Overall view

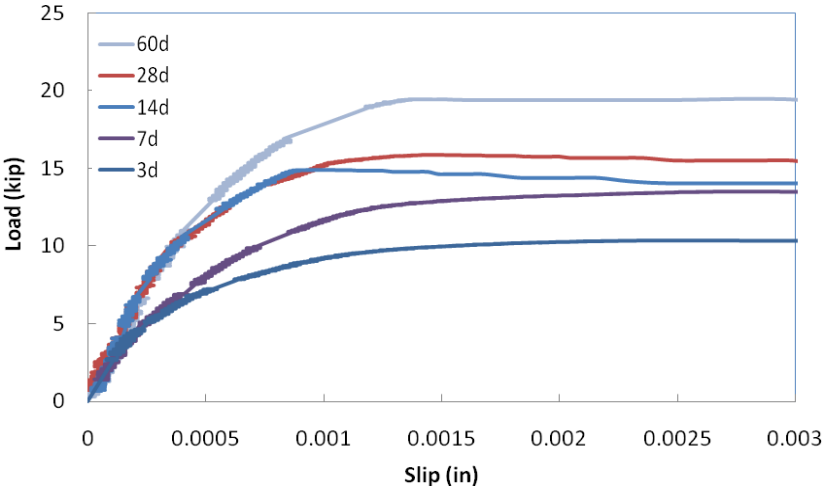

(b) Expanded view

Figure 4.14 Load-slip curves of specimens with concrete at various curing ages.

The average and range of the ultimate bond strengths of three uncoated specimens are plotted in Figure 4.15 as a function of curing age. As can be seen from Figure 4.15, the bond strength of uncoated rebar in concrete with Rolla Ready Mix is twice as high at 3 days and approximately 1.8 times as high at 28 days, compared to the MoDOT Bridge Mix design. This is because the concrete compressive strength (5.2 ksi) for Rolla Ready Mix is significantly higher than that (3.95 ksi) for MoDOT Bridge Mix. Note that the bond strength is often considered proportional to $\sqrt{f_c'}$ [ACI318-08, 2008]. In this study, the ratio of $\sqrt{f_c'}$ between Rolla Ready Mix and MoDOT Bridge Mix is approximately 1.15, which is substantially smaller than the increase of bond strength from pullout tests.

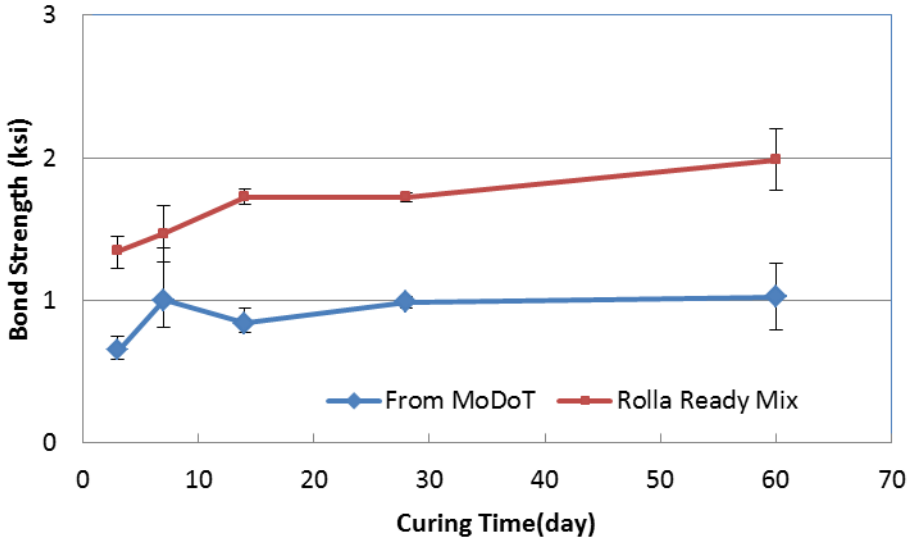

Figure 4.15 Bond strengths of specimens with various concrete mixtures.

4.3.2.3. Rebar size effect

Two sizes of enamel-coated rebar, #4 and #8, were tested to understand the effect of rebar size on bond strength. The average and range of the ultimate bond strengths of three specimens is plotted in Figure 4.16 as a function of curing age. They were determined by dividing the pullout force by the shear area using the 6.5-in. height of concrete cylinders. The larger rebar had smaller bond strength even though it took a larger pullout force due to its larger steel-concrete contact area and deeper deformations. The average bond strength ratio between the smaller and the larger rebar is approximately 0.63 at 28 days of curing ages, which is close to the ratio of 0.8 for #4 rebar and 1.0 for #8 rebar as required by ACI 318-08.

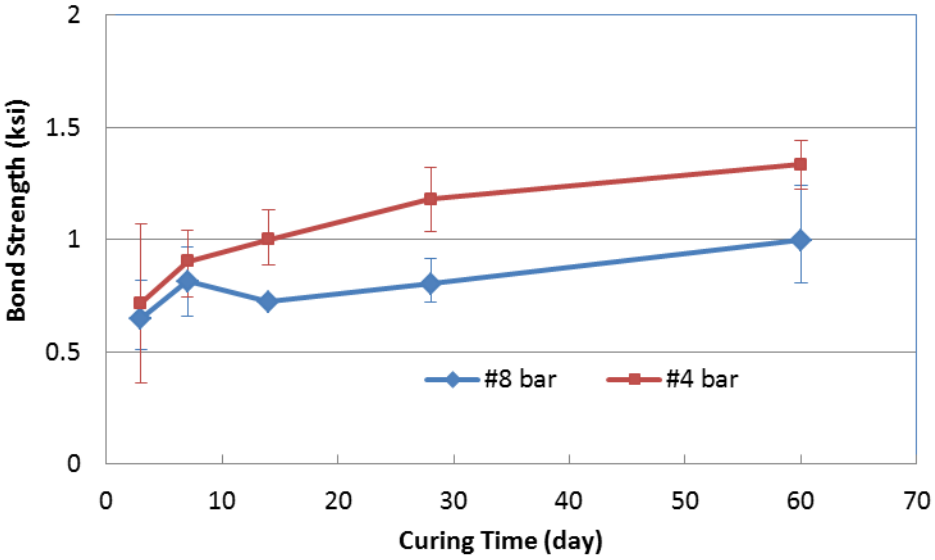

Figure 4.16 Bond strength of specimens with two rebar sizes.

Figure 4.17 shows the load-slip curves of two representative specimens with different rebar sizes. As can be clearly seen from Figure 4.17(a), the specimen with #4 rebar behaved in a ductile manner, corresponding to a pullout failure while the specimen with #8 rebar appeared more brittle due to concrete splitting failure as will be discussed in Section 4.3.2.3.

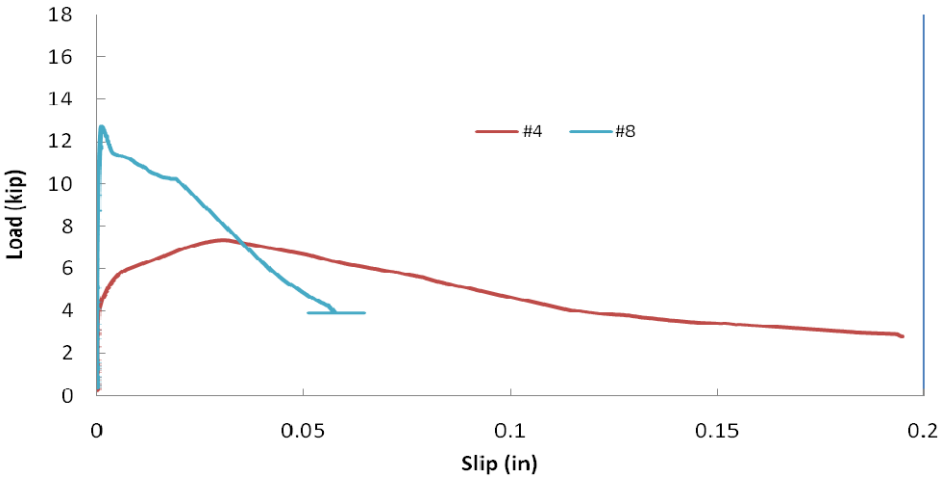

(a) Overall view

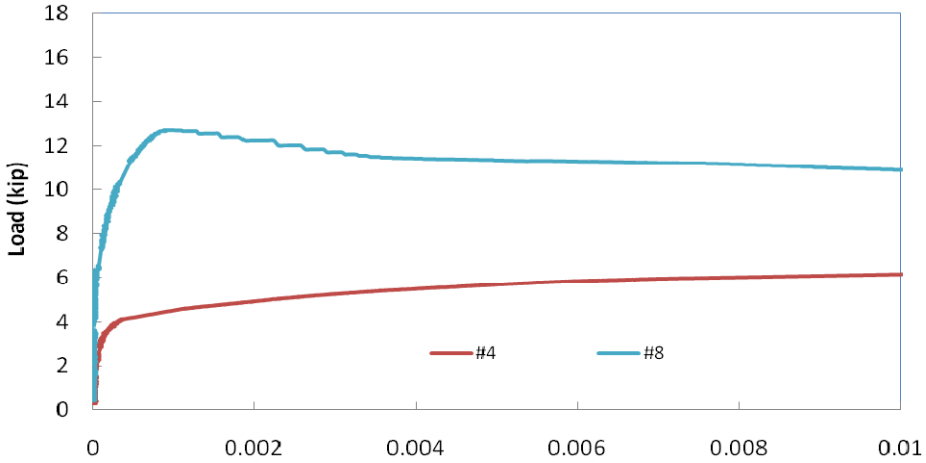

(b) Expanded view

Figure 4.17 Load-slip curves of specimens with two rebar sizes.

4.3.2.4. Failure modes

Throughout the rebar pullout test program, #4 rebar have been used to investigate the effects of coating and concrete mix on bond strength. For comparison, both #4 and #8 rebar were used to study the effect of rebar size. For all specimens with #4 deformed rebar, uncoated and coated, rebar was pulled out of the concrete, inducing no radial cracks in the concrete, as represented by Figure 4.18(a). For all specimens with #8 rebar, concrete splitting was observed as shown in Figure 4.18(b), except for the 3-day and 7-day tested specimens. The exception represented a combined failure mode of rebar pullout and concrete splitting as reflected by similar bond

strengths to #4 rebar as illustrated in Figure 4.16. It is attributable to the low early-age strength of concrete.

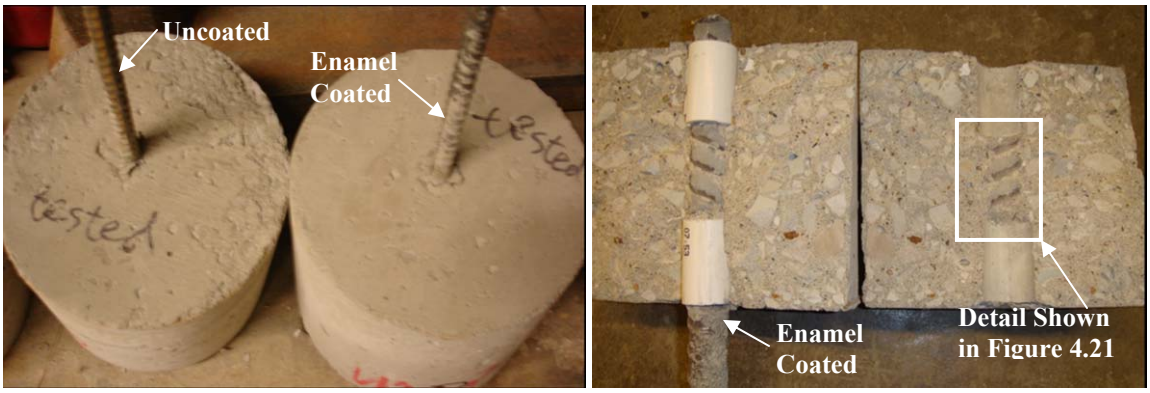

(a) Pullout failure (b) Split failure

Figure 4.18 Two representative failure modes of enamel-coated specimens.

To explain why the increase in bond strength with enamel-coated #4 rebar was only 5% compared to uncoated rebar, the detail of concrete-rebar interfaces is shown in Figure 4.19. As mentioned previously, all specimens with #4 rebar failed in rebar pullout. As indicated in Figure 4.19, failures occurred along a cylindrical surface connecting the tips of all rebar deformations. The effect of coating was only reflected in a small portion of the cylindrical surface around the tips of rebar deformations. Figure 4.19 also indicated that more concrete debris remained on the enamel-coated rebar compared to uncoated rebar, and no concrete debris was attached to the surface of epoxy coating. This examination indirectly supported the conclusion that enamel coating increased the bond strength between the concrete and steel, but the increase in bond strength is small for specimens failed in rebar pullout.

(a) Enamel-coated (b) Uncoated rebar (c) Epoxy-coated rebar

Figure 4.19 Details of concrete-rebar interfaces (#4 rebar).

Figure 4.20 shows the detail of concrete-rebar interfaces of specimens with #8 enamel-coated and uncoated rebar. Like the #4 rebar, concrete debris remained on the enamel-coated and uncoated steel rebar. However, in comparison with the #4 rebar, the concrete debris on the #8 rebar was much thinner mostly located between the rebar deformations as clearly seen in Figure 4.20(b). This observation indicated that the failure surface was mainly along the concrete-steel interface.

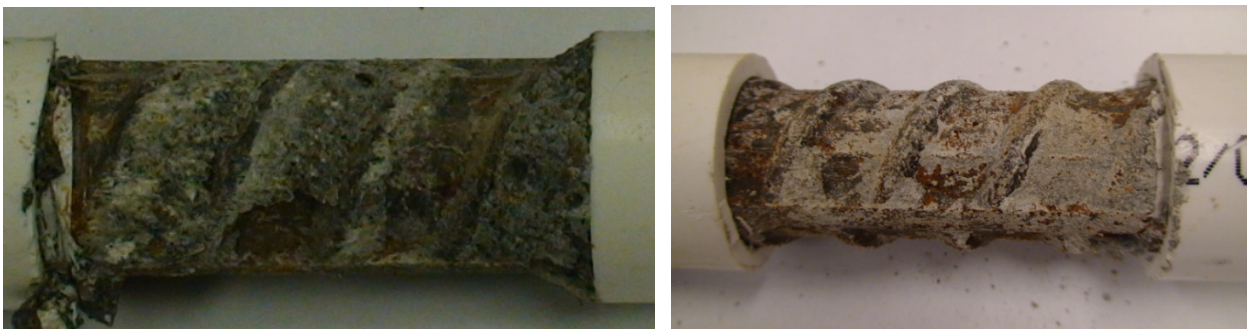

(a) Enamel-coated rebar (b) Uncoated rebar

Figure 4.20 Details of concrete-rebar interfaces (#8 rebar).

The expanded view of the splitting concrete surface enclosed in the rectangle in Figure 18(b) is presented in Figure 4.21. The traces of adhesion, friction, and concrete bearing effects are evident. Figure 4.22 summarizes the failure mechanisms of rebar pullout and concrete splitting with two schematic views. With a failure mode of rebar pullout shown in Figure 4.22(a), the bond strength between the concrete and steel was dominated by the shear strength of concrete. When concrete splitting occurred as illustrated in Figure 4.18(b), the bond strength depended on the adhesion, friction, and concrete bearing as shown in Figure 4.21. In this study, the face angle of the rebar used was over 45°, allowing the partial separation of rebar from its surrounding concrete at their interface. In this case, the effect of coating expects to be more significant than that for specimens failed in rebar pullout along the shear surface of concrete.

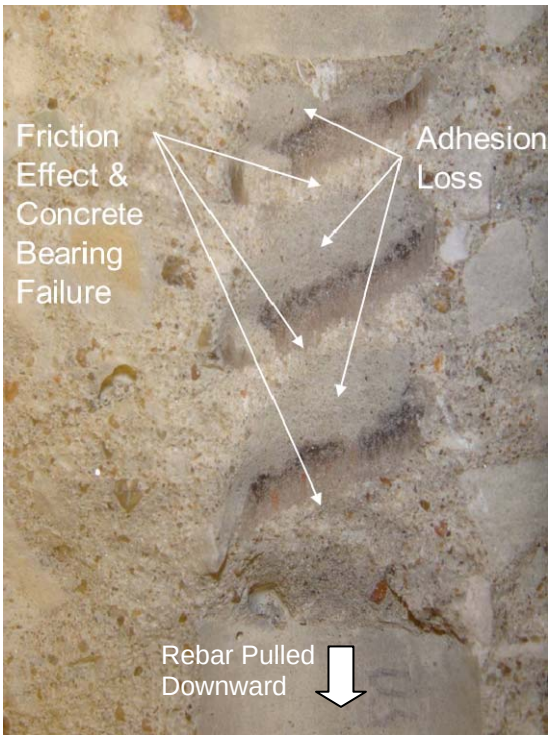

Figure 4.21 Traces of rebar movement.

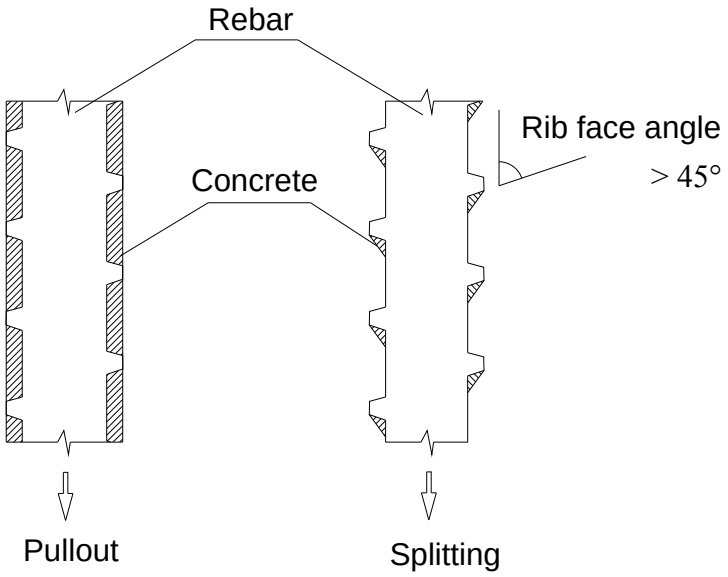

(a) Rebar pullout (b) Concrete splitting

Figure 4.22 Schematic views of concrete-rebar interface conditions for rebar pullout and concrete splitting failure modes.

4.4. Conclusions Based on Pullout Tests

The bond strength between an enamel-coated steel rod and mortar increases with increasing levels of calcium silicate within the coating. Considering its good bond performance and the ease of coating on steel rebar in practical applications, a mixture of 50% enamel and 50% calcium silicate or 50/50 enamel coating is recommended for bond strength between steel and concrete.

The pin pullout specimen with a ¼-in.-diameter steel rod embedded in a mortar cylinder failed in slipping (pullout) when the rod was coated with pure enamel but failed in splitting the mortar cylinder when the rod has a 50/50 enamel coating. The steel pullout and concrete splitting represent a ductile and a brittle bond failure mode of tested concrete cylinders, respectively. As the curing age increases, the mortar strength increases. Thus, the pullout failure mode becomes less ductile.

The rebar pullout specimens with enamel-coated reinforcement have a larger adhesion force and a steeper slope for the load-slip curves than those with epoxy-coated and uncoated rebar, exhibiting less slippage at the same load level. For all tested specimens with various coatings, the post-peak portions of load-slip curves are parallel and linearly decrease with increasing slip, reflecting a continual wearing condition on the rebar-concrete surface as rebar is being pulled out of the concrete. Although the adhesion and friction forces between rebar and concrete are increased with the use of enamel coatings, the ultimate bond strength is dominated by the concrete shear strength. As a result, the ultimate bond strength with an enamel coating only increases by 5% over uncoated rebar, while that with epoxy coating decreases 10% compared to

uncoated rebar. Overall, the ultimate bond strength with enamel-coated rebar is approximately 17% greater than that with epoxy-coated rebar.

The rebar size effect on bond strength of specimens with enamel-coated rebar can be represented by a rebar size factor in the ACI 318-08 development length equation. On the other hand, based on the limited number of tests, the ACI 318-08 equation may be overly conservative with respect to the concrete mix effect on bond strength.

All tested specimens with #4 deformed bars, coated or uncoated, fail in rebar pullout. For specimens with #8 enamel-coated rebar, the failure mode is dominated by concrete splitting. The exception is for early-tested specimens at 3 and 7 days of curing when concrete strength is still low.

5. SPLICE AND ANCHORAGE OF ENAMEL-COATED REBAR

5.1. Background

The use of reactive enamel coatings for steel rebar in civil engineering applications has been studied for the past five years [Day et al., 2006; Hackler et al., 2006]. At present, the understanding of the properties of the enamel material has been improved to a certain degree. To date, the maximum rebar length that manufacturers can provide is about six feet though alternative manufacturing techniques using electrostatic applications or plasma sprays are promising to lift the length limitations. Therefore, large scale tests of this technology have been limited. To facilitate the application of this material in bridge designs, the splice and anchor performance of enamel-coated rebar were investigated and is discussed in this section. Based on the data collected, design equations for splice and anchorage lengths are recommended.

5.2. Beam Tests

5.2.1. Technical Approach

The test program of beam specimens consisted of 12 rectangular concrete beams reinforced with enamel-coated, #6 or #8 deformed bars. Each beam measured 11 ft. in length and rested on two interior pin or roller supports, dividing it into three spans with two equal, cantilevered end spans. The cross section measured 12 in. wide and 18 in. deep with an effective depth of 16.5 in. or 15.75 in. depending on the rebar size. The middle span of each beam was designed for pure flexure, in which two reinforcing bars were longitudinally lap spliced at different lengths and transversely tied in close contact. A concrete compressive strength of 4.5 ksi was used for the design. As presented in Table 5.1, the test matrix contains detailed information of the splice specimens.

Table 5.1 Test matrix of beam spliced specimens

Specimens	Bar Size	Cover (in.)	Beam Size (B×H, in.)	Effective Depth (in.)	# of Spliced Bars	Splice Length (in.)
B-6-1*	#6	1.25	12×18	16.5	2	12
B-6-2*	#6	1.25	12×18	16.5	2	16
B-6-3	#6	1.25	12×18	16.5	2	12
B-6-4	#6	1.25	12×18	16.5	2	16
B-6-5*	#6	1.25	12×18	16.5	2	32
B-6-6*	#6	1.25	12×18	16.5	2	36
B-6-7	#6	1.25	12×18	16.5	2	32
B-6-8	#6	1.25	12×18	16.5	2	36
B-8-1*	#8	1.5	12×18	16.25	2	36
B-8-2	#8	1.5	12×18	16.25	2	36
B-8-3*	#8	1.5	12×18	16.25	2	43
B-8-4	#8	1.5	12×18	16.25	2	43

Note: * with transverse hoop bars.

In this study, the bond properties of coated bars in normal concrete were investigated through several key parameters, including the bar size, cover thickness, splice length, and confinement in the spliced region (transverse reinforcement). Both #6 and #8 rebar was selected since they are commonly used in bridge applications. The concrete cover thickness provided in Column 3 of Table 5.1 is for both the top and side clear cover to the spliced bar. The transverse reinforcement was provided to study the influence of confining stress on the bond behavior of enamel coated rebar.

ACI 318-08 recommends Eq. (5.1) for the determination of the minimum development (or splice) length in order to develop the full tensile strength of deformed bars. For uncoated #6 deformed bars in normal concrete having a compressive strength of 4.5 ksi, the calculated minimum development lengths were 22 in. and 31 in. with and without transverse reinforcement, respectively. For uncoated #8 deformed bars, the minimum development lengths became 35 in. and 58 in. with and without transverse reinforcement, respectively. To examine this design range and take into account the limitations in fabrication (6 ft. maximum at the beginning of this study), the selected splice lengths for coated rebar ranged from 12 in. to 43 in.. These lengths correspond to approximately 55% of the minimum value and 75% of the maximum value for development length.

$$l_d = \left(\frac{3}{40} \frac{f_y}{\lambda \sqrt{f_c'}} \frac{\psi_t \psi_e \psi_s}{\left(\frac{c_b + K_{tr}}{d_b} \right)} \right) d_b \tag{5.1}$$

where l_d is the minimum development length, f_y is the yield strength of reinforcement, λ = 1.0 for normal weight concrete, f_c' is the compressive strength of concrete, ψ_t =1.3 is the traditional reinforcement location factor to reflect the adverse effect of gravity on the top reinforcement during casting, ψ_e is a coating factor, ψ_s is a bar size factor (0.8 for #6 rebar or smaller and 1.0 for #8 rebar), c_b is the smallest side cover, d_b is the rebar size in diameter, and K_{tr} represents a factor of confining effect. The confining effect can be further determined by

$$K_{tr} = \frac{40 A_{tr}}{sn} \tag{5.2}$$

in which A_{tr} is the area of transverse reinforcement, s is the stirrup spacing, and n is the number of rebar spliced along the plane of splitting.

Sufficient shear reinforcement was provided in the two end spans of beam specimens to prevent any premature shear failure. For comparison, the middle span of some beam specimens was also confined transversely with #3 and #4 stirrups when they were spliced with #6 and #8 rebar, respectively.

5.2.1.1. Test specimens and material properties

Figure 5.1 shows the reinforcement and splicing details of the two groups of specimens: with and without confinement. The rebar cage fabrication and concrete casting are presented in Figure 5.2

and Figure 5.3, respectively. Due to the limitation in laboratory space, the splice specimens were cast in two groups with the same concrete mix design. The cast specimens were then kept moist and cured at room temperature for 7 days before the formwork was disassembled.

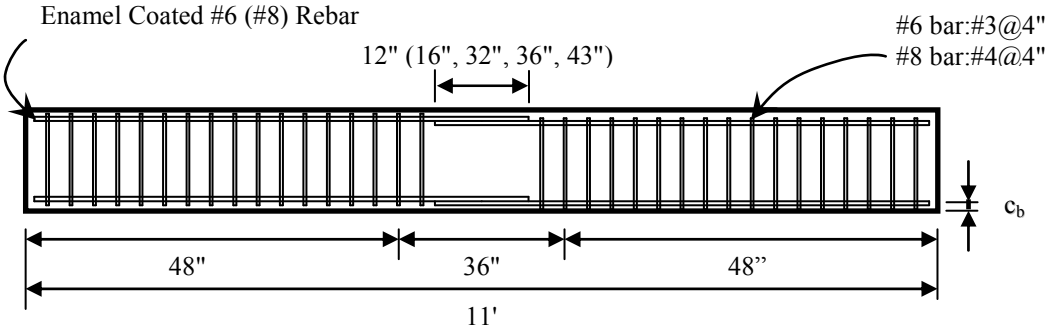

(a) Without confinement in the splice region

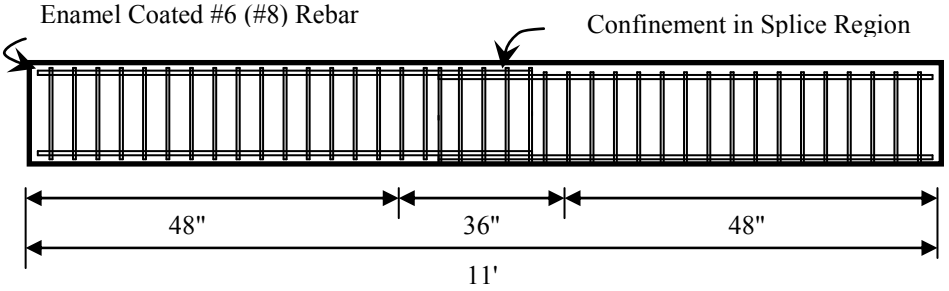

(b) With confinement in the splice region

Figure 5.1 Reinforcement details of beam specimens.

(a) Rebar cage of beams

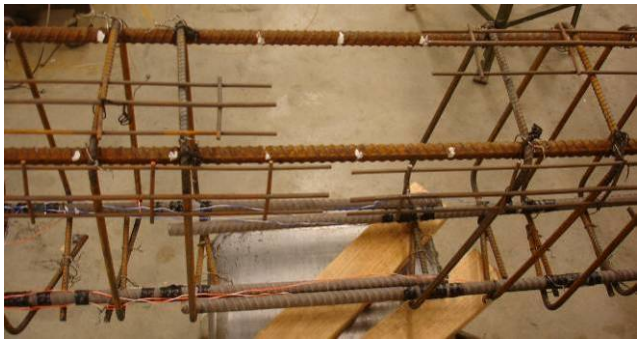

(b) View of spliced areas

Figure 5.2 Rebar caging.

(a) Curing of beams

(b) Finished beam specimens

Figure 5.3 Concrete casting.

The material specifications of the steel used in this study met the requirements of ASTM A615. The concrete mix design met the specified compressive and tensile strength, fracture energy, and modulus of elasticity as provided by Rolla Ready Mix, a local plant. Table 5.2 presents the actual concrete mix proportions provided by Rolla Ready Mix, Inc.

Table 5.2 Concrete mix proportions (Rolla Ready Mix, Inc.).

Material	**Quantity (lb/yd^3)**
Cement	658
Fine Aggregate	1505
Coarse Aggregate	1945
Water	110
Air Entrainment	0.6
High-Range Water Reducer	4.3

To determine the actual concrete compressive strength, test cylinders with a height of 12 in. and diameter of 6 in. were made according to ASTM C31 (2003) during the casting of beam specimens. The cylinders were then capped with Rediron 9000 sulfur capping compound according to ASTM C 617 (1998) and tested according to ASTM C 39 (2005) at curing ages of 7, 21, and 28 days. The mechanical properties of concrete for different groups of tested beams are provided in Table 5.3. The testing apparatus and typical failure mode of the cylinders are shown in Figure 5.4(a) and Figure 5.4(b), respectively.

The #3, #4, #6, and #8 reinforcing bars used in the splice specimens were provided by NUWAY Inc. The #6 and #8 rebar were coated by ProPerma Engineered Coating with the reactive 50/50 enamel coating. To determine the yield strength, the ultimate strength, and the modulus of elasticity, direct tensile strength tests were conducted using a Tinius-Olsen universal testing machine. The test setup is presented in Figure 5.5 with one extensometer used to measure the relative deformation in the middle portion of the specimen.

Table 5.3 Mechanical properties of concrete

Day	Group	Compressive Strength (ksi)	Average Compressive Strength (ksi)	Modulus of Elasticity (ksi)
7	1	3.2	3.25	N/A*
		3.0		
		3.3		
	2	3.1		
		3.4		
		3.5		
21	1	4.0	4.08	N/A
		4.1		
		3.9		
	2	4.1		
		4.3		
		4.1		
28	1	4.3	4.49	3,820
		4.5		
		4.4		
	2	4.7		
		4.7		
		4.4		

* Not Available

(a) Test apparatus

(b) Failure mode

Figure 5.4 Uniaxial compression test of concrete cylinders.

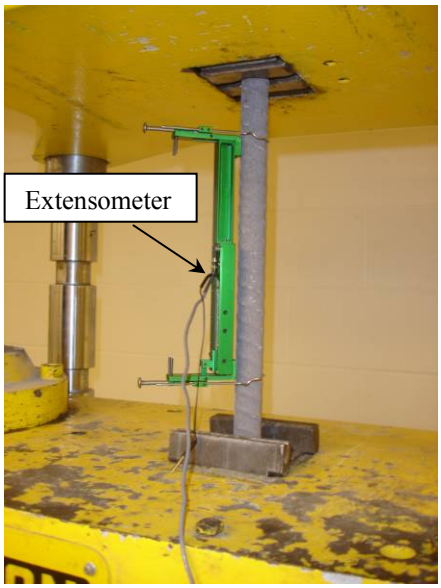

Figure 5.5 Tensile test setup and instrumentation of reinforcing steel bars.

The loading protocol for the tensile tests met the requirements of ASTM A370 (2005). The average load rate was kept at 0.5 in. per minute throughout each test. Crack initiation of the enamel coating was observed at an average strain of 3000 με. As the load continued to increase, the cracks on the coating surface widened until spalling occurred at the necking portion as illustrated in Figure 5.6.

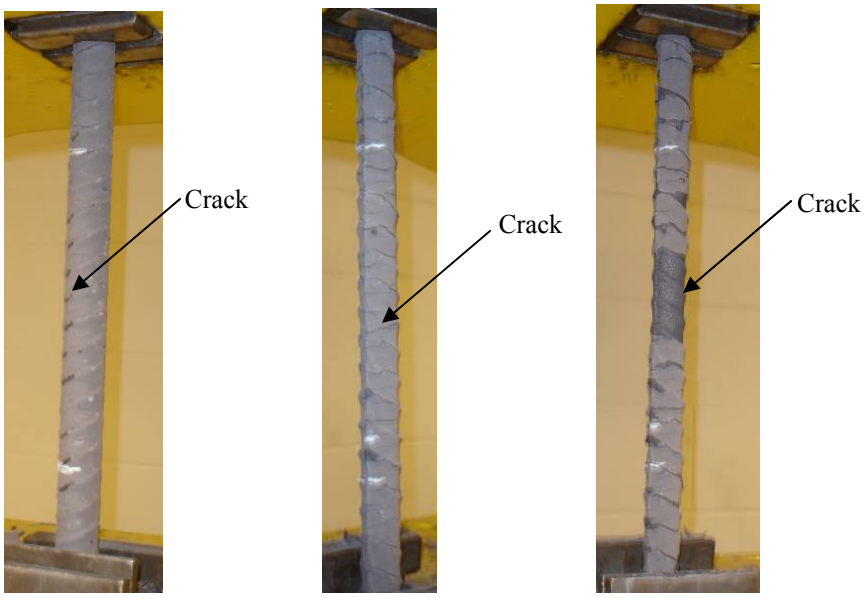

(a) Initiation of cracks (b) Crack widening (c) Enamel spalling

Figure 5.6 Tensile tests of enamel-coated rebar.

Table 5.4 lists the mechanical properties of the three #6 and three #8 specimens tested in this study. The average yield strengths of tested specimens were 60.6 ksi and 58.4 ksi for #6 and #8 coated rebar, respectively. The stress-strain curves of all tested specimens are presented in Figure 5.7. The test results are consistent, particularly for #8 rebar.

Table 5.4 Mechanical properties of coated rebar (Grade 60)

Property	#6 Coated Rebar	#8 Coated Rebar
Modulus of Elasticity, ksi	31,760	29,880
Yield Stress, ksi	60.6	58.4
Peak Stress, ksi	95.5	90.3

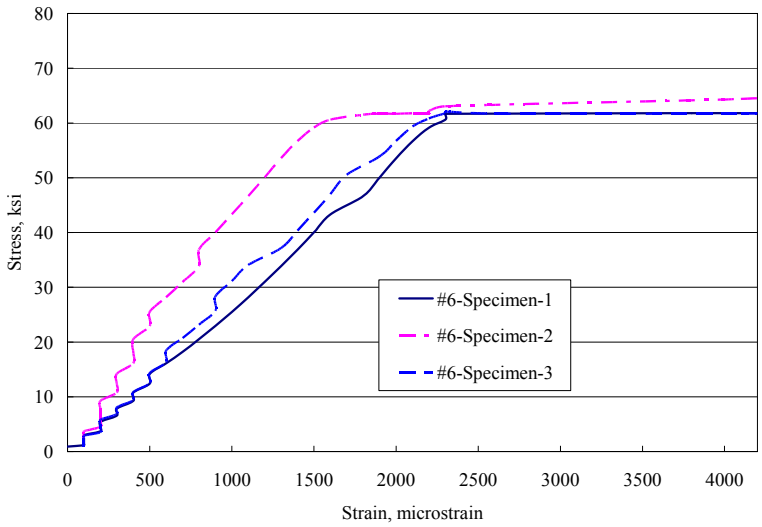

(a) #6 rebar

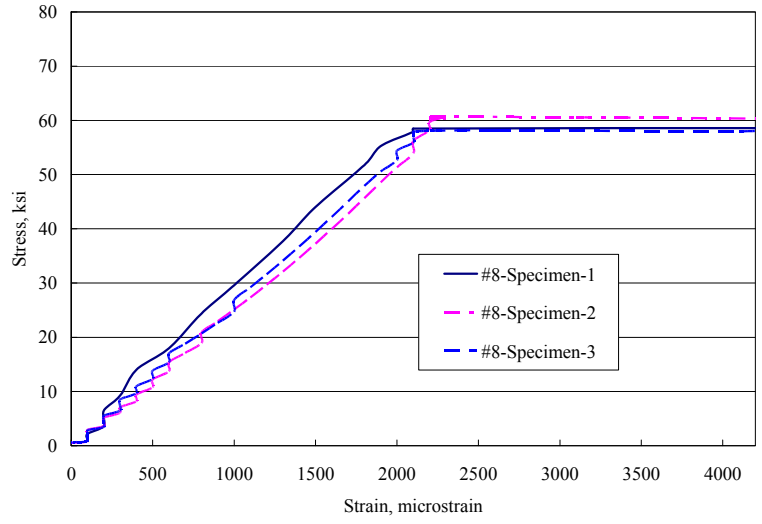

(b) #8 rebar

Figure 5.7 Stress-strain curves of enamel-coated deformed bars

5.2.1.2. Test setup, instrumentation, and loading protocol

Each beam was supported on two steel supports that were located 4 ft. from the two ends of the beam. As shown in Figure 5.8, the beam was tested under two equal loads at both ends of the beam, creating two cantilevered end spans and one center span that is subjected to pure flexure. The applied loads were provided by two hydraulic jacks placed between the ends of the beam and two double-channel reaction beams that were anchored to the strong floor through fine threaded Dywidag bars. Ball joint loading plates were placed between the jacks and beam ends to assure a vertical loading direction. The distance between the loading points was 9 ft.

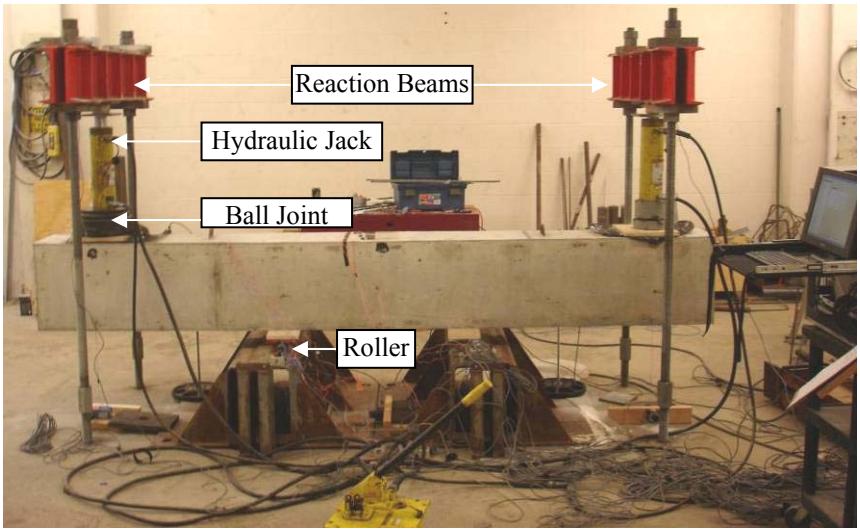

(a) Front view

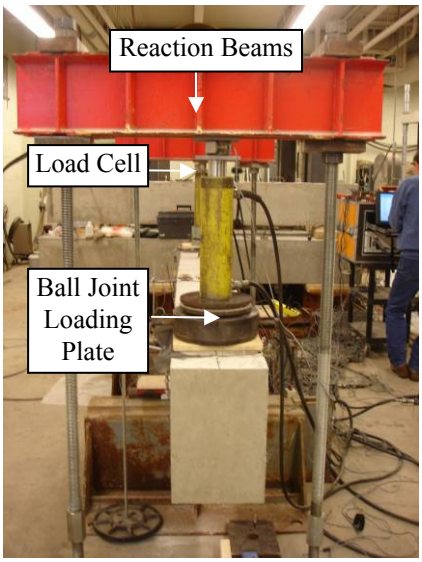

(b) End view and loading device

Figure 5.8 Test setup of a beam specimen.

Each beam specimen was instrumented with two 3-in. strain gauges on the top surface of the specimen to record the extreme fiber concrete tensile strain, as shown in Figure 5.9. In addition, eight strain gages were installed on the spliced rebar within the splice region of each specimen to monitor the strain variation of the coated rebar during testing. These gauges were located at the end of the splice and nine inches away from the end of the splice to provide an average strain reading for the coated rebar. Details of the strain gauge distribution are presented in Figure 5.10.

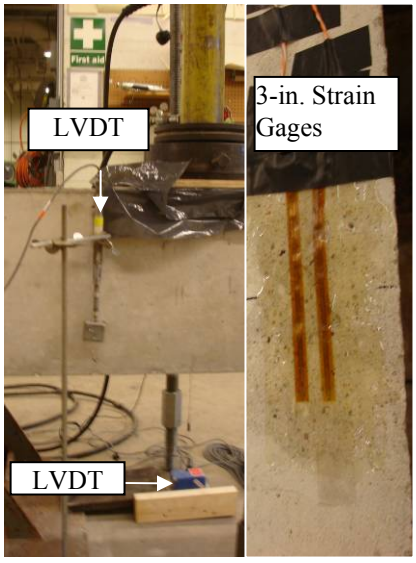

Figure 5.9 Instrumentation with LVDT and concrete strain gauges.

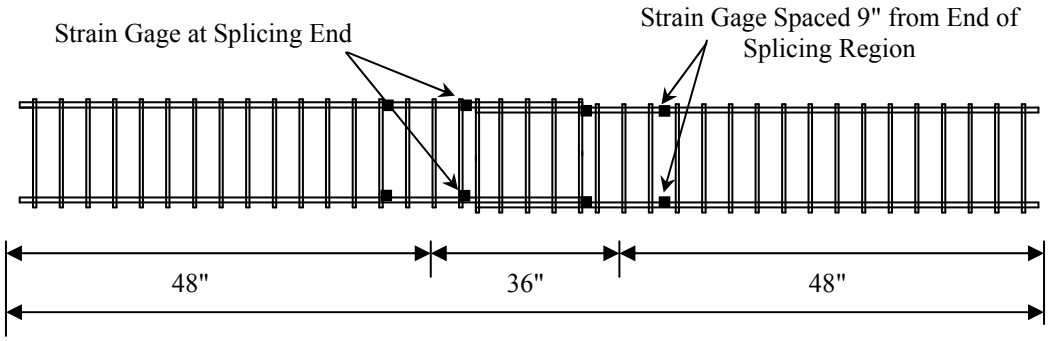

Figure 5.10 Strain gauge distribution around the splice area.

As illustrated in Figure 5.9, four LVDTs were used to monitor the deflections of a specimen during each test. Two LVDTs were located at the ends of the specimens. The other two were placed at each side of the beam at mid-span to obtain an average value of the mid-span deflection. Two 200-kip capacity load cells were mounted on top of the hydraulic jacks to monitor the load applied during the test. An overall view of external sensors is presented in Figure 5.11.

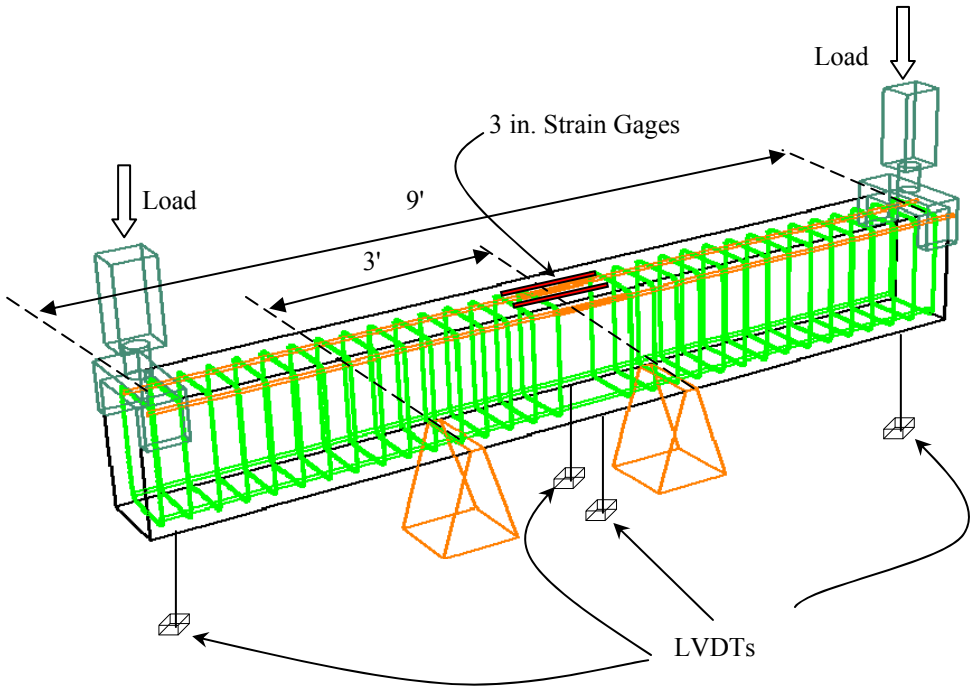

Figure 5.11 Illustration of sensor distribution (excluding embedded sensors).

The two hydraulic jacks were installed in parallel with the hydraulic pump to maintain equal loads at each end of the beam. The average loading rate was kept at 1 kip per minute throughout the test. The specimen was loaded monotonically until it failed either in splitting failure or in flexural failure initiated by yielding of the longitudinal reinforcement.

5.2.2. Results and Discussion

5.2.2.1. Visual observations

Three types of potential failure modes were expected during testing of the beam specimens: pullout of rebar, concrete splitting, and steel yielding in the lap splice area. Pullout failures were not observed throughout the test program. Therefore, the following discussions will be focused on the last two potential failure modes.

Both flexural and splitting failures were observed during the beam tests. For flexural failures, the main cause for load capacity reduction was steel yielding. For splitting failures, the main cause for load capacity reduction was the splitting of concrete along the stressed rebar. It is commonly known that concrete splitting always occurs after the steel reinforcement experiences yielding and a large strain. In several cases of this testing program, however, concrete splitting occurred immediately after yielding of the steel reinforcement but before it went through a large strain. Therefore, steel yielding and concrete splitting together result in a sudden and significant drop in the load capacity of the beams. Detailed discussions on the flexural and splitting failures were given with representative specimens of B-6-2 and B-6-3.

5.2.2.1.1. Flexural Failure of Specimen B-6-2

Specimen B-6-2 failed in flexure, as shown in Figure 5.12(a). As the applied load increased, cracks were initiated in the center span of the beam, subjected to a constant bending moment as shown in Figure 5.12(b). The cracks widened significantly as illustrated in Figure 5.12(c) as the beam approached failure. A typical flexural failure was observed as expected from this specimen. No obvious longitudinal cracks were observed throughout the test. At failure, the maximum crack width observed in the concrete was 0.5 in. when the load capacity of the beam was suddenly reduced as will be discussed later with the use of load-displacement curves. No concrete spalling was observed after the sudden drop in load capacity. After the concrete pieces from the cracked section were removed carefully, the coating of the rebar in the overlapped region remained intact on the steel rebar as illustrated in Figure 5.13.

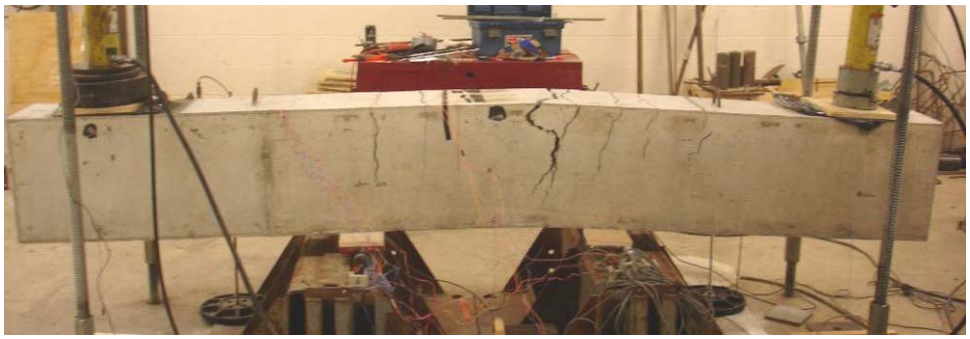

(a) Overview of the failed specimen

(b) Initial cracks

(c) Cracks at failure

Figure 5.12 Flexural failure of Specimen B-6-2.

Figure 5.13 Enamel coating remained on steel rebar.

5.2.2.1.2. Splitting Failure of Specimen B-6-3

Specimen B-6-3 failed in concrete splitting mode. After initial flexural cracks were observed as shown in Figure 5.14(a), longitudinal cracks occurred within the spliced region. As the longitudinal reinforcement approached the yield strain, the longitudinal cracks along the spliced rebar widened rapidly as indicated in Figure 5.14(b). Two minutes after the onset of longitudinal cracks, the specimen failed in sudden splitting as a visible reduction in load capacity was observed from the load-deflection curve displayed. Concrete spalling was observed as expected.

(a) Initiation of longitudinal cracks (b) Widened longitudinal cracks at failure

Figure 5.14 Representative splitting failure of Specimen B-6-3.

At the completion of testing, the spalled concrete chunks were removed from the overlapped region to reveal the details of rebar, concrete, and their interface. As shown in Figure 5.15(a), no evidence of relative slippage between the two spliced reinforcing bars was found in the damaged area. Fine concrete pieces were still attached to the coated rebar in the overlapped region as shown in Figure 5.15(a). A closer examination of the cracked concrete piece removed from the overlapped region indicated no coating material remained on the concrete, as illustrated in Figure 5.15(b). These observations indicated an effective bond formed between the enamel coating and the steel rebar. On the other hand, there was strong evidence of systematic concrete bearing failures where the rebar deformations were supported along the length of the rebar. As indicated in Figure 5.15(b), the remaining deformation tracks in the concrete have signs of bearing failures along the two opposite directions associated with potential slippage between the two lap-spliced bars. In addition, the concrete between the two reinforcing bars appeared to have been sheared off in the longitudinal direction. These findings indicated a strong adhesion between the enamel coating and concrete.

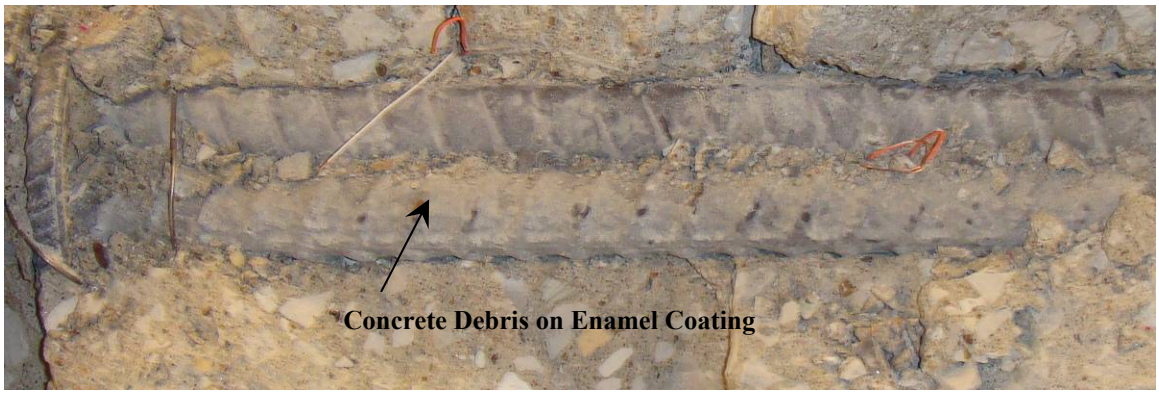

(a) Exposed enamel-coated rebar

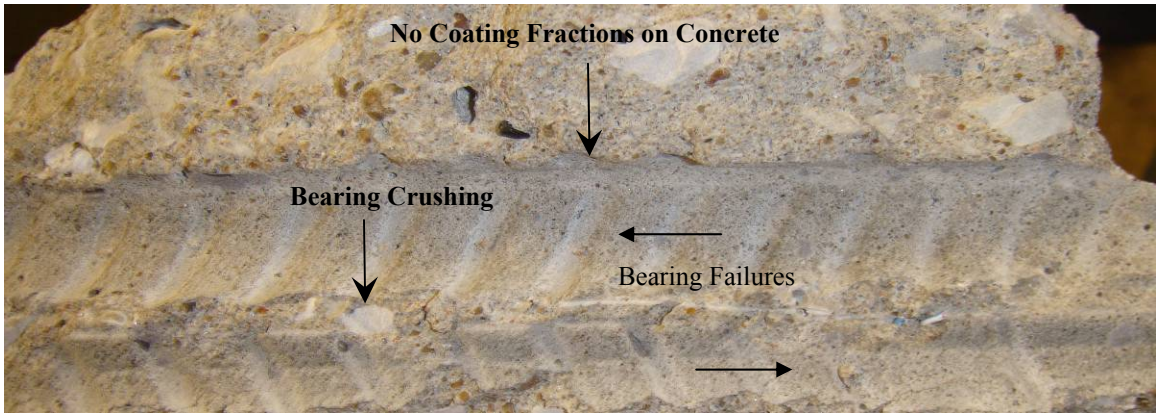

(b) Removed piece of cracked concrete

Figure 5.15 Forensic investigation of the failed specimen in splitting.

5.2.2.1.3. Overview of Failure Modes of All Specimens

Failures of all the tested beam specimens are illustrated in Figure 5.16. In general, a flexural failure indicated the effective bond between coated rebar and concrete, and the sufficient length of lap splices so that steel yield strength can be achieved at failure. The split failure indicated that either the bond between the coated rebar and concrete was insufficient to transfer the load from the rebar to its surrounding concrete or the lap splice was too short to transfer the tension force from one rebar to another rebar, locally resulting in high stress and breaking of the concrete.

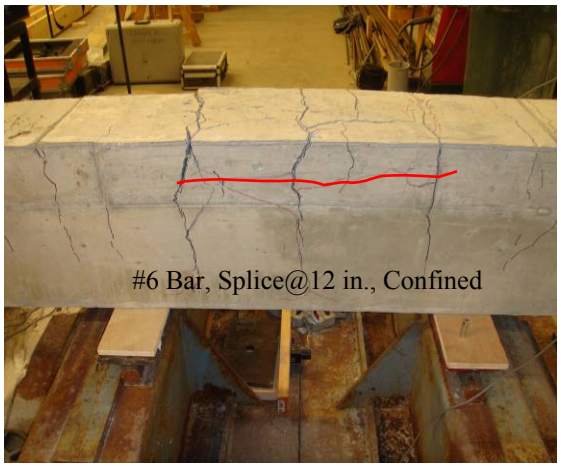

(a) Split failure of B-6-1 with steel yielding

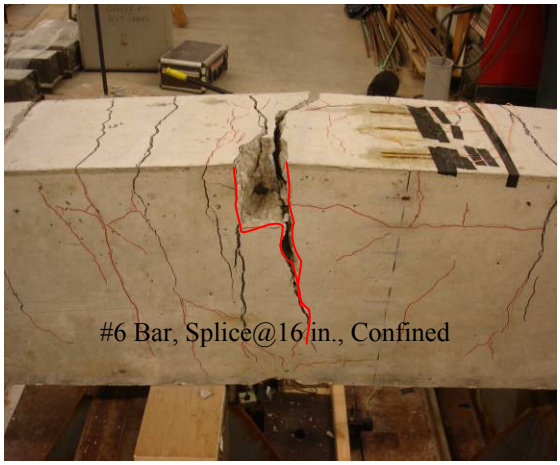

(b) Flexural failure of B-6-2

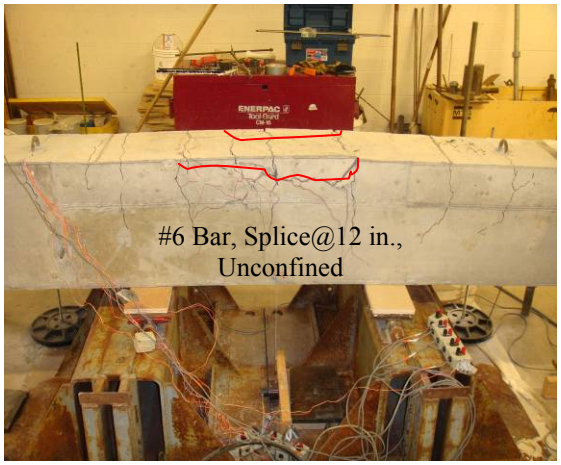

(c) Split failure of B-6-3 with steel yielding

(d) Split failure of B-6-4

(e) Split failure of B-8-1 with steel yielding

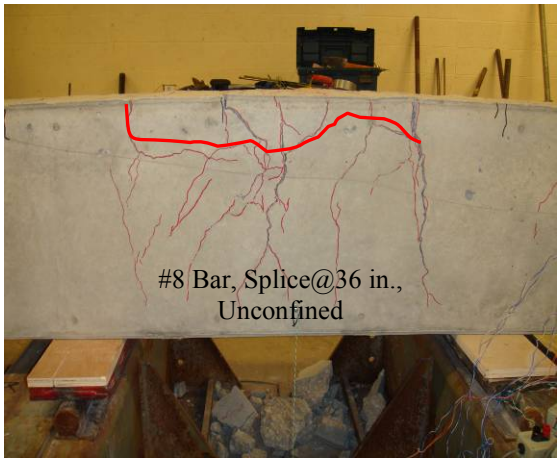

(f) Split failure of B-8-2 with steel yielding

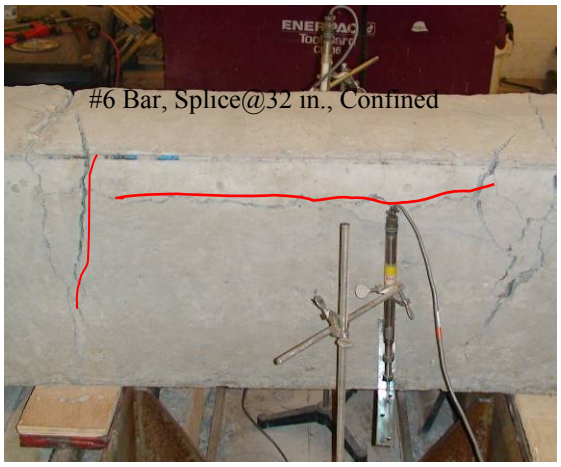

(g) Flexural failure of B-6-5 followed by splitting

(h) Flexural failure of B-6-6

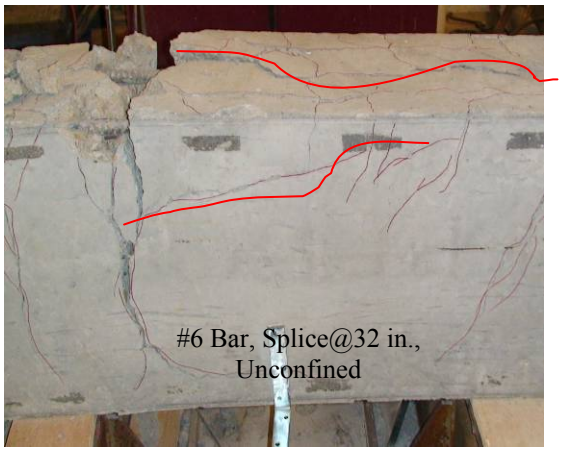

(i) Flexural failure of B-6-7 followed by splitting

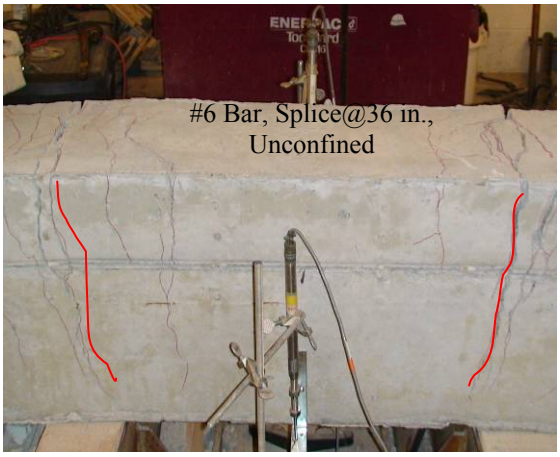

(j) Flexural failure of B-6-8

(k) Flexural failure of B-8-3

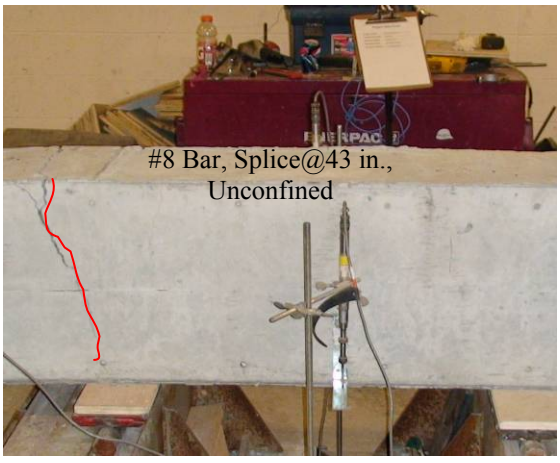

(l) Flexural failure of B-8-4

Figure 5.16 Failure modes of various tested beams.

5.2.2.2. Data analysis and discussions

The applied load is plotted in Figure 5.17 as a function of mid-span deflection with respect to the two ends of each of the 12 tested beams. It is also plotted as a function of the average strain of the two coated bars at the end of overlapped splices in Figure 5.18. Based on the load-deflection and load-strain curves, the condition under which a sudden reduction in load capacity and its corresponding failure mode can be identified as given in Figure 5.16.

(a) Specimen B-6-1

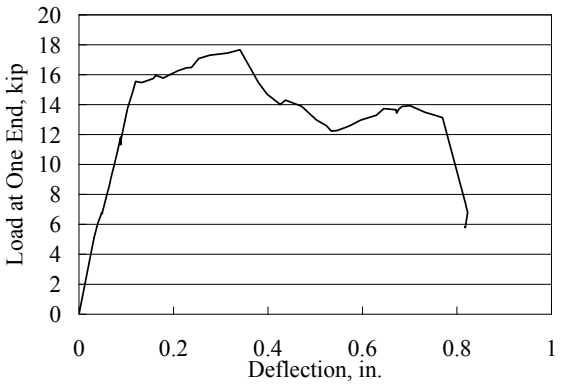

(b) Specimen B-6-2

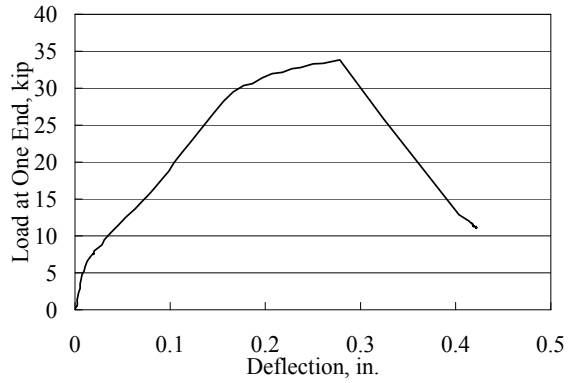

(c) Specimen B-6-3

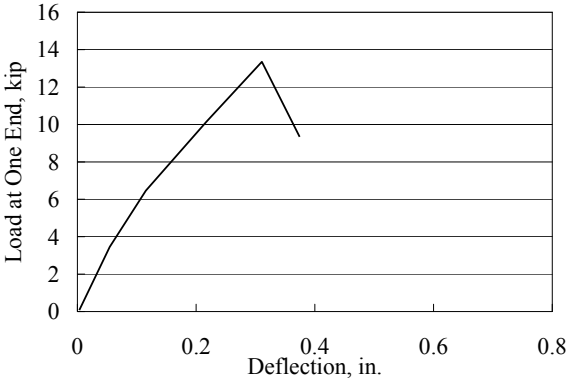

(d) Specimen B-6-4

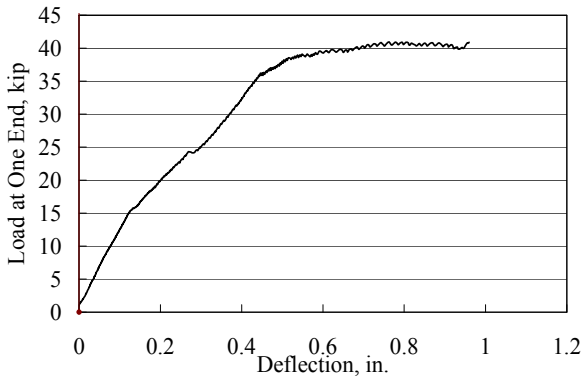

(e) Specimen B-6-5

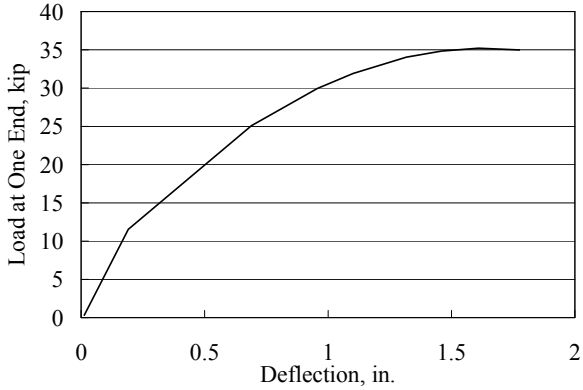

(f) Specimen B-6-6

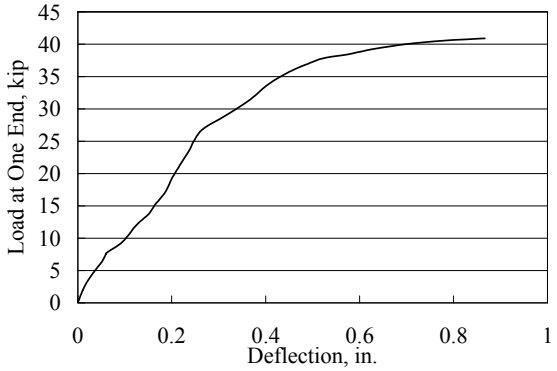

(g) Specimen B-6-7

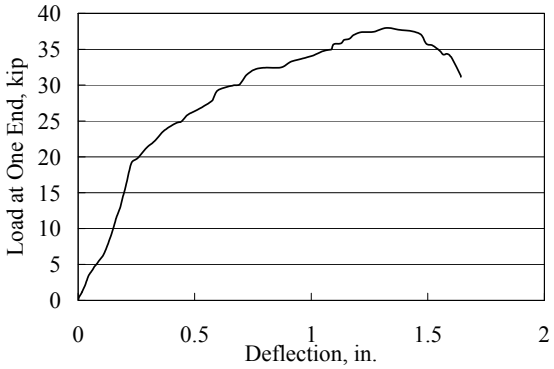

(h) Specimen B-6-8

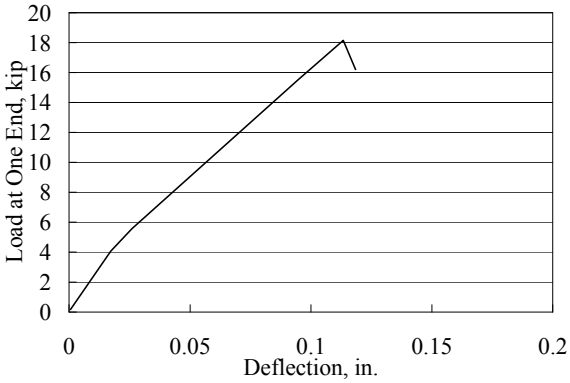

(i) Specimen B-8-1

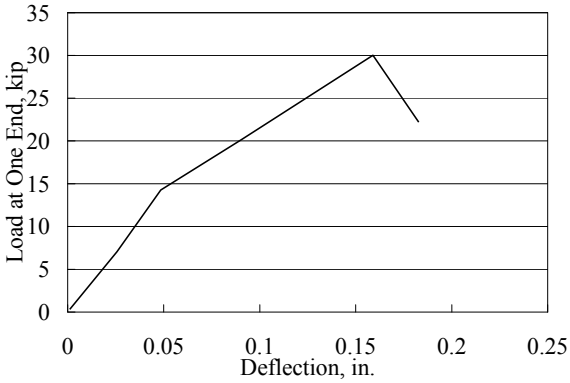

(j) Specimen B-8-2

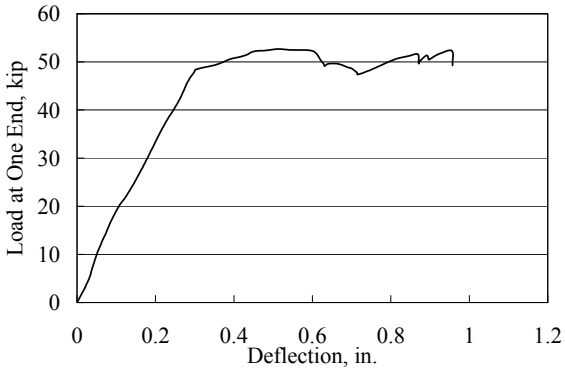

(k) Specimen B-8-3

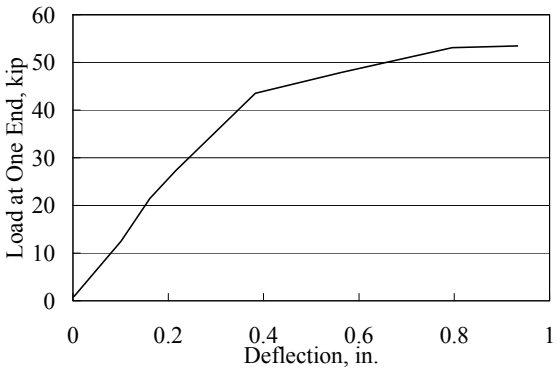

(b) Specimen B-8-4

Figure 5.17 Load-deflection curves of 12 tested beams.

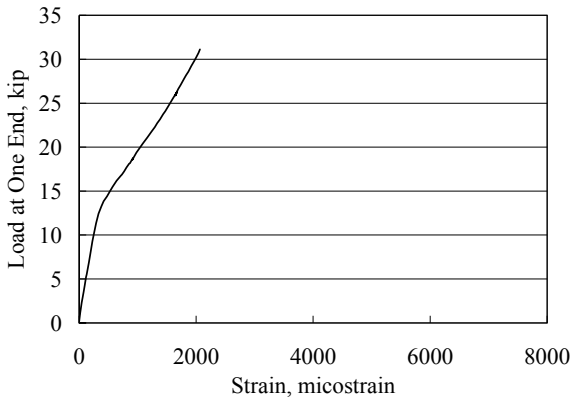

(a) Specimen B-6-1

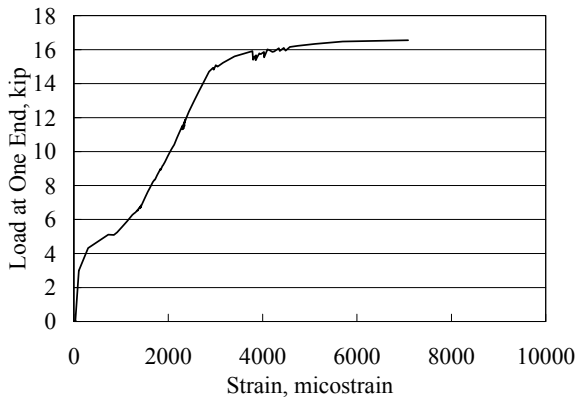

(b) Specimen B-6-2

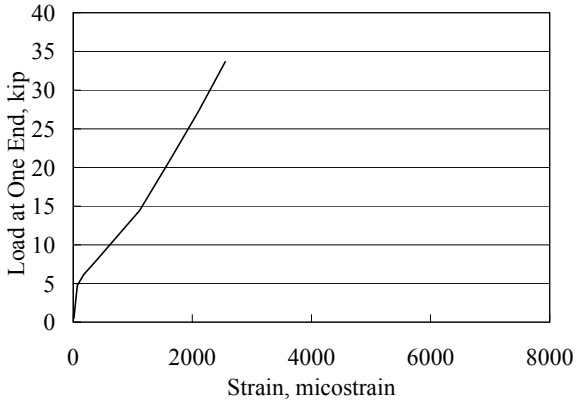

(c) Specimen B-6-3

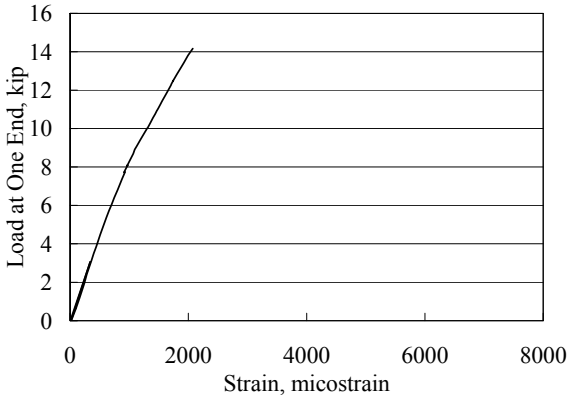

(d) Specimen B-6-4

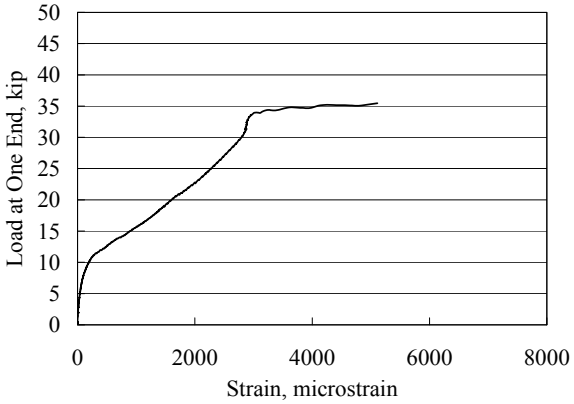

(e) Specimen B-6-5

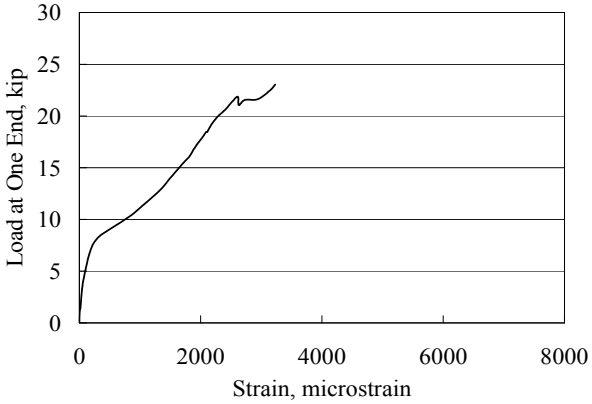

(f) Specimen B-6-6

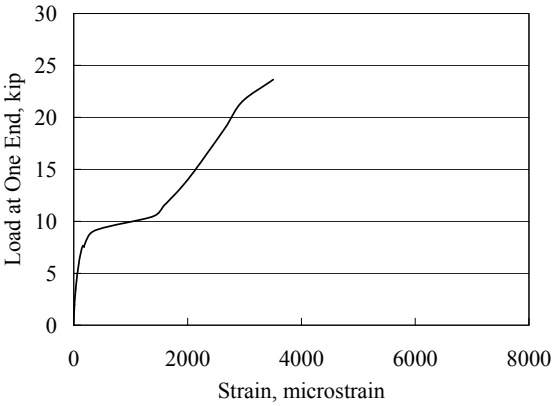

(g) Specimen B-6-7

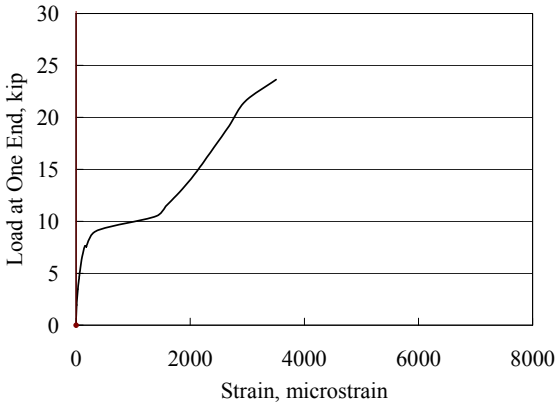

(h) Specimen B-6-8

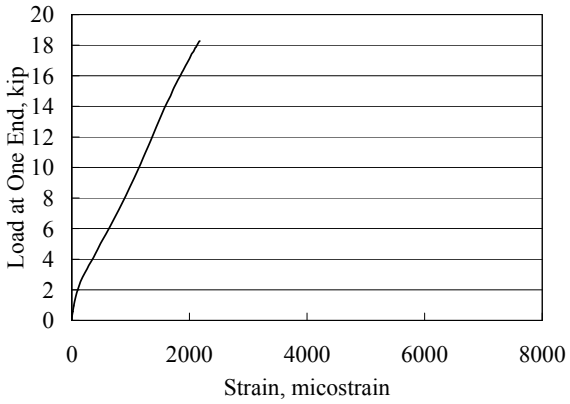

(i) Specimen B-8-1

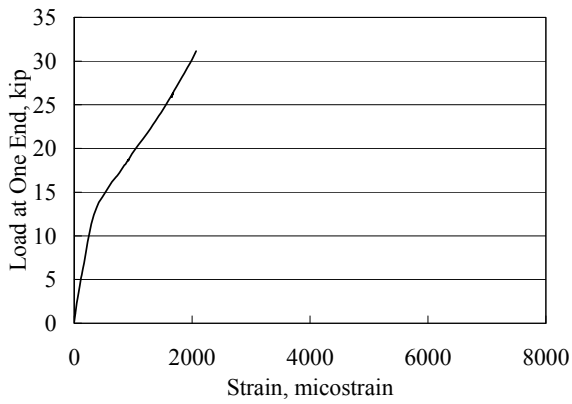

(j) Specimen B-8-2

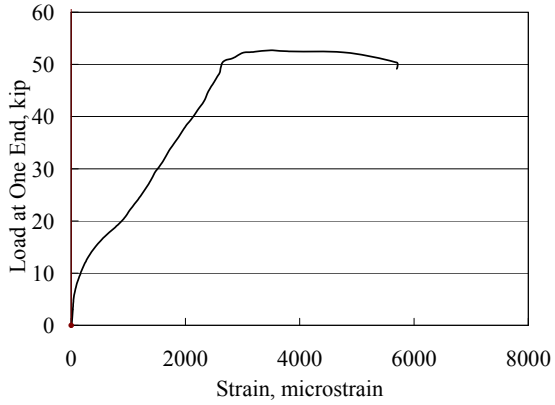

(i) Specimen B-8-3

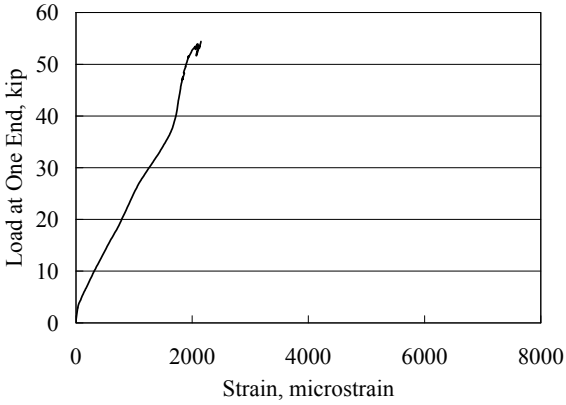

(j) Specimen B-8-4

Figure 5.18 Load-strain curves of 12 beam specimens.

The failure modes and the experimental average stresses of coated rebar for all beam specimens are presented in Table 5.5. The stresses of uncoated black rebar determined according to the ACI 318-08 development length equation are also included in Table 5.5, corresponding to various development lengths used in this study. The detail of their calculations is given below.

Table 5.5 Summary of test results

Specimens	Failure Mode	Experimental Average Stress in Coated Rebar (ksi)	ACI 318-08 Stress for Uncoated Rebar (ksi)	Relative Index
B-6-1*	Split with yielding	60	34.4	0.57
B-6-2*	Flexure	60	45.87	0.76
B-6-3	Split with yielding	60	22.93	0.38
B-6-4	Split	60**	30.58	0.51
B-6-5*	Flexure followed by splitting	60	60 (91.74)	1
B-6-6*	Flexure	60	60 (103.2)	1
B-6-7	Flexure followed by splitting	60	60 (61.16)	1
B-6-8	Flexure	60	60 (68.8)	1
B-8-1*	Split with yielding	60	60 (61.92)	1
B-8-2	Split with yielding	60	37.15	0.62
B-8-3*	Flexure	60	60 (73.96)	1
B-8-4	Flexure	60	44.38	0.74

* with confinement, ** minimum stress at failure due to damage of strain gauges in the spliced region. The number in parenthesis represents the stress directly calculated by Eq. (5.3) for linear material.

Corresponding to the splice length of a reinforcing steel bar, l_d, Eq. (5.1) can be rearranged to estimate the stress that would be developed in the steel bar if the steel were elastic and the steel-concrete were perfectly bonded. That is,

$$f_s = \frac{l_d}{d_b}\left[\frac{40\sqrt{f_c'}}{3(1.3)\Psi_e\Psi_s}\frac{c_b + K_{tr}}{d_b}\right] \tag{5.3}$$

in which the traditional rebar location factor ψ_t in Eq. (5.1) was replaced by 1.3 as more than 12 in. of fresh concrete was cast below the rebar. Considering a coating factor of ψ_e=1.0, the stress of an uncoated bar corresponding to the development lengths used in this test program can be estimated by Eq. (5.3) and listed in Column 4 of Table 5.5. The tested average stresses of coated rebar for all tested specimens are listed in Column 3 of Table 5.5. A relative index was defined as the ratio between the determined stress of an uncoated bar and the average stress of a coated bar. The calculated index values are recorded in Column 5 of Table 5.5.

Table 5.5 indicates that the experimental average stress of coated rebar in the spliced region reached the yield strength of steel based on strain measurements. On the other hand, some of the stresses of uncoated rebar, corresponding to various development lengths used in this study, are less than the yield strength of steel. In these cases, the relative index shown in Table 5.5 is less than 1.0 or, with equal development lengths, a coated reinforcing bar can be subjected to higher stress than an uncoated bar. This result reflected the increase in bond strength between the coated rebar and concrete.

For beam specimens reinforced with #6 enamel-coated steel bars, the relative index is plotted as a function of splice length in Figure 5.19(a) when lateral stirrups are used to restrain the longitudinal rebar in the spliced region and in Figure 5.19(b) when no lateral stirrup is provided in the spliced region. The minimum splice lengths required for a #6 uncoated bar in 4.5 ksi concrete, 22 in. with confinement and 31 in. without confinement, are also included in Figure 5.19(a) and Figure 5.19(b), respectively. The value, 1.0-relative index, represented by the shaded

areas in Figure 5.19 means the increased development stress due to enamel coating. Therefore, the increased development stresses in unconfined cases is approximately 50% higher than that in confined cases, indicating a more significant increase in bond strength when no transverse reinforcement was provided.

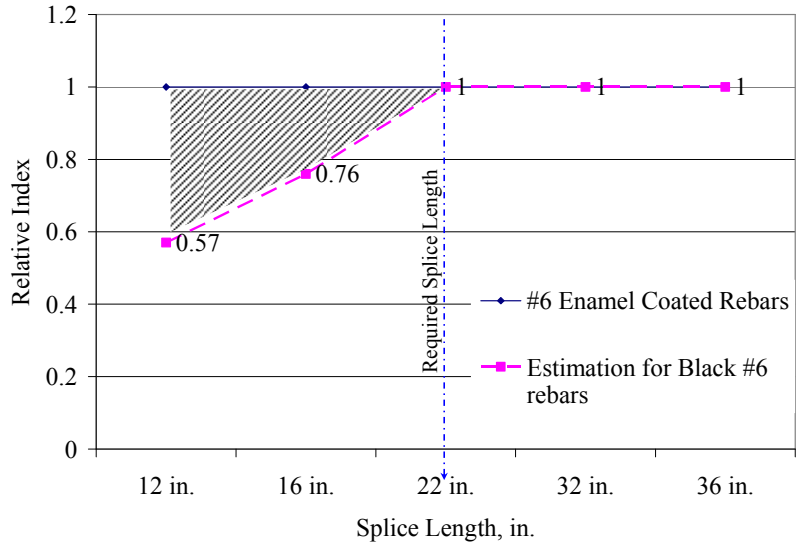

(a) With confinement

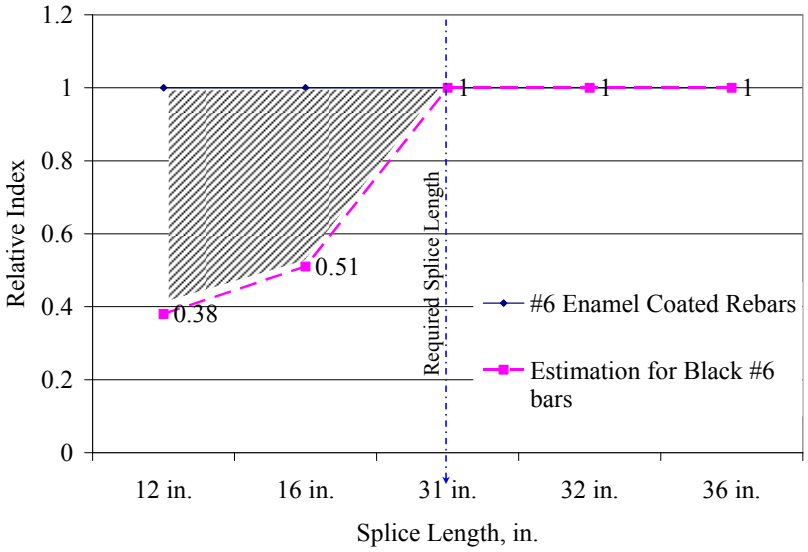

(b) Without confinement

Figure 5.19 Relative index variations with splice length for #6 rebar.

Similarly, the relative index is plotted in Figure 5.20 as a function of splice length for specimens with #8 steel reinforcing bars. In this case, the minimum development lengths required are 35 in. for confined rebar and 58 in. for unconfined rebar. They are also shown in Figure 5.20(a) and Figure 5.20(b), respectively. It is clearly observed that Specimens B-8-1 and B-8-2 with lateral confinement have sufficient splice lengths with uncoated/black steel reinforcement. When the

longitudinal rebar in the spliced region was not restrained with lateral stirrups, however, the minimum development length of uncoated rebar in 4.5 ksi concrete becomes significantly longer (from 35 in. to 58 in.), which makes Specimens B-8-3 and B-8-4 insufficient in splice length unless their steel reinforcing bars are coated with reactive enamels.

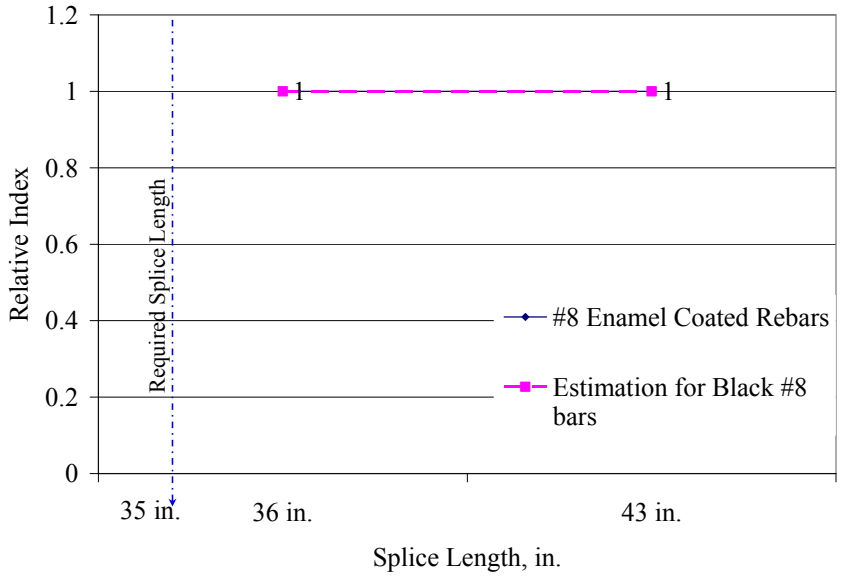

(a) With confinement

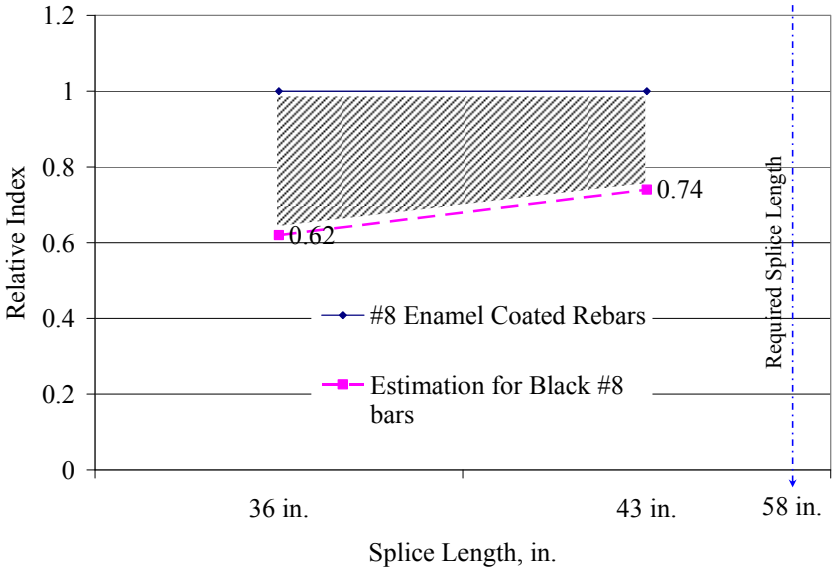

(b) Without confinement

Figure 5.20 Relative index variations with splice length for #8 rebar.

To reflect the increase in bond strength for coated rebar, a new coating factor is introduced and used in Eq. (5.1). Since the development stress f_s in Eq. (5.3) is proportional to $1/\Psi_e$ (coating factor), a new coating factor equal to the relative index is introduced in order to increase the

relative index from what is given in Table 5.5 for uncoated/black rebar to a value close to 1.0 for coated rebar.

A relative index of 1.0 in Table 5.5 will not be changed with the use of a new coating factor (<1.0) since the development stress is mechanically limited by the yield strength of steel. As such, the new coating factor can be chosen from the relative indices less than 1.0 in Table 5.5. The mean and the standard deviation of the relative index population (0.57, 0.76, 0.38, 0.51, 0.62, and 0.74 in Table 5.5) are approximately 0.60 and 0.13. The mean plus two standard deviations equals to 0.86. In this study, a coating factor of 0.85 is proposed for the determination of lap splice length in design.

The calculated design stresses using the new coating factor were compared in Figure 5.21 with the measured stresses and the values estimated with a coating factor of 1.0 for uncoated rebar. In Figure 5.21, the shaded area shows the difference between the calculated stress using the proposed coating factor and the actual testing values. The proposed factor of 0.85 is very conservative against the test data. The dotted area represents the corrected portion from the previous calculations using a coating factor of 1.0 for uncoated/black rebar.

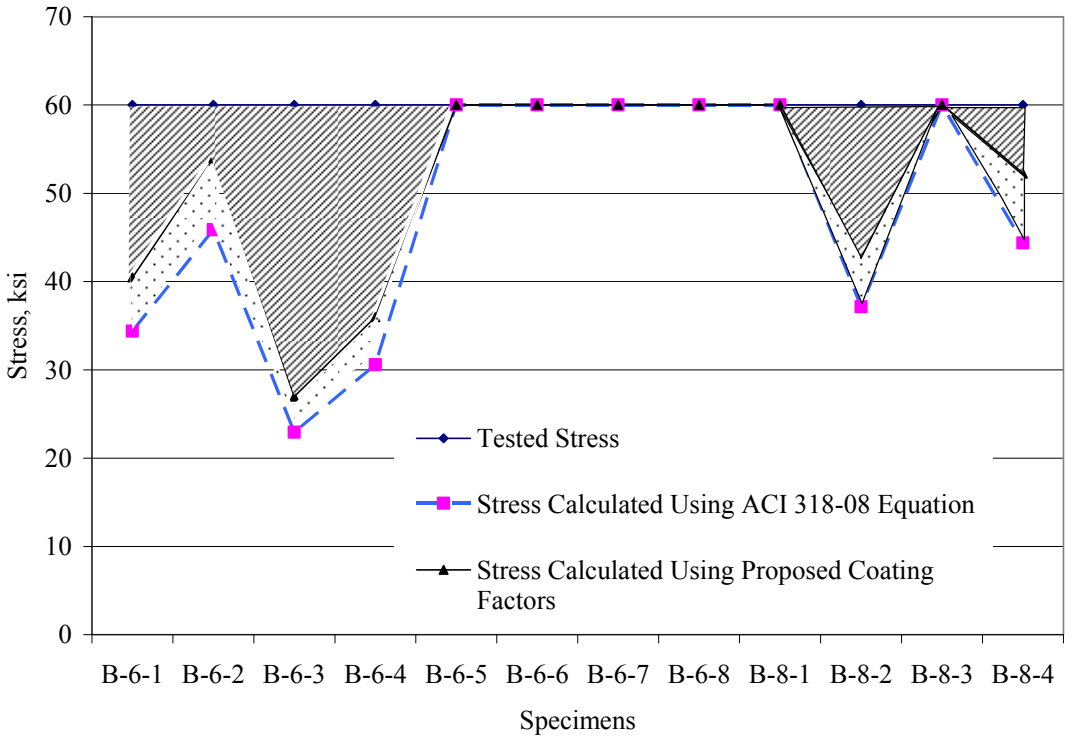

Figure 5.21 Stress comparisons among measured, calculated for black rebar, and calculated for enamel-coated rebar with the new coating factor.

5.2.3. Conclusions Based on Beam Tests

In comparison with the calculated stress in spliced rebar from the ACI 318-08 Equation, it is evident that the bond strength increased when the longitudinal reinforcing bars in a spliced

region were coated with enamel. The increment of bond strength in lap splices is approximately 50% larger when the longitudinal cracks are not restrained by transverse stirrups. For simplicity, one coating factor of 0.85 is recommended for both unconfined and confined cases. If a less conservative coating factor is desired, additional tests on beam specimens particularly with uncoated steel reinforcement must be performed.

5.3. Short Column Tests

This section deals with the understanding of anchorage behavior at beam-column or column-footing connections and quantifies the required anchor length of enamel-coated rebar in practical designs. These goals are achieved through testing of a series of short columns with embedded dowel bars simulating the beam action on the columns.

5.3.1. Technical Approach

The short column test program included 16 concrete column specimens in four groups based on their concrete strength and rebar size. As shown in Table 5.6, each group has four specimens: one control specimen reinforced with uncoated/black rebar and three coated with the 50/50 reactive enamel. The control specimen has the minimum development length as stipulated in ACI 318-08. The development lengths of the other three specimens with enamel-coated reinforcement were selected to be 60%, 80%, and 100% of the minimum development length for uncoated rebar in order to quantify the coating effect on anchor lengths.

Table 5.6 Test matrix for short columns

Specimen	Group	Coated	Rebar Size	Standard Hook Length (in.)	Column Cross Section (in.)	Development Length (in.)	Compressive Strength (psi)
C-6-1	I	No	#6	9	17.25×18	14.75	4000
C-6-2		Yes	#6	9	11.25×18	8.75	4000
C-6-3		Yes	#6	9	14.25×18	11.75	4000
C-6-4		Yes	#6	9	17.25×18	14.75	4000
C-6-5	II	No	#6	9	14.25×18	11.75	6000
C-6-6		Yes	#6	9	9.5×18	7.0	6000
C-6-7		Yes	#6	9	12×18	9.5	6000
C-6-8		Yes	#6	9	14.25×18	11.75	6000
C-8-1	III	No	#8	12	22×18	19.5	4000
C-8-2		Yes	#8	12	14×18	11.5	4000
C-8-3		Yes	#8	12	18×18	15.5	4000
C-8-4		Yes	#8	12	22×18	19.5	4000
C-8-5	IV	No	#8	12	18×18	15.5	6000
C-8-6		Yes	#8	12	12×18	9.5	6000
C-8-7		Yes	#8	12	15×18	12.5	6000
C-8-8		Yes	#8	12	18×18	15.5	6000

The basic development length specified in ACI 318-08 or the 2007 AASHTO LRFD Bridge Design Specifications can be determined by

$$l_{hb} = \frac{38.0 d_b}{\sqrt{f_c'}} \tag{5.4}$$

where l_{hb} is the required development length, d_b is the rebar diameter, and f_c' is the compressive strength of concrete. Figure 5.22(a) shows an isometric view of a short column specimen with a height of 60 in. and a width of 18 in. Each specimen is reinforced with two #6 or #8 rebar with standard 90° hooks to simulate a typical beam-column connection. The dimensions and reinforcement details are presented in Figure 5.22(b, c).

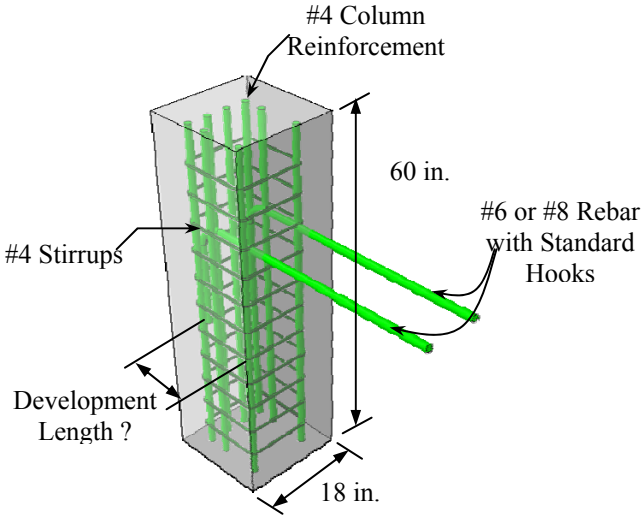

(a) Isotropic view

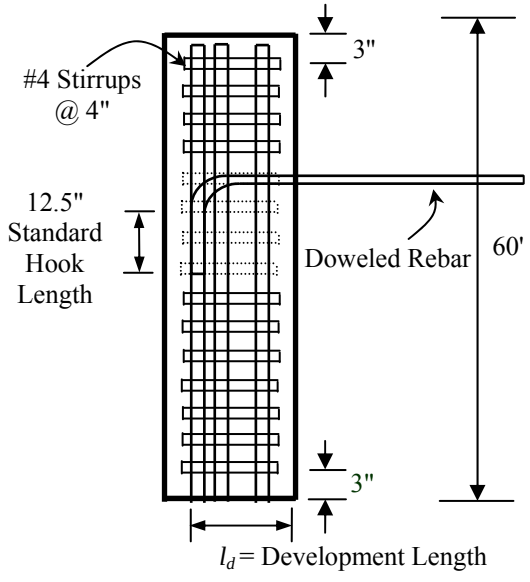

(b) Side view

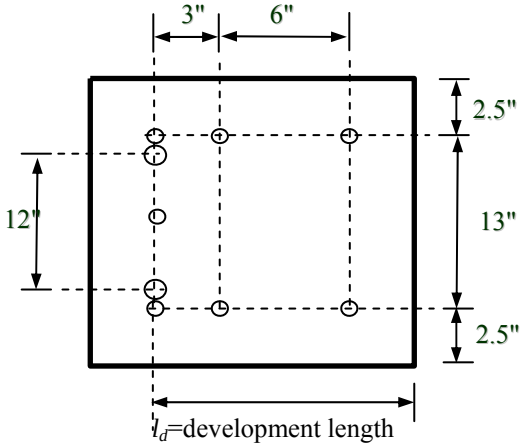

(c) Cross sectional view

Figure 5.22 Isotropic view of a column specimen.

Vertical reinforcement with #4 rebar was provided in all column specimens to withstand the moment created by pulling the dowel bars out of columns. No. 4 stirrups were provided to prevent potential shear failures.

5.3.1.1. Short column specimens and material properties

5.3.1.1.1. Construction of Short Column Specimens

To facilitate the construction of reinforcement cages, wood frames were built to fix the vertical reinforcing bars of columns through holes drilled on the top and bottom laminate sheets as shown in Figure 5.23. The short column specimens were cast twice for different concrete strength requirements.

(a) Wood frame (b) Steel formwork and concrete casting

Figure 5.23 Fabrication of column specimens.

5.3.1.1.2. Material Properties

The dowel rebar used in the column specimens was bent from straight rebar in the laboratory. Tension tests of coated and uncoated rebar were conducted on sample dowel bars similar to those for beam specimens in Section 5.2.1.1. The mechanical properties of both uncoated and coated rebar are listed in Table 5.7. The properties of coated rebar are close to those in Table 5.4 from previous tests, indicating no effect from the heat treatment process during coating of the rebar.

Table 5.7 Mechanical properties of dowel bars

Properties	#6 Coated Rebar	#8 Coated Rebar	#6 Uncoated Rebar	#8 Uncoated Rebar
Modulus of Elasticity, ksi	31,763	31,763	31,425	30,987
Yield Stress, ksi	60.6	59.4	62.5	60.2
Ultimate Stress, ksi	95.5	90.3	94	90.1

The concrete design mix used for the splice specimens was 4 ksi concrete. To achieve 6 ksi concrete, a different concrete mix was applied to meet design requirements as given in Table 5.8. Cylinder tests were performed to evaluate the mechanical properties of concrete as listed in Table 5.9.

Table 5.8 Concrete mix proportions (Rolla Ready Mix, Inc.)

Material	Quantity (lb/yd^3)
Cement	780
Fine Aggregate	1410
Coarse Aggregate	1945
Water	110
Air Entrainment	0.5
High-Range Water Reducer	5

Table 5.9 Mechanical properties of concrete used in short column specimens

Day	Group	Compressive Strength (psi)	Average Strength (psi)	Modulus of Elasticity (ksi)
7	I & III	3,900	3,730	N/A
		3,500		
		3,800		
	II & IV	4,132	4,120	
		4,008		
		4,217		
21	I & III	4,381	4,150	N/A
		3,916		
		4,152		
	II & IV	5,012	5,120	
		5,203		
		5,145		
28	I & III	4,462	4,370	3,770
		4,210		
		4,423		
	II & IV	5,675	6,020	4,420
		6,102		
		6,278		

5.3.1.2. Test setup, instrumentation, and loading protocol

The test setup for short column specimens is shown in Figure 5.24. A reaction frame containing two steel columns with footings and two C-channels was erected for the column test. Against the C-channels was a hydraulic jack that, together with a load beam, applied an upward load to the two dowel bars of a column specimen. To induce two tension forces on the column specimen through the dowel bars, the other end of the column must be fixed. For this purpose, two support beams were anchored down to the strong floor with two Dywidag bars each. On the top of the

support beams were placed two steel bearing tubes spanning over and holding down the column specimen.

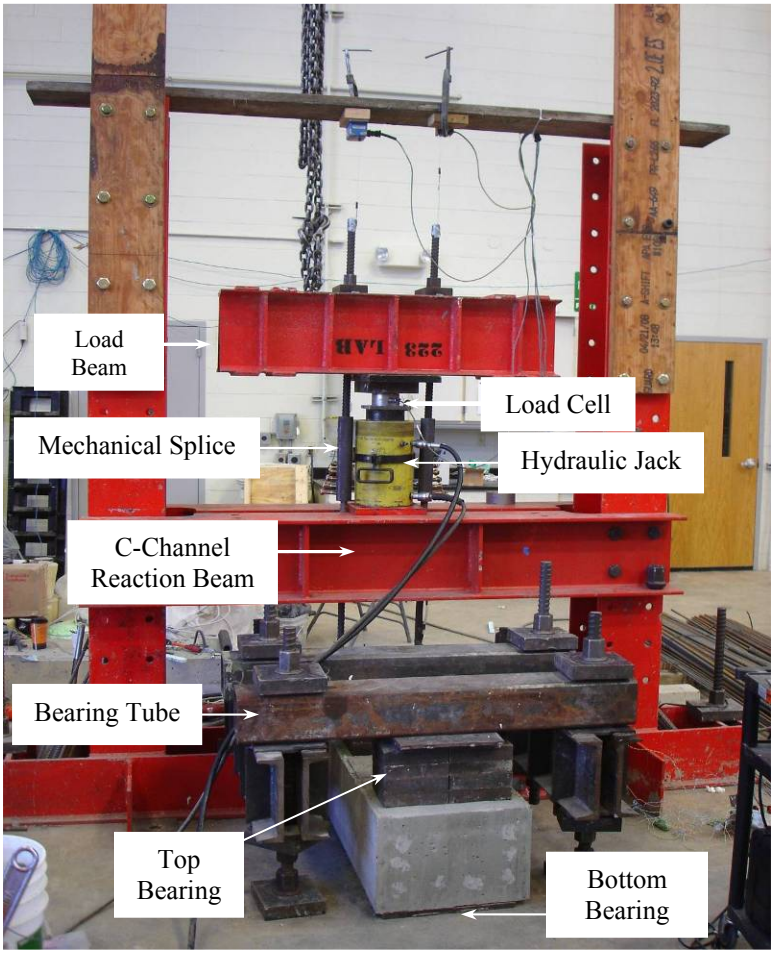

Figure 5.24 Test setup of a short column specimen.

The bearing tube farthest from the two dowel bars provided a pre-compressed force on the concrete column through several steel plates by prestressing the two Dywidag bars to 1 kip each. In this setup, neither rotation nor slip was allowed to occur at the column end. The bearing tube near the dowel bars also provided a pre-compressed force on the column by jacking the two Dywidag bars to 1 kip each. Moreover, it added a distributed compressive force on the column as the dowel bars were being pulled out of the concrete. The dowel bars and the nearby bearing tube together simulated the action of a reinforced concrete beam that connected to the column specimen in practical applications.

The hydraulic jack has a capacity of 200 kips powered by a manual pump. To facilitate the test setup, the two dowel bars were extended by two Dywidag bars with mechanic splices. Therefore, as the hydraulic jack was powered, tensile forces were applied on the dowel bars. Each specimen was loaded monotonically to failure at a constant loading rate of 5 kips per minute.

The displacements at the ends of both dowel bars were measured with two linear motion transducers. The rebar slips against concrete were measured on the top surface of the column near the dowel bars with two LVDTs. The third LVDT was placed on the floor to measure the tilt of the column at the location of the dowel bars. Three strain gages were installed at the middle of the stirrups on one side of the tested specimen, as seen in Figure 5.25. Another three strain gages were installed on one of the two dowel bars in each specimen at locations as illustrated in Figure 5.26.

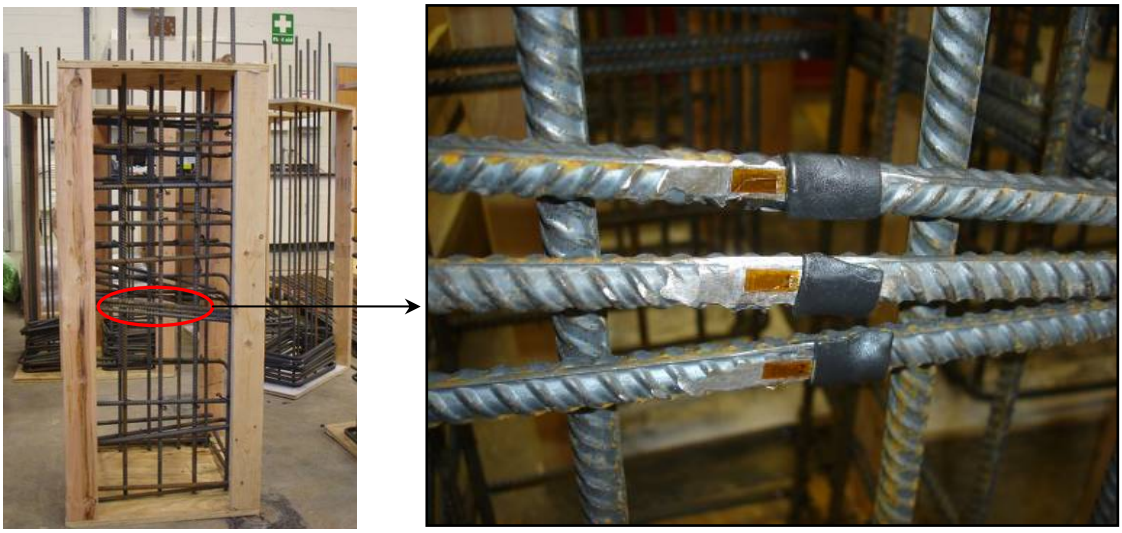

(a) Location of instrumented bars (b) Location of strain gauges

Figure 5.25 Strain gauges on stirrups.

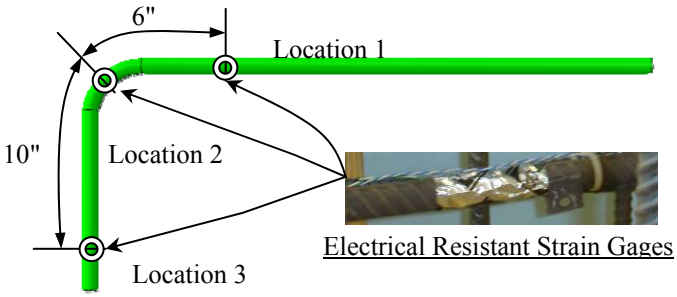

Figure 5.26 Strain gauges on dowel bar.

In addition to strain gages, three fiber Bragg grating (FBG) sensors were installed on the other dowel bar to capture the stain variation at the same locations as the strain gages but on a different dowel bar. The installation of optical fiber sensors was done on eight specimens. The benefit of using optical fiber sensors was less reduction in the bonding area, which can be critical to the understanding of actual anchor behaviors. To properly install FBG sensors, a groove was cut along the rib of a dowel bar as shown in Figure 5.27. Since an uncoated optical fiber has a

diameter of 125 μm, it can be easily embedded into a groove of 1/8 in. deep with epoxy as illustrated in Figure 5.28. The epoxy also protected the FBG sensors from moisture and impact effects.

(a) Groove cutting (b) Finished grooves on dowel bars

Figure 5.27 Preparation for optical fiber sensors.

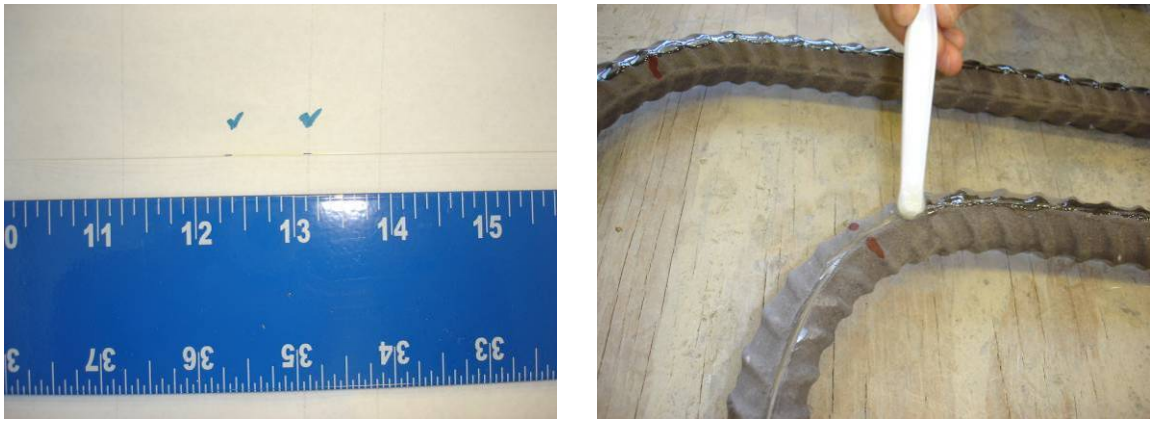

(a) FBG sensors and measurement points (b) Installation of FBG sensors

Figure 5.28 FBG sensors embedded into dowel bars.

5.3.2. Results and Discussion

After 28 days of curing, each short column was subjected to external forces as shown in Figure 5.29. The first compression force farthest from the dowel bars in tension is mainly provided by pretension of the anchored rods. As the tension force increases, the second compression force next to the dowel bars increases. Together, the tension and the second compression forces apply a moment and bend the short column to simulate the beam action at a beam-column joint in practical applications.

All of the tested specimens failed in rebar yielding, including those with enamel-coated rebar whose development lengths were 40% shorter than the required length by ACI318-08. During testing of all specimens, no concrete spalling was observed but cracks around the dowel bars were commonly seen on the tested specimens. The details of the failed specimens are illustrated here with crack patterns observed during the tests.

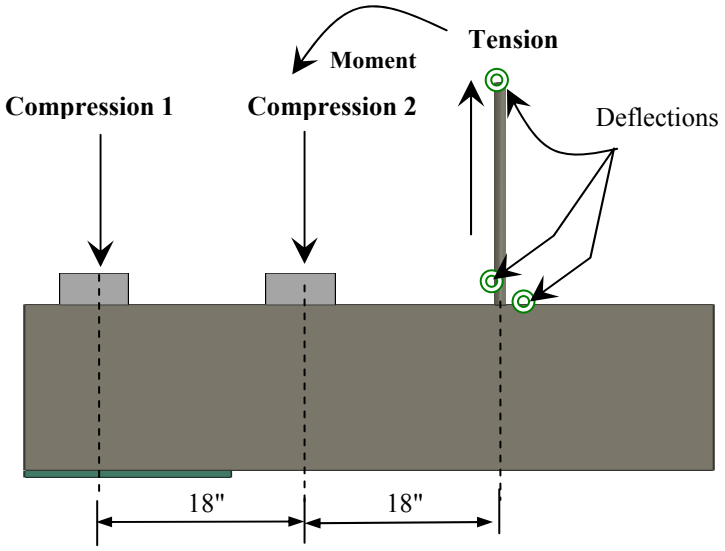

Figure 5.29 Forces applied on a column specimen (strong floor reaction not shown).

The following section is focused on visual observations, load-slip curves, and strain measurements. The overview of the test results is given by a summary of the load-slip curves of all tested specimens and the slip corresponding to steel yielding. Visual observations and strain measurements are illustrated in detail. The tested specimens in Groups I and IV represent the two extreme cases with the lowest and highest loading capacities of concrete and rebar.

5.3.2.1. Overall behavior of short column specimens

Figure 5.30 presents the load-slip curves of all the tested short columns as described in Table 5.6 except Specimen C-8-2 that was tested with a different setup and thus not included in the following discussions. Overall, all load-slip curves have similar trends. The load-slip curves of the two deepest columns in each group with coated and uncoated rebar provide envelopes for the remaining shallower columns. For #6 rebar, the deepest columns have higher slopes on the load-slip curves than the shallower columns in the same group. On the other hand, the deepest columns with #8 rebar have the slopes of the load-slip curves similar to those of other shallower specimens in the same group. However, the ultimate loads of all specimens in each group are similar, corresponding to the yield strength of rebar used in various tested specimens. The exception to this is the results from Specimen C-6-1 with uncoated #6 rebar due likely to its unexpected high material strength. Table 5.10 summarizes the slips at initial yielding of dowel bars in all specimens. The slips range from 0.04 to 0.12 in.

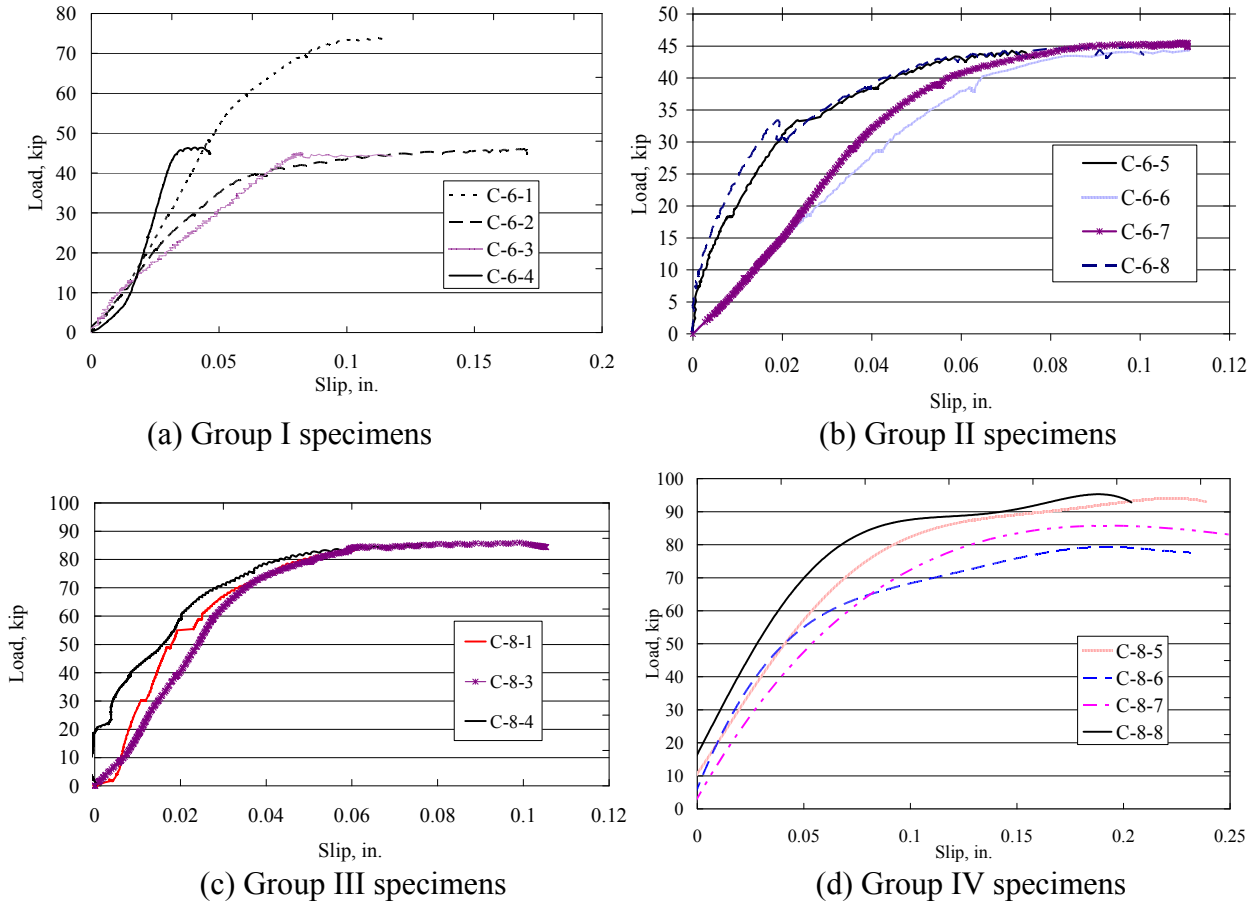

(a) Group I specimens

(b) Group II specimens

(c) Group III specimens

(d) Group IV specimens

Figure 5.30 Load-slip curves of all tested specimens.

Table 5.10 Summary of rebar slips at initial yielding

Specimen	Slip at Initial Yielding of Rebar (in.)
C-6-1	0.10
C-6-2	0.12
C-6-3	0.08
C-6-4	0.04
C-6-5	0.06
C-6-6	0.08
C-6-7	0.09
C-6-8	0.06
C-8-1	0.06
C-8-2	0.02 (not used in this study)
C-8-3	0.06
C-8-4	0.05
C-8-5	0.12
C-8-6	0.16
C-8-7	0.13
C-8-8	0.11

5.3.2.2. Group I specimens

Group I consisted of four reinforced concrete (RC) column specimens with two #6 Grade 60 dowel bars embedded in each column. The 28-day concrete compressive strength for Group I was 4.37 ksi. The top views of the failed specimens are shown in Figure 5.31. Cracks near the two dowel bars of each specimen were initiated from their side covers and propagated toward each other across the top surface. A cross-over crack was finally formed on the top surface as seen in Figure 5.31. The exception to this observation was the crack pattern on the top surface of Specimen C-6-4. As can be clearly observed in Figure 5.31(d), the two cracks initiated around the dowel bars of Specimen C-6-4 were not connected together though the development length of these dowel bars is equal to that of dowel bars in Specimen C-6-1. The only difference between the two specimens is the presence of enamel coating in Specimen C-6-4. This comparison indicates a better bond performance of dowel bars in concrete when coated with reactive enamel. As a result, the coated dowel bars engaged more concrete as they were pulled out of the concrete column, leading to less stress concentrations in the concrete around the dowel bars.

(a) Specimen C-6-1

(b) Specimen C-6-2

(c) Specimen C-6-3

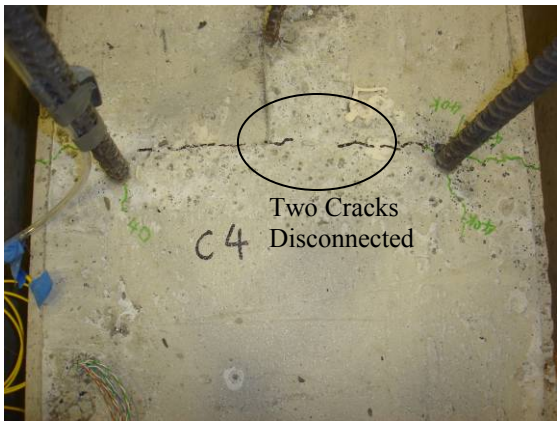

(d) Specimen C-6-4

Figure 5.31 Top views of various tested specimens in Group I.

Cracks on the sides of Specimens C-6-1 to C-6-4 were mapped and illustrated in Figure 5.32. It is clearly seen from Figure 5.32 that less cracks in number were observed as the development lengths increased from Specimen C-6-2 to C-6-4. With equal development lengths, Specimen C-6-4 and C-6-1 experienced similar cracks. The former appeared to have less cracks near the dowel bar, which is likely related to the use of enamel coating in Specimen C-6-4. It was interesting to note that severe cracks occurred but no concrete spalling was observed on Specimen C-6-2 even though only 60% of the required length for uncoated bars was considered. Due to the strong bond between enamel-coated rebar and concrete, the cracked concrete pieces most likely remained attached to the rebar in Specimen C-6-2.

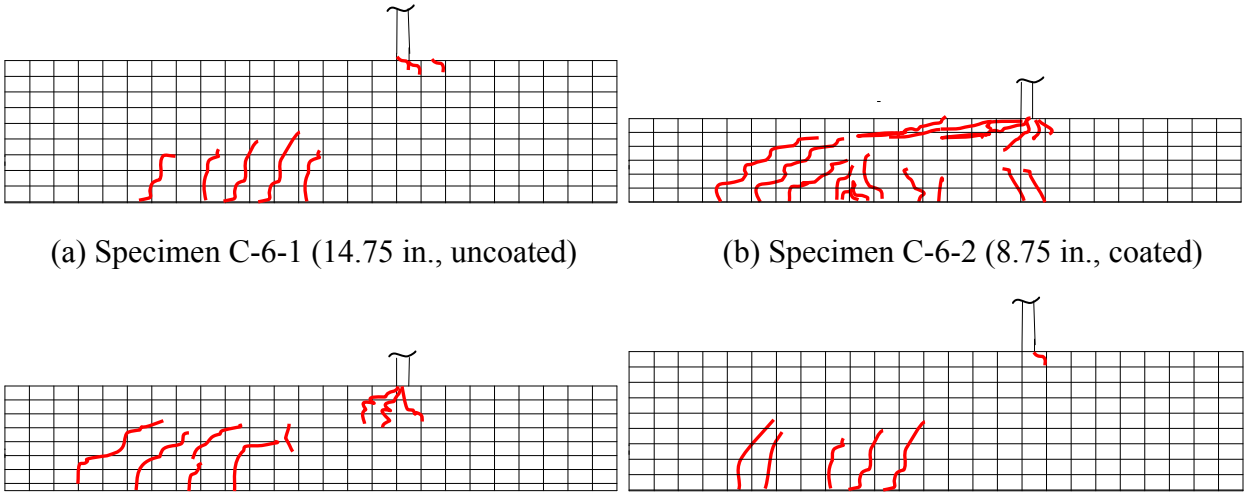

(a) Specimen C-6-1 (14.75 in., uncoated)

(b) Specimen C-6-2 (8.75 in., coated)

(c) Specimen C-6-3 (11.75 in., coated)

(d) Specimen C-6-4 (14.75 in., coated)

Figure 5.32 Crack patterns on the side of various specimens in Group I (marks traced on the pictures in B&W).

5.3.2.3. Group IV specimens

Group IV consisted of four RC column specimens with two #8 Grade 60 dowel bars embedded in each column. The 28-day concrete compressive strength for Group IV was 6.02 ksi. Similar to Group I, cross-over cracks between dowel bars were observed on the top surface of all specimens in Group IV except for Specimen C-8-8 as demonstrated in Figure 5.33. The exception with Specimen C-8-8 is likely attributable to the stronger steel-concrete bond associated with the longer development length of enamel-coated dowel bars compared to Specimens C-8-6 and C-8-7. In comparison with Specimen C-8-5, C-8-8 had the equal development length but did not experience any visible crack on the top surface of the column.

(a) Specimen C-8-5

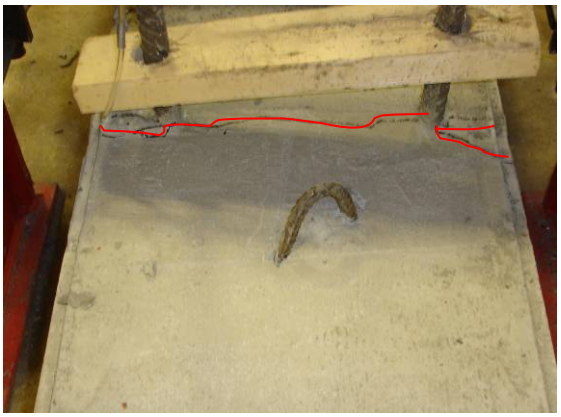

(b) Specimen C-8-6

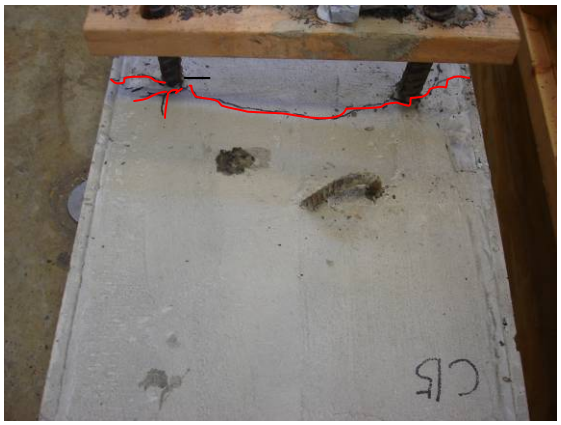

(c) Specimen C-8-7

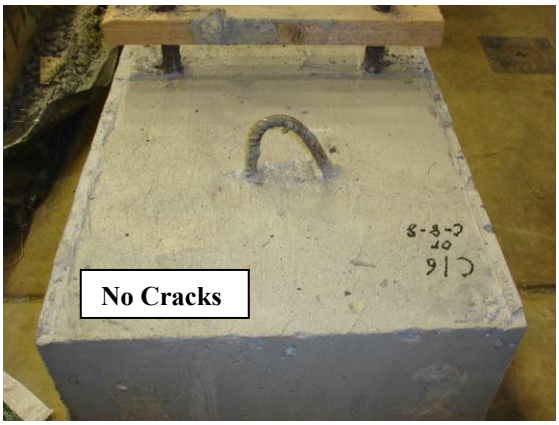

(d) Specimen C-8-8

Figure 5.33 Top views of various tested specimens in Group IV.

The crack patterns on the sides of the tested columns in Group IV were mapped and illustrated in Figure 5.34. Comparison among the three columns with enamel-coated dowel bars (C-8-6, C-8-7, and C-8-8) clearly indicated that the number of flexural cracks on the side face of columns increased as the development length decreased. The shorter development length means shallower cross section of columns and thus the lower moment resistance, resulting in more flexural cracks. By comparing Specimen C-8-8 with C-8-5 with equal development lengths, it was found that the column with enamel-coated dowel bars experienced smaller cracks near the dowel bars and on the side face of the column. This is likely because the two concentrated loads applied through the dowel bars can be distributed over a wider area of concrete when the dowel bars are better bonded to the concrete with the use of enamel coating. Therefore, the slip of enamel-coated dowel bars from the top surface of the column expects to be smaller as demonstrated in the comparison of load-slip curves of four column specimens in Figure 5.30(d).

In comparison with Group I specimens, Group IV specimens experienced much less cracks both in number and length. This result is due to the use of higher concrete strength in Group IV specimens.

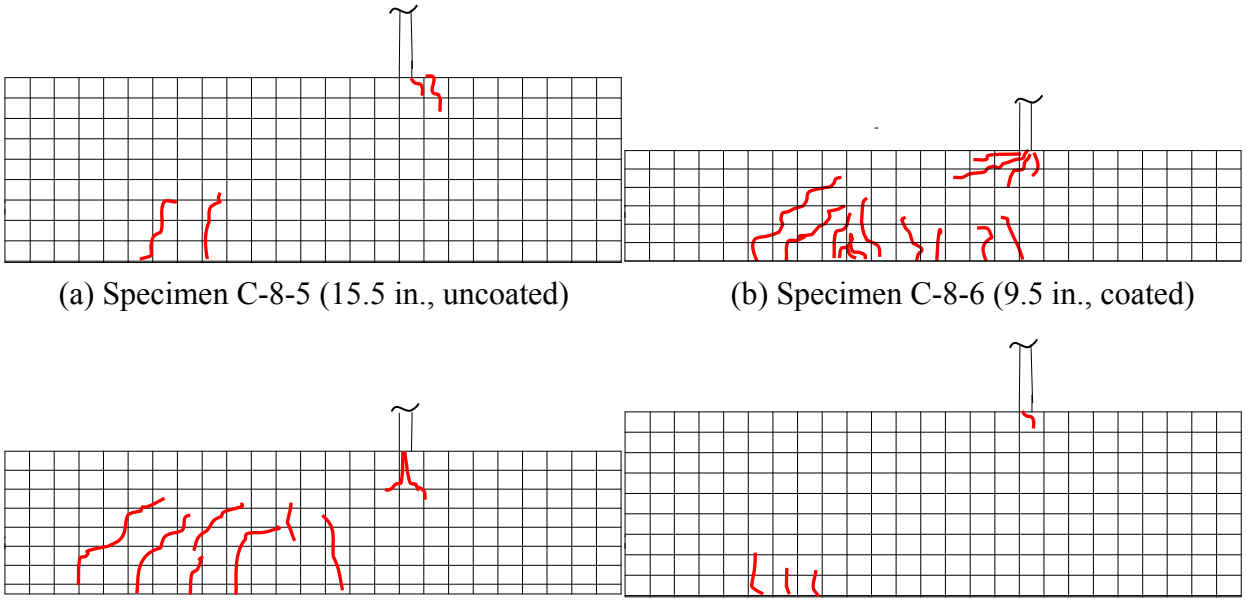

(a) Specimen C-8-5 (15.5 in., uncoated)

(b) Specimen C-8-6 (9.5 in., coated)

(c) Specimen C-8-7(12.5 in., coated)

(d) Specimen C-8-8 (19.5 in, coated)

Figure 5.34 Crack patterns on the side of various specimens in Group IV (marks traced on the pictures in B&W).

5.3.2.4. Strain measurements with optical fiber sensors

As discussed previously, eight column specimens were instrumented with FBG sensors that were deployed as shown in Figure 5.26 on each dowel bar. Unfortunately, the 90° bend of each dowel bar made the installation of optical fibers extremely difficult. Only three optical fiber sensors functioned as expected during the various tests.

Bragg gratings of pure glass were written on a single mode optical fiber that has a small inner core (a few μm in diameter) and a relatively large outer cladding (125 μm in diameter). Due to the difference in their refractive indices, light only travels through the core of an optical fiber. When Bragg gratings are stretched by a force, their period (distance between gratings) increases, resulting in a wavelength change of the light reflected from the gratings. The change in wavelength is proportional to the change of strain applied on the gratings. Multiple FBG sensors can be designed with different characteristic wavelengths and multiplexed for simultaneous measurements of strains along one optical fiber. More detailed discussions on the measurement principle of FBG sensors and their extensive case studies in civil engineering are referred to Ou et al. [2010].

Figure 5.35 illustrates the test setup with an optical sensing interrogator and an external PC for the measurements of strain data from FBG sensors. A snapshot of the computer screen is presented in Figure 5.36 during the strain measurement of Specimen C-6-6, in which three characteristic wavelengths are displayed. The differences in wavelength before and after loading a column specimen are directly related to the measured strains by the interrogator that has been well calibrated in the factory.

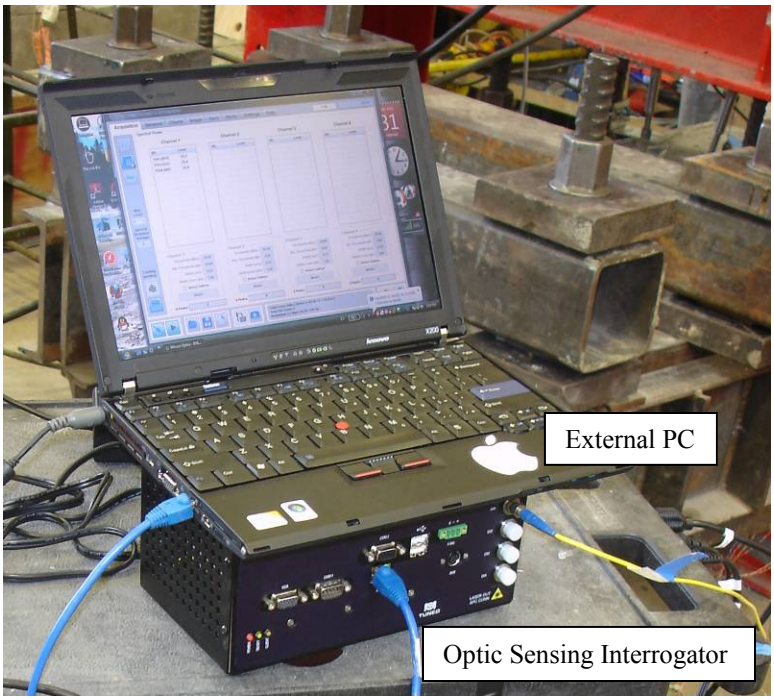

Figure 5.35 Optical fiber sensing system during testing.

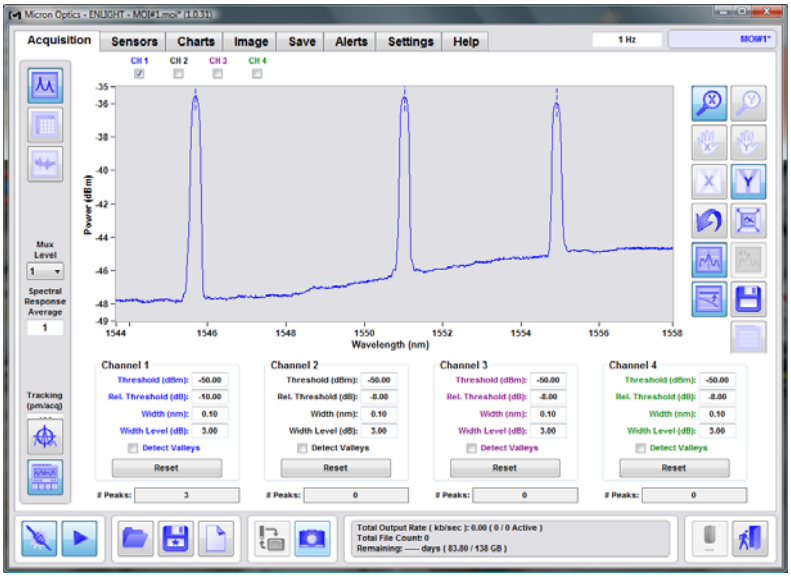

Figure 5.36 Reflection responses of three FBG sensors.

The load-strain curves of Specimen C-6-6, using the measured strains by three FBG sensors, are presented in Figure 5.37. The strains at Locations 2 and 3 are proportional to the applied load. Both are very small and negligible in comparison with that at Location 1. The load-strain curve using the measured strains at Location 1 indicates that the dowel bar experienced significant yielding. For Specimen C-6-6 with a development length of 7 in., Location 1 is 1 in. away from the top surface of the RC column. Therefore, the conclusion about rebar yielding is consistent

with what was observed from the load-slip curves in Figure 5.30(b). Note that the maximum load in Figure 5.37 is smaller than that in Figure 5.30(b) since the FBG sensors began to malfunction at approximately 38.5 kips.

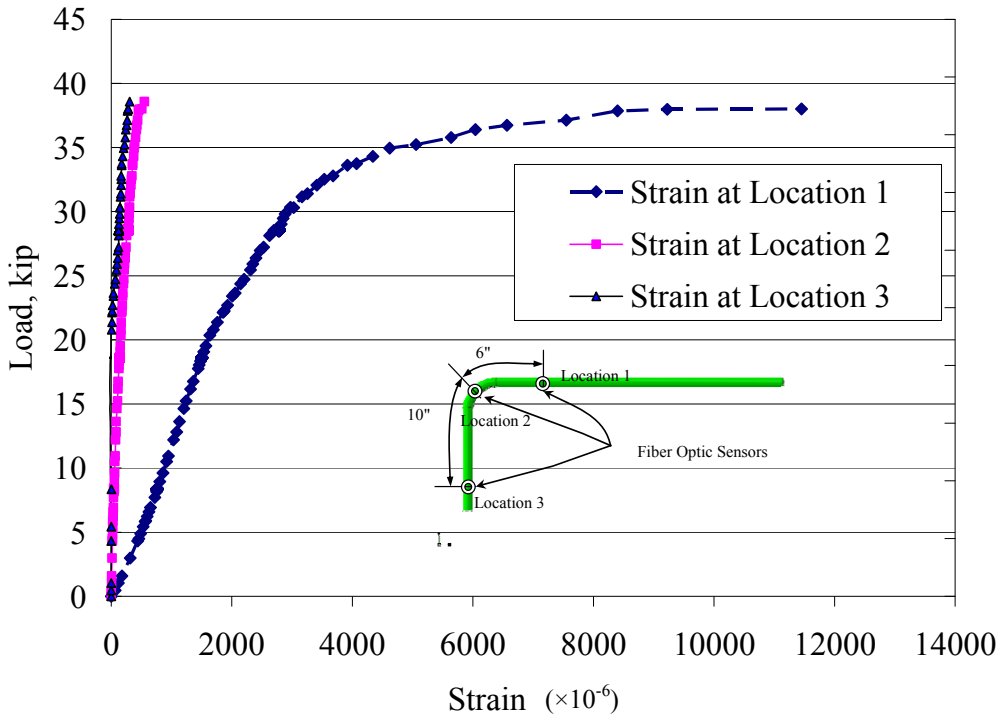

Figure 5.37 Measured strains at three locations by FBG sensors.

5.3.3. Conclusions Based on Short Column Tests

All RC column tests consistently showed steel bar yielding and no concrete spalling even though 60% of the development length required for uncoated bars by ACI 318-08 was considered for the design of the enamel-coated dowel bars. The severely cracked concrete pieces were still attached to the enamel-coated rebar. These results and observations indicated a strong bond between the enamel-coated rebar and concrete.

With equal development lengths, the column specimen with enamel-coated dowel bars experienced fewer (or no) concrete cracks near the steel bars than was found with uncoated dowel bars. The isolated cracks around the enamel-coated bars were not connected together and thus did not penetrate through the width of all tested columns.

More flexural and shear cracks were observed on columns when the development length of the dowel bars was reduced. This is mainly because the cross section of the columns became smaller as the development length decreased, thus generating higher stresses under the same load.

Although better installation methods and optical fiber packaging are needed to improve their survivability during installation, FBG sensors have been successfully applied to measure the

strain distribution along the length of a dowel bar. Such data is valuable to understand the true bond behavior at a steel-concrete interface since commonly used strain gauges may unintentionally weaken the bond interface.

5.4. Large Column Tests

The large column test program deals with the test and validation of the equation for splice length with the new coating factor recommended in Section 5.2. In this case, the main reinforcement of the columns is spliced with dowel bars into footings, simulating a representative detail in practical applications.

5.4.1. Technical Approach

Two large-scale columns were designed, fabricated, and tested to investigate the bond performance of spliced bars: one control specimen with uncoated reinforcement and the other with 50/50 enamel-coated reinforcement. As illustrated in Figure 5.38, each column specimen consisted of three structural components: load stub, circular column, and footing. The dimensions and reinforcement details are also shown in Figure 5.38.

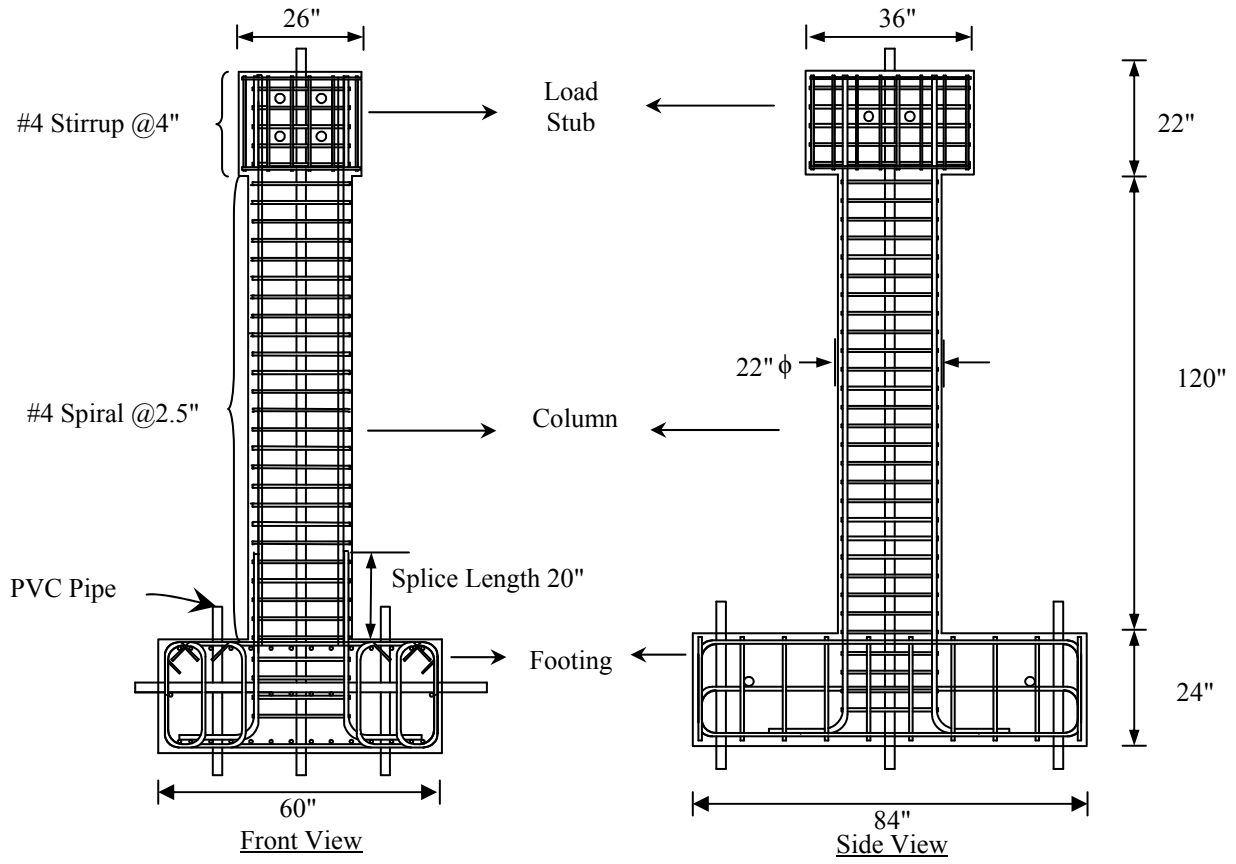

Figure 5.38 Dimensions and reinforcement details of column specimens.

The footing of each column was designed to simply help anchor the column down to the strong floor in the laboratory. It may not fully comply with design specifications. A 20-in. splice region was considered, starting from the top surface of footing. According to ACI 318-08 or the 2007 AASHTO LRFD Bridge Design Specifications, the required splice length for dowel bars in the footing was 28 in. In this study, a 70% reduction of the required splice length was used based on the beam test results as summarized in Table 5.5. The relative stress ratios of two specimens with confined stirrups (B-6-1 and B-6-2) are 0.57 and 0.76. The value 70% is close to the upper bound of the stress ratio from the tests. The final design of a splice length of 20 in. was selected.

5.4.1.1. Column specimens and material properties

5.4.1.1.1. Construction of Large-Scale Columns

The reinforcement cages for the column and footing of each specimen were separately fabricated and then assembled together prior to casting of the column as illustrated in Figure 5.39. To build the column reinforcement cage, dowel bars were first passed through the holes on a wood template. They were then lap spliced and tied with the main reinforcement of the column. Next, spiral ties were pulled along the main reinforcement of the column and tied together with tie-wires as shown in Figure 5.39(b). The spliced region is detailed in Figure 5.40(a) and the cross-sectional view of the column reinforcement cage is shown in Figure 5.40(b).

(a) Footing reinforcement cage (b) Column reinforcement cage

Figure 5.39 Fabrication of steel cages.

(a) Detail of lap splices (b) Cross-sectional view of column cage

Figure 5.40 Details of steel cages.

The wood formwork for the load stub and the steel formwork for footing and column are shown in Figure 5.41. The two column specimens were cast together with one batch of concrete. To bear the gravity load applied on the footing by the wet concrete in the column and load stub, the top of each column footing was covered with a strong laminate wood plate that was pressured down with cross beams. A wood platform was built to assist in the casting of concrete from the top of the load stub.

(a) Formworks (b) Casted column specimens

Figure 5.41 Casting of concrete columns.

5.4.1.1.2. Material Properties

Sample steel reinforcing bars were tested in tension. Their mechanical properties are presented in Table 5.11. The concrete mix was selected to have a compressive strength of 6 ksi in 28days. The concrete mix design is listed in Table 5.12 and the concrete properties at various curing ages are given in Table 5.13.

Table 5.11 Mechanical properties of reinforcing bars used in large-scale columns

Reinforcement	Modulus of Elasticity (ksi)	Yield Stress (ksi)	Ultimate Strength (ksi)
#4 Uncoated Sprial	31,760	78.5	100.5
#6 Uncoated Rebar	31,760	65.0	85.6
#8 Uncoated Rebar	29,880	60.6	95.5
#8 Coated Rebar	29,880	58.4	90.3

Table 5.12 Concrete mix design for large-scale column specimens

Material	Quantity (lb/Yd^3)
Cement	705
Fine Aggregate	1455
Coarse Aggregate	1945
Water	100
Air Entrainment	0.5
High-Range Water Reducer	5

Table 5.13 Concrete properties for large-scale column specimens

Day	Compressive Strength (psi)	Average Strength (psi)	Modulus of Elasticity (ksi)
7	4,205	4,444	N/A
	4,805		
	4,323		
21	5,210	5,223	N/A
	5,301		
	5,150		
28	6,600	6,340	4,560
	6,003		
	6,417		

5.4.1.2. Test setup, instrumentation, and loading protocol

Each column specimen was tested against the strong reaction wall in the Highbay Structures Laboratory, as shown in Figure 5.42. The cast specimen was first placed on top of the two concrete bases/pedestals that are in turn fixed to the strong floor by two Dywidag bars each. The column footing was then secured by two bearing beams that were in turn held down by two tie-down beams. Each tie-down beam was anchored to the strong floor with four Dywidag bars pretensioned to 5 kips. The load was applied on the load stub by two hydraulic actuators of 140 kip capacity each in tension. Efforts were made to provide two equal forces from the two hydraulic actuators to eliminate any torsional loading and thus apply only flexural forces to the columns.

To simulate the dead load effect in practical applications, each column was subjected to an axial load of approximately 133 kips. The axial load was provided by seven steel strands of 0.3 in. in diameter, which were inserted through a pre-embedded PVC pipe along the center of each column. The strands were anchored at the bottom face of the footing and prestressed with the hydraulic jack mounted on top of the loading stud as shown in Figure 5.42. The PVC pipe was sized to allow free rotations of the strands during the column tests in order to maintain a stable axial load.

A total of 64 strain gages were installed on the reinforcement of each column before the steel cage was assembled as shown in Figure 5.43. They included 44 gauges on the main/longitudinal reinforcing bars and 20 on the transverse spirals. They were distributed along the height of each column as illustrated in Table 5.14.

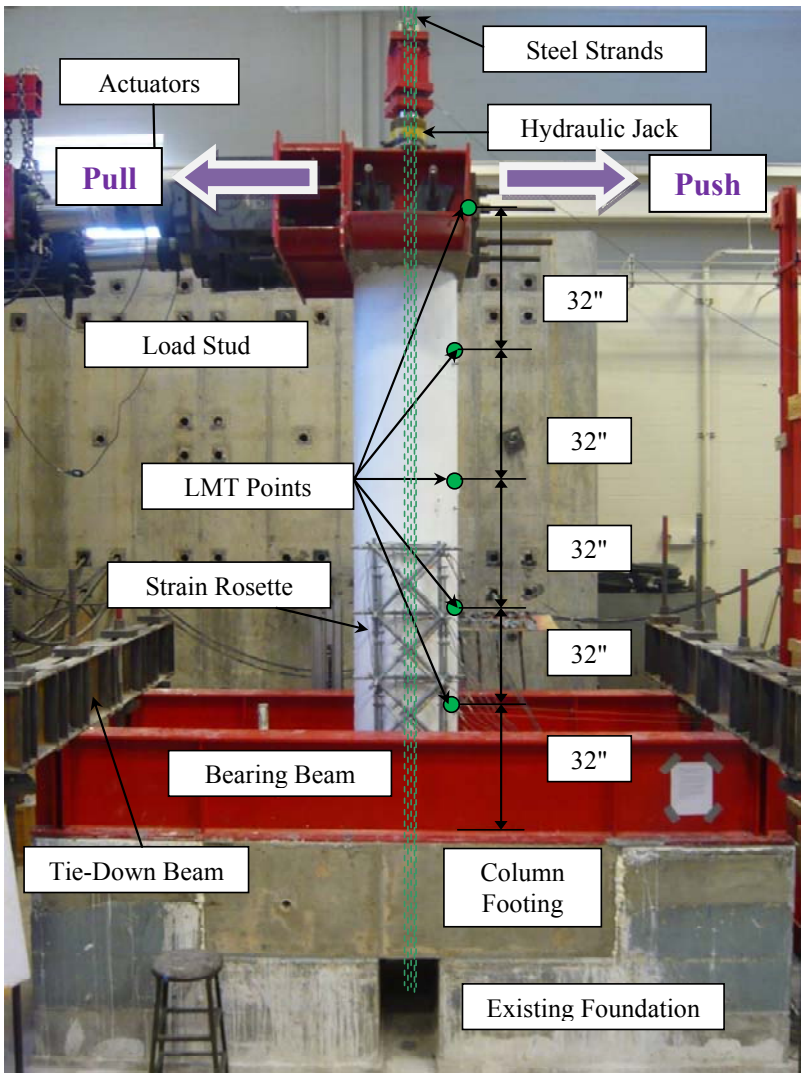

Figure 5.42 Test setup of a large-scale column.

(a) Strain gauges on main reinforcement

(b) Gauges on main and spiral reinforcement

Figure 5.43 Installation of strain gauges.

Table 5.14 Strain gauge profile on each column specimen

Gage Location No.	Rebar No				* Strain Gages Installed on Spirals
11	A	B	C	D	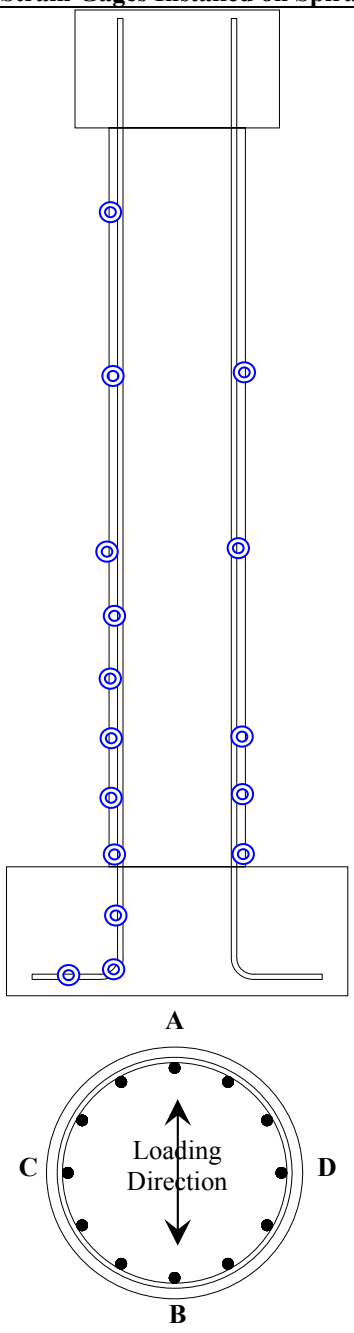
10	A*	B*	C*	D*	
9	A*	B*	C*	D*	
8	A	B	C	D	
7	A	B	C	D	
6	A*	B*	C*	D*	
5	A*	B*	C*	D*	
4	A	B	C	D	
3	A	B	C	D	
2	A	B	C	D	
1	A	B	C	D	

To measure the deflection distribution over the column height, ten linear motion transducers (LMT) were installed at five different elevations as shown in Figure 5.42. Two LMTs were located at each elevation to obtain an average value of the measured deflections. A load cell was installed on top of the hydraulic jack to monitor the axial load applied on the test specimen. Two MTS actuators used to provide the lateral loads had built-in load cells and displacement transducers (LVDTs).

Prior to tests, an axial load of 133 kips was applied to each column specimen. As shown in Figure 5.44, the column was tested under cyclic loading at three force control levels first and at six displacement control levels later. The three force loading levels (12 kips, 24 kips, and 36 kips from two actuators) were selected to correspond to 25%, 50%, and 75% of the theoretical/estimated yield load of the column specimen (approximately 24 kips/actuator at 3 in.). The six displacement loading levels (3 in., 3.75 in., 4.5 in., 5.25 in., 6 in. and 9 in.) tested the column to a theoretical ductility level of 3. At each loading level, the column was pushed and pulled for three complete cycles at a loading rate of 6 kip/actuator/min. or 0.75 in/min.

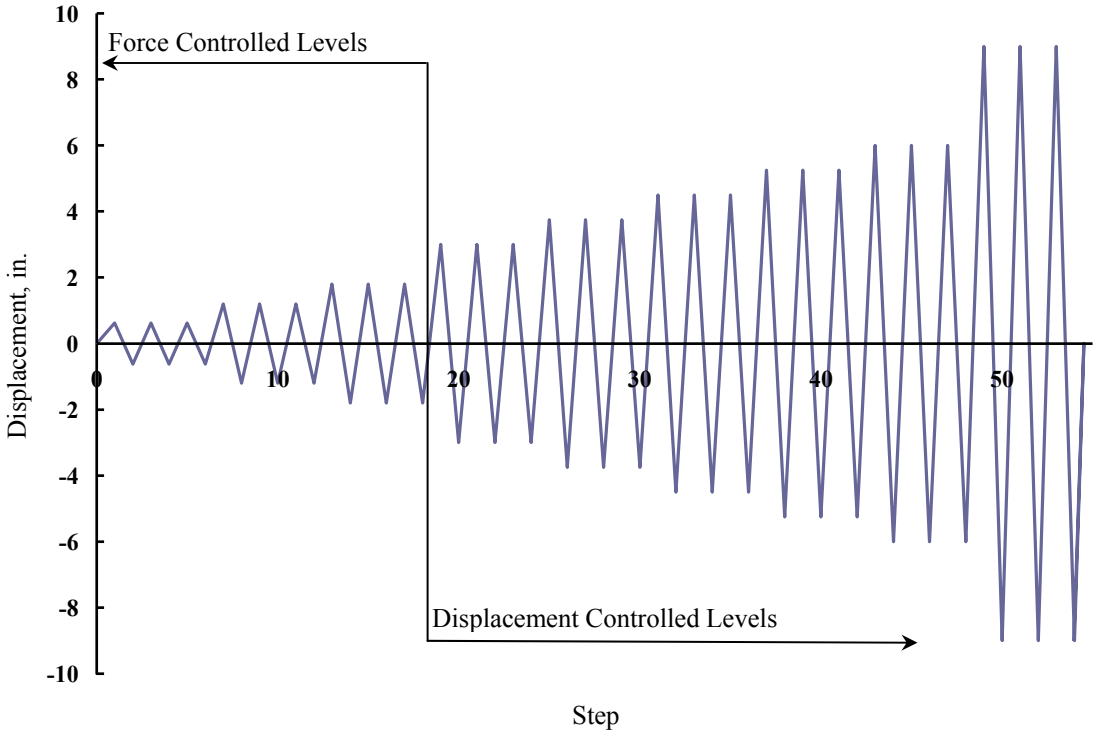

Figure 5.44 Loading protocol (displacement specified).

5.4.2. Results and Discussion

The crack patterns, failure modes, load-displacement curves, and energy dissipations of two column specimens are discussed and compared in this section. For clarity, the specimen reinforced with uncoated rebar was designated as Column #1 and the specimen with enamel coated reinforcement was designated as Column #2.

5.4.2.1. Visual observations

At 12 kips (6 kips per actuator), both columns performed elastically, returning to their undeformed position when completely unloaded. Neither cracks nor residual deformation were observed. At 24 kips (12 kips per actuator), flexural cracks were observed on both columns but no concrete spalling occurred. As shown in Figure 5.45(a, b), the crack patterns on the two columns are similar. Some of the cracks on Column #2 are shorter and disconnected.

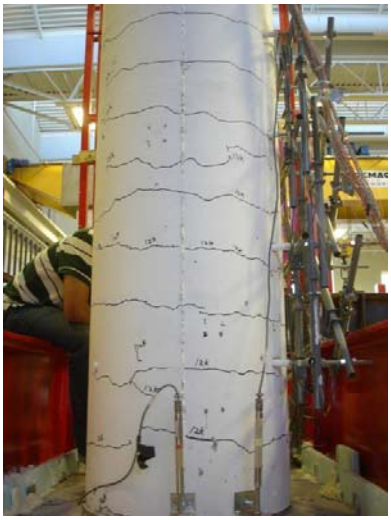

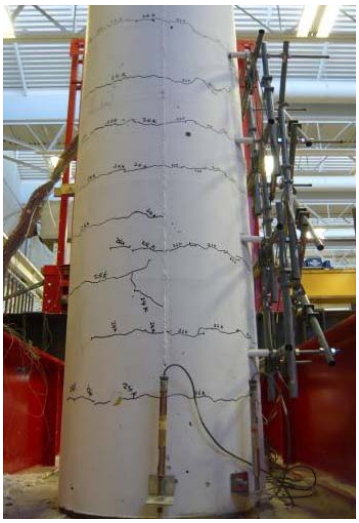

Column #1(marked load from one actuator) (b) Column #2 (marked load from two actuators)

Figure 5.45 Crack patterns at 24 kips.

At 36 kips (18 kips per actuator), longitudinal cracks started to appear at the bottom portion of both columns. However, as shown in Figure 5.46, more and longer longitudinal cracks were observed on Column #1, particularly around the end of the spliced bars. No concrete spalling occurred on both columns. At this stage, the strain gauges installed on the longitudinal rebar indicated that the strains approached the yield strain. Therefore, the column continued to be tested in displacement control.

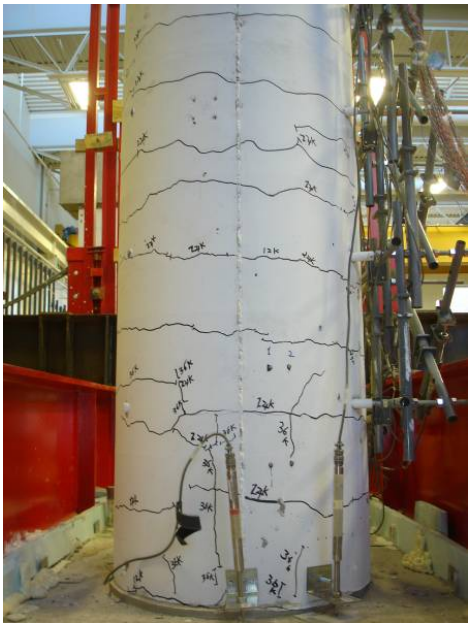

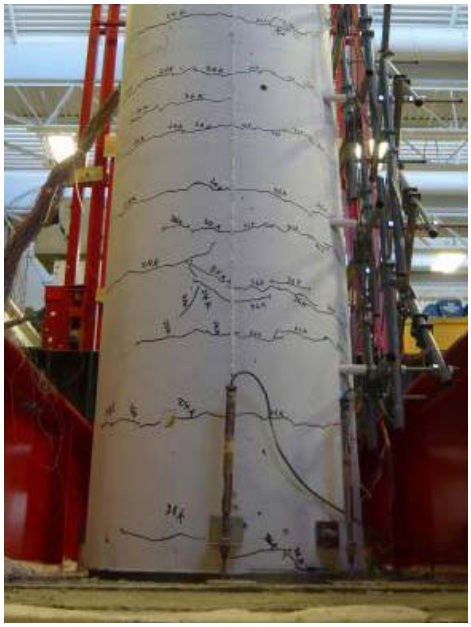

(a) Column #1 (b) Column #2

Figure 5.46 Crack patterns at 36 kips.

At a maximum displacement of 3 in., more longitudinal cracks were observed on both columns as concrete split as shown in Figure 5.47. The transverse cracks also extended significantly. On one hand, concrete spalling started to appear on Column #1 around the column-footing joint due to pinching effects as the concrete cover was pinched by the footing and internal longitudinal reinforcement. As the corresponding load was 44 kips from two actuators, the concrete splitting failure in Column #1 was initiated when the longitudinal rebar approached yielding. On the other hand, the longitudinal reinforcement of Column #2 reached the yield strength at the column-footing joint, as indicated by the installed strain gages. Minor concrete spalling also occurred on the opposite side due to pinching effects. This can be simply understood as the over-stretching of the longitudinal reinforcement (yielding) destroyed the compatibility between the steel and concrete which led to the cracks propagating and spalling of the concrete cover.

(a) Column #1 (b) Column #2

Figure 5.47 Crack patterns and concrete spalling at 3 in.

When Column #1 was subjected to a displacement of 6 in., the slippage between spliced longitudinal bars increased and the corresponding load capacity was significantly reduced. With accumulative pinching effects due to the increasing displacement and increasing slippages between spliced rebar, the longitudinal cracks were extended significantly and substantial concrete spalling occurred as shown in Figure 5.48(a). Note that the cracks marked in green color in Figure 5.48 and in black color in Figure 5.47 were induced when the actuators were pulled and pushed, respectively, as illustrated in Figure 5.42.

At a displacement of 9 in., Column #1 significantly lost its load capacity. As shown in Figure 5-48(b), the concrete cover in the spliced area was completely lost; the slippage between the spliced bars increased; and the stress transfer capability was significantly reduced. As a result, part of the transversely confined concrete core degraded and a significant crack developed in the

concrete core near the end of spliced rebar as indicated in Figure 5.48(b). The presence of the hollow concrete core was a strong indication of the column failure at the spliced joint.

(a) At 6 in. displacement (b) At 9 in. displacement

Figure 5.48 Concrete cover spalling and concrete core degradation of Column #1

As the extent of longitudinal rebar yielding continued to move upward with increasing displacements, the two spliced bars slowly slipped with each other; concrete splitting and spalling increased. At a displacement of 9 in., the concrete core of Column #2 began degrading at the bottom of the column as shown in Figure 5.49. This mainly resulted from the joint rotation associated with yielding of the longitudinal reinforcement.

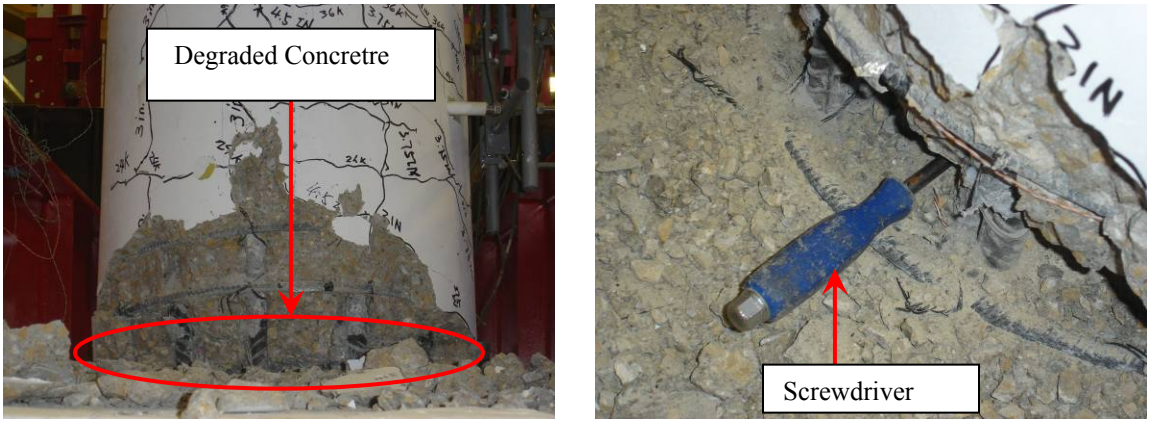

(a) Overview of damage (b) Expanded view

Figure 5.49 Concrete cover spalling and concrete core degradation of Column #1

5.4.2.2. Data analysis and discussions

The heights of spalling concrete areas are compared in Figure 5.50 for the two columns. It is clearly seen that the maximum heights of the spalling area at the same displacement of 9 in. are 25 in. and 12 in. for Column #1 and Column #2, respectively. This comparison indicates that Column #2 is much stiffer than Column #1.

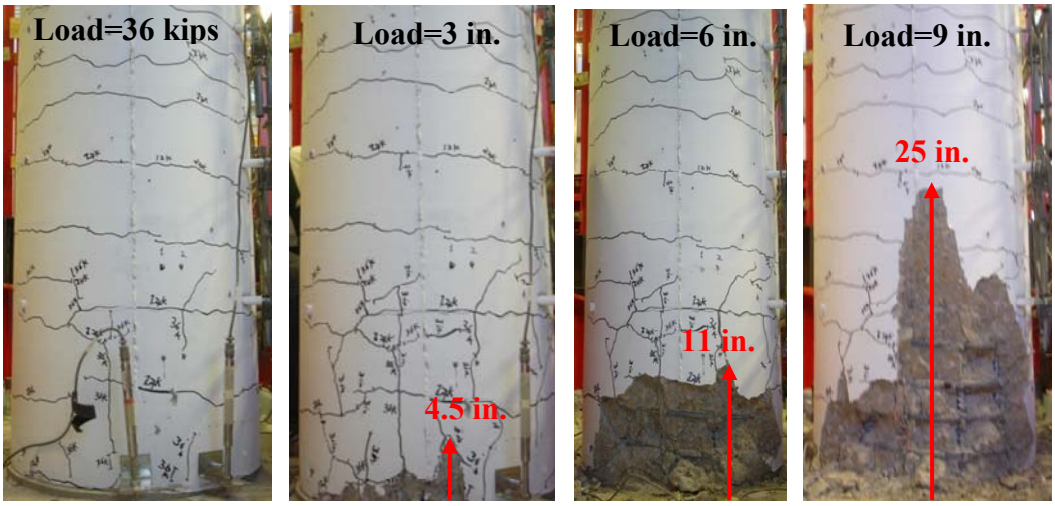

(a) Column #1

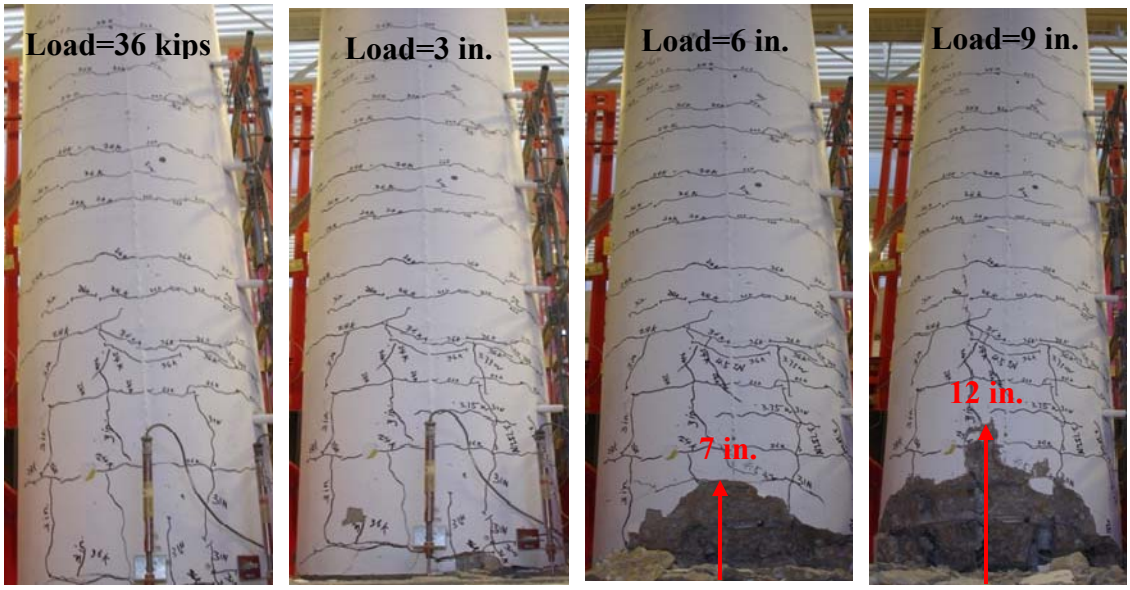

(b) Column #2

Figure 5.50 Increasing spalling areas of two columns.

The load level corresponding to a displacement of 3 in. was 44 kips for both columns. With the increasing displacement, the total load applied from two actuators is listed in Table 5.15. The

secant stiffness calculated from the applied load and displacement and the increase in secant stiffness from Column #1 to Column #2 are also given in Table 5.15. It can be seen from Table 5.15 that the increase in stiffness ranges from 23% to 40%.

Table 5.15 Applied displacement, corresponding load, and secant stiffness

Applied Displacement (in)	Corresponding Load (kip)		Secant Stiffness (kip/in)		Increase in Secant Stiffness (%)
	Column #1	Column 2	Column #1	Column #2	
3.75	28.52	38.90	7.60	10.4	37%
4.50	22.64	30.24	5.04	6.72	25%
5.25	18.05	23.56	3.44	4.48	30%
6.00	14.52	20.36	2.42	3.40	40%
9.00	12.56	15.44	1.40	1.72	23%

The load-displacement curves of two columns are compared in Figure 5.51. In this report, an average tangential stiffness of a column was introduced to measure the overall rigidity of the column over a displacement range. It is defined as the arithmetic average of tangential stiffness at all measured displacement points. Figure 5.51 indicates that the increase in tangential stiffness from Column #1 to Column #2 is approximately 30.9%. The stiffness increase is consistent with the change in damaged area as shown in Figure 5.50.

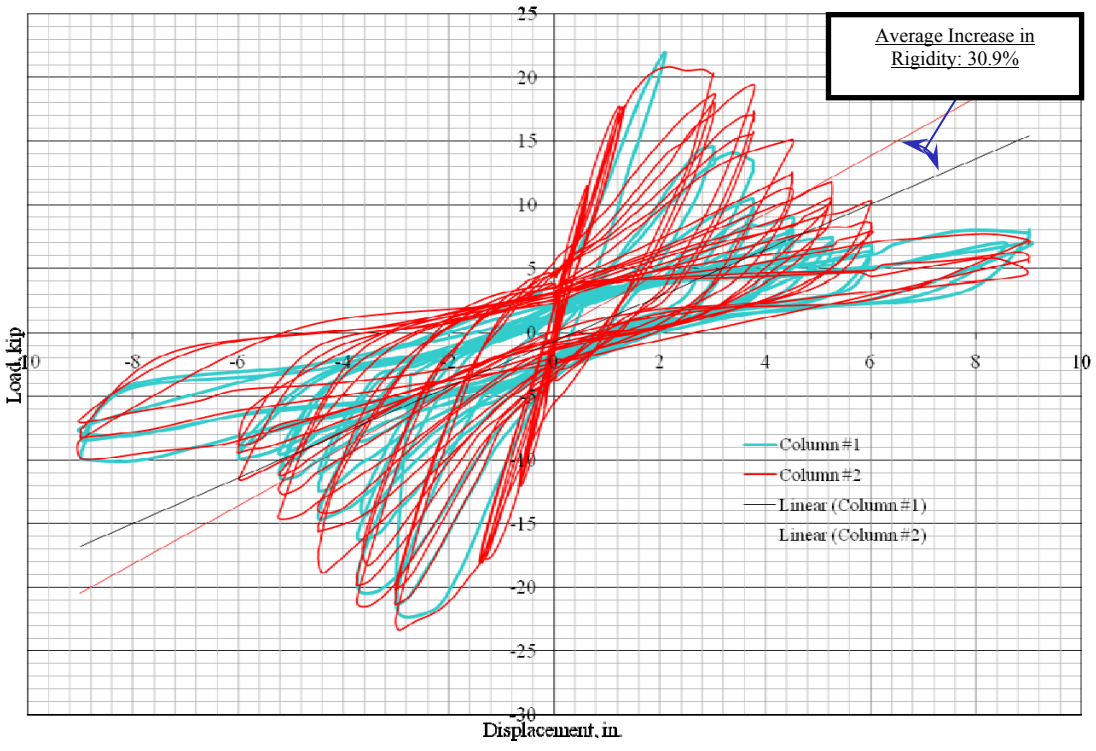

Figure 5.51 Load-displacement curves of two columns.

It can also be observed from Figure 5.51 that the envelope of the load-displacement curves of Column #2 basically covers that of Column #1. In two consecutive cycles, Column #1 suddenly experienced a maximum drop of 35.2% in load capacity whereas Column #2 gradually dropped a maximum of 11.6% in load capacity. In comparison with Column #1, Column #2 can dissipate 30.8% more energy over a range of the test displacement, as illustrated and evaluated in Figure 5.52. Here, the energy dissipated is measured by the shaded area in Figure 5.52.

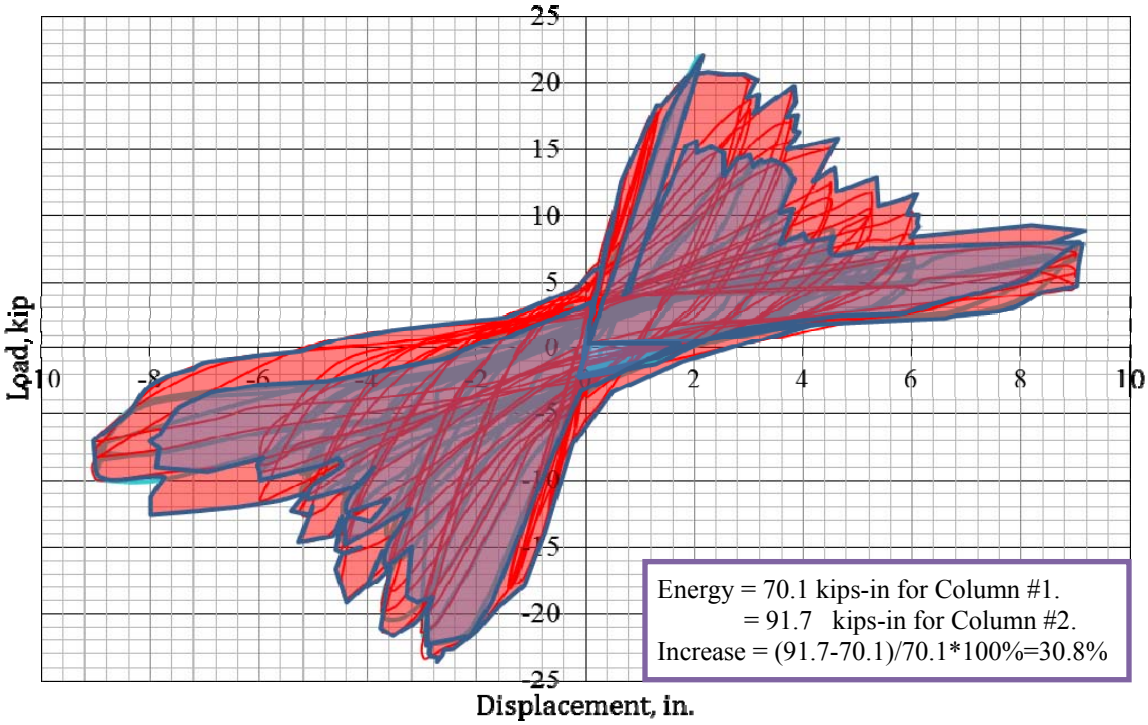

Figure 5.52 Dissipated energy in two columns.

By comparing Figure 5.48(b) with Figure 5.49(b), it can be concluded that Column #1 failed at the upper end of the spliced joint whereas Column #2 at the lower end of the spliced joint due to significant steel yielding. As such, the positive effect of the enamel coating was clearly demonstrated in this study.

5.4.3. Conclusions Based on Testing of Large-Scale Columns

The comparisons of two large-scale column tests clearly demonstrated the enhancement of steel-concrete bond strengths when the steel rebar was coated with 50/50 enamel coatings. This conclusion is supported by the increases in secant and tangential stiffness, energy dissipation, and concrete spalling areas. The difference in the location of concrete core degradations in two columns reflects the different failure modes. Column #1 with uncoated reinforcement mainly failed in lap splice with excessive spliced rebar slippages at the upper end of the spliced joint even though the maximum stress in main reinforcement approached the yield strength of steel. Column #2 with enamel-coated rebar failed in rebar yielding followed by extensive spliced rebar slippages, resulting in concrete core degradation at the column-footing connection.

6. CORROSION RESISTANCE OF ENAMEL-COATED BARS

6.1. Background

Corrosion is a complex electrochemical process. Its onset and severity cannot be detected accurately with one specific test or evaluation method. In this study, five tests were conducted to understand and quantify the process of corrosion in enamel-coated steel bars and deformed rebar. They include salt spray tests, accelerated corrosion tests (ACT), ponding tests, potentiodynamic (PD) tests, and electrochemical impedance spectroscopy (EIS) tests. Table 6.1 lists the five test methods and the parameters they can provide for corrosion evaluation. For ACT and ponding tests with RC specimens, both concrete resistivity and half-cell measurements were taken.

Table 6.1 Corrosion test methods and their outcomes

Test	Corrosion Current	Corrosion Potential	Corrosion Rate	Corrosion Probability	Impedance	Surface Characteristics
Salt Spray						√
ACT	√	√		√		
Ponding		√		√		
PD	√	√	√			
EIS					√	

The following sections discuss the details of each corrosion test. The test methodology, sample preparation, test setup, and protocol are presented.

6.2. Salt Spray

Originally proposed in 1914 by Mr. J. A. Capp and later adopted by the National Institute of Standards and Technology (NIST), salt spray testing has become a widely recognized method for examining the corrosion resistance of protective coatings. In 1939 the American Society for Testing and Materials (ASTM) International developed ASTM B117, a standard salt spray test method specifically designed to evaluate the relative corrosion resistance of various metals and/or coatings. Today salt spray chambers are designed according to the ASTM B117 standard and are automated to maintain a specified environment within the chamber.

A schematic representation of a typical salt spray chamber is shown in Figure 6.1. As can be seen from Figure 6.1, a salty fog is injected into the enclosed chamber through a nozzle (or atomizer) centrally located along the chamber's floor. The atomizer is continually supplied with saltwater that is stored within a reservoir positioned along the right side of the chamber and a steady stream of clean compressed air. Built-in heating units are used to maintain an elevated temperature inside the chamber. A chamber's lid is typically sloped so to avoid any solution that

has accumulated along the inner surface of the lid from falling upon the specimens lying below. The solution that accumulates inside the chamber is disposed of through a drain positioned within the chamber's floor.

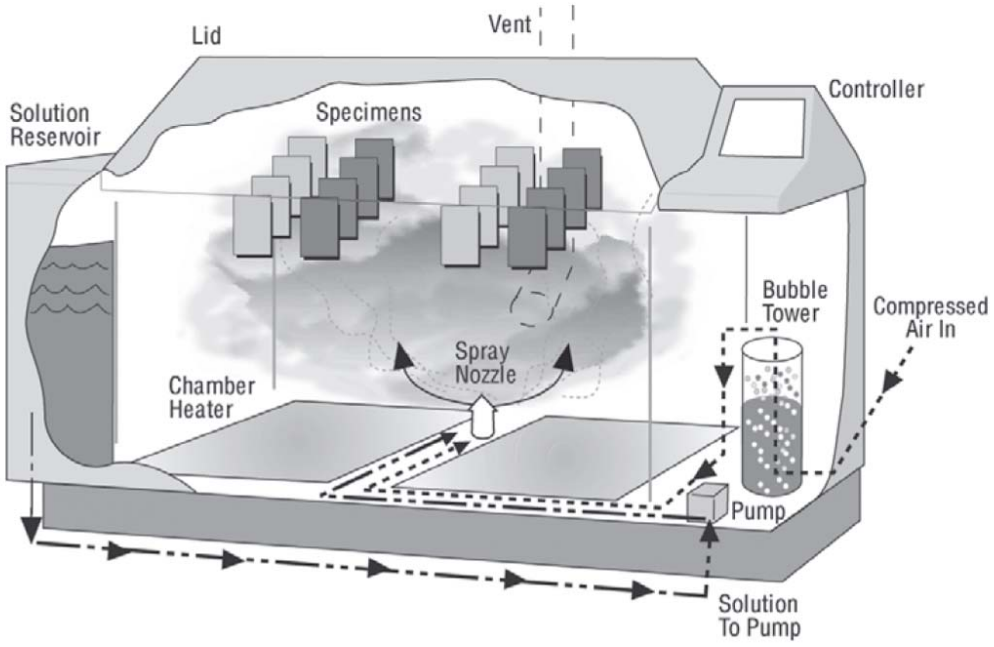

Figure 6.1 A schematic representation of a salt spray chamber (Courtesy of the Q-Lab Corporation).

6.2.1. Technical Approach

Using a Q-Fog salt spray chamber manufactured by the Q-Lab Corporation, the corrosion resistance of three enamel coating configurations along with a standard epoxy coating was evaluated. The test consisted of subjecting a total of 64 specimens to a series of wet/dry cycles over a period of twelve weeks. Half of the 64 specimens were coated smooth steel bars while the remaining 32 specimens were coated deformed steel bars. Each group of 32 specimens contained eight 50/50 enamel-coated bars, eight double enamel-coated bars, eight pure enamel-coated bars, and eight epoxy-coated bars. After testing, the uniformity of each coating, as well as the steel-coating bond along both the deformed and smooth bars, was evaluated through visual and microscopic cross-sectional examination.

6.2.1.1. Test samples

Each specimen was approximately 11 in. (279 mm) in length and was made from either ½-in.-diameter (13 mm) smooth steel dowels or No. 4 (No. 13) deformed bars, with all steel conforming to ASTM A615 Grade 60. After the specimens were sectioned to the proper length, the ends were beveled and two layers of Loctite's Aquamarine Epoxy were uniformly applied along the ends of each specimen, as shown in Figure 6.2. While applying the second layer of epoxy, specimens were examined for areas of damage which may have been caused through handling and/or transporting of the specimens. Each area exhibiting signs of damage received

one layer of epoxy. A layer of epoxy was also applied to any rare imperfections that were observed within each coating. These areas of imperfections were deemed as manufacturing defects and were seen within each type of coating.

Figure 6.2 Typical smooth and deformed salt spray specimen prior to testing.

Prior to testing, one end of each specimen was labeled with either "D," "F," "P," or "EP" so to indicate whether a specimen was coated with double enamel, 50/50 enamel, pure enamel, or epoxy, respectively. The sides and back of each specimen were also labeled so to assist in systematic repositioning of each specimen within the salt spray chamber throughout the twelve weeks of testing.

6.2.1.2. Test procedure and preparation

During the twelve weeks of testing, the set of 64 specimens was broken up into two groups of 32 specimens. Group 1 contained all of the deformed bars, and Group 2 contained all of the smooth bars. Each specimen remained within its assigned group throughout the entire testing period.

During the course of testing, the two groups were subjected to wet and dry environments at alternate times. For example, while the deformed specimens were subjected to the dry condition, the smooth specimens would have been subjected to the wet condition, or vice versa. The two groups of specimens were transferred from one condition to the other on Monday, Wednesday, and Friday of each week.

The total duration of the salt spray test was 2000 hours with each of the two groups spending half of the time in a dry environment and the remaining 1000 hours in a wet (salty fog) environment. With the two groups of specimens being transferred from one environment to the other on Monday, Wednesday, and Friday of each week, the typical duration of the wet or dry phase of testing was approximately 48 or 72 hours long. After a group had spent 72 hours within the wet environment, the group would spend the following 72 hour phase in the dry environment. This cycling was maintained throughout the 2000 hours of testing and resulted in each group spending an equal amount of time in both the wet and dry environments.

6.2.1.2.1 Wet Phase

Specimens were repositioned within the salt spray chamber in a systematic order after every wet/dry cycle. This repositioning of the specimens ensured that each specimen received an

equivalent amount of exposure to the corrosive environment by the time the test had been completed. As shown in Figure 6.3, four holding racks, spaced 6 in. (152 mm) on center, were located within the chamber. Each holding rack supported a total of eight specimens that were spaced approximately 4 in. (102 mm) from each other. The eight specimens contained along a holding rack were coated with the same coating. The holding rack to which each of the four groups of specimens was designated depended upon where the specimens were positioned during the previous wet phase.

Figure 6.3 Specimen layout during the wet phase of testing.

The four holding racks contained within the salt spray chamber were constructed of vinyl trays that spanned the width of the salt spray chamber and plastic zip-ties which were spaced every 4 in. (102 mm) along the lengths of fiberglass rods, as shown in Figure 6.3. The fiberglass rods were spaced 6 in. (152 mm) on center from one another and were offset 4 in. (102 mm) from the chamber's side wall. Each specimen within the chamber was oriented at an angle of approximately 15 degrees from vertical in accordance with ASTM B117. A minimum distance of 3 in. (76 mm) was maintained between the walls of the chamber and the specimens. At no time during the test were any two specimens in contact with one another and a specimen never obstructed another specimen's exposure to the salt fog.

The salt fog that was constantly distributed throughout the chamber had an average fall-out rate of approximately 2.37 fl-oz (70 mL) per 12.4 sq-in. (8000 sq-mm) of horizontal surface area over a period of 48 hours. The solution used throughout the testing period was composed of distilled water and 5 percent USP grade sodium chloride (NaCl) by weight. The temperature within the salt spray chamber was maintained at 95 ± 3 °F (35 ± 2 °C) throughout the twelve weeks of testing.

6.2.1.2.2. Dry Phase

The dry phase of the test consisted of placing 32 specimens in a dry environment with an average ambient temperature of 68 °F (20 °C) and a relative humidity of 40 to 60 percent. Racks constructed of wood and two carbon rods were used to support the ends of each specimen. The racks suspended each specimen approximately ½ in. (13 mm) above the underlying shelf on which they were stored. A total of eight specimens, each spaced 1 in. (25 mm) on center, were distributed along the width of each rack. The eight specimens assigned to a rack were all of the same type and corresponded to the grouping within the salt spray chamber. At no time during the course of testing were any of the specimens in contact with each other or any foreign object other than the wooden portion of the rack within which they resided. Figure 6.4 shows a representative view of how a group of 32 specimens were stored during the dry phase of the test.

Figure 6.4 Specimen layout during the dry phase of testing.

6.2.1.2.3. Cross-Sectional Examination

When a cross-section of a selected specimen was taken, the specimen was first cut into two pieces at a location that was approximately ½ in. (13 mm) from an area of interest. Depending upon availability or maintenance issues, the saw used to cut the specimens was either a band-saw or a diamond-bladed chop-saw that incorporated the use of water during the cutting process. If the chop-saw was used, the two remaining pieces of the specimen were immediately dried upon the completion of the cut with the use of paper towels. The piece of the specimen containing the area of interest was then mounted within an epoxy.

Mounting of the specimens involved a PVC mold and a low viscosity, clear epoxy. The epoxy used during this process was manufactured by Allied High Tech Products, Inc. and required a resin to hardener ratio of 10 to 3, by weight. A polyvinyl chloride (PVC) cap, with an inner diameter of 1 in. (25 mm), was used to form the epoxy around the selected specimen. Prior to casting the epoxy, a thin uniform layer of petroleum jelly was applied along the mold's inner surface to act as a bond breaker. The epoxy and rebar specimen were then placed into the PVC mold and allowed to cure for at least 12 hours. Once cured, the specimen was removed from the PVC mold and cleaned. A slice of the specimen was then taken across the area of interest using one of the two saws previously mentioned. The slice was then labeled according to the specimen from which it was taken and then subsequently polished.

The face of the exposed steel was held against an 8-in.-diameter (203 mm) rotating platform that contained polishing paper. An assortment of five polishing papers, all of different grit, was used during the polishing process. The order of the five grits used, starting with the coarsest and ending with the finest was 180, 320, 600, 800, and 1200. The polishing papers were made with silicon carbide grit and were manufactured by Allied High Tech Products, Inc. A steady stream of water was used to continually saturate the surface of the polishing paper fixed upon the rotating platform. Once polishing was complete, the specimen was removed from the platform and carefully wiped dry with a Kimwipe tissue. Polishing of a specimen was deemed complete when a smooth transition zone between the coating and the steel was obtained. Examination of a finished cross-section was then conducted using a Hirox digital microscope.

6.2.2. Results and Discussion

The results discussed within this section are based on visual observations during the course of the salt spray testing, as well as microscopic examination of sections taken at the conclusion of the test period. Values stated within this section are approximate unless otherwise noted. Photographs indicating the overall condition of each specimen are contained in Appendix A.

6.2.2.1. 50/50 enamel

The deformed 50/50 enamel-coated specimens performed relatively well until the 6th week of testing. Each specimen only showed minor amounts of "pin sized" areas of corrosion as shown in Figure 6.5(a). However, during the remaining tests, each specimen gradually showed increasing amounts of corroded areas along both the transverse and longitudinal ribs. By the 10th week, the 50/50 enamel coating began to crack along a portion of the transverse ribs that had previously shown signs of corrosion. This cracking of the coating is shown in Figure 6.5(b). When the test was complete, it was determined that most, if not all, of the visible corrosion had taken place along the transverse and longitudinal ribs of each specimen. On average, 57 percent of a specimen's transverse ribs and 12 percent of its longitudinal ribs showed signs of corrosion.

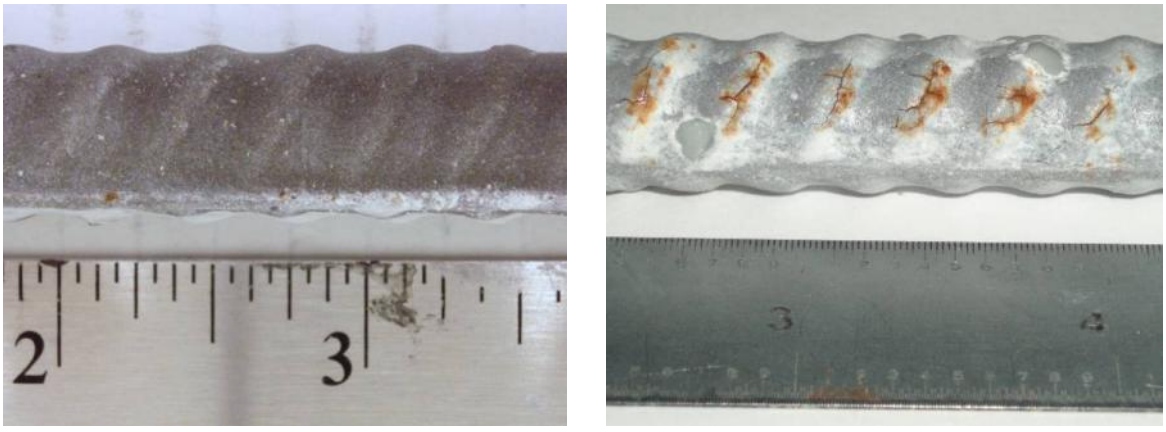

(a) 5th week (b) 12th week

Figure 6.5 A typical condition of a deformed 50/50 enamel-coated specimen after testing.

Similar to the deformed specimens, the smooth 50/50 enamel-coated specimens appeared to have performed well up until the 8th week of testing. Prior to the 8th week, specimens only exhibited minor "pin sized" areas of corrosion that were spread out uniformly along the length of each specimen. It wasn't until the 10th week of testing when the severity of each specimen's condition began to show. During the 10th week of testing, the 50/50 enamel coating began to show signs of spalling around the areas that exhibited earlier signs of corrosion. When the test was completed two weeks later, 42 percent of the coating along an average specimen showed signs of spalling. When the coating along a spalled area was removed, an extensive amount of corrosion was seen along the surface of the underlying steel bar, which is shown in Figure 6.6(a). Figure 6.6(b) indicates a typical piece of the 50/50 enamel coating that shows "pin sized" areas of corrosion along its surface while having an extensive amount of rust throughout its inner surface.

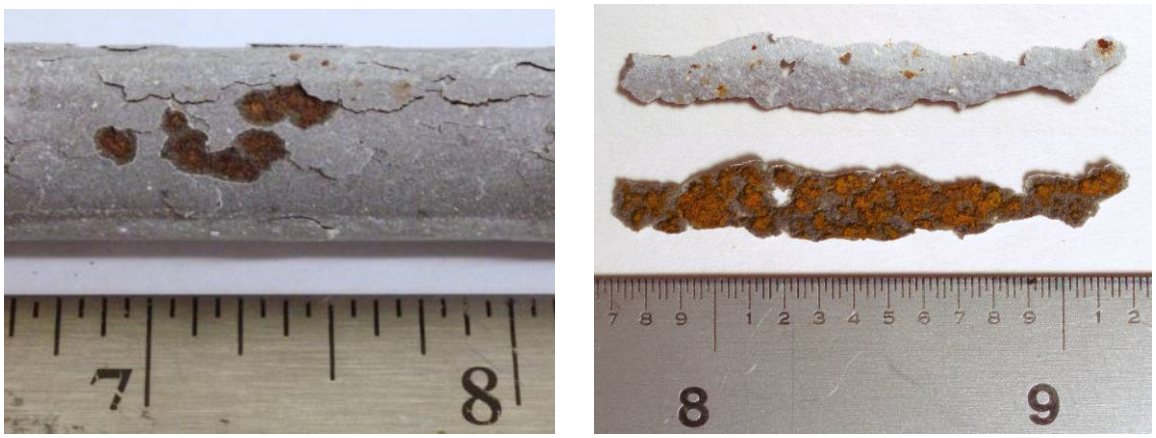

(a) Spalling of enamel coating (b) Top and bottom views of fallen-off pieces

Figure 6.6 A typical condition of 50/50 enamel coating along a smooth specimen.

Cross-sectional examination of the 50/50 enamel-coated specimens revealed that the thickness of the coating along a smooth specimen was between 7.9 and 11.8 mils (200 and 300 microns); whereas the thickness of the coating along a deformed specimen ranged from 7.9 and 29.5 mils (200 to 750 microns). This variation within the coating thickness was seen near transverse and longitudinal ribs, as shown in Figure 6.7.

The 50/50 enamel coating, throughout each cross-section, exhibited a grainy texture, which is shown in Figure 6.7(b), and a grayish brown color. However, at locations where the steel had begun to corrode, the color of the coating resembled that of red rust. This rusty-red coloring was not always uniform throughout the thickness of the coating. At times the outer surface of the coating would maintain its original grayish brown color while the inner surface of the coating became rusty-red due to corrosion, as shown in Figure 6.7(c).

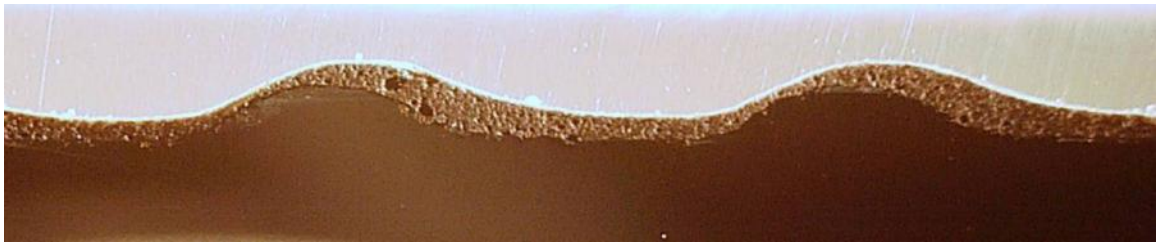

(a) Longitudinal view

(b) Granular texture

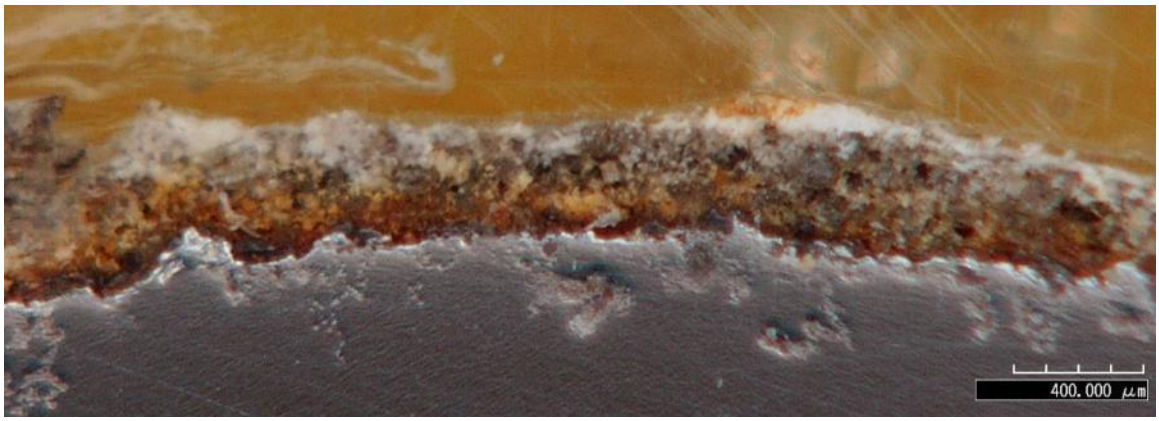

(c) Color gradient within and along a corroded section

Figure 6.7 Representative condition of 50/50 enamel coating along a deformed rebar specimen**.**

6.2.2.2. Double-coat enamel

The deformed double enamel-coated specimens showed "minor" signs of corrosion along a random portion of the transverse ribs within the first four weeks of testing. These areas of corrosion became more significant over the course of the remaining eight weeks. By the time the test was complete, 18 percent of the transverse ribs along an average specimen exhibited "moderate" signs of corrosion and 31 percent showed "minor" signs of corrosion. Therefore, after the twelve weeks of testing, a total of 49 percent of an average specimen's transverse ribs showed either "minor" or "moderate" signs of corrosion. The difference between "minor" and "moderate" signs of corrosion along a corroding rib may be seen in Figure 6.8. The longitudinal

ribs of each specimen showed minimal signs of corrosion with only one or two “pin sized” areas throughout each rib.

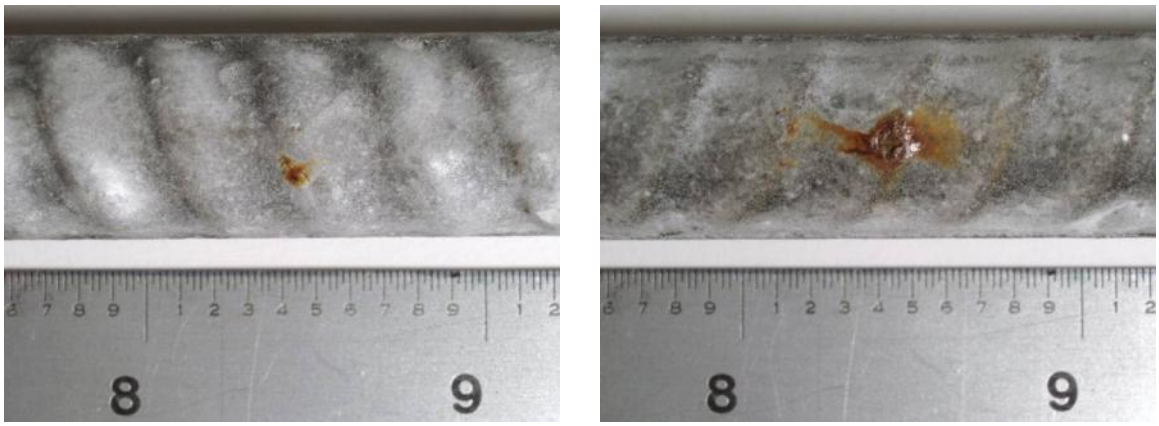

(a) “Minor” sign of corrosion (b) “Moderate” sign of corrosion

Figure 6.8 Typical transverse ribs along a double enamel-coated, deformed rebar specimen.

The smooth double coated enamel specimens showed little signs of corrosion throughout the twelve weeks of testing. When the test was complete, each of the eight specimens had, on average, a total of eight areas that exhibited signs of corrosion. Areas that showed signs of corrosion were classified as either “minor” or “moderate.” A typical “minor” and “moderate” area of corrosion may be seen in Figure 6.9. On average, three out of the eight areas that showed signs of corrosion were classified as “moderate.”

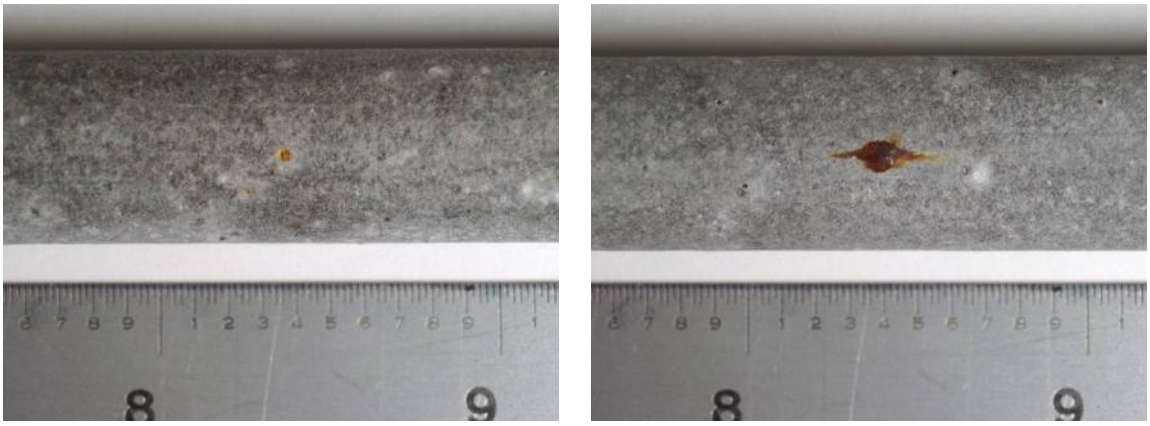

(a) “Minor” sign of corrosion (b) “Moderate” sign of corrosion

Figure 6.9 A typical surface condition along a double enamel-coated, smooth rebar specimen.

The cross-sectional evaluation of the double coated enamel specimens revealed that a boundary between the first and second applied coating was maintained during the second round of firing

and that only a minor amount of calcium silicate from the 50/50 enamel outer coating had percolated through the surface of the inner coating.

The double enamel coating was uniformly distributed along the length of each smooth specimen, which resulted in a coating thickness of around 15.7 mils (400 microns), as can be seen in Figure 6.10(d). However, the thickness of the coating along a deformed specimen fluctuated from 5.9 to 29.5 mils (150 to 750 microns). This fluctuation within the thickness of the coating was seen along the transverse ribs of the deformed specimens. At the locations where the coating was 29.5 mils (750 microns) thick, the boundary between the two layers was easily seen; whereas at locations along a specimen where the coating was thin, the boundary did not exist. When the boundary did not exist, the coating mainly consisted of a combination of the two applied coatings with a varying amount of calcium silicate. A typical distribution of the double enamel coating along a deformed specimen is shown in Figure 6.10(a-c).

(a) Typical longitudinal view of double coating on a deformed rebar

(b) Thick portion of double coating on a deformed rebar showing a distinct boundary

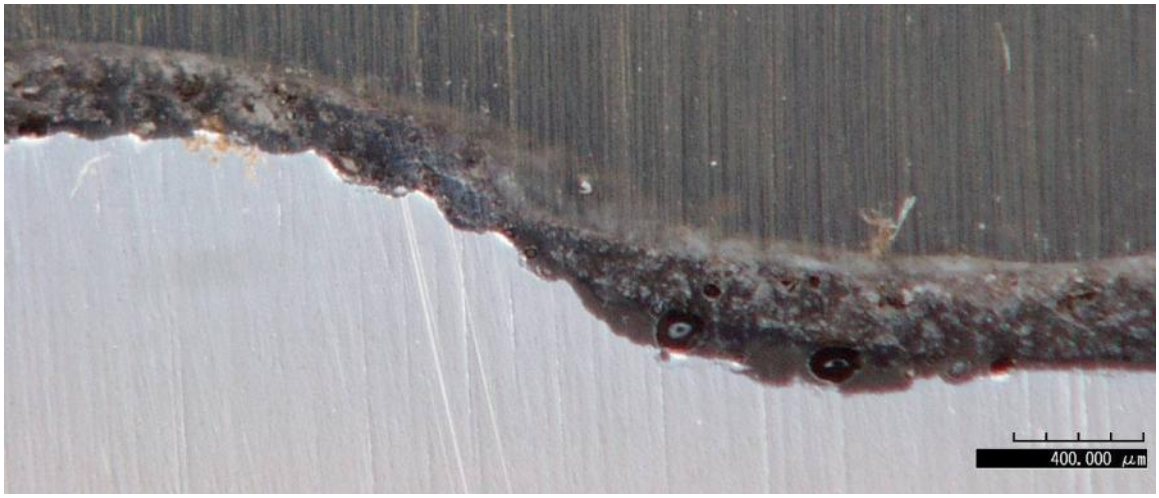

(c) Thin portion of double coating on a deformed rebar showing no distinct boundary

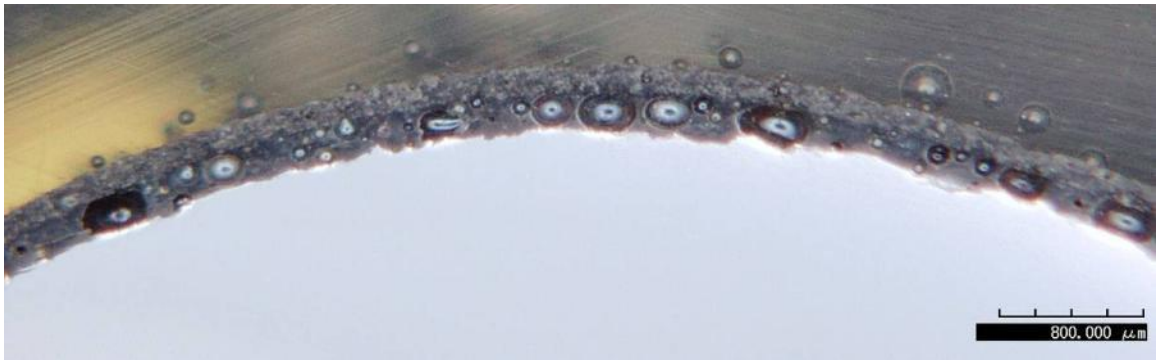

(d) Typical cross-sectional view of a smooth bar

Figure 6.10 Double coating condition on smooth and deformed bars.

6.2.2.3. Pure enamel

Within the first three days of testing, three out of the eight deformed pure enamel-coated specimens showed moderate signs of corrosion. By the second week, it was evident which of the eight specimens were performing well and which ones were not. The variation of test results is shown in Figure 6.11.

Of the three specimens that showed a poor performance throughout the test, 83 percent of their transverse ribs showed signs of either “minor” or “significant” corrosion after the test was finished. The difference between “minor” and “significant” corrosion for the deformed black enamel-coated specimens is shown in Figure 6.12. An average of 58 percent of the transverse ribs that exhibited signs of corrosion along the three specimens were labeled as “significant” and 31 percent of the area along the specimens’ longitudinal ribs showed extensive signs of corrosion. On average, 7 percent of the transverse ribs along the five remaining specimens showed “minor” signs of corrosion while 2 percent of the longitudinal ribs showed “significant” signs of corrosion. Among these five specimens, the average longitudinal rib showed corrosion along 3 percent of its length.

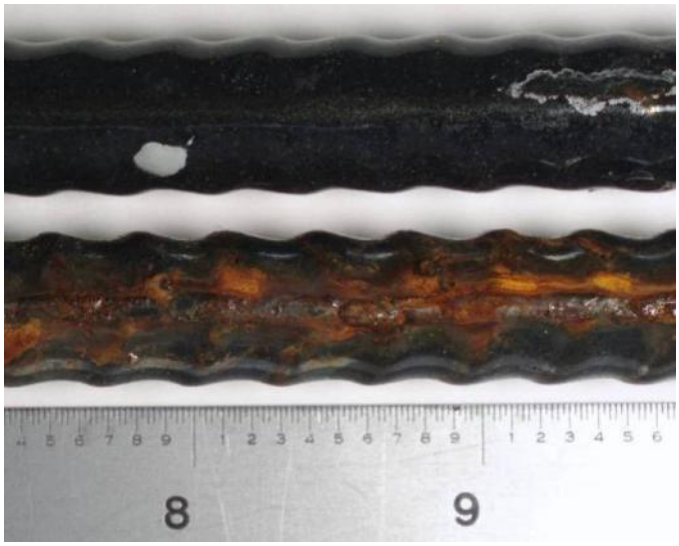

Figure 6.11 Variation within the test results for pure enamel-coated, deformed rebar specimens.

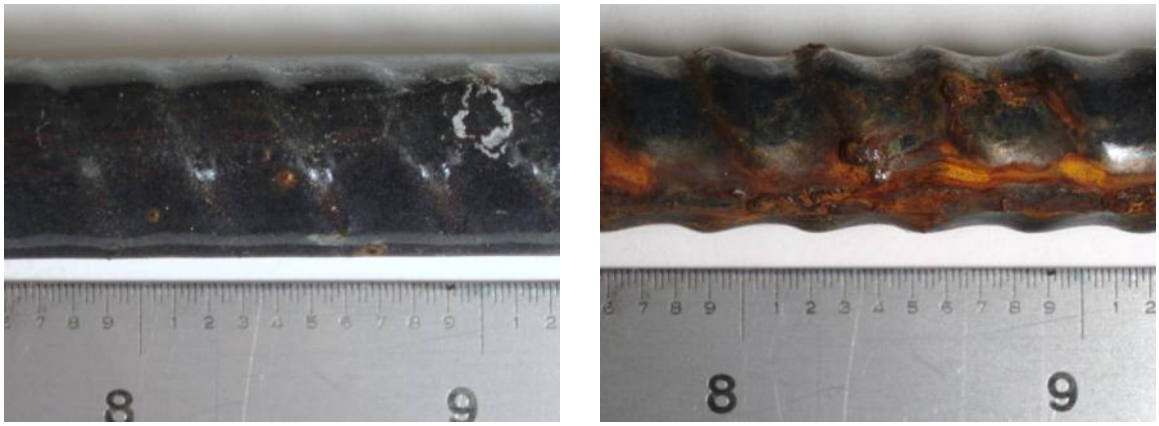

(a) “Minor” signs of corrosion (b) “Significant” signs of corrosion

Figure 6.12 A typical pure enamel-coated deformed rebar specimen showing corrosion along its transverse and longitudinal ribs.

The set of smooth pure enamel-coated specimens performed well throughout the twelve weeks of testing. When the test was complete, minor signs of corrosion were seen along the length of each specimen. Figure 6.13 shows a typical representation of the surface condition along a pure enamel-coated, smooth bar specimen after testing.

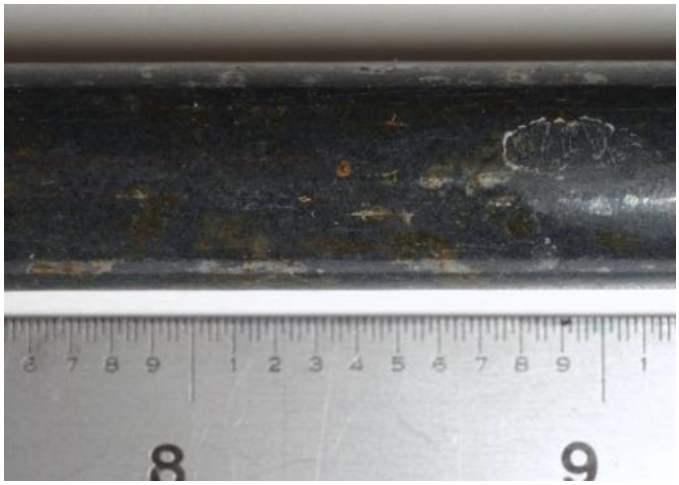

Figure 6.13 Surface condition along a pure enamel-coated smooth bar specimen after testing.

As seen in Figure 6.14, cross-sections of the smooth and deformed pure enamel-coated specimens revealed similar coating distribution patterns as those seen within the cross-sections of the 50/50 enamel-coated and double enamel-coated specimens. The coating was uniformly distributed along the smooth specimens and was approximately 9.8 mils (250 microns) thick, as shown in Figure 6.14(d). On the other hand, depending upon which of the eight deformed specimens were being examined, the thickness of the coating along an individual specimen ranged from 2.0 to 17.7 mils (50 to 450 microns) or 7.9 to 39.4 mils (200 to 1,000 microns), as shown in Figure 6.14(b). Figure 6.14(c) shows two images along a portion of the cross-section of a deformed bar that includes a damaged area within the coating. As shown in the two images, the bond between the enamel coating and the steel was maintained and only the exposed steel has corroded (i.e., no undercutting of the enamel coating occurred).

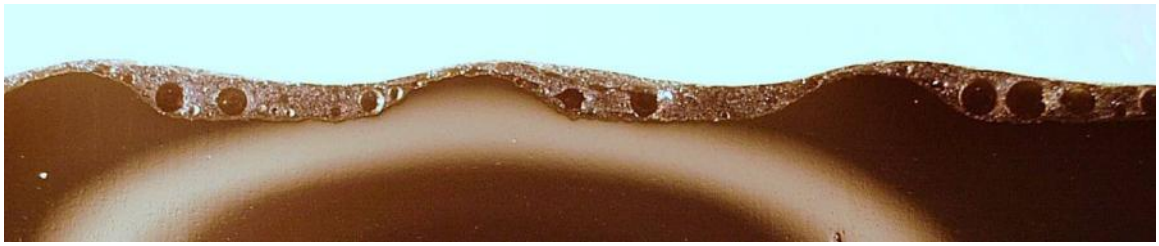

(a) Longitudinal view of a deformed bar that performed well

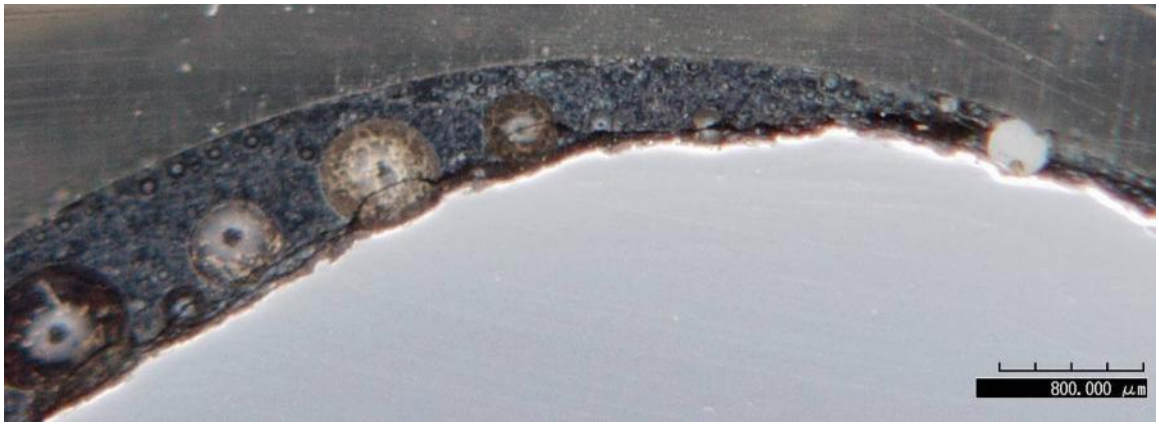

(b) Thickness variation of coating in a deformed bar

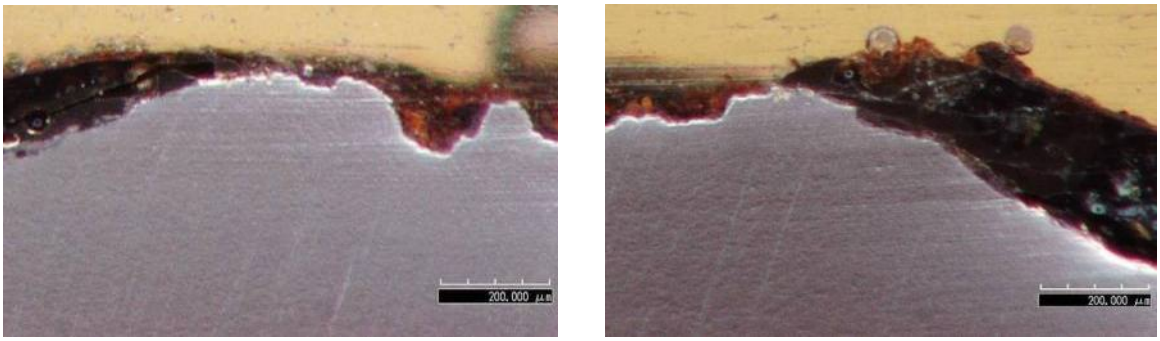

(c) No undercutting of coating even after significantly damaged on a deformed bar

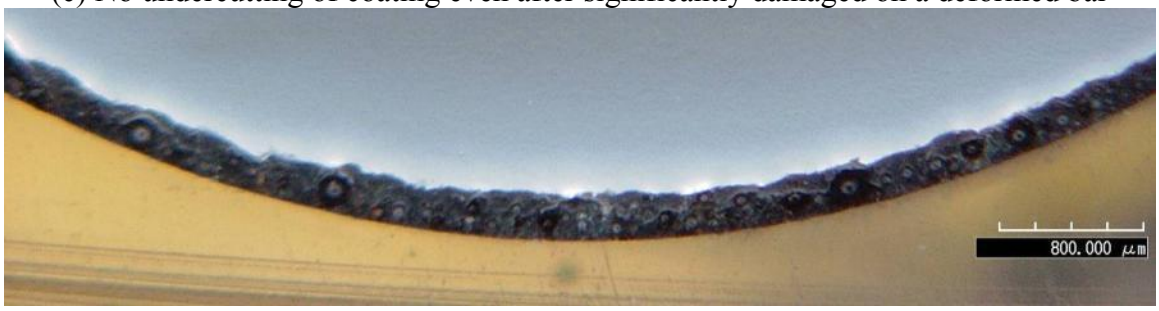

(d) Cross-sectional view of a smooth bar after testing

Figure 6.14 Thickness variation and corrosion condition of pure enamel coating.

6.2.2.2. Epoxy

Both the deformed and smooth epoxy-coated specimens performed well throughout the duration of the test. After testing, each specimen showed minor spots of corrosion that were between 7.9 and 15.7 mils (200 and 400 microns) in size. Typically these spots were low in number and uniformly distributed throughout the length of each specimen, as shown in Figure 6.15(a, b). However, these spots tended to increase in quantity and size along areas of the coating that appeared to have been degraded by excessive light exposure, as shown in Figure 6.15(c).

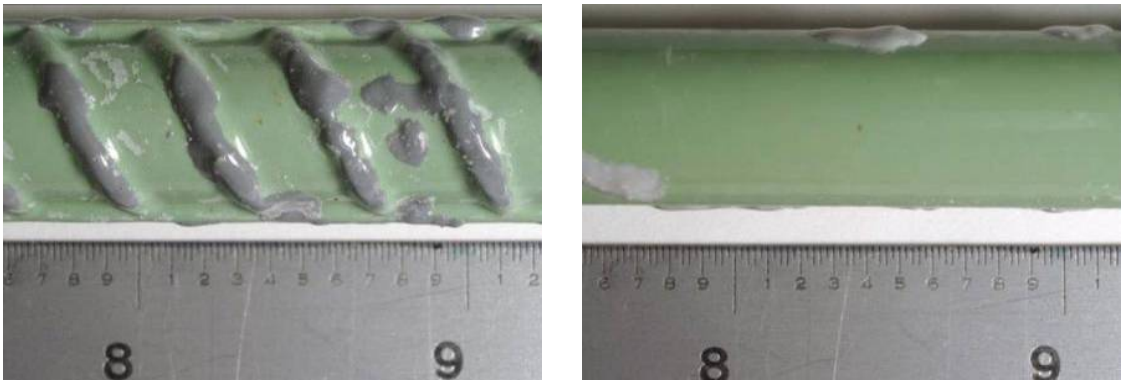

(a) Typical spots of corrosion in a deformed and a smooth bar after testing

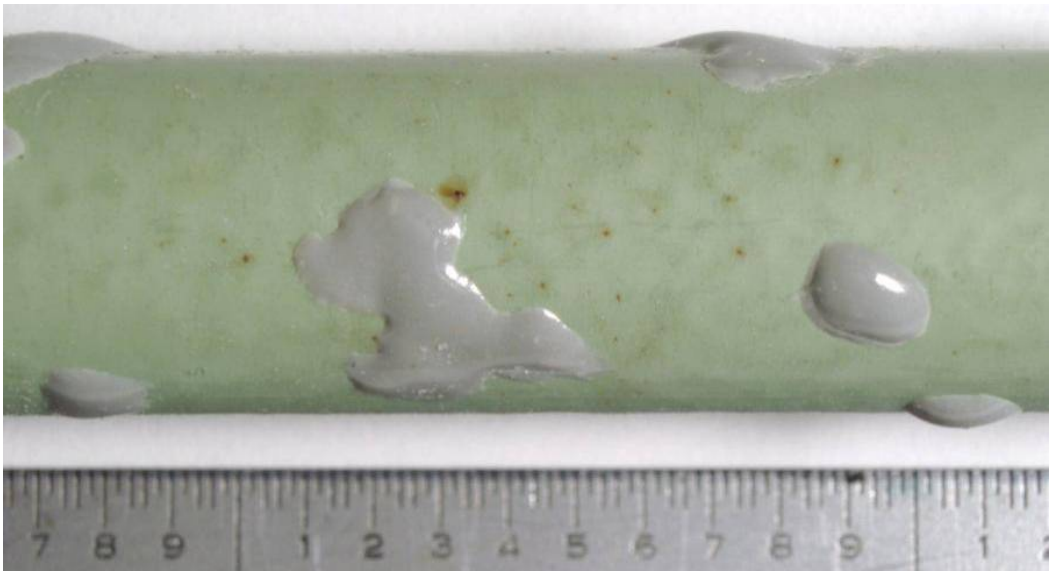

(b) Sign of degradation of an epoxy-coated smooth bar

Figure 6.15 Surface conditions of epoxy-coated bars**.**

Cross-sections of the epoxy-coated specimens indicated a uniformly distributed coating along the lengths of both the smooth and deformed specimens. The thickness of the coating ranged from 7.9 to 13.8 mils (200 to 350 microns) and when intact, appeared to be well bonded to the steel, as shown in Figure 6.16. However, at locations along a specimen where the coating was breached, a separation between the coating and the steel was observed and the underlying steel had begun to corrode. This undercutting of the coating is shown in Figure 6.16(b).

(a) Longitudinal view of a deformed bar

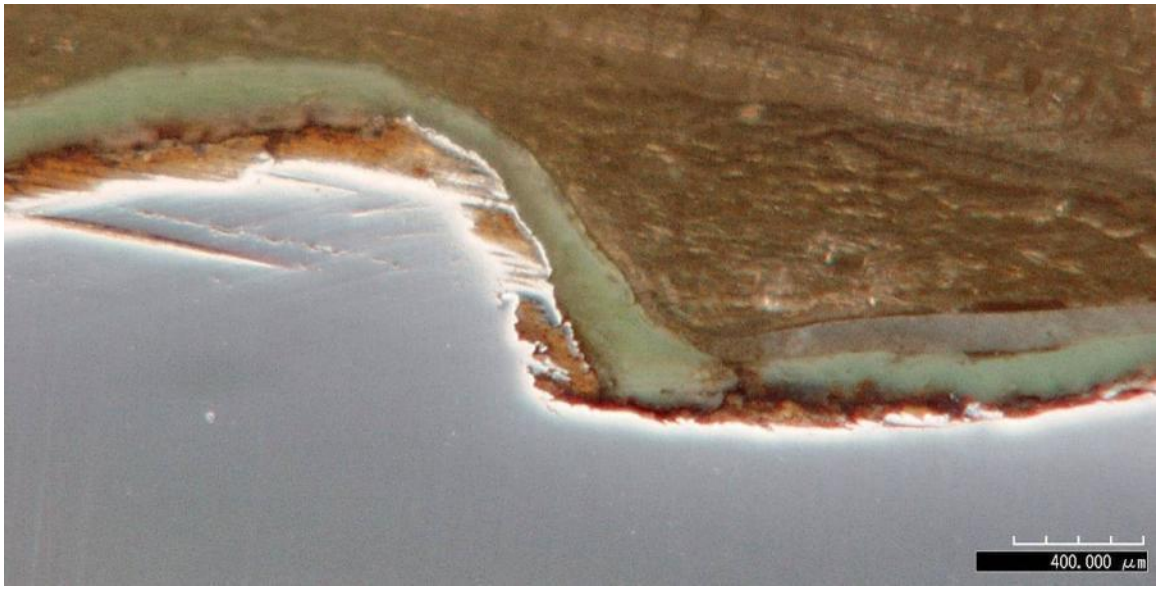

(b) Steel corroding underneath a slightly damaged section of epoxy coating after testing

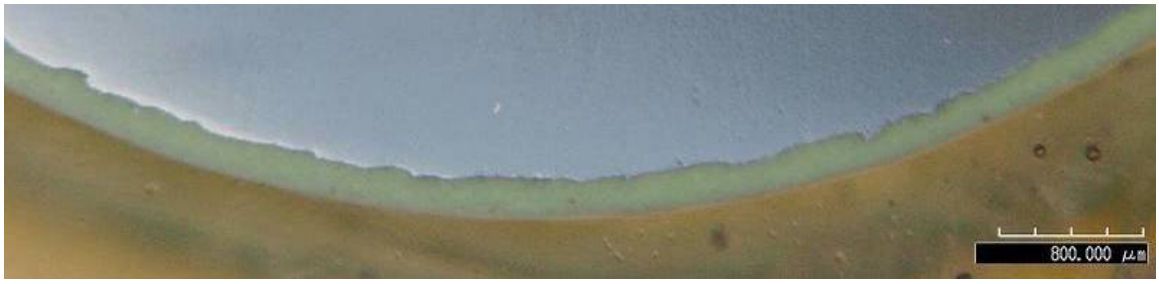

(c) Typical cross-sectional view of an epoxy-coated smooth bar after testing

Figure 6.16 Corrosion conditions of epoxy-coated bars.

6.2.3. Conclusions Based on Salt Spray Tests

The performance of the three enamel coatings largely depended upon the coating's thickness and the concentration of calcium silicate within the coating. The uniformly coated smooth specimens, with an average coating thickness of around 7.9 to 15.7 mils (200 to 400 microns), outperformed the inconsistently coated deformed specimens that possessed thinly coated areas along their transverse and longitudinal ribs. However, although having similar thickness distribution to the pure and double enamel coating, the 50/50 enamel coating performed better on

deformed specimens than on smooth specimens. This is likely attributable to a large quantity of calcium silicate within the coating.

When a large quantity of calcium silicate is added to a pure enamel mixture and then fired to create 50/50 enamel, a porous material is created. The pores throughout the 50/50 enamel, as shown in Figure 6.7(b), provide pathways for oxygen, moisture, and chlorides to reach the steel. The iron oxide formed during the corrosion process then slowly begins to outwardly diffuse toward the exterior surface of the coating, as shown in Figure 6.7(c). Therefore, the time it takes for a 50/50 enamel specimen to show any significant signs of corrosion is a function of the coating's thickness and the rate of diffusion of both the corrosive elements and the iron oxide. This would explain why the deformed 50/50 enamel specimens showed signs of corrosion earlier than the smooth specimens and why the visual signs of corrosion along the smooth specimens increased dramatically between the 8^{th} and 10^{th} week of testing.

The pure enamel, double enamel, and epoxy specimens all performed relatively well throughout the testing period. However, the deformed double enamel-coated specimens did show areas of weakness along a portion of their transverse ribs. These areas of weakness were thinly coated with what appeared to be an amalgamation of the two applied coatings. This mixing of the two coatings would, at times, lead to large concentrations of calcium silicate within the thinly coated sections of the coating. As a result, the coating along these sections exhibited similar properties to that of the 50/50 enamel.

The performance of a deformed pure enamel-coated specimen directly correlated to the minimum thickness of the applied coating along that specimen. The three specimens that performed poorly during the test had a minimum coating thickness of 2.0 mils (50 microns); whereas the five specimens that performed well during the test had a minimum coating thickness of 7.9 mils (200 microns). When damaged, the pure enamel coating maintained its bond with the steel and no undercutting was observed.

Both the deformed and smooth epoxy-coated specimens were uniformly coated and no significant signs of corrosion were observed along the surface of the specimens. However, when the coating showed signs of degradation in the form of discoloration, an increase in the amount of "pin-sized" areas of corrosion were observed. Undercutting of the coating was also observed along a section of a specimen that had a breach in the coating.

6.3. Accelerated Corrosion Test

Initially developed as a test to evaluate the corrosion resistance of post-tensioning grouts [Thompson et al., 1992], the accelerated corrosion test (ACT) method has been extended to evaluating the corrosion resistance of steel coatings [Volz et al., 2008]. Typically, the samples consist of cylindrically cast elements, each containing a single reinforcing bar, which are then placed into a 5 percent by weight NaCl electrolyte corrosion cell. Once positioned within the corrosion cell a constant potential is applied to the specimen and the resulting current is measured over time. The test is completed at the onset of intense corrosion, which is detected from an abrupt increase in the monitored electric current. The length of time to complete this test depends on the ability of the system to resist the onset of corrosion. In general, these tests run between 300 and 1500 hours, not including sample preparation.

The benefit of the ACT is that the applied potential will force the chloride ions to attack the coated rebar. This test will thus expose any material or processing defects in the coating that would allow the transport of chloride ions to the steel surface and allow initiation of corrosion. The test will also partially determine whether the enamel coating has the ability to heal itself through hydration of the embedded calcium-silicate.

Indirectly, the test also examined the ability to effectively coat a deformed bar through the dipping process used for the enamel coatings. This was accomplished by testing both smooth and deformed coated bars. As a basis for comparison, both uncoated and epoxy-coated bars were included within this test.

Testing began on August 11, 2009 and was completed on August 1, 2010. During that time, a total of 144 specimens were tested. Of the 144 specimens, 80 were grouted and 64 were non-grouted. Sixty-four out of the 80 grouted specimens contained bars that were coated with one of the four coatings examined within this test. The four coatings tested were: 50/50 enamel, double enamel, pure enamel, and epoxy. Half of the remaining 16 grouted specimens contained a smooth uncoated steel bar while the remaining eight specimens contained a deformed uncoated steel bar. Eight out of the 16 specimens with one of the four coatings are deformed bars and the remaining eight are smooth bars.

6.3.1. Technical Approach

6.3.1.1. Test specimens

A specimen consisted of one, 15-inch long (381 mm), coated or uncoated steel bar that was either grouted or non-grouted. Depending upon the specimen, the bar was either a smooth dowel ½″ (13 mm) in diameter or a No. 4 (No. 13), grade 60, deformed bar. After the bars were sectioned to the proper length, a portion of the coating along each bar was removed. The removal of a bar's coating occurred along a ¾-inch (19 mm) long section that was located at one end of the bar, as shown in Figure 6.17. This section was located above the electrolyte of the corrosion cell and provided the electrical connection necessary for the test. While preparing the epoxy-coated bars, two additional steps were taken. The two additional steps involved beveling the end of the bar that was still partially coated and then cleaning the bar with soap and water.

Figure 6.17 A typical smooth and deformed coated bar examined during ACT testing.

Two layers of Loctite's Aquamarine Epoxy were uniformly applied along the beveled end of each specimen, as shown in Figure 6.17. While applying the second layer of epoxy, specimens

were examined for areas of damage which may have been caused through handling and/or transporting. Each area exhibiting signs of damage received one layer of epoxy. A layer of epoxy was also applied to any rare imperfections that may have been seen within each coating. These areas of imperfections were deemed as manufacturing defects and were seen within each type of coating.

Bars were grouted within polyvinyl chloride (PVC) molds that were constructed using three pieces of PVC piping. The three pieces measured 5.9 in. (150 mm), 3.5 in. (90 mm), and 2.4 in. (60 mm) in length, as shown in Figure 6.18. Prior to constructing the molds, two longitudinal slits were cut along each 3.5-inch (90 mm) long section of PVC. Constructing a mold involved connecting the three pieces of PVC, in the order shown in Figure 6.18, with silicone and duct tape. After securely connecting the three pieces of PVC, any silicone that had accumulated along the interior surface of the mold was removed with the use of paper towels. The partially completed mold was then set aside for a period of approximately 24 hours. After the silicone had cured, each mold was then capped using a properly sized PVC cap and PVC cement. When completed, a mold measured approximately 12.2 in. (310 mm) in length and had an inner diameter of 1¼ in. (32 mm).

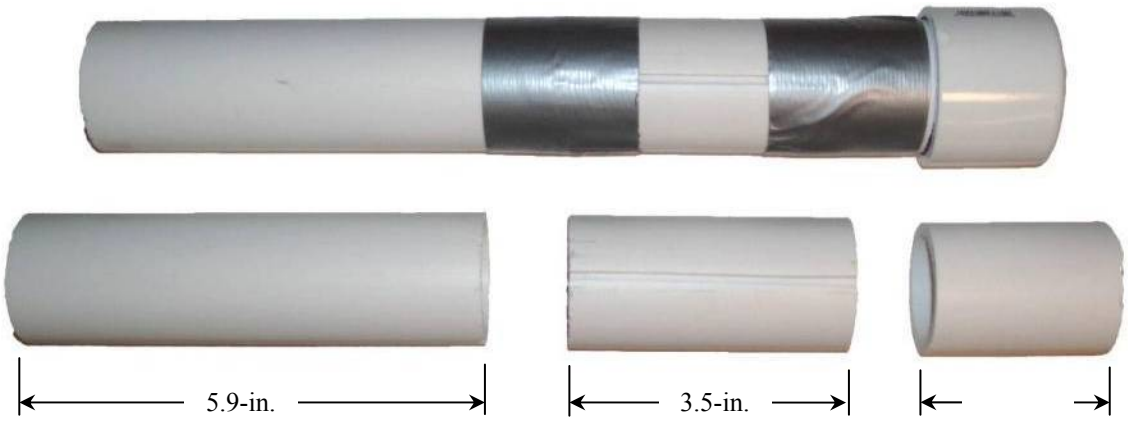

Figure 6.18 The three sections of PVC piping alongside a completed mold which was used during the casting of a grouted ACT specimen.

A total of nine specimens were cast with what is commonly referred to as a "neat grout." A batch of grout was prepared using approximately 10 lbs. (4.5 kg) of Type II portland cement and a water-to-cement ratio of 0.45. The grout was batched within a 2 gallon (7.6 liter) container using a high-shear mixer. After the grout had been thoroughly mixed, half of the grout was transferred to a pitcher. A plastic spacer and the epoxy-coated end of a bar were then placed within the mold. The plastic spacer was used to centrally position the bar along the bottom of the mold. Any bar that was coated with 50/50 or double enamel was first doused with deionized water using a squirt bottle. Dousing a bar with deionized water was considered complete when the coating of the bar had been fully saturated and excess water began to drip from the epoxy-coated end of the bar. Once a bar was properly positioned within a mold, the mold was then filled with grout in three equally sized lifts. After each lift the bar was slowly twisted while the mold was tapped. Once fully grouted, the bar was then centrally positioned along the top of the mold using a second plastic spacer. A plastic bag was then placed over the top of the specimen

and secured with a rubber band. The specimen was then transferred to a curing chamber for 28 days. The same procedure was then repeated for the remaining eight specimens within the set.

6.3.1.2. Test preparation and setup

6.3.1.2.1. Single Specimen Test

Preparation of the non-grouted specimens varied slightly depending on the particular specimen coating with unhydrated calcium silicates. Therefore, as a way to promote the hydration of the calcium silicate prior to testing, each specimen coated with reactive enamels was first placed within a pitcher containing deionized water for a period of three days. After three days of soaking, the specimen was then permitted to air-dry for a minimum of 24 hours prior to initiating the test. Specimens containing no calcium silicate within their coating, such as the pure enamel-coated and epoxy-coated specimens, were cleaned with soap and water before they were tested.

Pretest preparations for grouted specimens were identical for all specimen types. Preparing a set of grouted specimens began after at least 28 days of curing. After removing the nine specimens from the curing chamber, they were immediately placed within a 5 gallon (18.9 liter) container partially filled with tap water. The two portions of duct tape used to connect the three sections of PVC were removed and the exterior surface of each specimen was cleaned using tap water. Using sandpaper, any rust that had gathered along the end of the specimen which contained the ¾ in. (19 mm) section of exposed steel was removed. After the surface of each specimen was cleaned, the 3.5-inch (90 mm) long section of PVC containing two longitudinal slits was removed from each specimen. Any silicone that remained along the surface of the freshly exposed grout was removed while the grout was inspected for voids and/or defects. Any specimen containing a void larger than that shown in Figure 6.19 was omitted from the test. If no individual specimen exhibited any detrimental defects within its grout, eight randomly selected specimens were chosen for the test.

Figure 6.19 A void detrimental to the specimen's performance in the ACT test.

After prepping a set of specimens, each specimen was then placed within a corrosion cell, as shown in Figure 6.20. The corrosion cell consisted of a glass beaker that contained approximately 0.8 gallons (3 liters) of electrolyte. The electrolyte was composed of deionized water and 5 percent ACS grade sodium chloride (NaCl) by weight. Before batching the solution, the deionized water was given a minimum of 24 hours to reach an ambient temperature of approximately 68°F (20°C). Once a specimen was positioned within the solution, a plexiglass top was placed over the beaker. A brass grounding clamp was then attached to the exposed steel located at the top of the specimen. Both the counter and reference electrodes were then partially inserted into the solution. The centroids of the counter and reference electrodes were equally spaced at a distance of approximately 2.4 in. (60 mm) from the center of the specimen (the working electrode). As shown in Figure 6.20, the counter and reference electrodes were supported by the plexiglass top and were located on opposite sides of the specimen. The counter electrode, supported approximately ½ in. (13 mm) above the bottom of the beaker, was made of a graphite rod that was ½ in. (13 mm) in diameter and 12 in. (305 mm) in length. The graphite rod, manufactured by Graphtek LLC, was a grade GM-10. A gel-filled saturated calomel electrode (SCE), manufactured by Fisher Scientific, was used as the reference electrode and was positioned at a depth of approximately 3½ in. (89 mm) within the solution. After the electrodes were partially immersed within the solution, they were then individually connected to an eight-channel ECM8 multiplexer which was attached to a Series G300 potentiostat. Both the multiplexer and the potentiostat were manufactured by Gamry Instruments.

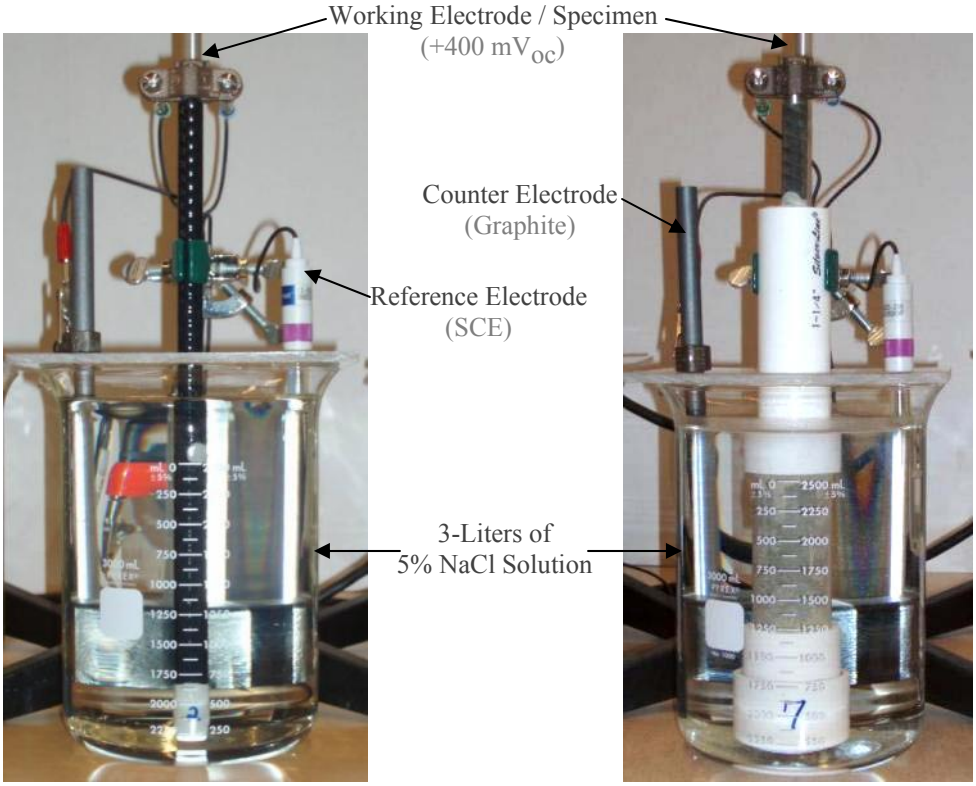

(a) Non-grouted specimen (b) Grouted specimen

Figure 6.20 Test setup of a typical specimen in a beaker.

After properly connecting each of the eight corrosion cells to the multiplexer, the open circuit (OC) potential of each specimen was measured using the potentiostat and a computer that had Gamry Instruments Framework software, Version 5.50. The accuracy of the potentiostat in measuring the OC potential of a specimen was within ±1 mV of its actual value. Once the OC potential of each specimen had been measured, a constant +400 mV potential was applied to each specimen. The accuracy of the potentiostat in applying a potential to a specimen was within ±2 mV of the specified value. Depending upon the type of specimen being tested, the corrosion current of each specimen was recorded every 5 or 30 minutes. The accuracy of the potentiostat in measuring the corrosion current of a specimen was within ±50 pA. Testing of a specimen was considered complete the moment a continual and/or substantial increase in a specimen's corrosion current was reported. When the testing of a specimen was complete, the specimen was disconnected and removed from the corrosion cell in which it resided.

6.3.1.2.2. Multiple Specimen Test

To create the same corrosion environment, 12 deformed bars measuring 24 in. long were tested simultaneously in a rectangular plastic container measuring 44 in. long, 39 in. wide, and 24 in. deep. The specimens included two uncoated steel bars, five 50/50 enamel-coated bars, and five epoxy-coated bars. To study the effect of coating damage on the corrosion resistance of bars, epoxy-coated and enamel-coated rebar were pre-damaged using an impact test apparatus designed according to the ASTM G14. As shown in Figure 6.21, the apparatus consists of a 2-lb. (0.91 kg) steel rod with a hemispherical head, a vertical section of hollow aluminum tubing to guide the rod, and a horizontal section of steel angle to position the rebar. The bars were secured to the steel angle with clamps, and the tup was dropped from a height of 36 in. (914 mm) to damage the coatings. The five coated bars of each type (enamel- or epoxy-coated) were then further divided into: one undamaged and four damaged at 1 in., 2 in., 3 in., and 4 in. intervals, respectively. The epoxy- and enamel-coated rebar specimens with approximately 1-in.-interval damage are presented in Figure 6.22.

Figure 6.21 Impact test apparatus.

(a) Intact epoxy-coated rebar

(b) Damaged epoxy-coated rebar

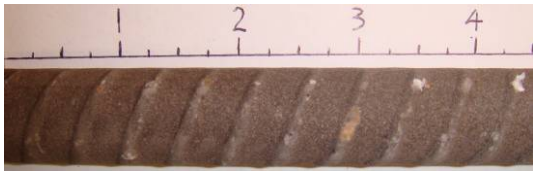

(c) Intact enamel-coated rebar

(d) Damaged enamel-coated rebar

Figure 6.22 Surface conditions of epoxy- and enamel-coated rebar specimens.

All specimens were submerged in a solution of distilled water and 15% NaCl by weight. The distilled water was added periodically to compensate for evaporative loss.

As illustrated in Figure 6.23, the 12 specimens were arranged in a circular configuration around a central graphite rod, which serves as the cathod. Graphite was chosen to minimize the effects of corrosion on the cathode. The 12 24-in. bars were suspended from an acrylic glass top that was placed on the container, but also allowed to rest on the bottom of the container. Each bar had 14 in. of its length submerged into the NaCl solution. Machine screws were welded to the top of each bar, and a wire attached to the machine screws. The wire led to a 10-ohm resistor, across which a differential voltage measurement was taken. Each of these wires was then connected in parallel to a voltage source which provided a constant 50mV to the tested bars. A diagram of the corrosion test setup can be seen in Figure 6.24. The rebar specimens were connected to the positive end of the power supply and the graphite rod was connected to the negative end of the power supply. The external electrical potential forced the rebar to corrode. The corrosion levels were evaluated using the corrosion current, which was calculated from the voltage drop across each resistor. The test lasted for 1400 hours. Data measurements were taken every minute for the duration of the test.

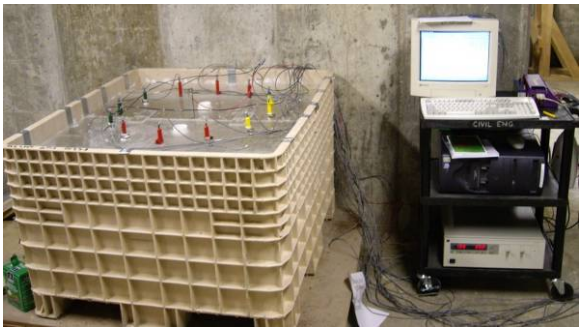

Figure 6.23 ACT setup in a container.

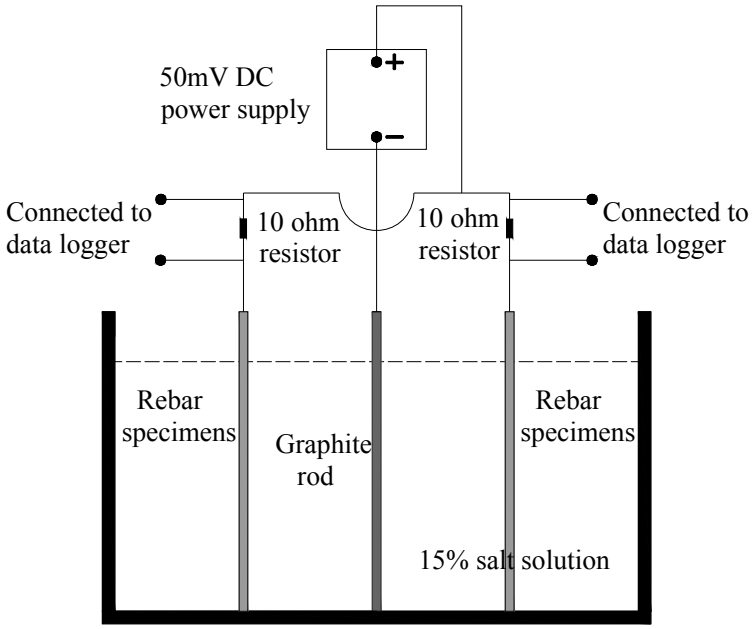

Figure 6.24 ACT schematic diagram with multiple specimens.

6.3.2. Results and Discussion

6.3.2.1. Single specimen tests

The complete results for each individual specimen are presented in Appendix B. The ACT results are typically reported as the average of the time-to-corrosion (t_{corr}) values for a set of eight specimens of the same type. When a t_{corr} value corresponding to a single specimen fell outside the range of two standard deviations above or below the set's mean t_{corr} value, the specimen was discarded from the calculation as an outlier. Moreover, if a grouted specimen reported erratic corrosion current readings within the first 24 hours of testing, the result obtained from that specimen was excluded from the calculation. Of the 18 specimen sets, three sets contained a specimen that was excluded from the calculation of the set's average t_{corr}. Those three sets were: grouted deformed uncoated, grouted deformed 50/50 enamel-coated and non-grouted deformed 50/50 enamel-coated. However, although normally reported as an average of eight specimens, the ACT testing protocol allows for a minimum of six specimens to represent t_{corr} for a set.

In some cases, there is a degree of judgment on determining the t_{corr} for a particular specimen. Three commonly observed test results are shown within Figure 5.25. The result labeled "A" in Figure 5.25 was commonly seen while testing a typical non-grouted specimen; whereas the results labeled "B" and "C" were commonly seen while testing grouted specimens. When a test result for a non-grouted specimen resembled that of "A," the specimen received a t_{corr} value of zero (0) hours. The justification for assigning a t_{corr} value of 0 hours is that a significant level of corrosion current was reported throughout the duration of the test and visible signs of corrosion were seen along the specimen shortly after the test was initiated. Conversely, a specimen that produced a result similar to that which is labeled "B" in Figure 5.25 would have received a t_{corr}

value that was measured from the start of the test to the moment when the well defined spike in corrosion current first appeared. For example, the specimen that produced the result labeled "B" in Figure 5.25 received a t_{corr} value of 530 hours. If a specimen exhibited a minor increase in corrosion current over a long period of time that was then followed by a more significant increase in corrosion current, the t_{corr} value for that specimen would have been measured from the start of testing to the point at which the first significant increase in corrosion current was first detected. For instance, the specimen that produced the result labeled "C" in Figure 5.25 was assigned a t_{corr} value of 690 hours.

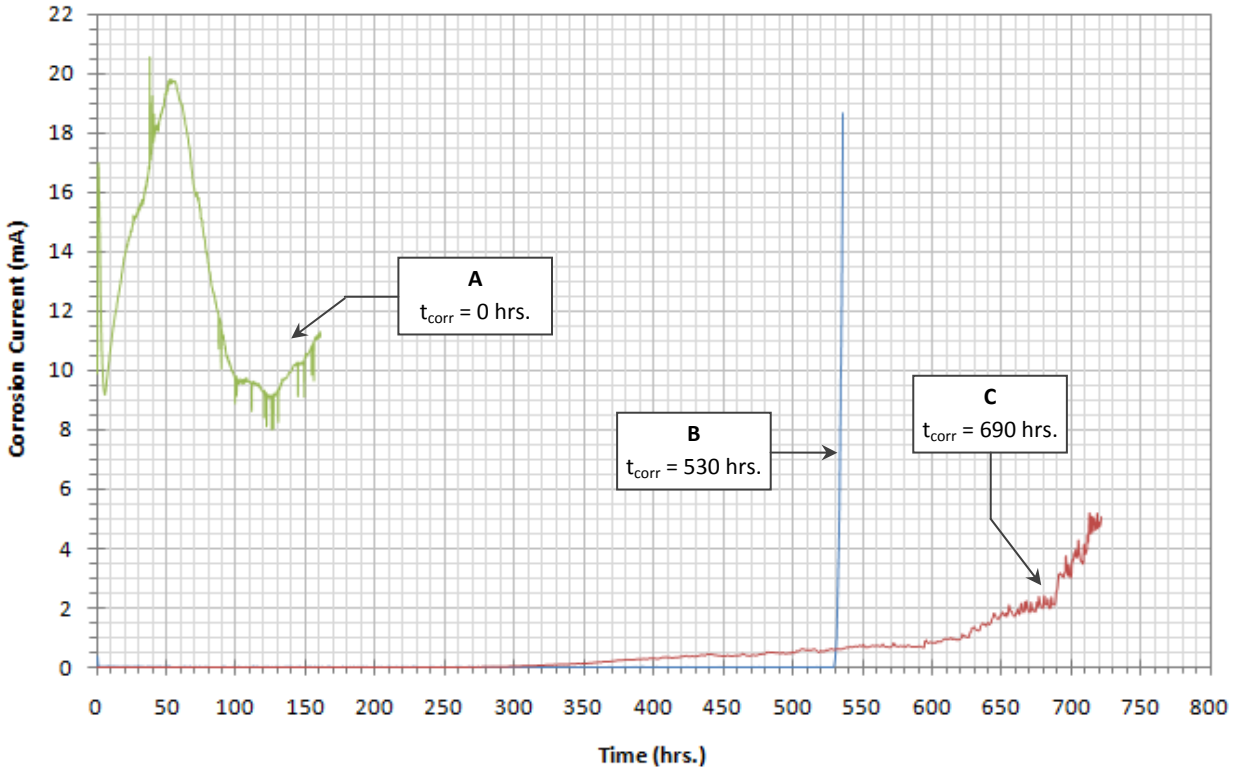

Figure 6.25 Three test results commonly seen during the ACT phase.

6.3.2.1.1. Non-Grouted Specimens

A summary of the ACT results for the non-grouted specimens is shown in Figure 6.26. The 95 percent confidence interval for each set's average t_{corr} is also included in Figure 6.26. A set's confidence interval was developed using the standard error of a set's mean value (SEM). The SEM for a set of specimens was calculated by dividing the standard deviation of the sample set by the square root of the number of specimens used in deriving the set's average t_{corr} value.

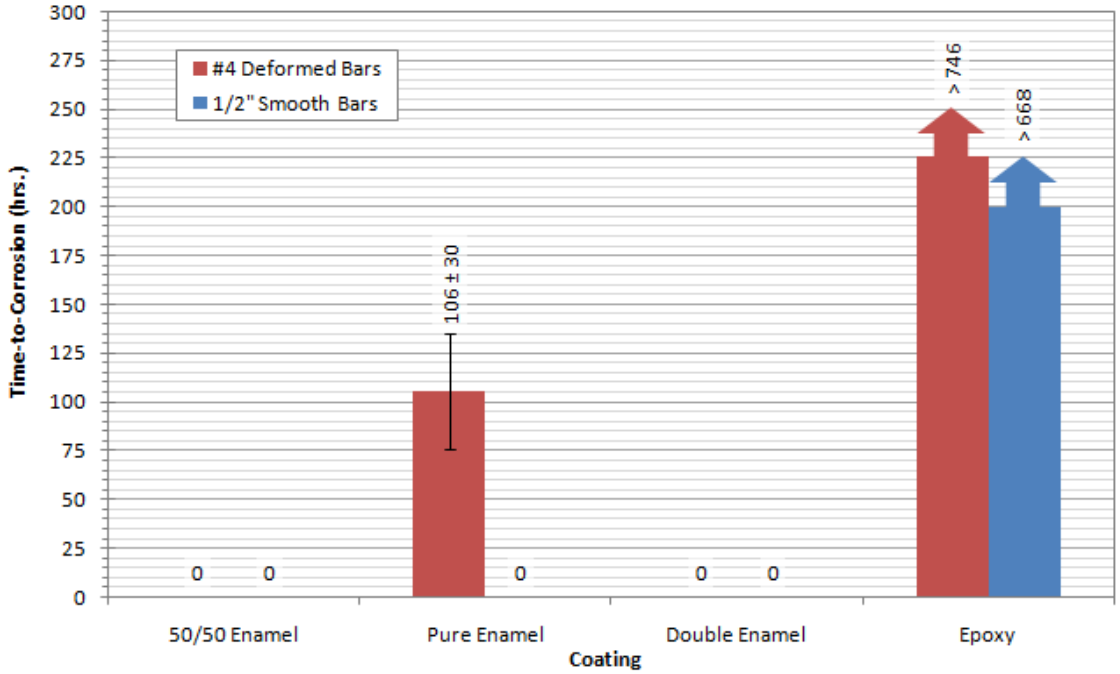

Figure 6.26 Test result summary for the non-grouted specimens.

Of the eight non-grouted specimen sets, only three sets resisted corrosion for an appropriate time. Those three sets included deformed pure enamel-coated bars and both smooth and deformed epoxy-coated bars. As shown within Figure 6.26, the deformed pure enamel-coated bars reported an average t_{corr} of 106 hours, while both the smooth and deformed epoxy-coated bars exhibited no visible signs of corrosion after 668 and 746 hours of testing, respectively. Testing of the epoxy-coated specimens ended prematurely, so to avoid any complication with the scheduling of the remaining tests.

6.3.2.1.2. Grouted Specimens

A summary of the ACT results for the grouted specimens is shown in Figure 6.27. The 95 percent confidence interval for each set's average t_{corr} is also included in the figure. A set's confidence interval was developed using the standard error of a set's mean value (SEM). The SEM for a set of specimens was calculated by dividing the standard deviation of the sample set by the square root of the number of specimens used in deriving the set's average t_{corr} value.

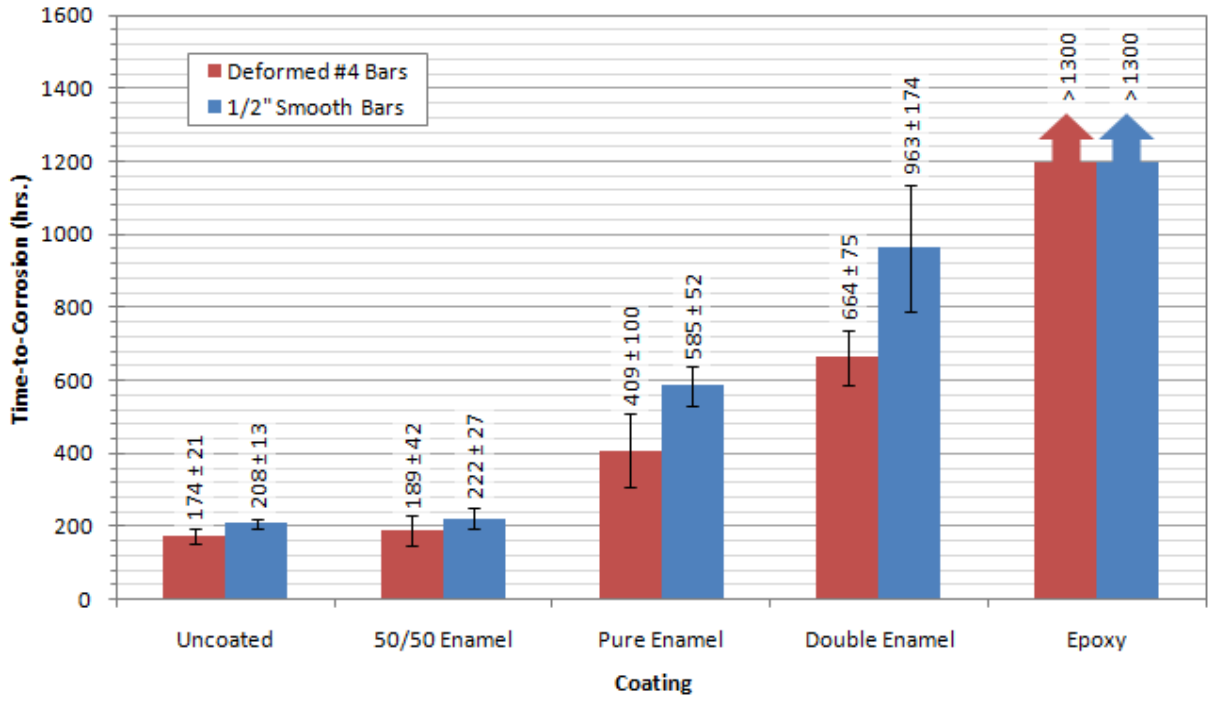

Figure 6.27 Test result summary for the grouted specimens.

Figure 6.27 clearly indicates the relative ability of each of the coating types to protect the underlying steel. Also, in general, the smooth bars exhibited a longer t_{corr} value than the deformed bars, with the difference becoming more pronounced as the relative coating performance improved. A minor difference was observed between the average t_{corr} values obtained for both the grouted uncoated and grouted 50/50 enamel-coated specimens. The average t_{corr} values for the grouted pure and double enamel-coated specimens, on the other hand, were approximately 2.4 and 4.0 times greater than that of the grouted 50/50 enamel coated specimens, respectively. However, among the pure and double enamel-coated specimens, the average t_{corr} for the deformed specimens varied significantly from that of the smooth specimens. For example, as shown in Figure 6.27, the average t_{corr} values for the smooth and deformed pure enamel-coated specimens were 409 and 585 hours, respectively. These two values corresponded to a 43 percent difference in t_{corr}. However, using the 95 percent confidence interval, the difference between those two values may vary from as low as 5 percent to as high as 106 percent. The coating that reported the greatest difference between the average t_{corr} of the smooth and deformed specimens was the double enamel-coating. Using a 95 percent confidence interval, the difference between the grouted smooth and deformed double enamel-coated specimens may vary from 7% to 193%. As indicated in Figure 6.27, the deformed double enamel-coated specimens reported an average t_{corr} value of 664 hours, which was 31% lower than that of the smooth double enamel-coated specimens.

Of the grouted specimens, the highest t_{corr} value was reported by both the smooth and deformed epoxy-coated specimens. The testing of both sets lasted for a period of approximately 1300 hours. Similar to the testing of the non-grouted epoxy-coated specimens, testing of the grouted epoxy-coated specimens was completed prematurely due to deadlines within the study.

6.3.2.2. Multiple specimen tests

Figure 6.28 presents the recorded corrosion currents from all specimens as a function of time. For uncoated (Br) and for enamel-coated (EN) rebar, the corrosion current increased with time and approached a nearly constant value after 600 hours. The asymptotic corrosion current is between 2.00 mA and 2.25 mA for uncoated rebar, and between 0.25 mA and 0.50 mA for enamel-coated rebar. The corrosion current for epoxy-coated (EP) bars are always less than 0.1 mA. The corrosion current densities for all the tested rebar are listed in Table 6.2. The corrosion current of enamel-coated steel bars lies between those of uncoated bars and epoxy-coated bars. The corrosion current density is approximately 77.4 uA/in^2 (12 uA/cm^2) for uncoated rebar, 12.9 uA/in^2 (2.00 uA/cm^2) for enamel-coated rebar, and 0.3 uA/cm^2 for epoxy-coated rebar. Note EN-1" in Figure 6.28 and Table 6.2 means an enamel-coated specimen with damage at 1 in. interval.

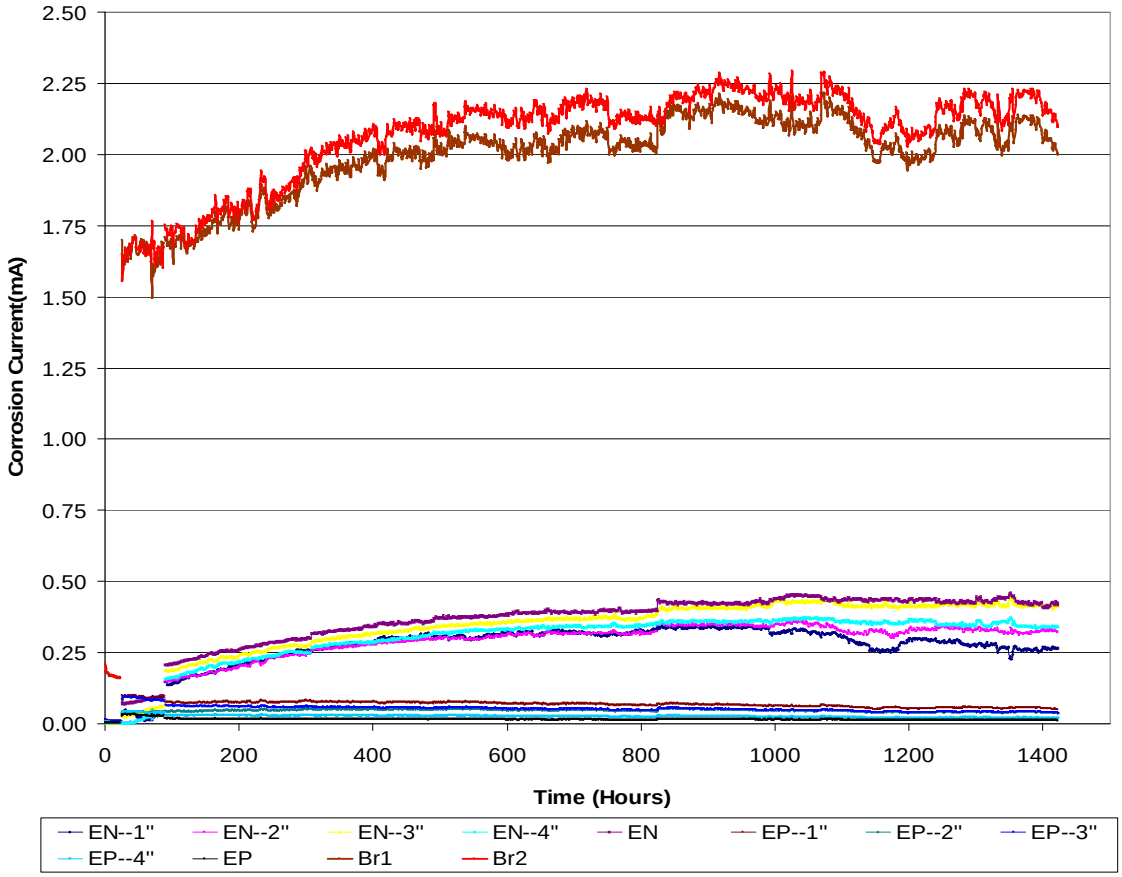

Figure 6.28 Corrosion currents of the 12 tested bars.

Table 6.2 Corrosion current (uA) and current densities (uA/in^2)

Specimen	Br1	Br2	EN	EN-1″	EN-2″	EN-3″	EN-4″	EP	EP-1″	EP-2″	EP-3″	EP-4″
Current	12.00	12.15	1.70	2.40	1.86	2.32	1.98	0.09	0.37	0.27	0.28	0.14
Density	77.4	78.37	10.97	15.48	12.00	14.96	12.77	0.58	2.39	1.74	1.81	0.90

Figures 6.29 and 6.30 are plots of corrosion current as a function of time for enamel- and epoxy-coated rebar, respectively. For enamel-coated rebar, a closer damage spacing or larger damage area does not necessarily indicate a greater corrosion current. As illustrated in Figure 6.31, this observation can be verified by inspection of the surface conditions of enamel-coated rebar after testing; corrosion did not always occur around the damaged areas and undamaged areas can be corroded as well. This result is likely due to pores in the enamel coating. For epoxy-coated rebar, intact rebar indicates the lowest corrosion current in comparison with damaged ones, and the 1″-interval damage caused the highest corrosion current. Abrupt changes in the plots coincide with interruption of the tests for data retrieval.

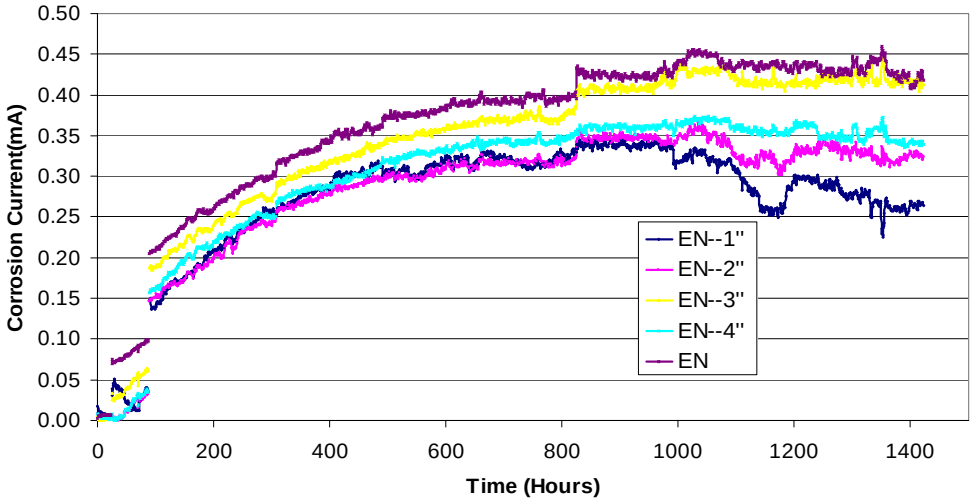

Figure 6.29 Corrosion current of enamel-coated rebar.

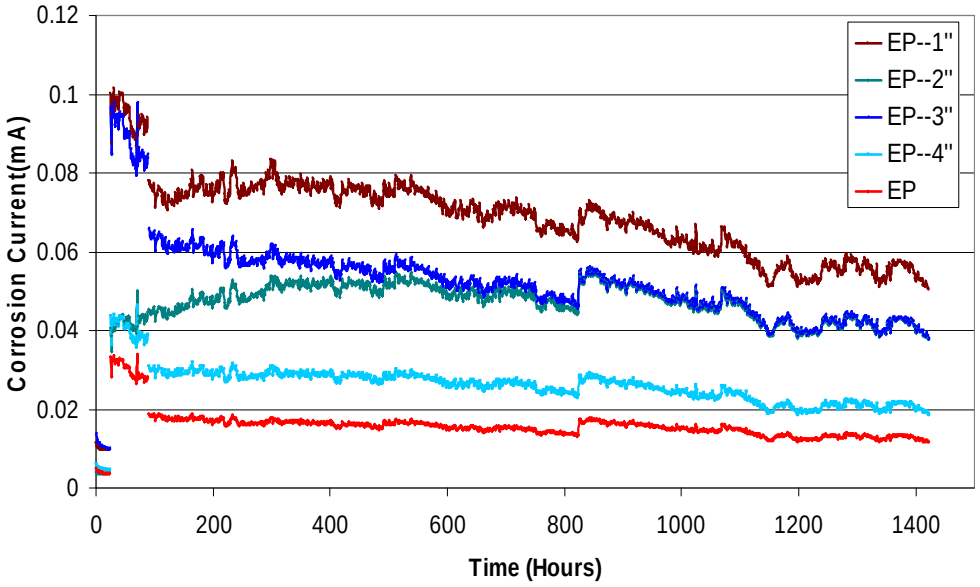

Figure 6.30 Corrosion current of epoxy-coated rebar.

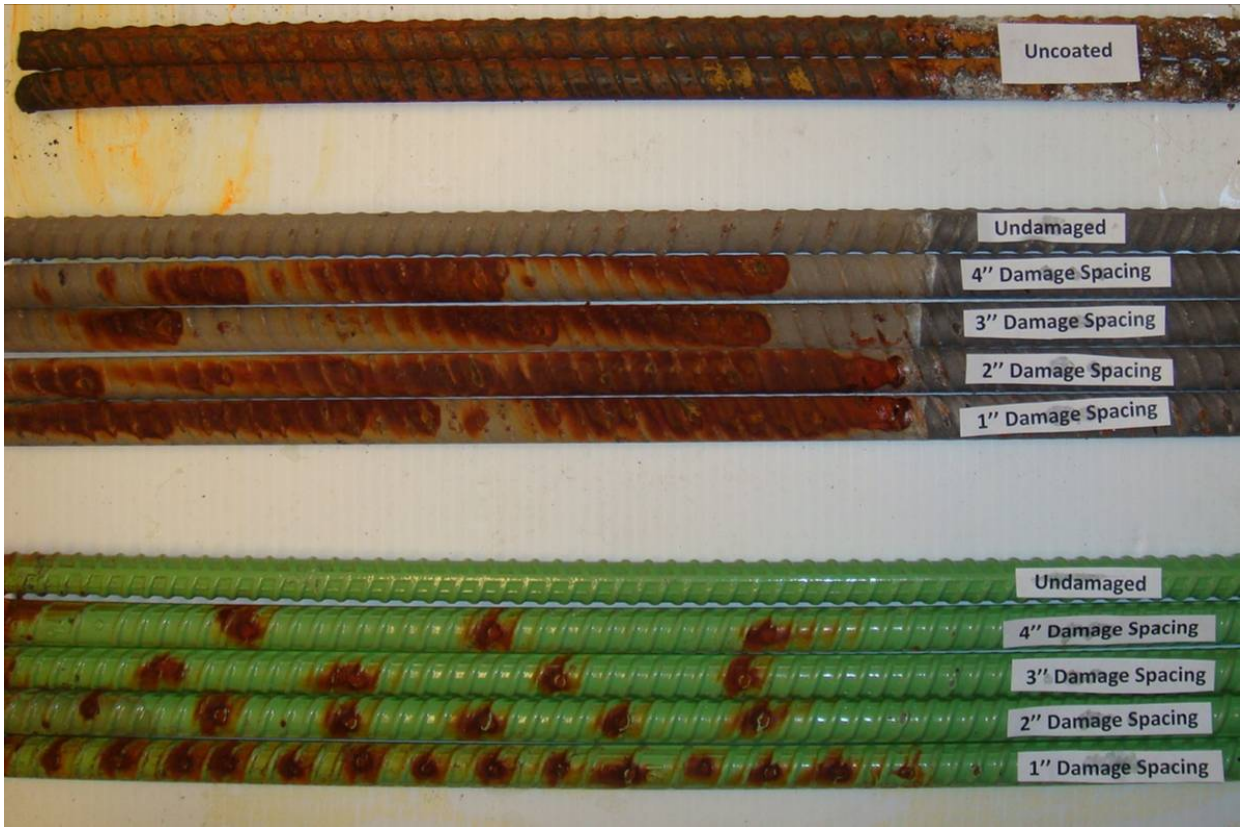

Figure 6.31 Surface conditions of all tested rebar after testing

Figure 6.31 shows the surface conditions of all tested rebar at completion of testing. It can be observed from Figure 6.31 that epoxy-coated rebar only corroded around the damaged areas due to undercutting effects as observed during salt spray tests. For enamel-coated rebar, corrosion occurred on a large area due to porosity of the 50/50 coating. However, due to the chemical bond between the enamel and steel, undercutting did not occur. Uncoated rebar show the highest degree of corrosion. These relative comparisons support the conclusions drawn from the salt spray tests.

6.3.3. Conclusions Based on Accelerated Corrosion Tests

Testing of non-grouted, enamel-coated bars revealed that 50/50 enamel and double enamel coatings were unable to protect the underlying steel for any measureable amount of time. The only enamel coating that can postpone the onset of corrosion was the pure enamel coating as applied to the deformed bars. The exterior surface of each of the eight pure enamel-coated deformed bars appeared identical to one another and resembled that of the non-corroded specimen. Following the cross-sectional examination procedure stated within the technical section of the salt spray test, a cross-section was developed from one of the eight bars. The cross-section revealed a coating thickness that ranged from approximately 7.9 to 39.4 mils (200 to 1,000 μm) and was similar to that shown in Figure 6.14(a).

Testing of grouted specimens revealed a definite trend in the corrosion resistance of the different coatings. The uncoated specimen groups have the lowest t_{corr} values, but just slightly lower than

those obtained from the 50/50 enamel-coated specimens. A significant increase in corrosion resistance of a specimen was observed when the 50/50 enamel coating was replaced by pure enamel. The corrosion resistance of the pure enamel coating can be increased by approximately 64% when a second coating composed of 50/50 enamel was applied to the exterior surface of the coated bar to form double enamel. Although the double enamel coating provided a great deal of corrosion protection to the underlying steel bar, the greatest t_{corr} values were reported by both groups containing epoxy-coated bars.

The pure and double enamel coatings can generally increase a smooth bar's corrosion resistance by approximately 181% and 363%, respectively, when grouted. However, those percentages decreased by approximately 24% when the smooth bar was replaced by a deformed bar. This decrease in corrosion resistance is mainly caused by the inconsistent coating thickness in double and pure enamel-coated deformed bars that resulted in a thin coated layer near transverse ribs, while the double and pure enamel-coated smooth bars were uniformly coated and possessed a coating thickness that was greater than the minimum coating thickness on the transverse ribs. Although the 50/50 enamel-coated bars shared identical coating distribution patterns to that of the double and pure enamel-coated bars, the thinly coated areas along a deformed bar appeared to have little effect on the reported t_{corr} values. In fact, the 50/50 enamel coating increased the t_{corr} value of an uncoated bar by only 8%. The inability of the 50/50 enamel coating to provide a substantial amount of protection can be explained by the semipermeable calcium silicate particles embedded within the coating and the network of voids seen throughout the coating's thickness.

The epoxy coating showed an exceptional ability in protecting both smooth and deformed steel bars from corrosion when either grouted or non-grouted. Each non-grouted specimen withstood a minimum of 664 hours of testing without showing any signs of corrosion. The grouted specimens showed no signs of corrosion after being tested for a period of 1300 hours.

6.4. Ponding Test

Commonly used to determine a concrete's resistance to chlorides, the AASHTO T259 standard was incorporated to study the corrosion resistance of 50/50 enamel-coated, epoxy-coated, and uncoated reinforcing bars when placed within a high alkaline environment. A total of 20 reinforced and 5 unreinforced concrete ponding specimens were subjected to a continuous two week wet / one week dry cycle, for a period of 54 weeks. The 20 reinforced concrete ponding specimens were divided into five groups, with four specimens to each group. The five groups were: uncoated, "perfect" epoxy, damaged epoxy, "perfect" 50/50 enamel, and damaged 50/50 enamel. The name of each group corresponded to the type of coated reinforcing bars embedded within a group's four specimens. The five unreinforced specimens were constructed as control specimens for concrete resistivity measurements.

The control specimens were used to obtain a "representative" concrete resistivity value for the overall set of specimens. Concrete resistivity and half-cell potential readings were carried out every 6 weeks over the course of the testing period. Upon completion of the test, chloride profiles were developed from randomly selected specimens. After developing the chloride profiles, specimens contained within each group were then forensically evaluated.

6.4.1. Technical Approach

6.4.1.1. Test specimens and material properties

Specimens measured 18 in. × 18 in. (457 mm x 457 mm) in plan and 3½ in. (89 mm) in height. Each specimen contained a 15-in. (381 mm) square by 1-in. (25 mm) deep reservoir along its surface, as shown in Figure 6.32.

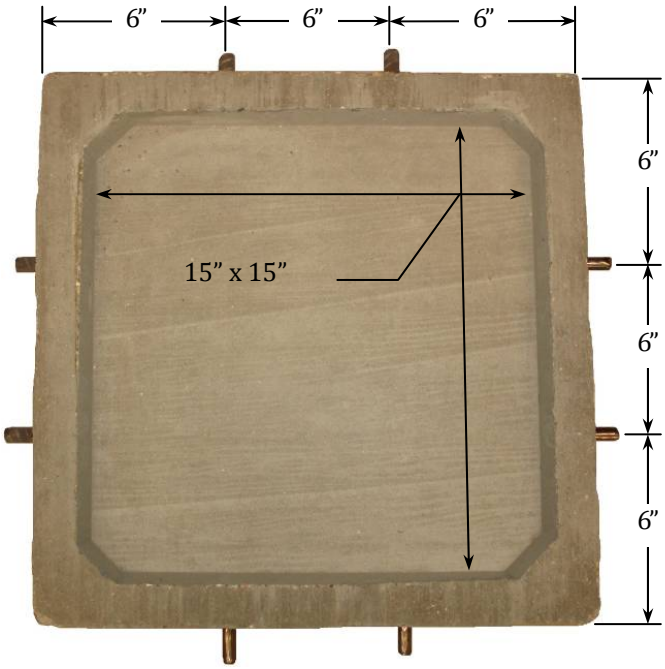

Figure 6.32 Typical reinforced ponding specimen.

Four 21-in. (533 mm) long segments of deformed, No. 4 (No. 13), Grade 60 rebar were embedded within each of the 20 reinforced specimens. Two of the four bars were positioned in the longitudinal direction and were given ½ in. (13 mm) of cover with respect to the surface of the reservoir. The remaining two bars were positioned directly beneath and in contact with the two longitudinal bars, but in the transverse direction. The bars were spaced in plan as shown in Figure 6.32.

After cutting the bars to a length of 21 in. (533 mm), half of the epoxy and enamel-coated bars were intentionally damaged. Each bar was damaged at three locations along one of its sides. With respect to either end of a bar, the three locations were at distances of 4½ in. (114 mm), 10½ in. (267 mm), and 16½ in. (419 mm). The three areas of damage along each bar were created under the same level of impact energy with the impact device shown in Figure 6.21.

Figure 6.33 shows a damaged enamel-coated and an epoxy-coated rebar. The 50/50 enamel coating exhibited an average area of damage that was approximately 3/8 in. × 1/2 in. (10 mm × 13 mm), whereas the epoxy coating showed an average area of damage that was approximately 1/16 in. × 1/8 in. (2 mm × 3 mm).

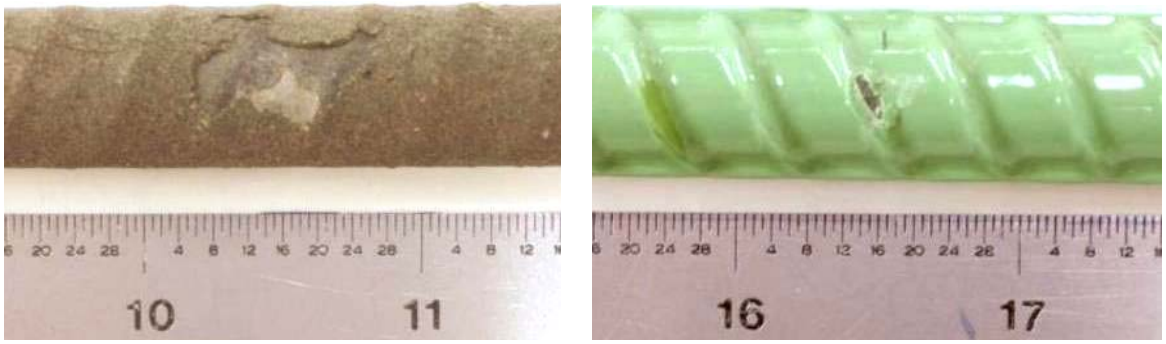

(a) A 50/50 enamel-coated specimen (b) An epoxy-coated specimen

Figure 6.33 Representative view of an average intentionally damaged area.

The bars were then cleaned thoroughly. First, a wire brush was used to remove any rust from the uncoated bars. Next, the uncoated and epoxy-coated bars were cleaned with a mild soap and water. After cleaning the bars, the epoxy and 50/50 enamel-coated bars were examined for unintentionally damaged areas. Any area along a bar that was unintentionally damaged received two coats of Rebar Green Epoxy Paint manufactured by Aervoe Industries, Inc.

Both uncoated and "perfectly" coated bars were randomly oriented within the forms. Bars that were intentionally damaged were oriented with the side containing the three areas of damage facing downward towards the bottom of the form, which would eventually become the top surface of the specimens. In an effort to prevent any rotation and/or movement of the bars during casting, plastic zip ties were used to connect the bars running perpendicular to one another, as shown in Figure 6.34 below.

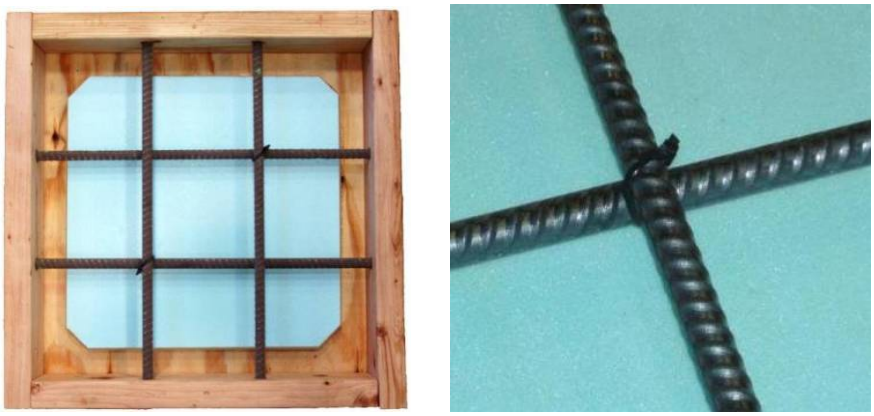

Figure 6.34 Formwork and rebar detail**.**

The forms used to cast the specimens were constructed of lumber and 1-in. (25 mm) thick polyisocyanurate foam. The walls of each form were made of four pieces of 1½-in. × 3½-in. (38 mm × 89 mm) lumber. Two ⅝-in.-diameter (16 mm) holes were drilled through each of the walls at locations of the rebar. A 21-in. × 21-in. × ¾-in. (533 mm × 533 mm × 19 mm) section of plywood was used as the bottom of each form. Centrally located on the top of the plywood was a 15-in. × 15-in. × 1-in. (381 mm × 381 mm × 25 mm) section of polyisocyanurate foam.

The foam was secured to the plywood using Polyurethane Premium Construction Adhesive manufactured by Henkel Corporation. Prior to using the forms, the interior surface of each form was coated with a layer of release agent that was manufactured by Dayton Superior. A typical form may be seen in Figure 6.34. A detailed drawing of a typical form may be found in Appendix C.

A standard 4000 psi (27.56 MPa) concrete was used for each of the 25 specimens. The mix had a 0.50 water-to-cement ratio and incorporated no chemical or mineral admixtures. Coarse and fine aggregate used within the mix consisted of ⅜-in. (10 mm) pea gravel and Jefferson City sand, as listed in Table 6.3. Batching of the concrete took place at a local ready-mix plant and was delivered to the lab where it was then placed indoors.

Table 6.3 Concrete constituents by weight

Type I Cement	⅜-in. Pea Gravel	Sand (Jefferson City)	Water
658 lbs	1562 lbs	1562 lbs	329 lbs

Casting of the 25 specimens was broken up into three pours which occurred on three separate days over the course of a 7 month period. The first pour was on December 9, 2008 with the casting of the first and second specimen within each of the five groups containing reinforcement. Casting of the third and fourth specimen, within each of the five groups, occurred on February 2, 2009. The third and final pour took place on May 22, 2009 and consisted of casting the five unreinforced control specimens.

For each of the three pours, a total of five test cylinders, measuring 6 in. × 12 in. (152 mm × 305 mm), were cast alongside the ponding specimens. After each casting, plastic sheeting was used to cover the specimens and plastic caps were placed over the cylinders. The cylinders and specimens were moist cured for seven days. After curing, the specimens were demolded, labeled, and transported to the room in which they were stored during the 54 weeks of testing. However, before transporting the epoxy and 50/50 enamel specimens, the coating along one end of each of the four exposed bars was removed through grinding to provide the electrical connection necessary for the subsequent half-cell readings.

The 7 and 28-day compressive strengths of each pour were determined using four of the five cylinders that were cast and cured alongside the specimens. Before testing, the ends of each cylinder were capped following ASTM C617. All cylinders were tested in accordance with ASTM C39. The 7 and 28-day strengths were determined through testing 1 and 3 cylinders, respectively. The average 28-day compressive strength of the three cylinders, along with the 7-day compressive strength based on one cylinder, for each of the three pours may be found in Table 6.4.

Table 6.4 Compressive strength of concrete

Age *(Days)*	Strength *(psi)*		
	Pour 1	Pour 2	Pour 3
7	2147	2729	2724
28	4359	4379	3869

6.4.1.2. Test method, setup, and protocol

During the 54 weeks of testing, specimens were stored within a room that had an average ambient temperature of 68°F (20°C) and a relative humidity of 40 to 60%. They were subjected to a series of 18 consecutive wet/dry cycles. The wet phase of a wet/dry cycle lasted for a total of two weeks and poured 0.53 gallons (2 liters) of saltwater into a specimen's reservoir. The saltwater consisted of distilled water with 5% ACS grade sodium chloride (NaCl) by weight, and remained within a specimen's reservoir during the entire two weeks. To prevent any evaporation of the saltwater, each specimen was covered with plastic sheeting that was held down with an elastic band. An image of a typical specimen during the wet phase of testing may be seen in Figure 6.35(a).

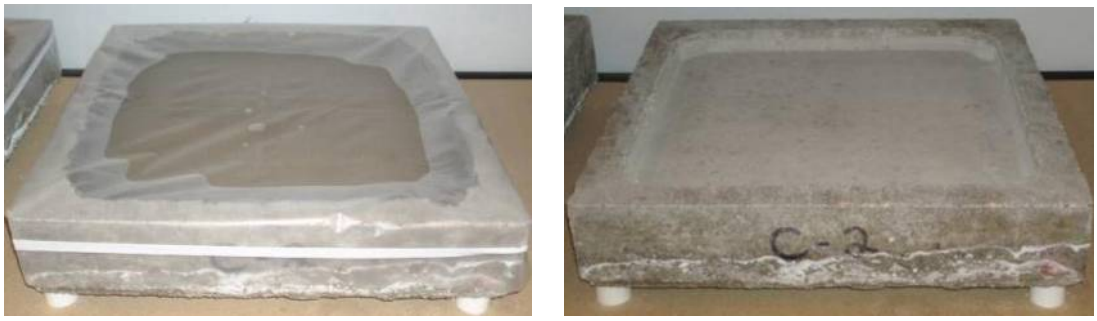

(a) Wet phase of testing (b) Dry phase of testing

Figure 6.35 Typical specimens.

The dry phase of a wet/dry cycle began when the saltwater contained within the specimen's reservoir was removed with the aid of a vacuum. The specimen was then permitted to air dry, as illustrated in Figure 6.35(b) for a period of one week.

The wet/dry cycling of the specimens began directly after collecting the baseline resistivity and corrosion potential measurements for each specimen. Baseline readings were conducted within the first week after a group of specimens were cured for 28 days. Once the baseline measurement had been recorded the first wet/dry cycle began. Concrete resistivity and corrosion potential readings were then performed after every two consecutive wet/dry cycles (6 weeks).

6.4.1.2.1. Concrete Resistivity Measurements

The resistivity of each specimen was measured every six weeks with the use of a Canin^{+}, a corrosion analyzing instrument manufactured by Proceq. Canin^{+} incorporated the use of a Wenner Probe, also known as a four probe resistivity meter, which has a fixed electrode spacing of 2 in. (51 mm) and a nominal alternating current (AC) output of 180 μA at a frequency of 72 Hz. The equipment had an impedance of 10 MΩ and an operating range of 0 to 99 kΩcm. The Canin^{+} along with the Wenner Probe may be seen in Figure 6.36(a).

(a) Canin^{+} equipment and the Wenner Probe (b) Measurement point layout

Figure 6.36 Ponding test specimen and preparation.

A specimen's resistance was measured approximately 30 minutes after a wet phase of testing had been completed. This 30 minute period between empting the specimen's reservoir and conducting the resistivity measurements allowed for the evaporation of any excess saltwater along the surface of the specimen's reservoir. Each specimen's resistivity was consistently measured at the six locations shown in Figure 6.36(b).

6.4.1.2.2. Corrosion Potential Measurements

The corrosion potential of the rebar embedded within a specimen was measured immediately after the specimen's resistivity readings were recorded. Using the Canin^{+} equipment, which had an operating range of ±999 mV and incorporated a copper/copper sulfate half-cell, the corrosion potentials at three locations along the length of each embedded bar were measured. The three locations were spaced 6 in. (152 mm) on center and were offset a distance 3 in. (76 mm) from a specimen's side. A schematic layout of the locations in which potential readings were taken along the surface of a specimen may be seen in Figure 6.37(b).

(a) The copper/copper sulfate half cell (b) Locations with corrosion potential taken

Figure 6.37 Half cell measurements

Before measuring the corrosion potential of an embedded bar in concrete, the exposed steel along one end of the bar was cleaned. Cleaning of the steel was considered complete when a bright metal to bright metal connection between the bar and the voltmeter (or Canin^{+}) was achieved. The connection between the positive terminal of the voltmeter and the bar was made through the use of an alligator clip, as shown in Figure 6.37(a). After securely connecting the voltmeter to the bar, the half-cell was then connected to the voltmeter's negative terminal. The sponge attached to the end of the half-cell was then dipped into distilled water until it became fully saturated. Once the sponge was saturated, the three points along the rebar, as can be seen in Figure 6.37(b), were located with the use of a ruler. Measurements were then carried out by gently placing the half-cell upon each of the three locations. The recorded values were based off of the Canin^{+}'s ability to automatically acquire a value once a reading had become stable. After the three values were recorded, the sponge was then re-saturated and the corrosion potential values for the three remaining bars embedded in concrete were obtained using the same procedure.

6.4.1.2.3. Forensic Evaluation and Chloride Analysis

Upon completion of the 54-week-long ponding test, a forensic evaluation was conducted on each group of specimens. The forensic evaluation involved a visual examination of the reinforcing bars embedded within a specimen after they were carefully removed from the concrete by dividing a specimen into nine sections. Each section was removed in a systematic order using an air chisel as shown in Appendix C. After removing the four pieces of rebar from a specimen any loose material along the length of each of the four bars was removed by hand. Afterwards, each bar was visually examined and photographed.

When necessary, areas along selected bars were cross-sectioned following the same procedure as explained within the salt spray section of this report and examined microscopically to further

understand the coating's characteristics. Prior to the removal of the reinforcement, cores were taken from a portion of the selected specimens and the chloride profiles were developed.

Among the 25 specimens, three specimens were chosen to undergo a chloride content analysis. Of the three specimens, one contained epoxy-coated rebar, one contained 50/50 enamel-coated rebar, and one contained uncoated rebar. The chloride analysis conducted upon these specimens involved determining the water soluble chloride content within multiple samples of concrete powder. The samples of powder were collected at various locations along the depth of a core, as shown in Figure 6.38. A 3-in. (76 mm) diameter core was removed from the middle of each specimen's reservoir and an additional core was taken from the corner of one of the three specimens.

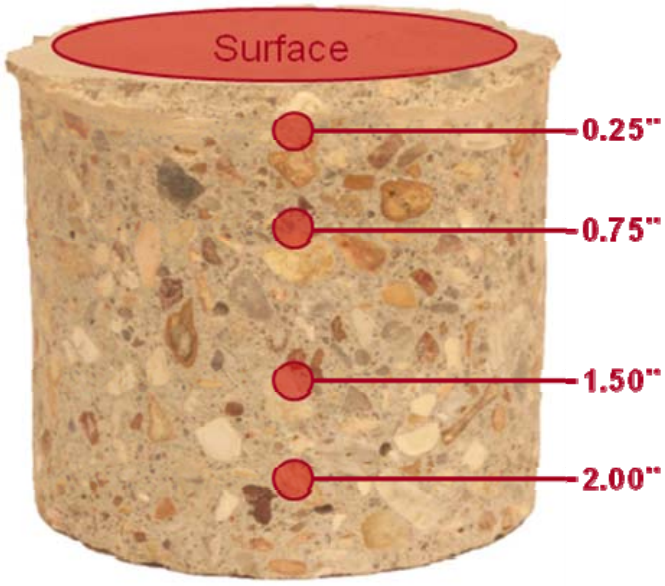

Figure 6.38 Locations where concrete powder samples were collected for chloride analysis.

Using Rapid Chloride Testing (RCT) equipment manufactured by Germann Instruments, Inc., the concentration of water soluble chlorides contained within each powder sample was determined. Using the graduated ampoule and compression pin that were included within the RCT kit, 0.053 oz (1.5 g) of concrete powder, which pertained to a single location along the height of a core, was measured. The powder was then transferred to a vial containing 0.304 fl-oz (9 mL) of an extraction liquid that was composed of 96% deionized water and 4% hydrogen peroxide (H_2O_2). The vial was then shaken for a period of 5 minutes. After a vial had been shaken, the contents within the vial were then filtered into a vial containing 0.034 fl-oz (1 mL) of a buffer solution. The buffer solution consisted of 24% hepes ($C_8H_{18}N_2O_4S$) and 76% deionized water. While filtering the contents from one solution to the other, the chloride selective electrode was prepped and calibrated according to the directions provided by the manufacturer.

The electrode was prepared by filling it with a wetting agent that contained 2% potassium nitrate (KNO_3), 3% potassium chloride (KCl), and 95% deionized water. Once prepped, the electrode was then connected to a voltmeter and inserted into one of four vials containing a solution with a

known chloride concentration. The four calibration liquids included within the RCT kit contained chloride concentration levels of 0.005, 0.020, 0.050, and 0.500%. Those four chloride concentrations produced voltage readings of approximately 100 mV, 72 mV, 49 mV, and -5 mV respectively. After removing the electrode from a vial, it was rinsed off using distilled water and then blotted dry with a tissue. The recorded voltage readings were then plotted upon a log chart that contained units of voltage in the x-axis and percent chlorides by weight of concrete in the y-axis. The four points were then connected by three straight lines which were drawn with the use of a straight edge. A data sheet containing this log chart may be seen in Appendix C.

After successfully filtering the solution from one vial to the other, the solution was then quickly shaken for 1 to 2 seconds. The calibrated electrode was then inserted into the vial and remained there until the voltage reading stabilized to within 0.2 mV. Once stable, the voltage reading was then recorded and the chloride content was determined by using the log chart that contained the data which was previously obtained from the calibration liquids. The electrode was then removed from the vial, rinsed with distilled water and blotted dry with a tissue.

6.4.2. Results and Discussion (Evaluation)

6.4.2.1. Concrete resistivity measurements

The resistivity for each specimen group over the course of the 54 weeks of testing is shown in Figure 6.39. Each data point in Figure 6.39 represents the overall resistance of a specimen group or the average value of measurements on various specimens in each group. Error bars, representing a 95% confidence interval for each data point, are also shown in Figure 6.39. A data point's confidence interval was developed using the standard error of a set's mean value (SEM) [ASTM G16, 2010]. A data set consisted of four individual sets of six resistivity values which were gathered from the four specimens contained within each specimen group. Therefore, a data point's SEM was equal to the standard deviation of these 24 resistivity values divided by the square root of 24. A table of the resistivity values pertaining to a specific specimen within a specimen group may be found in Appendix C.

As shown in Figure 6.39, the resistivity for each group of specimens remained relatively constant during the testing period. Both the "perfect" and damaged 50/50 enamel specimens have approximately the same resistance throughout the 54 weeks of testing. Similarly, both the "perfect" and damaged epoxy groups have the overall resistance values of 11.0 kΩcm. A specimen group's overall resistance was calculated by averaging the group's ten data points shown within Figure 6.39. The overall resistance for each of the six groups of specimens, along with the 95% confidence interval corresponding to each value, is shown in Figure 6.40.

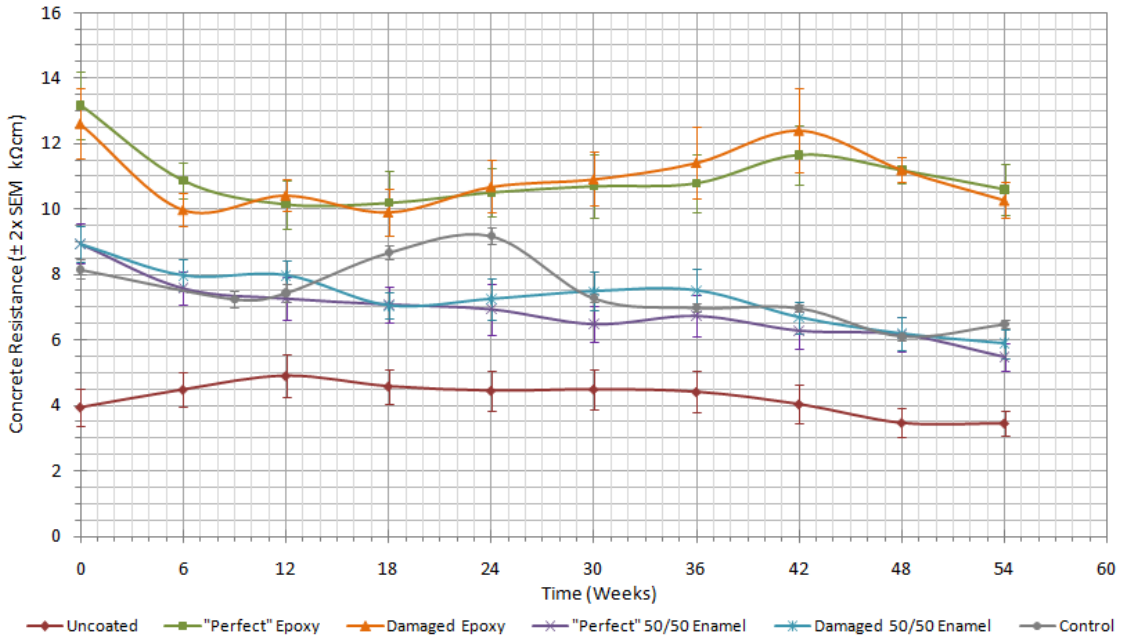

Figure 6.39 Average resistance of each specimen type during the 54 weeks of testing.

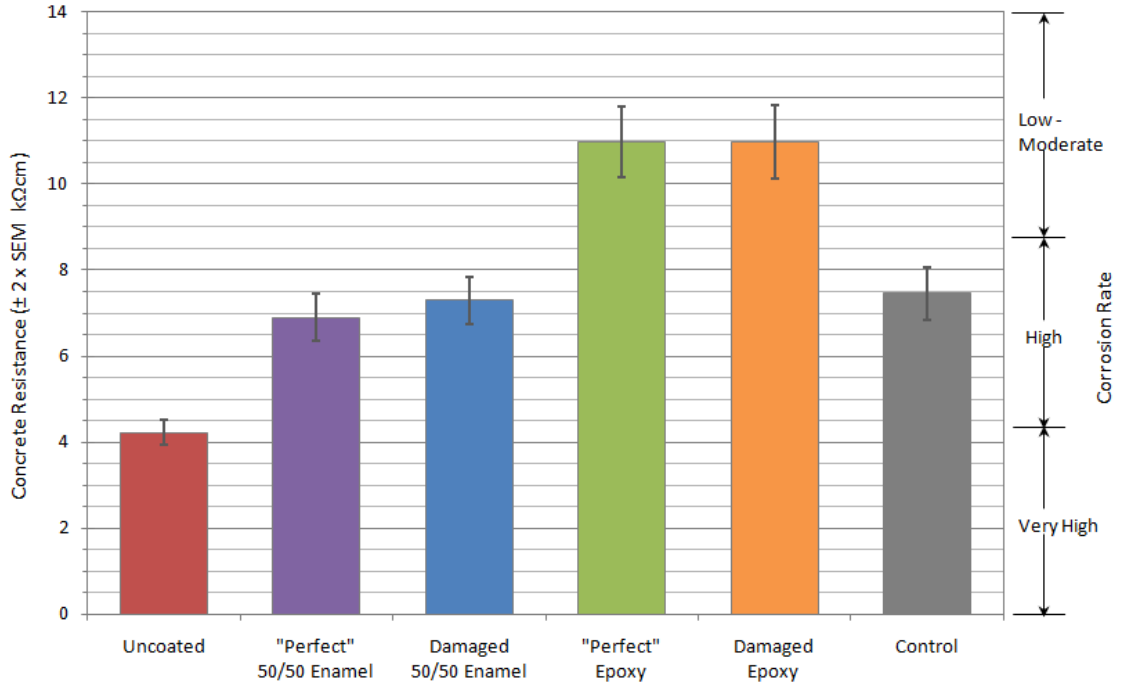

Figure 6.40 Average resistance of each specimen type.

Using the relation established by ACI [2001], as given in Table 6.5, and the overall resistance values reported within Figure 6.40, the corrosion rate of the reinforcing bars contained within each specimen group was generalized assuming that the bars were depassivated. With an overall

resistance value of 4.2 kΩcm, the uncoated specimens exhibited the lowest resistance out of the six specimen groups. This low resistance correlated to a "very high" corrosion rate of the uncoated reinforcement. As stated earlier, both groups containing 50/50 enamel-coated reinforcement reported similar resistivity values throughout the testing period. The average overall resistance of the two groups was approximately 7.1 kΩcm, which correlated to a "high" corrosion rate of the 50/50 enamel-coated bars. The highest overall resistance was reported by the two groups containing epoxy-coated rebar, which is 11.0 kΩcm corresponding to a "low to moderate" corrosion rate of the epoxy-coated reinforcement. As a basis for comparison, the group containing unreinforced specimens has an overall resistance of 7.5 kΩcm.

Table 6.5 Correlation between concrete resistivity and the rate of corrosion for a depassivated steel bar embedded within the concrete [ACI, 2001].

Concrete Resistivity (kΩ cm)	Rate of Corrosion
> 20	Low
10-20	Low to Moderate
5-10	High
< 5	Very High

6.4.2.2. Corrosion potential measurements

Corrosion potential measurements for the five groups of reinforced specimens are shown in Figure 6.41. Each data point in Figure 6.41 represents an average potential value of the four specimens in each group. Error bars, representing a 95% confidence interval for each data point, are also shown in Figure 6.41. A data point's confidence interval was developed using the standard error of a data set's mean value (SEM). A data set consisted of four individual sets of twelve potential measurements which were gathered from the four specimens in each group. Therefore, a data point's SEM was equal to the standard deviation of these 48 potential measurements divided by the square root of 48. A table of potential measurements pertaining to a specific specimen within a specimen group may be found in Appendix C.

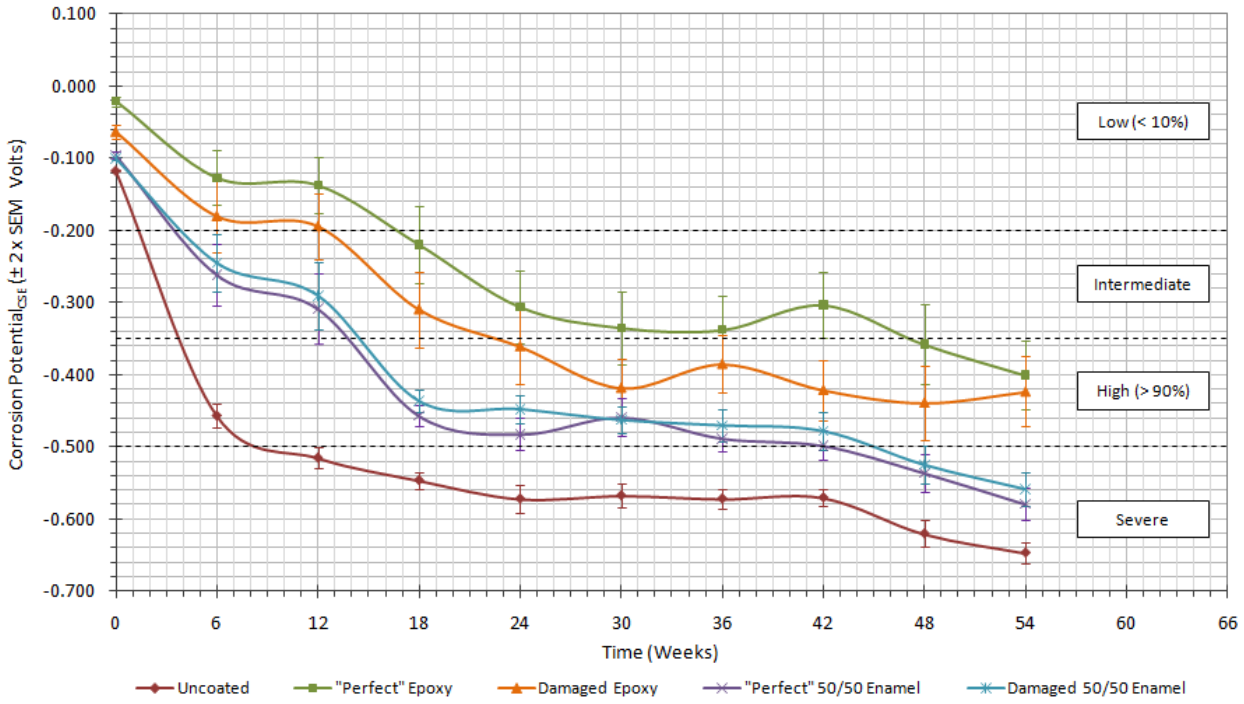

Figure 6.41 Average corrosion potential of each specimen group during the 54 weeks of testing.

As shown in Figure 6.41, all five groups follow a similar trend in corrosion resistance, which decreases over time. However, there are relative differences between the groups. Throughout the 54 weeks of testing, the two groups containing epoxy-coated bars reported the greatest corrosion resistance (more positive half-cell potential) of the five groups, while the lowest corrosion resistance (more negative half-cell potential) was reported by the uncoated group. The two 50/50 enamel groups reported a corrosion resistance (half-cell potential) between the epoxy and uncoated specimens. Furthermore, the two enamel groups reported similar potential values throughout the test, with the "perfect" 50/50 enamel group consistently reporting the lower (more negative) of the two potential values.

As shown in Figure 6.41, the average potential for each specimen group changed significantly within the first 24 weeks of testing. During the 30 weeks that followed, the potential of each specimen group gradually decreased and by week 54 each group reported an average potential of less than -350 mV, which would indicate a high probability of corrosion. The final potential value for each specimen group is shown in Figure 6.42. The average potential values stated in Figure 6.42 were calculated using the final potential measurements collected from all the specimens in a group. Using error bars, the standard error within a specimen group's final potential value is also shown in Figure 6.42. Of the five groups, both the "perfect" epoxy group and damaged epoxy group reported the greatest distribution in potential measurements; whereas the potential measurements collected from the uncoated group showed the smallest distribution.

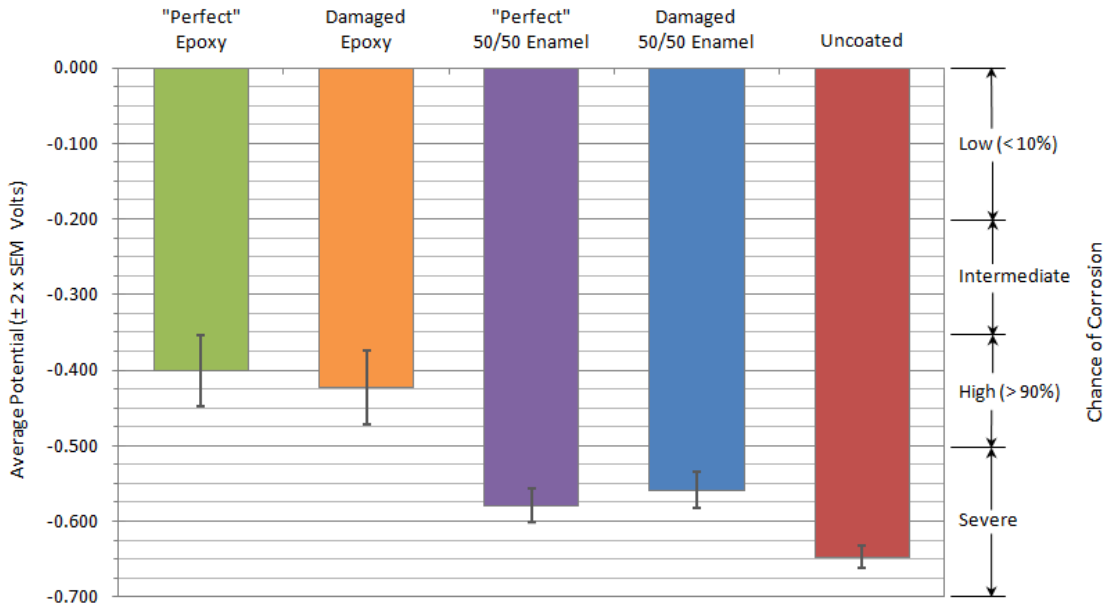

Figure 6.42 Average corrosion potential of each specimen group at the end of testing in week 54.

Using the relation established by Broomfield [2007], as given in Table 6.6, and the average potential values shown in Figure 6.42, the probability of corrosion in each specimen group was determined at the end of the testing period. Of the five specimen groups, the "perfect" 50/50 enamel group, damaged 50/50 enamel group, and the uncoated group reported final average potential values of less than -550 mV. Within those three groups, no individual specimen reported an average corrosion potential of greater than -500 mV. This indicted a "severe" chance that every specimen in the three groups had begun to corrode. The two remaining groups, "perfect" epoxy and damaged epoxy, had final average potential values of -400 mV and -425 mV, respectively. This correlated to a "high (> 90%)" chance that a specimen belonging to either of those two groups contained corroding reinforcement. Moreover, the average potential of each of the four individual specimens in the two groups varied significantly, as each group contained one specimen that possessed a "severe" chance of corrosion and another specimen that possessed an "intermediate" chance of corrosion.

Table 6.6 Correlation between the corrosion potential of a steel bar embedded in concrete and risk of corrosion [Broomfield, 2007].

Potential (CSE) **(mV)**	**Risk**
> -200	Low (< 10%)
-200 to -350	Intermediate
-350 to -500	High (> 90%)
< -500	Severe

6.4.2.3. Forensic evaluation and chloride analysis

Chloride profiles for three reinforced specimen groups are shown in Figure 6.43. As expected, a large concentration of water soluble chlorides was discovered along the surface of each specimen that was tested. The chloride concentration in each core dropped significantly from around 0.9% at the surface to approximately 0.35% at a depth of ¼ in. (6 mm). The chloride concentration then decreased further to a value of approximately 0.05% at a depth of 2.0 in. (51 mm). However, the chloride concentration within the core that was taken from the specimen containing uncoated reinforcement began to increase at some point between the depths of ¾ in. (19 mm) and 1½ in. (38 mm). As shown within Figure 6.43, the chloride concentration within this core continued to increase to a value of 0.6% at a depth of 2.0 in. (51 mm).

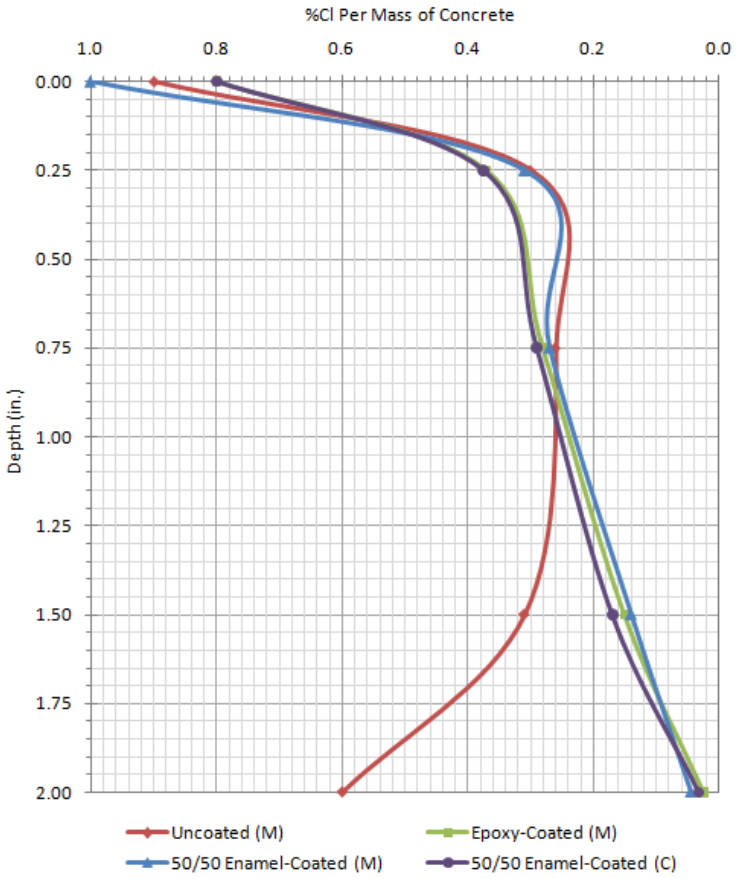

Figure 6.43 Typical chloride profiles for the 25 ponding specimens.

Using the chloride profiles that were developed for the epoxy and 50/50 enamel specimen, as shown in Figure 6.43, the average chloride concentration at depths of ½ in. (13 mm) and 1½ in. (38 mm) were approximately 0.27% and 0.17%, respectively. It was within that depth range that the reinforcement for each specimen was located. Using the two chloride concentrations, along with the information provided in Table 6.7, the reinforcement embedded within the 20 specimens was considered to be under a "high" risk of corrosion.

Table 6.7 Correlation between percent chloride by mass of concrete and corrosion risk [Broomfield, 2007].

% CL by Mass of Concrete	Risk
< 0.03	Negligible
0.03-0.06	Low
0.06-0.14	Moderate
> 0.14	High

Within the first 8 weeks of testing, a portion of the specimens containing uncoated reinforcement began to show hairline cracks along the surface of their reservoir. The cracks were located directly above the reinforcement that had a cover of ½ in. (13 mm). By the 17th week, the cracks were fully developed and half of the specimens began to show signs of leaking from the reservoir. The leaking of a specimen was attributed to the crack penetrating through the thickness of a specimen's reservoir wall. Each wall that showed signs of leaking was patched with one layer of Loctite's Aquamarine Epoxy. During the weeks that followed, the cracks continued to grow and by week 40, a portion of the cracks reappeared within the previously repaired sections with epoxy. A second layer of Aquamarine Epoxy was then applied to the newly formed cracks. An image of a typical crack that formed along the surface of a specimen's reservoir is shown in Figure 6.44.

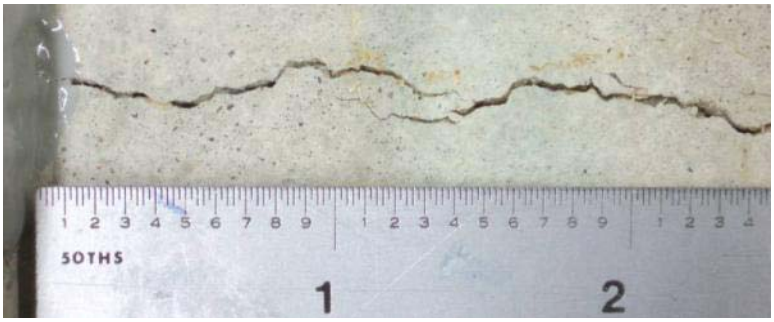

Figure 6.44 Cracking along the surface of the specimens with uncoated reinforcement.

6.4.2.3.1. Uncoated Rebar

The forensic evaluation of the uncoated group of specimens revealed that each of the four bars in a specimen exhibited signs of corrosion. Of the four bars, the two located closest to the surface of the specimen's reservoir showed significant signs of corrosion, and the other two bars lying furthest from the surface showed moderate signs of corrosion. This can be seen in Figure 6.45, which shows a typical set of four bars that were removed from a specimen that reported a maximum average potential of -662 mV at 54 weeks and an average resistance of 3.5 kΩcm throughout the testing period. The two bars labeled "3" and "4" in Figure 6.45 were positioned closest to the surface of the specimen's reservoir. Notice how bars "3" and "4" show more significant signs of corrosion than bars "1" and "2," which were positioned furthest away from the surface of the specimen's reservoir.

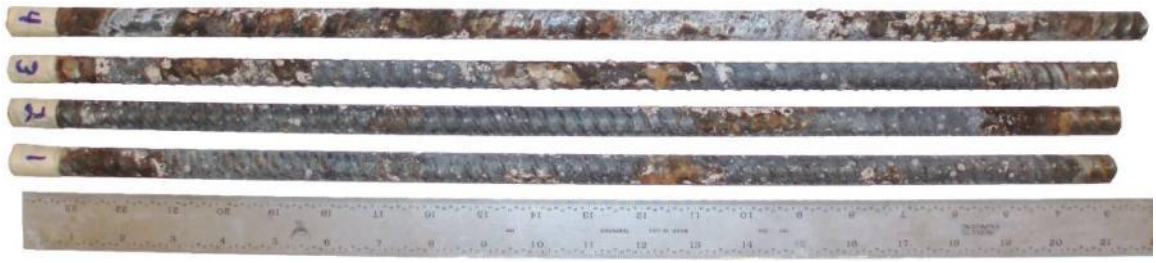

Figure 6.45 Uncoated reinforcing bars after removal from a ponding specimen.

The reason for the widespread corrosion along bar "4" was due to a crack that was located directly above the bar. The crack was fully developed by the 17th week of testing and extended the entire width of the specimen. This crack was either caused by or exacerbated by the buildup of corrosion along the bar. The local areas of corrosion seen along the three remaining bars are most likely due to the low concrete resistance and the high levels of chlorides that were observed within the specimen. Images of uncoated bars that were contained within the group's three remaining specimens are shown in Appendix C.

6.4.2.3.2. 50/50 Enamel Coated Rebar

A significant amount of the 50/50 enamel coating was unintentionally removed from each bar during the forensic examination. On average, a typical bar lost approximately 50% of its coating while being removed from a specimen. The majority of the coating that was detached from a bar was well adhered to the surrounding concrete. Portions of the coating that was attached to the concrete indicated red rust stains along its inner surface, as shown in Figure 6.46.

Figure 6.46 Red rust stayed on the concrete surface of a 50/50 enamel specimen.

The condition of the "perfect" and damaged 50/50 enamel-coated reinforcing bars was nearly identical. Similar to the uncoated specimens, both the "perfect" and damaged 50/50 enamel-coated specimens contained two bars that showed significant signs of corrosion (bars "3", "4", "7", and "8" in Figure 6.47), while the two remaining bars included within each specimen exhibited moderate signs of corrosion (bars "1", "2", "5", and "6"). A typical set of "perfect" and damaged 50/50 enamel-coated bars may be seen in Figure 6.47. The four "perfectly" coated

bars shown in Figure 6.47(a) were removed from a specimen that reported a maximum average potential of -589 mV at 54 weeks and an average resistance of 6.0 kΩcm throughout the testing period. The four damaged 50/50 enamel-coated bars shown in Figure 6.47(b) were removed from a specimen that reported a maximum average potential of -575 mV at 54 weeks and an average resistance of 6.8 kΩcm throughout the testing period. Images of "perfect" and damaged 50/50 enamel-coated bars that were removed from the three remaining specimens contained within each specimen group are shown in Appendix C.

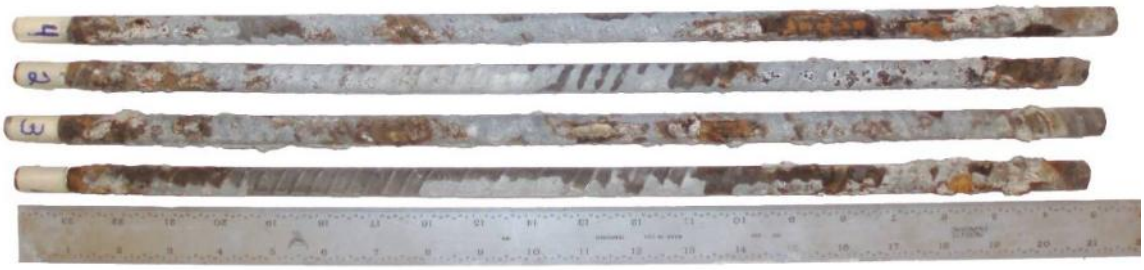

(a) "Perfect" 50/50 enamel-coated bars

(b) Intentionally damaged 50/50 enamel-coated bars

Figure 6.47 Reinforcing bars after removal from a specimen.

6.4.2.3.3. Epoxy-Coated Rebar

While visually examining the "perfect" epoxy-coated reinforcing bars, no significant signs of corrosion were observed. However, a typical bar did show minor signs of corrosion within damaged areas that appeared to have been pre-existing. As discussed in the section of ponding tests, two layers of Rebar Green Epoxy Paint were applied to all pre-existing areas of damage along each epoxy-coated bar prior to testing. However, while removing the epoxy-coated bars from the specimens, the Rebar Green Epoxy Paint adhered to the concrete and thus a portion of the pre-existing areas of damage were re-exposed, as shown in Figure 6.48(a). An overall view of a typical set of "perfectly" epoxy-coated bars may be seen in Figure 6.48(b). The bars shown in Figure 6.48(b) were removed from a specimen that reported an average potential of -316 mV at 54 weeks and an average resistance of 9.9 kΩcm throughout the testing period. Images of "perfect" epoxy-coated bars that were removed from the three remaining specimens in the group are shown in Appendix C.

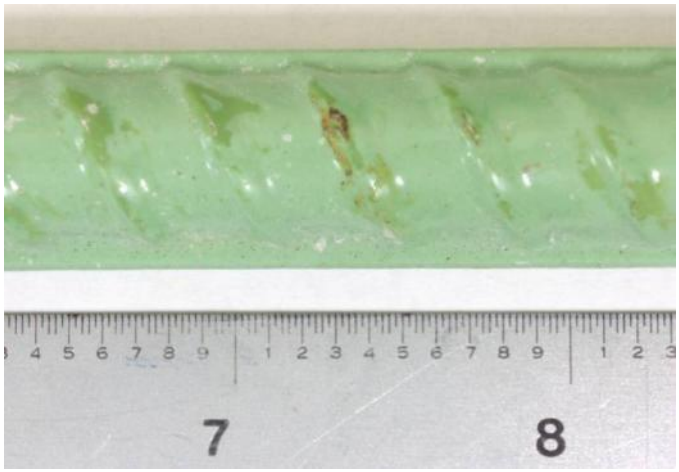

(a) Re-exposed area of damage

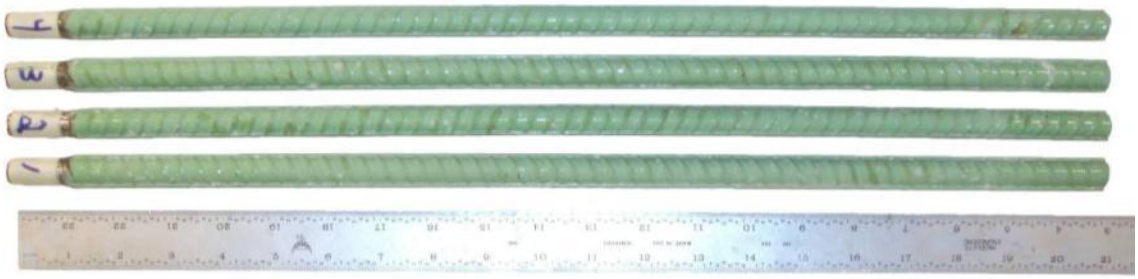

(b) “Perfect” epoxy-coated bars after removal from a specimen

Figure 6.48 Visual inspection on “perfect” epoxy-coated bars removed from a ponding specimen.

Similar to the “perfect” epoxy-coated bars, the intentionally damaged epoxy-coated bars experienced little corrosion. Each bar exhibited areas of pre-existing damage that were re-exposed while the bar was removed from a ponding specimen. On average, one of four intentionally damaged areas exhibited significant signs of corrosion, as can be seen in Figure 6.49(a). When a cross-section was taken through an area of damage that showed signs of corrosion, rust was observed beneath the coating as shown in Figure 6.49(b, c). However, a cross-section through an area of damage which exhibited no signs of corrosion revealed that the epoxy was well adhered to the steel and no rust was present beneath the coating. An overall view of a typical set of intentionally damaged epoxy-coated bars is shown in Figure 6.49(a). These bars were removed from a specimen that reported a maximum average potential of -440 mV at 54 weeks and an average resistance of 9.7 kΩcm throughout the testing period. Images of intentionally damaged epoxy-coated bars that were removed from the three remaining specimens in the specimen group are shown in Appendix C. Also included within Appendix C are additional cross-sectional images that were taken through areas within selected bars that showed signs of damage.

(a) Intentionally damaged epoxy-coated bars removed from a ponding specimen

(b) Detailed view of local damage (pre-test) and corrosion around the damage area (post-test)

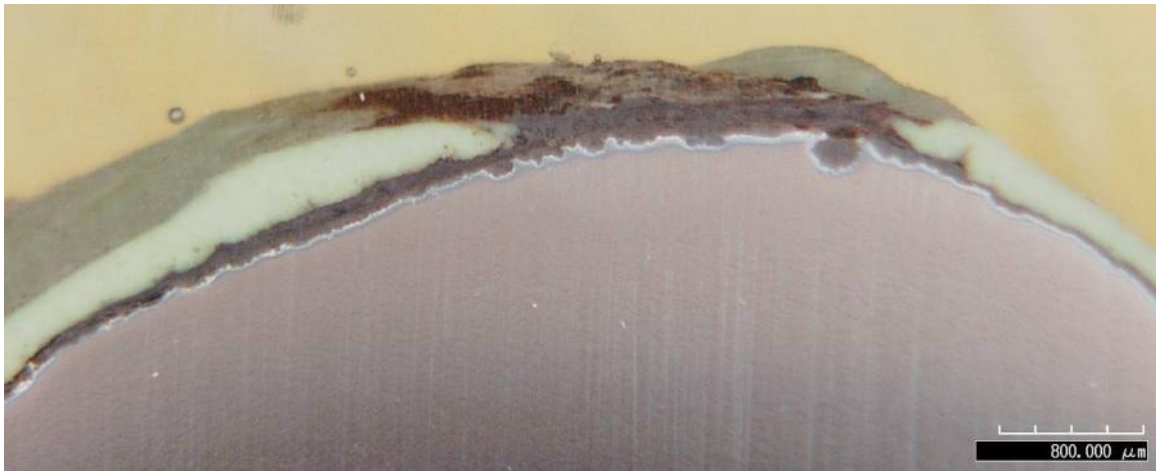

(c) Corrosion detail at d-d section

Figure 6.49 Corrosion conditions of intentionally damaged epoxy-coated bars.

6.4.3. Conclusions Based on Ponding Tests

As clearly demonstrated in Figures 6.39 and 6.40, the concrete resistance of a reinforced specimen is a function of the type of coating that is applied to the specimen's reinforcement. The intentionally created damage on the reinforcing bars appeared to have insignificant effects on their corrosion resistance, regardless of the type of coating used. In comparison with the unreinforced specimens, the average concrete resistances of specimens reinforced with either

"perfect" or damaged epoxy-coated bars, with either the "perfect" or damaged 50/50 enamel-coated bars, and with uncoated bars were 47% higher, similar, and 44% lower, respectively. Considering the use of same concrete and steel, these results indicated that the epoxy coating provided the greatest resistance to the applied electrical current, while the uncoated bar provided the least resistance. The 50/50 enamel-coated bars provided a degree of resistance between those of the epoxy and uncoated bars.

As demonstrated in Figure 6.41, the measured corrosion potentials of all specimens experienced a similar trend over time when exposed to a high chloride environment. They all started with a rapid reduction, then maintained at certain level, and finally decreased again. Similar to what were observed from concrete resistivity measurements, the epoxy coating provides the greatest degree of resistance, while the uncoated bars offer the least. The 50/50 enamel-coated bars offer a degree of resistance between those of the epoxy and uncoated bars. However, when examining similar coatings, there are some noticeable differences. As shown in Figure 6.41, a 28% decrease in corrosion resistance was observed due to damage in the epoxy coating and only a 4% variation in corrosion resistance was seen due likely to damage in 50/50 enamel coating. These observations verified the conclusions drawn on the undercutting effect of epoxy coating from salt spray tests. The final set of corrosion potential measurements indicated a "high (> 90%)" probability that the reinforcement contained in every specimen group actively corroded. With a severe chance that the reinforcement in the two 50/50 enamel groups and the uncoated group had begun to corrode.

Through chloride-ion analysis, a chloride profile similar to the one labeled "uncoated" in Figure 6.43 can develop when cracks form along the surface of a specimen's reservoir. However, only four out of the 25 specimens contained within this study showed signs of cracking along the surface. As indicated in Figure 6.43, a typical chloride profile developed from an uncracked specimen showed high levels of chlorides near the surface and a low concentration at a depth of around 2.0 in. (51 mm). Even so, the chlorides penetrated the concrete to the depth of the reinforcement in sufficient concentration to attack the passive layer and initiate corrosion.

Forensic evaluation revealed a significant variation in the condition of four bars in the uncoated specimen, the "perfect" 50/50 enamel-coated specimen, and the damaged 50/50 enamel-coated specimen. The reinforcing bars closest to the surface of a specimen's reservoir exhibited significant signs of corrosion, while the two remaining bars far away from the reservoir showed moderate signs of corrosion. On the other hand, the condition of the four reinforcing bars in either the "perfect" or damaged epoxy specimen were found to be substantially identical and exhibited only very limited corrosion.

A loss in adhesion between the epoxy coating and the steel was observed around the intentionally damaged area. When a loss in adhesion was observed, the steel beneath the coating indicated signs of corrosion. On the other hand, when a typical 50/50 enamel-coated reinforcing bar was removed from concrete, half of the coating was detached from that bar and securely attached to the surrounding concrete.

6.5. Potentiodynamic Test

The primary purpose of potentiodynamic polarization tests was to determine the corrosion current. These tests measured the rate of charge transfer between the anodic and cathodic reactions at a corrosion potential. The two reactions can be combined to generate the Butler-Volmer equation that involves I_{corr} and E_{corr}, the corrosion current in amps and the corrosion circuit potential in volts, respectively, β_a and β_c represent the beta coefficients in volts/decade for the anodic and cathodic reactions, respectively.

Figure 6.50 shows a representative polarization curve with two distinct branches largely described by the Butler-Volmer equation. The upper and lower branches represent the anodic and cathodic reactions, respectively. By extending the tangential lines at the initial and final applied potentials, the interception point of the two tangential lines gives the corrosion current. In this study, each sample was polarized using a forward scan from $E_{oc} - 200\,\text{mV}$ to $E_{oc} + 200\,\text{mV}$ at a scan rate of 0.5 mV/sec. in which E_{oc} is the open circuit potential that is measured at the beginning of each potentiodynamic test. Measurements were carried out monthly for a period of 10 months.

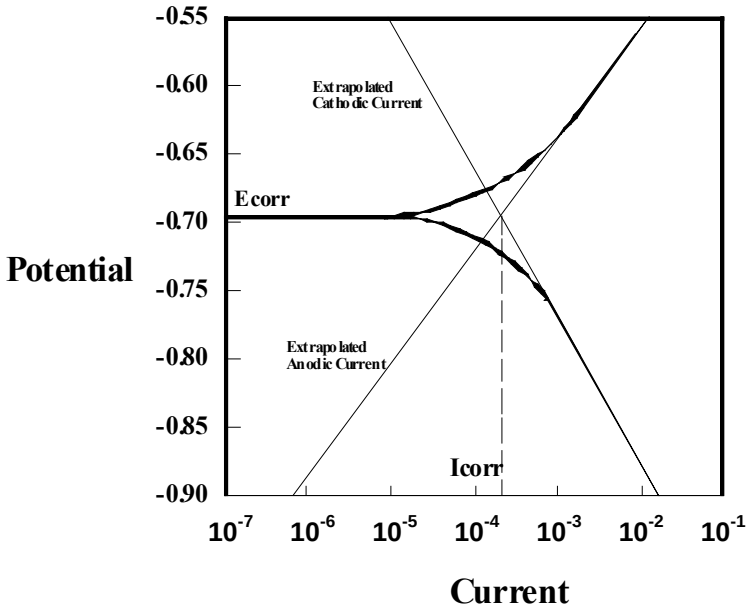

Figure 6.50 Typical polarization curves.

6.5.1. Technical Approach

6.5.1.1. Test specimens and material properties

Two types of samples were prepared for various potentiodynamic tests: steel discs and mortar cylinders. The steel discs investigated the corrosion resistance of various coatings, and the mortar cylinders studied corrosion-resistant performance of enamel-coated samples in actual applications.

6.5.1.1.1. Steel Disc Sample

Steel disc samples were made from #8, Grade 60, deformed rebar. The rebar was cut into 60 steel discs approximately 1″ in diameter and 0.5″ in thickness as shown in Figure 6.51(a). A nut was welded to each steel disc to provide an electrical connection after coating of the specimen. A copper wire was tightly tied around the thickness of the nut for several rounds as illustrated in Figure 6.51(b). The circular cross sections of each steel disc were polished with Grade 60, 180, 320 and 600 sand papers.

One third of the steel discs were coated with enamels by Pro Perma Engineered Coatings. The main chemical components of the enamel are given in Table 6.8. Each disc was dipped into enamel slip and then fired above 1400 °F. Before each test, the thickness of enamel coating measured approximately $78.8\pm3.94\times10^{-4}$in (200±10um).

(a) Set of steel disc samples (b) Sample polishing and wire connection

Figure 6.51 Preparation of steel disc samples.

Table 6.8 Chemical composition of enamel (%)

$CaSiO_3$	SiO_2	Al_2O_3	B_2O_3	CaF_2	Na_2O	CaO	K_2O	ZrO_2	MnO_2	NiO	CoO	Total
50.00	22.00	2.30	9.65	2.35	7.90	0.05	1.40	2.65	0.75	0.50	0.45	100.00

In order to force corrosion to occur in one circular cross section, epoxy resin was used to cover the remaining surfaces of each disc. For this purpose, a wood formwork was constructed with 100 divisions of 2.00″×1.50″×0.75″, as shown in Figure 6.52. After casting the epoxy, the resistance of each steel-copper connection was measured with an amp meter (approximately 0.8 ohm) to ensure a good electrical connection. After de-molding from the wood formwork, 60 uncoated steel disc samples and 60 enamel-coated samples were made as shown in Figure 6.53(a, b).

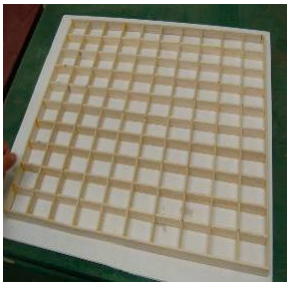

(a) Wood formwork

(b) Epoxy resin

(c) Sample casting

Figure 6.52 Casting process of steel disc samples.

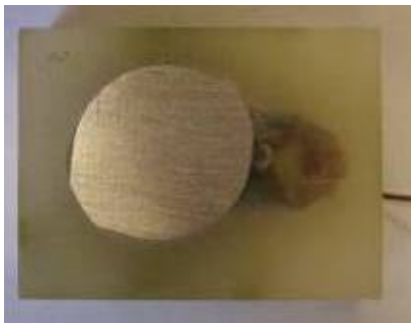

(a) Uncoated sample

(b) Enamel-coated sample

Figure 6.53 Steel disc samples for testing.

Note that, after one month of corrosion tests, cracks were observed on enamel coatings around the edge of several coated steel discs. As such, all enamel-coated steel disc samples were strengthened with marine epoxy around the edge of their cross section, as shown in Figure 6.53(b).

6.5.1.1.2. Mortar Cylinder Sample

Portland Cement Type I as specified in Table 6.9 was used in mortar cylinder samples. The mix design for the mortar cylinder specimens is shown in Table 6.10. The fine aggregate used was Missouri River sand with a ¼ in. maximum size and a fineness modulus of 2.80. Superplasticizer was not added to avoid any potential influence on the corrosion reaction of steel.

Table 6.9 Chemical analysis of Portland Cement Type I used in mortar specimens (%)

Ignition loss	SIO_2	AL_2O_3	CAO	MGO	SO_3	NA_2O	K_2O	CL^-	TIO_2	FE_2O_3	P_2O_5	Total
3.980	19.48	6.803	55.35	3.324	4.345	2.391	1.001	0.021	0.202	2.177	0.191	99.27

Table 6.10 Mortar mix design

Cement (lbs)	Sand (lbs)	Water (lbs)	Water/cement ratio
33.00	50.00	15.00	0.45

Each mortar specimen was a 1.5-in.-diameter and 4.5-in. tall cylinder reinforced with a #4 reinforcing bar along the centerline of the specimen as shown in Figure 6.54(a). The rebar was cut into 3.50 in. in length and a copper wire was connected at one end of the rebar. To limit the reactive rebar surface to the middle portion of the rebar and avoid crevice corrosion, the rebar ends were encased in PVC tubes containing epoxy resin, as shown in Figure 6.54(b). Therefore, the actual length of steel potentially exposed to the corrosion environment was approximately 2 in. long. The clear cover of concrete around the exposed portion of the rebar was 0.5 in. During casting, a 1.5-in.-diameter PVC pipe was used as a mold as illustrated in Figure 6.54(c). The rebar and PVC mold were held in place by grooves cut in the plywood bottom form. To ensure consolidation of the concrete, a ¼-in.-diameter steel rod was inserted 25 times within each of the three lifts. After casting, all the specimens were moisture cured for 28 days prior to testing.

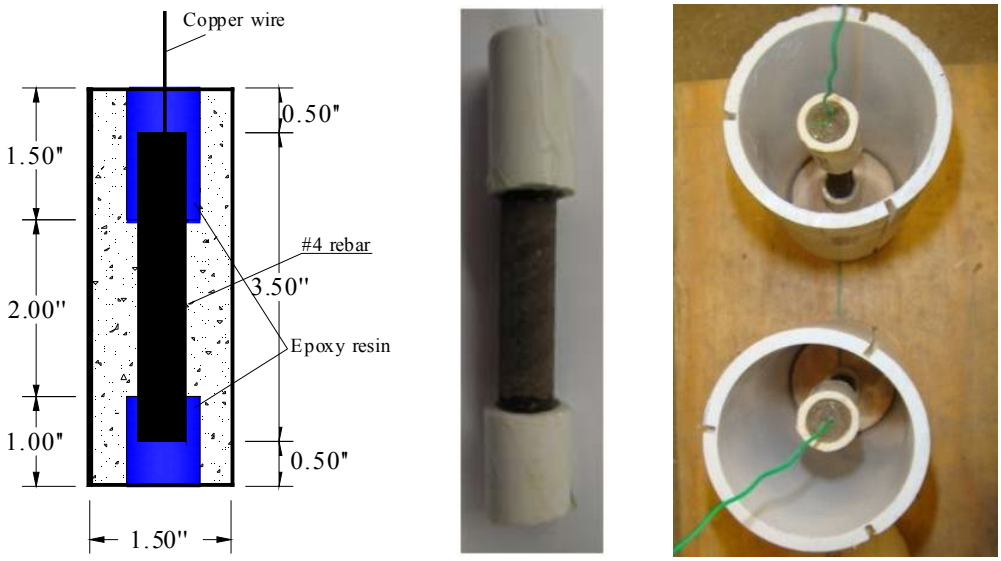

(a) Specimen design (b) Epoxy at both ends (c) PVC mold for casting

Figure 6.54 Mortar cylinder specimen and casting

6.5.1.2. Test method, setup, and protocol

After fabrication, 60 samples were immersed in 3.5% salt solution by weight at room temperature. The salt solution was made with distilled water and purified sodium chloride in a glass beaker. In order to keep a constant chloride concentration of the solution, distilled water was added biweekly to compensate for water evaporation.

Each disc or mortar cylinder sample was tested in a glass beaker with three electrodes, as shown in Figure 6.55. The three electrodes are the 1.00″×1.00″×0.05″ platinum sheet as a counter electrode, saturated calomel electrode (SCE) as a reference electrode, and the steel disc as the working electrode. All three electrodes were connected to Gamry Instrument for data acquisition.

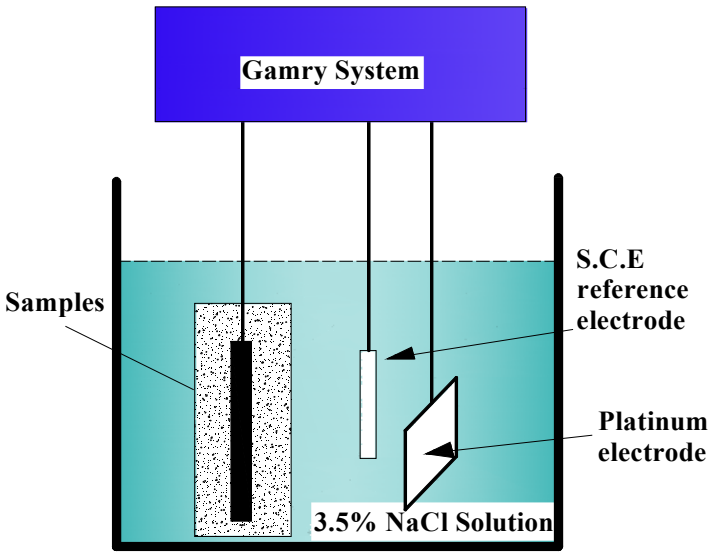

Figure 6.55 Test setup for EIS and potentiodynamic tests.

In addition to the measurements for corrosion current and corrosion potential, the pH of the solution was recorded every month before and after each test of steel disc samples with a Crison Model 2002 Ion Analyzer pH-meter. For mortar cylinder samples, chloride analysis was also done to confirm the conclusions drawn on the corrosion process of samples from other measurements. Chloride content was measured at three locations: 15/160 in., 45/160 in., and 70/160 in. from the mortar surface. For each mortar cylinder, three measurements were taken from three points symmetrically located around the rebar and their average was used to understand the diffusion process of chlorides in concrete.

6.5.2. Results and Discussion

6.5.2.1. Steel disc samples

The pH values, mass loss, and corrosion current were measured in various tests. Visual inspection was also conducted after each test. Their results are presented and discussed below.

Figure 6.56 shows pH changes of salt solution with time. The pH value of a solution plays an important role in the chemical reaction of steel with the solution. It was observed from Figure 6.56 that the pH of all samples did not change significantly with time, which shows a constant solution condition throughout the test period. The pH measured approximately 8.0 for enamel-coated samples and 7.0 for uncoated bars.

The mass loss of all steel disc samples is presented in Figure 6.57. The mass of the enamel-coated samples increased with time. In addition to the mass increase expected when the CS hydrates, these results can be explained by the facts that corrosion products were accumulated underneath coatings and the coatings held the corrosion products throughout the period of tests. For uncoated steel disc samples, however, their corrosion products were dissolved into salt solution during the corrosion process, reducing their mass with time. This explanation was also supported by visual inspection on the change of color in salt solution at the end of the test period.

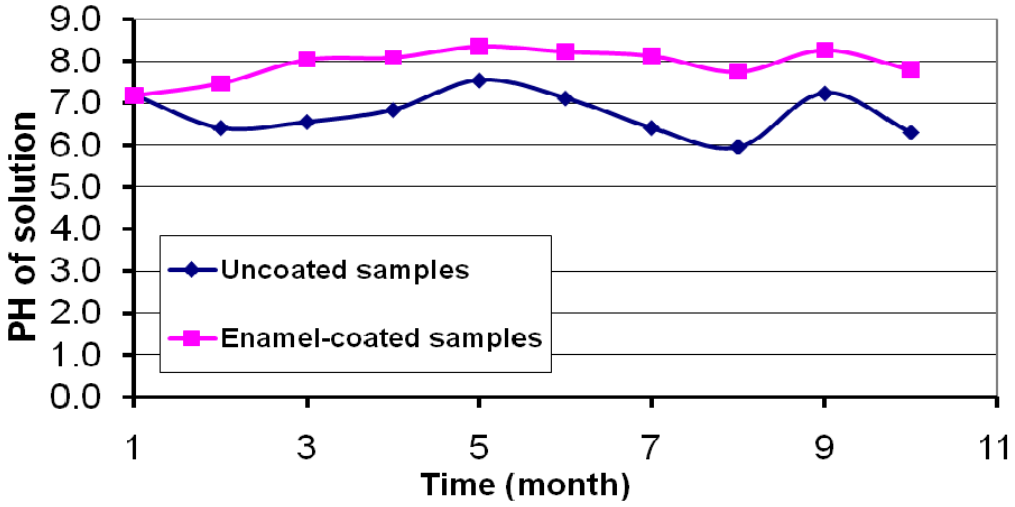

Figure 6.56 Change of the pH values of salt solution over time.

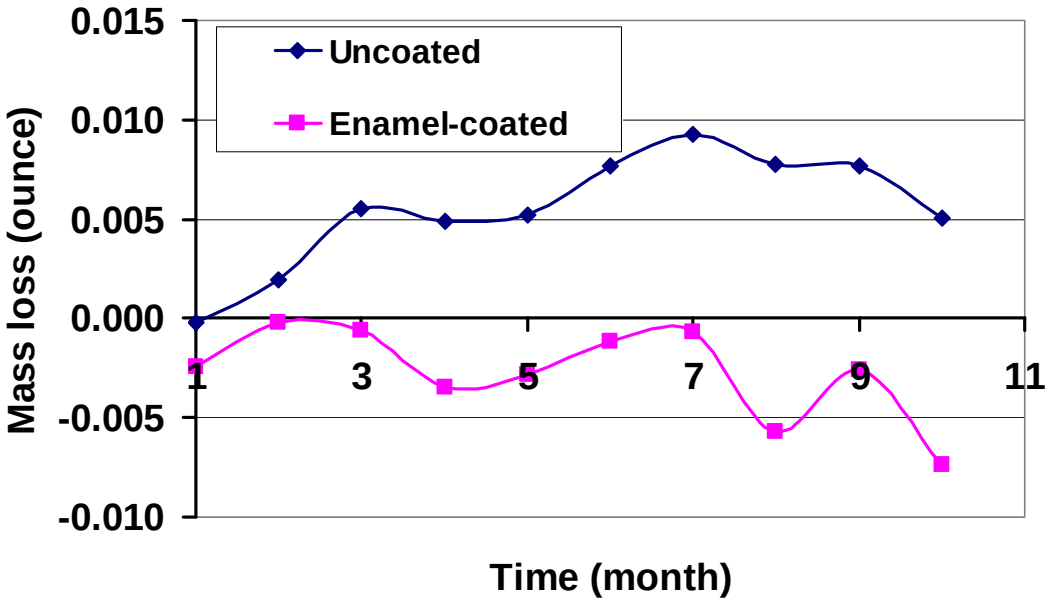

Figure 6.57 Mass loss of steel disc samples with time.

Potentiodynamic test results for enamel-coated and uncoated steel disc samples with different immersion times are presented in Figure 6.58. The corrosion currents are around 0.645 uA/in^2 (0.1 uA/cm^2) and 64.5 uA/in^2 (10 uA/cm^2) for enamel-coated and uncoated steel samples, respectively. Neither of the two sets of polarization curves for coated and uncoated samples showed a significant change over time, indicating that a stable corrosion process occurred. For uncoated samples, the corrosion environment represented by temperature, pH, and salt content changed little; the corrosion process thus remained stable all the time. For enamel-coated samples, this can be explained by the strong adhesion strength between enamel coating and steel

disc, which kept all samples in similar working conditions. In this case, the corrosion process is controlled by the diffusion of ions through the coating between the salt solution and steel surface. Note that the results in Figure 6.58(a) may be affected by the presence of marine epoxy used to strengthen enamel-coated steel discs.

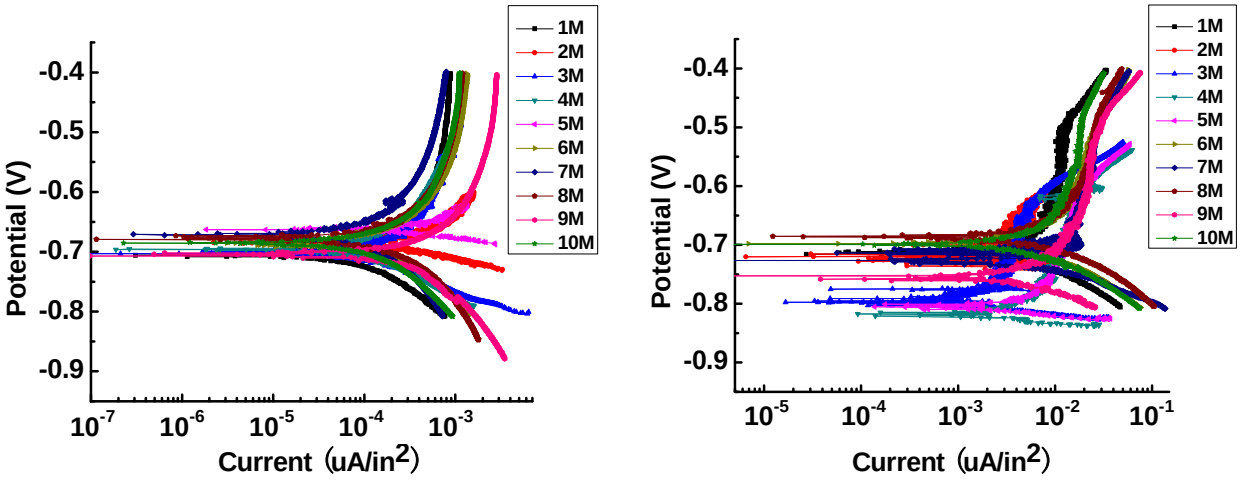

(a) With coating (b) Without coating

Figure 6.58 Tafel plots of steel disc samples

Table 6.11 shows the surface conditions of enamel-coated and uncoated samples with different immersion times. For example, 1M in Table 6.11 denotes one month. For enamel-coated samples, it can be clearly seen from Table 6.12 that the corrosion product increased over time. Throughout the tests, it was observed that the enamel coating remained intact after 10 months of immersion in salt solution. This observation was attributable to the strong adhesion between steel disc and enamel coating. For uncoated samples, steel rust can be seen on the surface of tested samples. For both coated and uncoated samples, there appeared to be a large variation of corrosion products over time. This is a reflection of the nature and complexity of the corrosion process. In addition, this is because potentiodynamic tests are generally destructive in nature. In this study, they were conducted on different samples every month. As a result, other factors except for immersion time may affect the corrosion process. In particular, coating thickness plays an important role in the process of corrosion.

Table 6.11 Surface conditions of steel disc samples

Enamel-Coated Samples									
		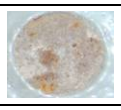	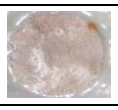	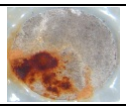	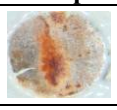	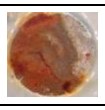	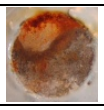	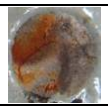	
1M	2M	3M	4M	5M	6M	7M	8M	9M	10M
Uncoated Samples									
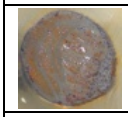		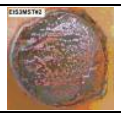							
1M	2M	3M	4M	5M	6M	7M	8M	9M	10M

6.5.2.1. Mortar cylinder samples

6.5.2.1.1. Chloride Profile Analysis

Figure 6.59 presents the average change of chloride contents with the distance from the surface of a mortar cylinder sample. Chloride content was measured at three distances every month. At each distance, three measurements were taken at three points symmetrically distributed around the center rebar of a mortar cylinder. For typical concrete mixtures, the critical chloride content for rebar corrosion is between 1 lbs (0.6 kg) and 1.51 lbs (0.9 kg) of Cl- per yd^3 (m^3) of concrete. In this study, a cement density of 200 kg/m^3 was considered as used in the standard MoDOT concrete mix design. Therefore, the critical chloride concentration may be expressed in terms of weight percent of cement. This value ranges from 0.3% to 0.45% as shown in the shadowed area in Figure 6.59.

Normalizing the chloride concentration by cement weight in Figure 6.59 provides a meaningful measure because it is related to the ratio of CL^- / OH^- that controls the formation of a depassivation layer on the surface of a reinforcing steel bar. After three to four months (3M to 4M) of immersion in salt solution, the chloride concentration at the surface of a steel bar exceeded its critical value, which means a great probability of corrosion initiation. Note that the concentration of chloride on the mortar surface, extrapolated from the diffusion curves, ranged from 1.019% to 1.138%. The lower and upper bounds corresponded to the measurements after five (5M) and two (2M) months, respectively. The other measurements (1M, 3M, 4M, and 6M) seemed quite consistent, ensuring the quality of measured data from this study.

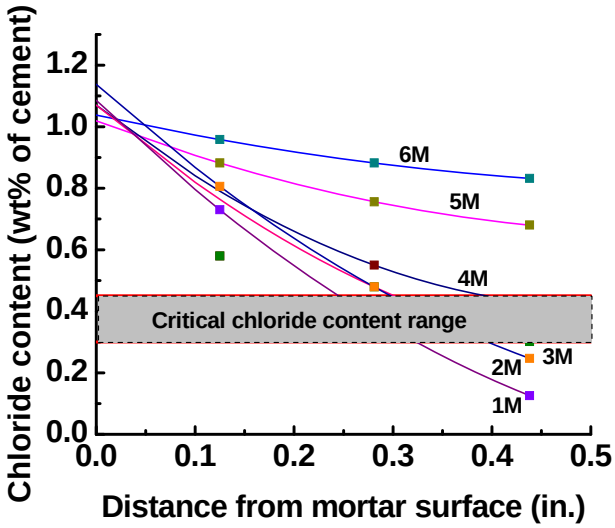

Figure 6.59 Chloride profiles at various immersion times.

6.5.2.1.2. Polarization Curves

Table 6.12 gives three indices for corrosion evaluation of steel [Building Research Establishment, 2000]. They include the polarization resistance, corrosion current, and corrosion penetration.

Table 6.12 Polarization resistance, corrosion current, and corrosion penetration [Building Research Establishment, 2000]

Rate of Corrosion	Polarization Resistance $R_p\,(k\Omega - in.^2)$	Corrosion Current Density $i_{corr}\,(\mu A/in.^2)$	Corrosion Penetration $p\,(\mu m/year)$
Very high	$0.037 < R_p < 0.37$	$64.5 < i_{corr} < 645$	$100 < p < 1000$
Moderate/high	$0.37 < R_p < 3.7$	$6.45 < i_{corr} < 64.5$	$10 < p < 100$
Low/moderate	$3.7 < R_p < 37.5$	$0.65 < i_{corr} < 6.45$	$1 < p < 10$
Passive	$37.5 < R_p$	$i_{corr} < 0.65$	$p < 1$

The polarization curves for mortar cylinder samples are presented in Figure 6.60. Four zones (passive, low/moderate, moderate/high, very high) corresponding to the corrosion currents listed in Table 6.12 are identified in Figure 6.60. It can be seen from Figure 6.60(a) that the coated samples stayed in passive state for two months of immersion in salt solution though their corrosion potential dropped from -260 mV to -350 mV. At three month (3M), corrosion seemed to begin in the coated sample or is in the low/moderate zone making a transition from passive to active corrosion. After four to six months of immersion time (4M-6M), the corrosion current of all samples significantly increased and they all fell into the moderate/high zone. This indicates that a stable corrosion process has formed in salt solution.

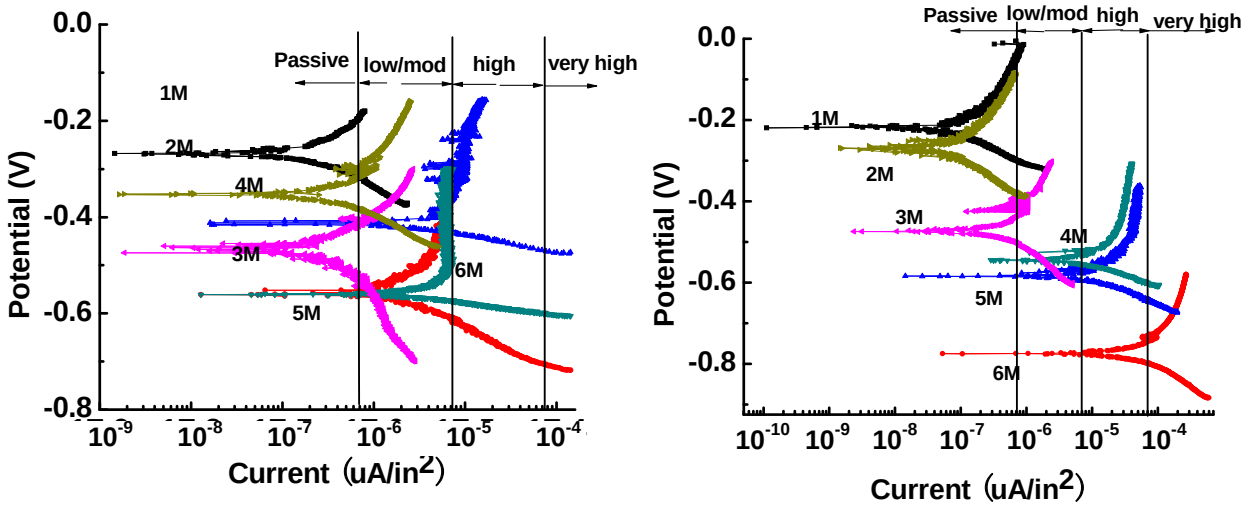

(a) Enamel-coated rebar (b) Uncoated rebar

Figure 6.60 Tafle plots of mortar cylinder samples.

The polarization curves for uncoated samples, as shown in Figure 6.60(b), indicate that, like the coated samples, they were in the passive state for the first two months (M1 and M2). Corrosion also seemed to start at three months of immersion (3M). However, unlike the coated samples, the corrosion current of uncoated samples significantly increased with immersion time after three months, indicating an active state of corrosion. Samples with four and five months of immersion (4M and 5M) have a high potential for corrosion. The sample tested at six months (6M) falls in

the very high zone. Overall, the uncoated samples corroded more significantly than the coated samples.

6.5.3 Conclusions Based on Potentiodynamic Tests

The use of enamel coating on steel rebar can increase the pH value of the corrosion environment to which the rebar is exposed. The level of increase varied with the immersion time but is around 10%. The corrosion currents of enamel-coated samples are generally lower than those of the uncoated samples, indicating less corrosion. The mass loss in coated samples was substantially less than those without coating. Thus, enamel coating can improve the corrosion resistance of steel.

Both chloride analysis and polarization curves confirmed that the coated and uncoated mortar cylinder rebar started corrosion after three months of immersion in the 3.5% NaCl solution. The coated rebar likely experienced moderate corrosion between three and six months. The uncoated rebar, however, was subjected to a high probability of corrosion after four to five months of immersion. At the end of six months, the probability of corrosion in the uncoated rebar became very high. Therefore, the enamel coating slows down the corrosion process limiting the diffusion of chloride ions through the coating.

6.6. Electrochemical Impedance Spectroscopy Test

Electrochemical Impedance Spectroscopy (EIS) is an electrochemical technique that allows the physical properties of a material to be related to its chemical properties. EIS provides a more thorough understanding of an electrochemical system than any other electrochemical techniques. Its experiment involves the application of a harmonic potential wave of low voltage amplitudes over a wide range of excitation frequencies to a sample material. The different frequency excitations allow the measurement of several electrochemical reactions that take place at very different rates as well as the measurement of the capacitance of an electrode. EIS is a powerful tool in the study of coating performance. It can be used to evaluate the deterioration of a coating based on the changes in impedance diagrams induced by the appearance of surface phenomena (pores or defects, delamination at metal/coating interface, water adsorption). In practice, the measured impedance information can be modeled as an equivalent circuit which consists of a number of electrical elements such as resistance, capacitance, inductance, and so on. From the change of simulated electrical elements, the change of coating and coating damage due to corrosion can be identified.

6.6.1. Technical Approach

6.6.1.1. Test specimens and material properties

The samples used for EIS tests are the same as those used for potentiodynamic tests. In this study, two groups of samples (steel disc and mortar cylinder) were fabricated as detailed in Section 6.5.

6.6.1.2. Test method, setup, and protocol

EIS tests share the similar setup to potentiodynamic tests as discussed in Section 6.5.1.2. Prior to impedance measurements, a period of 30 minutes was given to attain a stable value for the open circuit potential E_{oc}. The impedance measurements were performed under a sinusoidal potential wave of 10 mV around E_{oc} with excitation frequency ranging from 0.001 Hz to 100 kHz. They were taken at one month intervals for a period of 6 months for mortar cylinder samples and for a period of 10 months for steel disc samples, respectively.

6.6.2. Results and Discussion

6.6.2.1. Steel disc samples

For the uncoated samples, Figure 6.61(a) presents the Nyquist plots from various EIS tests at different immersion times, in which the real part of impedances is plotted as a function of the imaginary part of the impedances as the excitation frequency varies. These plots can be simulated by an equivalent electrical circuit (EEC) model of three circuit elements: a solution resistance connected in series with a parallel system of a polarization resistance (R_p) and a constant phase element (CPE), representing the steel-solution interface effect upon the corrosion resistance of steel discs. The best-fitted polarization resistances of uncoated steel samples are plotted in Figure 6.61(b) as a function of immersion time. The polarization resistance fluctuated but overall increased with immersion time.

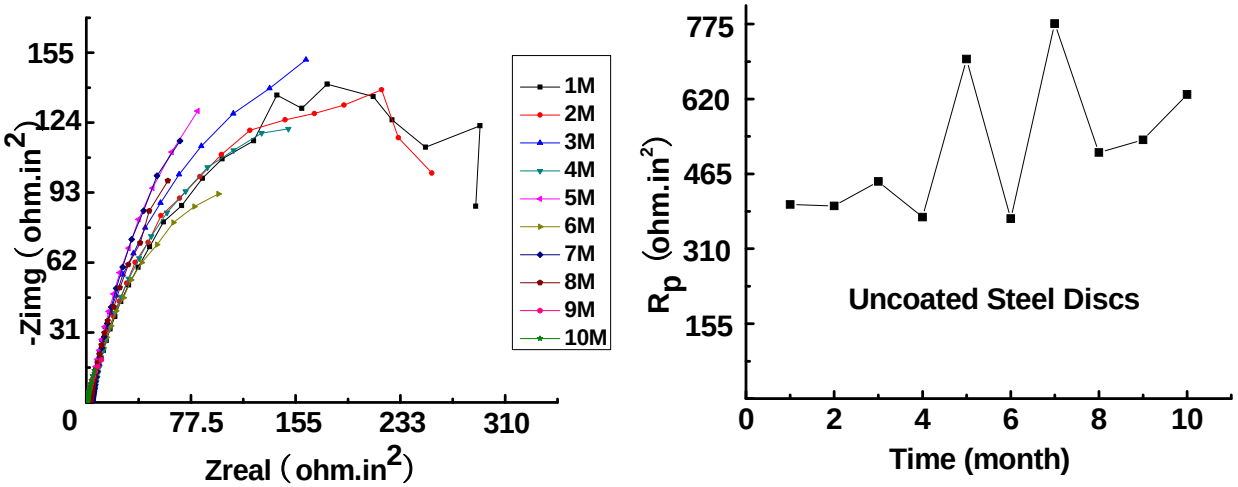

(a) Nyquist plots (b) Polarization resistance with time

Figure 6.61 EIS test results from uncoated steel disc samples.

For the enamel-coated samples, the Nyquist plots are presented in Figure 6.62(a). The results obtained in this case did not fit a typical solution-coating-steel EEC model. It was discovered at the end of this study that the Loctite Aquamarine Epoxy used to strengthen enamel coating around the edge of steel discs may have had significant influences on the corrosion process of enamel-coated steel disc samples. Figure 6.62(b) presents the Nyquist plot of a new steel disc sample strengthened with Loctite Professional Heavy Duty Epoxy before it was submerged into the salt solution. Unlike Figure 6.62(a), Figure 6.62(b) can be modeled as part of a semi-circle, giving a polarization resistance.

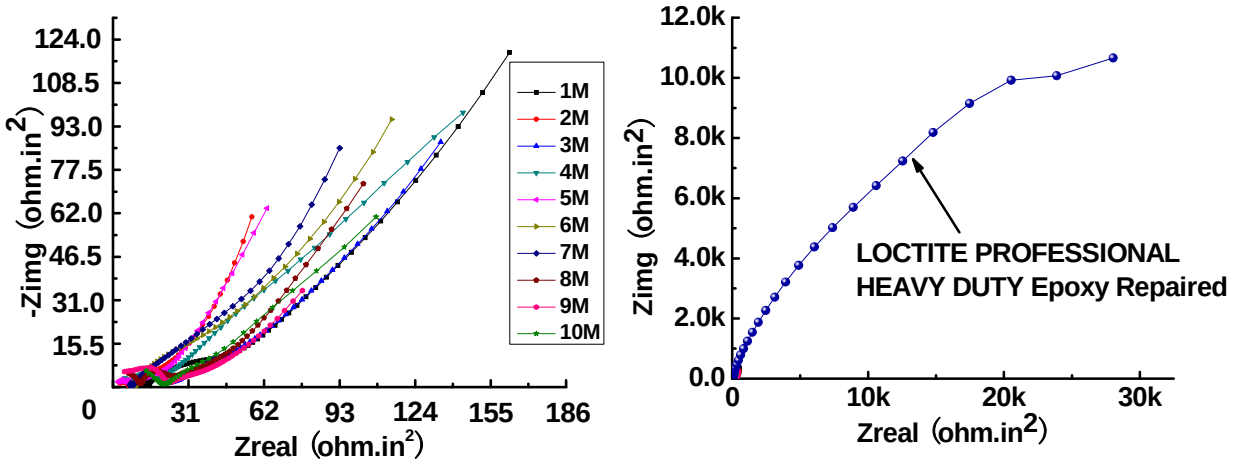

(a) Loctite aquamarine epoxy (b) Loctite professional heavy duty epoxy

Figure 6.62 Nyquist plots of enamel-coated steel discs strengthened with different epoxies.

6.6.2.2. Mortar cylinder samples

Figure 6.63 shows the typical impedance spectra of mortar cylinder samples with uncoated rebar. In general, both modulus and phase angle of the impedances decreased with the excitation frequency. The only exception to this overall performance is the fluctuation of phase angle around 100 Hz, corresponding to one month of immersion in salt solution. Considering the data from potentiodynamic tests, corrosion is mostly active after two to three months. Therefore, for the purpose of corrosion evaluation, the EIS results presented in Figure 6.63 are quite consistent. The impedance resistance of the solution-steel system rapidly decreased till approximately 0.1 Hz and then slowly reduced.

Figure 6.64 presents the impedance spectra of mortar cylinder samples with enamel-coated rebar. In general, the mortar cylinder samples with uncoated rebar exhibited similar corrosion behavior as observed for enamel-coated rebar. However, the magnitude of impedances is generally higher, particularly after the samples have been immersed in the salt solution for four to six months (4M-6M).

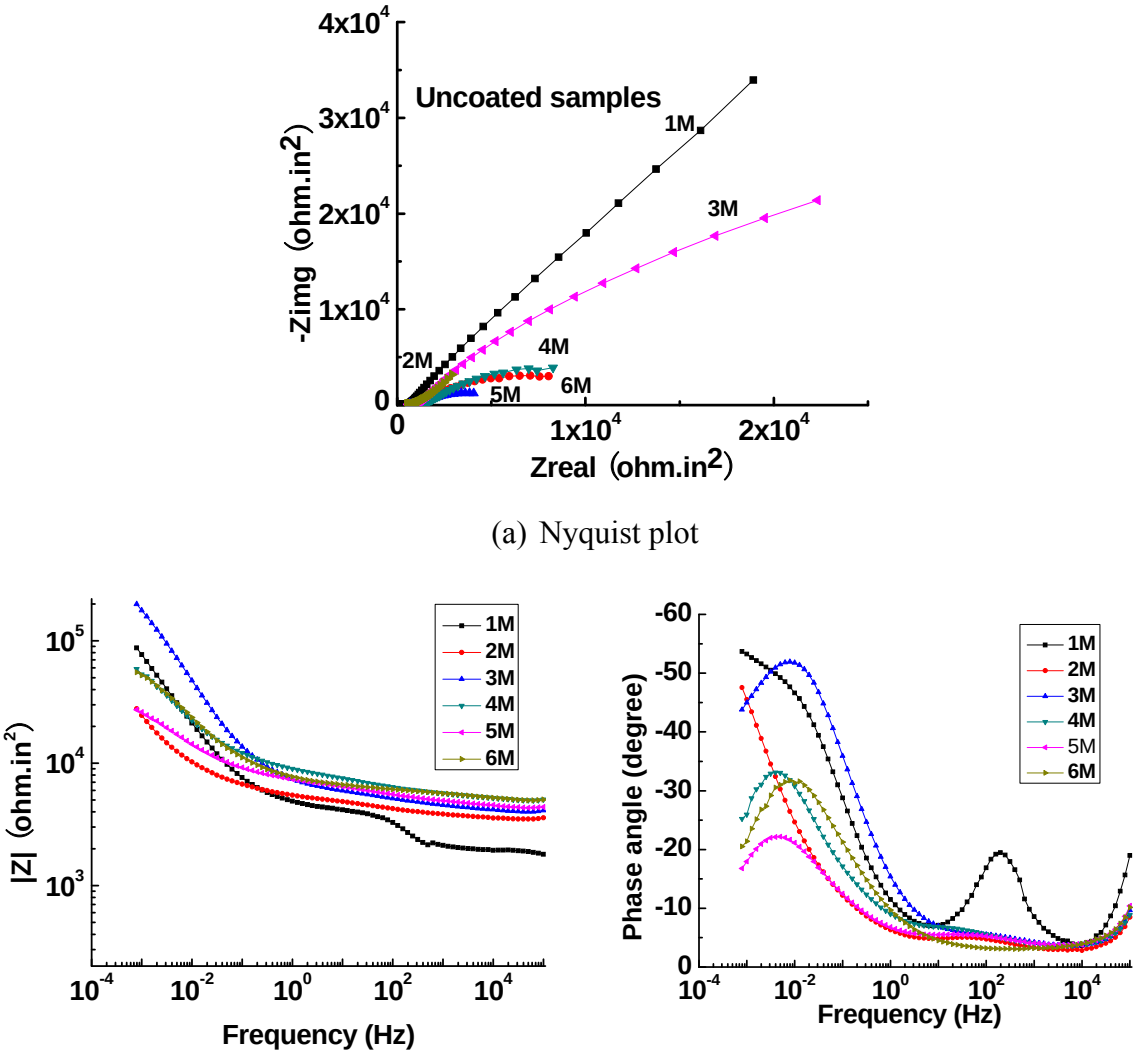

(a) Nyquist plot

(b) Impedance modulus

(c) Impedance phase angle

Figure 6.63 Impedance spectra of mortar cylinder samples with uncoated rebar at various immersion times.

The impedance spectra of a mortar cylinder sample can also be interpreted by an EEC model consisting of an electric resistance in series with a RQ network shown in Figure 6.65. The series resistance R_s accounts for the ionic conduction in the electrolyte filling the pores in the mortar. The CPE represents the total capacitance of the mortar covering of rebar, the enamel coating and the interface between steel and enamel coating. The parallel element R_p denotes the polarization resistance related to the process of corrosion.

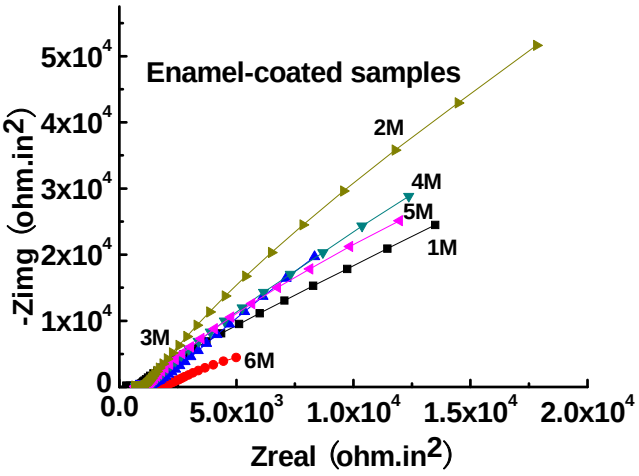

(a) Nyquist plot

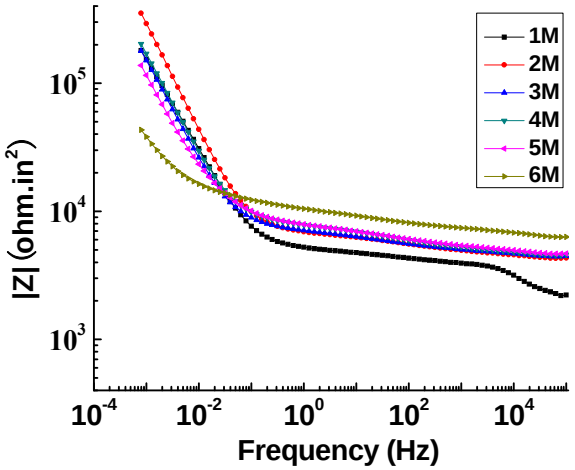

(b) Impedance modulus

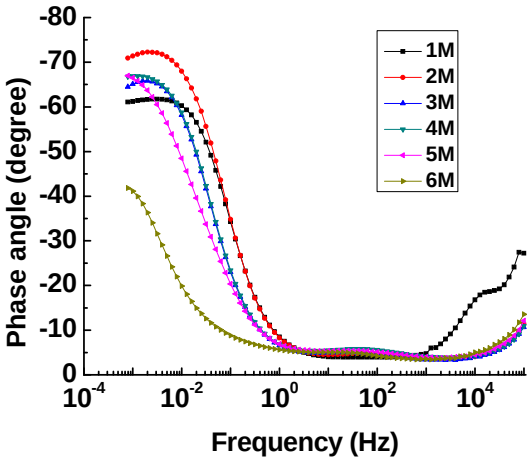

(c) Impedance phase angle

Figure 6.64 Impedance spectra of mortar cylinder samples with enamel-coated rebar at various immersion times.

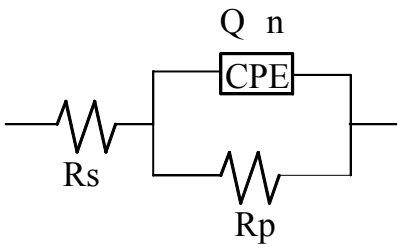

Figure 6.65 Equivalent electrical circuit (EEC) model of a mortar sample.

The CPE is an ideal but unreal circuit element used to represent the response of a real-world system. The Nyquist plot is ideally expected to be a semicircle with the center on the real axis; but in many EIS experiments, the observed plot is an arc of a circle with the center some distance below the real axis. One common explanation for this phenomenon is that "some property of the system is not homogenous or that there is a distribution of some physical properties of the system [Ekekwe, 2009]. Mathematically, a CPE's impedance is inversely proportional to the Q parameter and excitation frequencies. When n=1, the CPE resembles a capacitor.

After the EIS test data was fitted into the EEC model, various model parameters can be identified as listed in Table 6.13 or presented in Figure 6.66. The mortar resistances of enamel-coated and uncoated samples are compared in Figure 6.66(a). This resistance was calculated from simulation results of the high frequency response of the spectra, which can also be concluded from the bode plots shown in Figure 6.63(b) and Figure 6.64(b) in the range of high frequency. In theory, when the frequency of scanning potential reaches a very high value, the capacitance would be close to zero and the resistance of the system would dominate. The resistance of the mortar increased with immersion time for enamel-coated samples from 465 ohm.in^2 (3000 ohm.cm^2) for one month immersion to 1561 ohm.in^2 (10070 ohm.cm^2) for six months of immersion in salt solution. This can be explained by a decrease of voids inside the mortar due to hydration reactions and the carbonization process. However, the resistance for uncoated rebar samples did not increase but decreased after five and six months of immersion in salt solution. This observation is likely due to different samples tested over time.

Table 6.13 EEC model parameters for mortar cylinder samples with enamel-coated rebar immersed in salt solution for various times

Rebar	Time	Rs (ohm.in^2)	Q ($\times 10^{-4}$ F/in^2)	N	Rp ($\times 10^6$ohm.in^2)
Enamel-coated	1M	772	19.35	0.78	0.16
	2M	1085	16.13	0.85	0.66
	3M	1132	25.80	0.81	0.24
	4M	1247	22.58	0.81	0.43
	5M	1278	26.32	0.75	0.45
	6M	1725	44.12	0.59	0.02
Uncoated	1M	630	11.61	0.72	0.47
	2M	1013	70.31	0.62	0.40
	3M	1010	9.29	0.68	0.10
	4M	1341	17.42	0.57	0.02
	5M	1087	26.38	0.51	0.006
	6M	836	76.76	0.45	0.02

As shown in Figure 6.66(b), the charge transfer polarization resistances of enamel-coated rebar samples were always larger than those of uncoated rebar samples except for the first month test results, indicative of a lower corrosion rate of enamel coating. For uncoated rebar samples, the charger transfer resistance decreased with time consistently, which can be verified with the expected intersection values of curves with the real axis in Figure 6.63(a) and Figure 6.64(a). The decrease of charge transfer resistance with time indicates the increase of corrosion rate for uncoated-rebar samples.

The slope of each Nyquist plot in Figure 6.63(a) and Figure 6.64(a) can also be used as a corrosion behavior indicator. When the slope is close to 1.0, the capacitive behavior of mortar-rebar system dominates, revealing steel passivity. As shown in Figure 6.66(d), the slopes of enamel-coated rebar samples are always greater than those of uncoated rebar samples. Therefore, there is a more dominant capacitive behavior in enamel-coated samples than uncoated rebar samples. This result indicates the protective ability of enamel coating for steel rebar corrosion. The slopes of both coated and uncoated rebar systems decrease with time since more chloride ions have gradually penetrated through the mortar cover of a mortar cylinder sample. Eventually stable ion exchange passages were formed with the solution in the mortar pores.

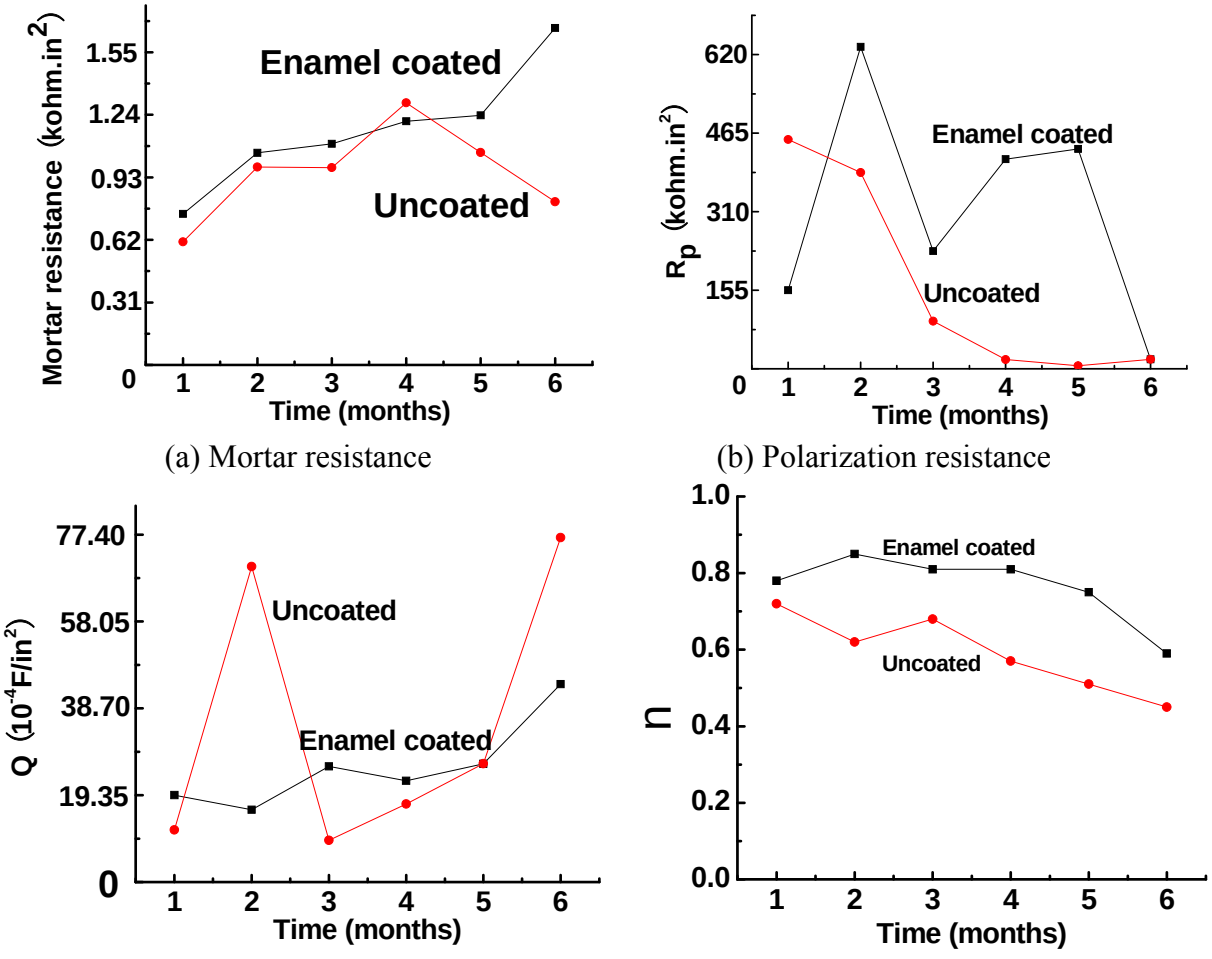

(a) Mortar resistance (b) Polarization resistance

(c) Q factor (d) n values

Figure 6.66 EEC model parameters changes over time.

6.6.3 Conclusions Based on EIS Tests

Corrosion test results are sensitive to several factors. In this study, local touchups around the edge of steel discs with marine epoxy were demonstrated to be a dominant uncertainty factor for enamel-coated steel discs. The next factor is the thickness of enamel coating. For mortar cylinder

samples, the coating thickness and the mortar quality can be two main sources of uncertainties among various EIS tests. Future tests shall be designed to minimize, if not completely eliminate, the effects of uncertainties.

The modulus of impedances for mortar cylinder samples rapidly drops until an excitation frequency of approximately 0.1 Hz and then decreases slowly. Both the modulus and phase angle of uncoated and coated rebar samples become much smaller after 1.0 Hz. For mortar cylinder samples, the impedance magnitude of enamel-coated rebar is generally higher than that of uncoated rebar. In comparison with uncoated rebar samples, the enamel-coated rebar samples have a more significant capacitive behavior that is closely related to steel passivity.

7. RECOMMENDATIONS

7.1. Concrete-Steel Bond Behavior

A mixture of 50% enamel and 50% calcium silicate or 50/50 enamel coating is recommended for a maximum increase of the bond strength between steel rebar and concrete. If corrosion is a concern, a double-coat system consisting of an inner layer of pure enamel and an outer layer of 50/50 enamel coating is recommended based on limited laboratory tests. Although the test results of pure enamel and 50/50 coating are indicative of the improved performance of a double-coat system both for bond strength and corrosion resistance, more tests should be conducted to validate the new coating system in field conditions.

7.2. Steel Corrosion Process

Pure enamel is recommended for a moderate protection of steel rebar in corrosive environments. The double-coat system with an inside pure enamel layer and an outside 50/50 coating is recommended for maximum corrosion protection when costs are less of a concern or where enhanced steel-concrete bond strengths are needed. Furthermore, a manufacturing technique that provides uniform coating thicknesses, such as electrostatic applications, will significantly improve the corrosion performance of the enamel coatings. The tradeoff between corrosion performance and coating cost shall be investigated with a case study of highway bridges.

7.3. Development Length and Splice Length Equations

The development length of enamel-coated steel bars in lap splice and anchorage areas shall be determined using the ACI 318-08 design equations. A coating factor of 0.85 is recommended for lap splice designs. Although 60% of the ACI 318-08 required anchorage length for uncoated rebar appears sufficient based on the limited number of tests, 85% of the anchorage length required by ACI 318-08 is recommended for the anchorage design of enamel-coated rebar.

8. IMPLEMENTATION PLAN

Extensive laboratory tests have concluded that a coating factor of 0.85 can be used to take into account the effect of enamel coating on rebar-concrete bond strengths in lap splice areas. In anchorage areas, the development length of enamel-coated rebar can be further reduced. Therefore, the use of enamel coating can reduce at least 15% steel in lap splice and anchorage areas. Considering that the use of epoxy coating in current practices adds at least 20~50% rebar development lengths, the cost saving associated with the use of enamel coating can amount to 35% ~ 65% in joint areas of a reinforced concrete structure provided that the unit price for enamel coating is equivalent to epoxy coating. Therefore, the enamel technology is a viable technology for field implementation.

To transfer the new coating technology into practice, a case study on a real-world bridge is needed to document the field performance and a combined effect of many environmental factors such as moisture, temperature, vibration at construction sites, etc.

9. BIBLIOGRAPHY

AASHTO T 259 (2002), *Resistance of Concrete to Chloride Ion Penetration*, American Association of State Highway and Transportation Officials, Washington D.C..

AASHTO (2004), *Standard Specifications for Highway Bridges*, American Association of State Highway and Transportation Officials, Washington D.C..

Abrams D.A. (1913), "Test of Bond between Concrete and Steel," *Bulletin No. 71*, Engineering Experiment Stiduation, University of Illinois, Urbana, III, 105pp.

ACI (2008), *Building Code Requirements for Structural Concrete and Commentary*, ACI 318-08, American Concrete Institute, Farmington Hills, MI.

ACI (2001), *Protection of Metals in Concrete Against Corrosion*, ACI 222R-01, American Concrete Institute, Farmington Hills, MI.

ASTM A 615 (2009), *Standard Specification for Deformed and Plain Carbon-Steel Bars for Concrete Reinforcement*, American Society of Testing and Materials, West Conshohocken, PA.

ASTM B 117 (2009), *Standard Practice for Operating Salt Spray (Fog) Apparatus*, American Society of Testing and Materials, West Conshohocken, PA.

ASTM C 39 (2009), *Standard Test Method for Compressive Strength of Cylindrical Concrete Specimens*, American Society of Testing and Materials, West Conshohocken, PA.

ASTM C109/C109M-08 (2007), *Standard Test Method for Compressive Strength of Hydraulic Cement Mortars (using 50-mm cube specimens)*, American Society of Testing Methods (ASTM).

ASTM C 617 (2009), *Standard Practice for Capping Cylindrical Concrete Specimens*, American Society of Testing and Materials, West Conshohocken, PA.

ASTM G 14 (2004), *Standard Test Method for Impact Resistance of Pipeline Coatings (Falling Weight Test)*, American Society of Testing and Materials, West Conshohocken, PA.

ASTM G 16 (2010), *Standard Guide for Applying Statistics to Analysis of Corrosion Data*, American Society of Testing and Materials, West Conshohocken, PA.

Broomfield, John P. (2007), *Corrosion of Steel in Concrete Understanding, Investigation and Repair*, Taylor & Francis (Second Edition).

Brown, M.C. and Weyers, R.E. (2003), "Corrosion protection service life of epoxy coated reinforcing steel in Virginia bridge decks," *Final Contract Report*, Virginia Transportation Research Council, Charlottesville, Virginia.

Building Research Establishment. (2000), "Corrosion of steel in concrete: investigation and assessment," *Digest* 444, Part 2, BRE, Garston, pp. 444-448.

Chen, G. D., Baird, J., Yan, D. M., and Koenigstein, M. (2010), "Blast tests of full-size wall barriers reinforced with enamel-coated steel rebar," *Final Report LWI191000*, Leonard Wood Institute, St. Robert, Missouri.

Chen, G.D., Brow, R., Baird, J., Reis, S., Yan, D. M., Koenigstein, M., and Malone, P. G. (2009), "Blast protection of critical infrastructure by use of concrete barriers reinforced with enamel coated steel rebar and fibers," *Final Report LWI61009*, Leonard Wood Institute, St. Robert, Missouri.

Day, D.C., Weiss, C.A., Malone, P., and Hackler, C.L. (2006), "Innovative method of bonding Portland cement concrete to steel using a porcelain interface," *Materials Science and*

Technology (MS&T) Conference Proceedings, The American Ceramic Society, Westerville, OH.

Ekekwe, N. (2009), *Electrochemical Impedance Spectroscopy : Corrosion Behavior Application Theory, Modeling, and Experimentation*, VDM Verlag Dr. Muller Aktiengesellschaft & Co. KG.

Fyles, K.M., and Shorrock, P. (1982), "Alkali resistant glass fibers for cement reinforcement," U.S. Patent 4,345,037, Assigned to Pilkington Brothers Ltd (GB).

Hackler, C., Koenigstein, M., and Malone, P. (2006), "The use of porcelain enamel coatings on reinforcing steel to enhance the bond to concrete and steel surfaces, " *Mater. Sci. & Tech. Conf. Proc.*, The American Ceramic Society, Westerville, Ohio.

Hartt, W.H., Powers, R.G., Leroux, V., and Lysogorski, D.K. (2004), "Critical literature review of high-performance corrosion reinforcements in concrete bridge applications," *Final Report FHWA-RD-04-093*, July.

NRC, *International Critical Tables*, McGraw-Hill, 2, p. 116, National Research Council (NRC), Washington, D.C., 1927.

Ou, J.P., Zhou, Z., and Chen, G.D. (2010), "Fiber Bragg grating sensors in civil engineering applications," Chapter 8 in Fiber Bragg Grating Sensors: Recent Advancements, Industrial Applications and Market Exploitation, Edited by Dr. Andrea Cusano from the Optoelectronic Division, Department of Engineering, University of Sannio, 82100 Benevento, Italy, Bentham Science Publishers, E-Book Program, www.bentham.org/ebooks.

Sagues, A. et al. (1994), "Corrosion of epoxy coated rebar in Florida bridges," *Final Report WPI No. 0510603*, Florida Department of Transportation.

Thompson, N.G., Lankard, D., and Sprinkel, M. (1992), "Improved grouts for bonded tendons in post-tensioned bridge structures," *Report No. FHWA-RD-91-092*, Federal Highway Administration, Cortest Columbus Technologies.

Volz, J.S., Schokker, A.J., and Pacheco, A.R. (2008), "Linear polarization resistance for acceptance testing of post-tensioning grouts," *Proc. Concrete Bridge Conference*, St. Louis, Missouri.

APPENDIX A: SALT SPRAY TEST

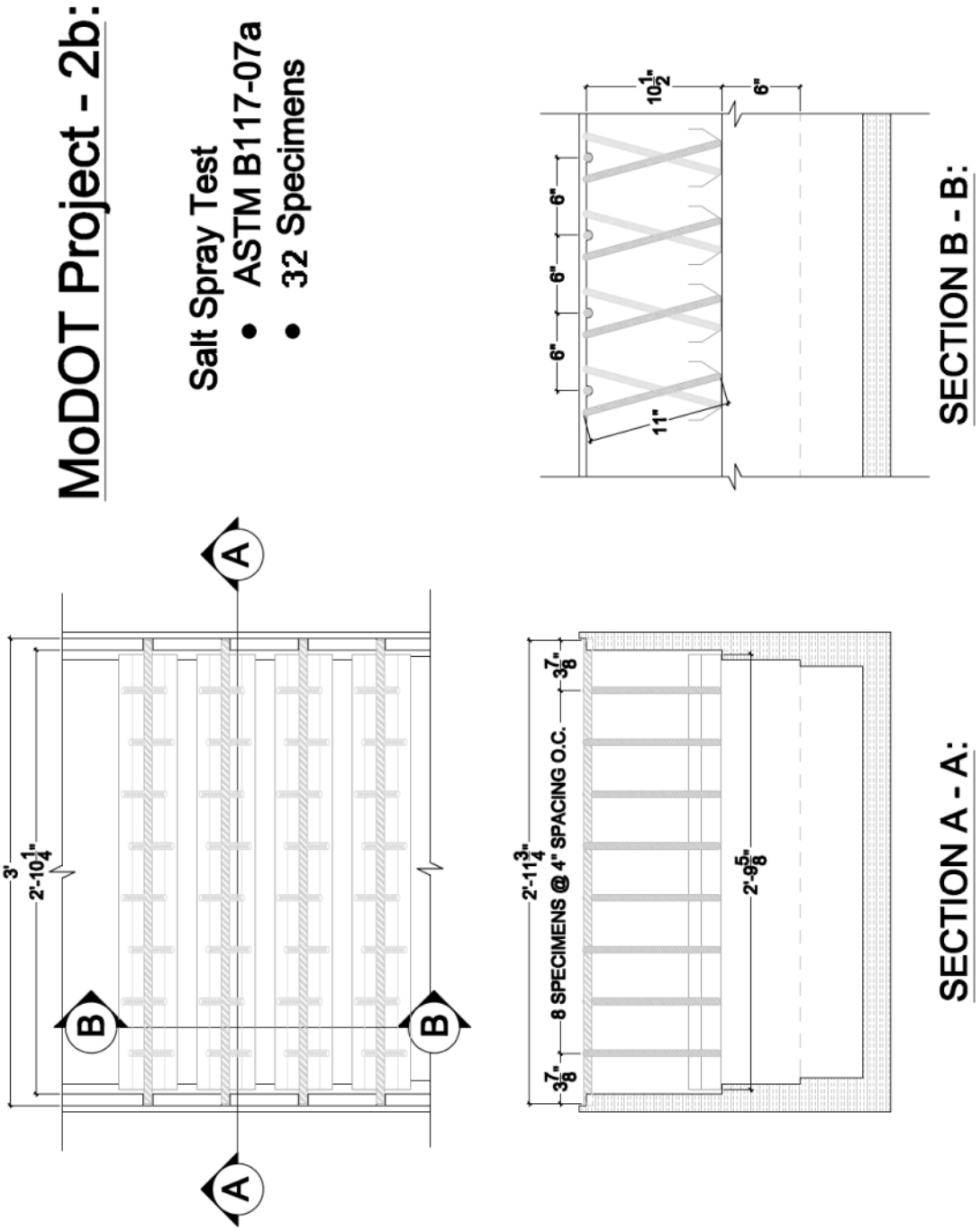

Figure A - 1: Salt spray specimen layout within the salt spray chamber.

Figure A - 2: Front side of the smooth 50/50 enamel-coated salt spray specimens after testing.

Figure A - 3: Backside of the smooth 50/50 enamel-coated salt spray specimens after testing.

Figure A - 4: Front side of the deformed 50/50 enamel-coated salt spray specimens after testing.

Figure A - 5: Backside of the deformed 50/50 enamel-coated salt spray specimens after testing.

Figure A - 6: Right side of the deformed 50/50 enamel-coated salt spray specimens after testing.

Figure A - 7: Left side of the deformed 50/50 enamel-coated salt spray specimens after testing.

Figure A - 8: Front side of the smooth double enamel-coated salt spray specimens after testing.

Figure A - 9: Backside of the smooth double enamel-coated salt spray specimens after testing.

Figure A - 10: Front side of the deformed double enamel-coated salt spray specimens after testing.

Figure A - 11: Backside of the deformed double enamel-coated salt spray specimens after testing.

Figure A - 12: Right side of the deformed double enamel-coated salt spray specimens after testing.

Figure A - 13: Left side of the deformed double enamel-coated salt spray specimens after testing.

Figure A - 14: Front side of the smooth pure enamel-coated salt spray specimens after testing.

Figure A - 15: Backside of the smooth pure enamel-coated salt spray specimens after testing.

Figure A - 16: Front side of the deformed pure enamel-coated salt spray specimens after testing.

Figure A - 17: Backside of the deformed pure enamel-coated salt spray specimens after testing.

Figure A - 18: Right side of the deformed pure enamel-coated salt spray specimens after testing.

Figure A - 19: Left side of the deformed pure enamel-coated salt spray specimens after testing.

Figure A - 20: Front side of the smooth epoxy-coated salt spray specimens after testing.

Figure A - 21: Backside of the smooth epoxy-coated salt spray specimens after testing.

Figure A - 22: Front side of the deformed epoxy-coated salt spray specimens after testing.

Figure A - 23: Backside of the deformed epoxy-coated salt spray specimens after testing.

Figure A - 24: Right side of the deformed epoxy-coated salt spray specimens after testing.

Figure A - 25: Left side of the deformed epoxy-coated salt spray specimens after testing.

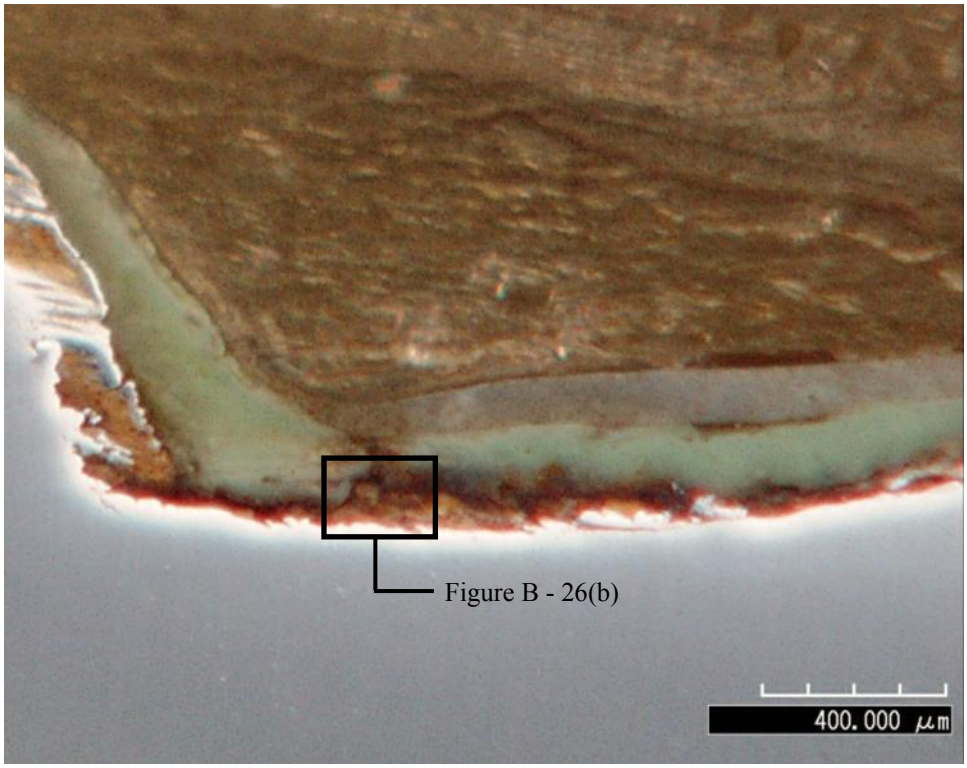

(a)

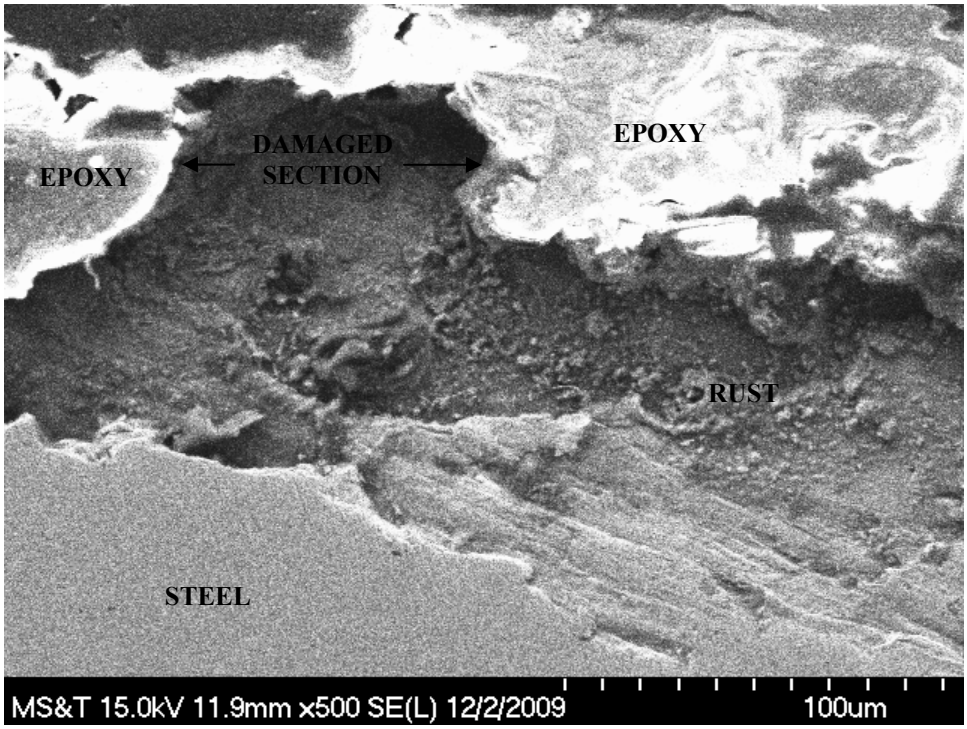

(b)

Figure A - 26: (a) Rust undercutting the epoxy coating near an unintentionally damaged section along salt spray specimen. (b) A close-up of the damaged section within the epoxy coating.

APPENDIX B: ACCELERATED CORROSION TEST

Table B - 1: T_{corr} values for the non-grouted smooth 50/50 enamel-coated ACT specimens.

Specimen No.	t_{corr} (hrs.)
1	0
2	0
3	0
4	0
5	0
6	0
7	0
8	0
Average t_{corr}:	0
Standard Deviation:	0
Standard Error:	0
COV:	- - - - -

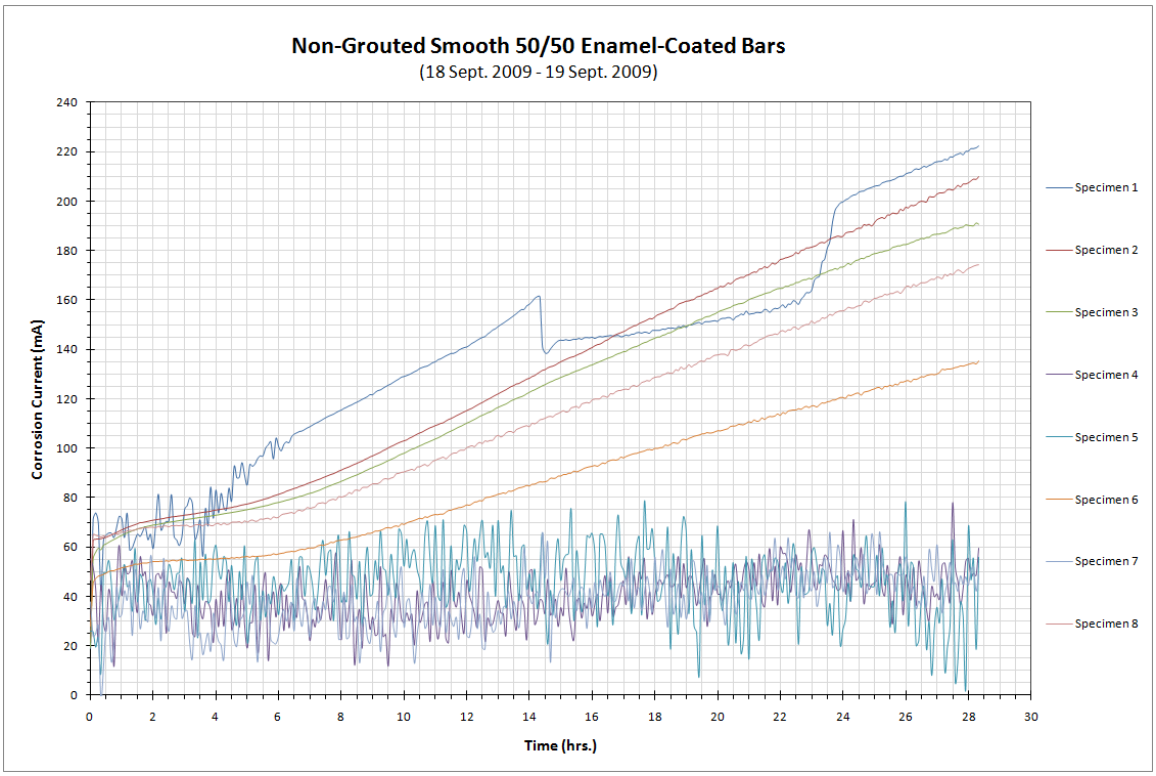

Figure B - 1: Corrosion current versus time plot for the non-grouted smooth 50/50 enamel-coated ACT specimens.

Table B - 2: T_{corr} values for the non-grouted deformed 50/50 enamel-coated ACT specimens.

Specimen No.	t_{corr} (hrs.)
1	0
2	0
3	0
4	OMITTED
5	0
6	0
7	0
8	0
Average t_{corr}:	0
Standard Deviation:	0
Standard Error:	0
COV:	- - - - -

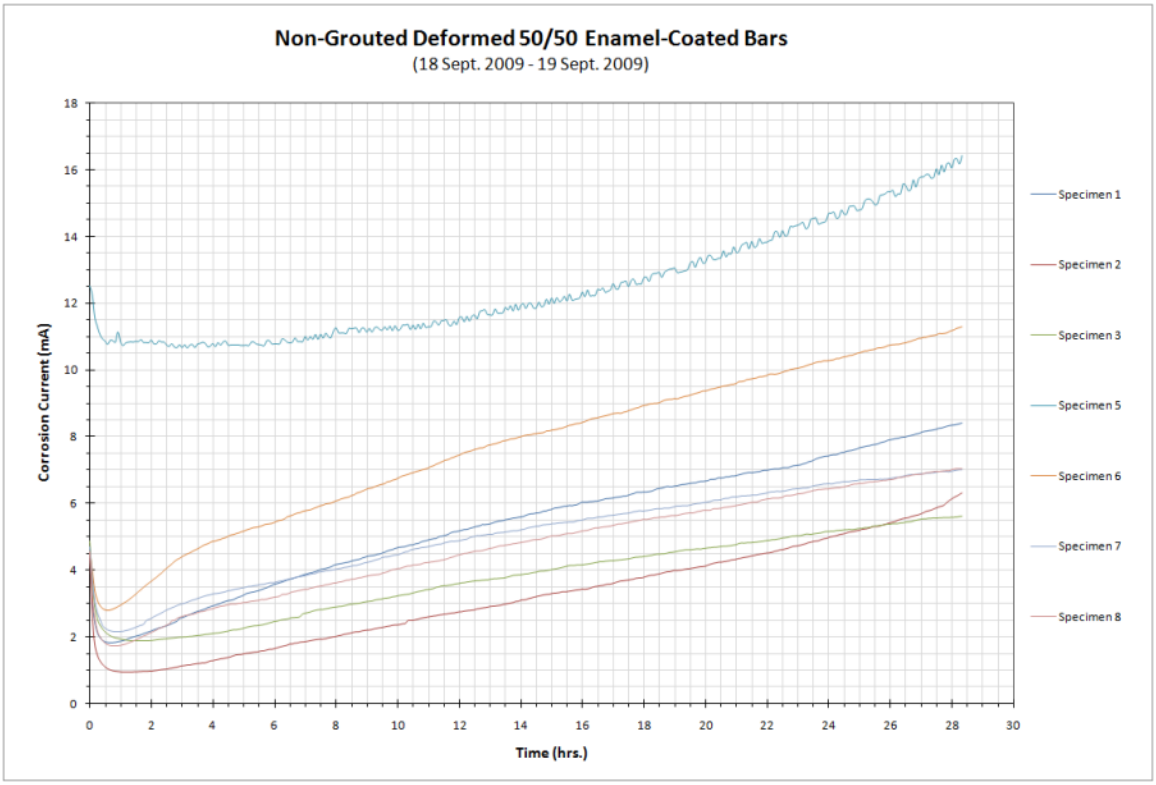

Figure B - 2: Corrosion current versus time plot for the non-grouted deformed 50/50 enamel-coated ACT specimens.

Table B - 3: T_{corr} values for the non-grouted smooth pure enamel-coated ACT specimens.

Specimen No.	t_{corr} (hrs.)
1	0
2	0
3	0
4	0
5	0
6	0
7	0
8	0
Average t_{corr}:	0
Standard Deviation:	0
Standard Error:	0
COV:	- - - - -

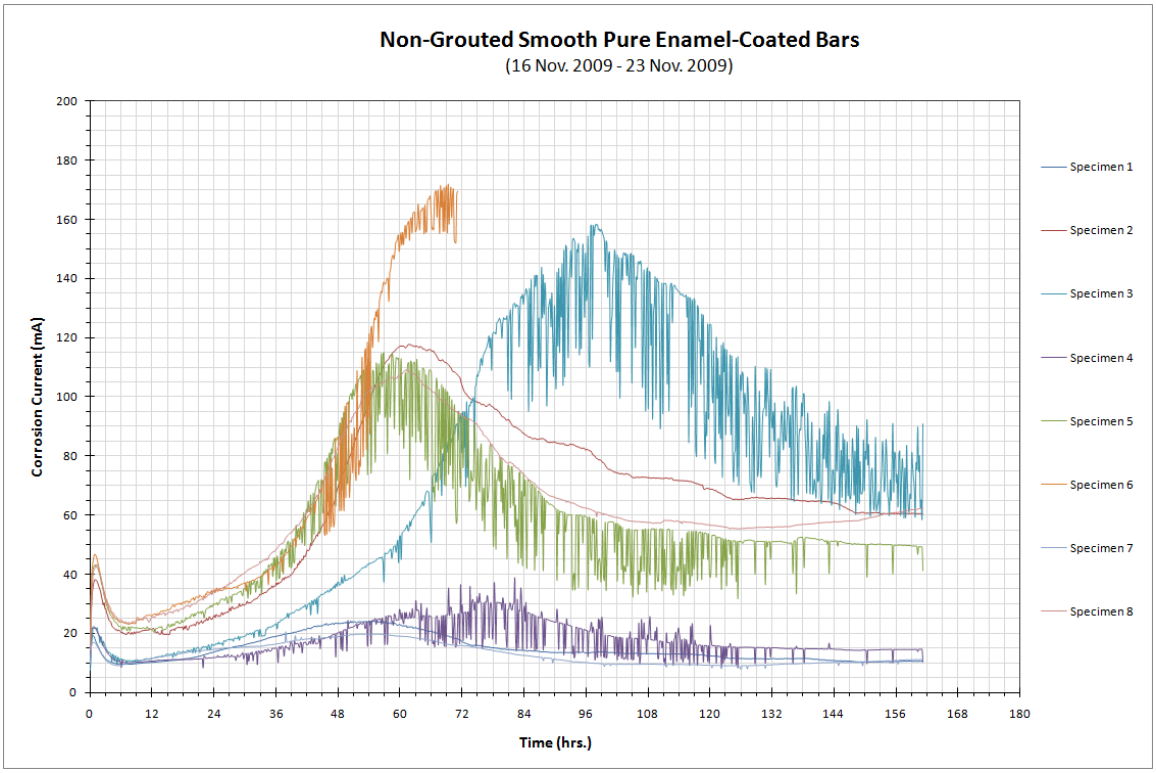

Figure B - 3: Corrosion current versus time plot for the non-grouted smooth pure enamel-coated ACT specimens.

Table B - 4: T_{corr} values for the non-grouted deformed pure enamel-coated ACT specimens.

Specimen No.	t_{corr} (hrs.)
1	68
2	175
3	99
4	151
5	66
6	131
7	66
8	90
Average t_{corr}:	106
Standard Deviation:	42
Standard Error:	15
COV:	39.7%

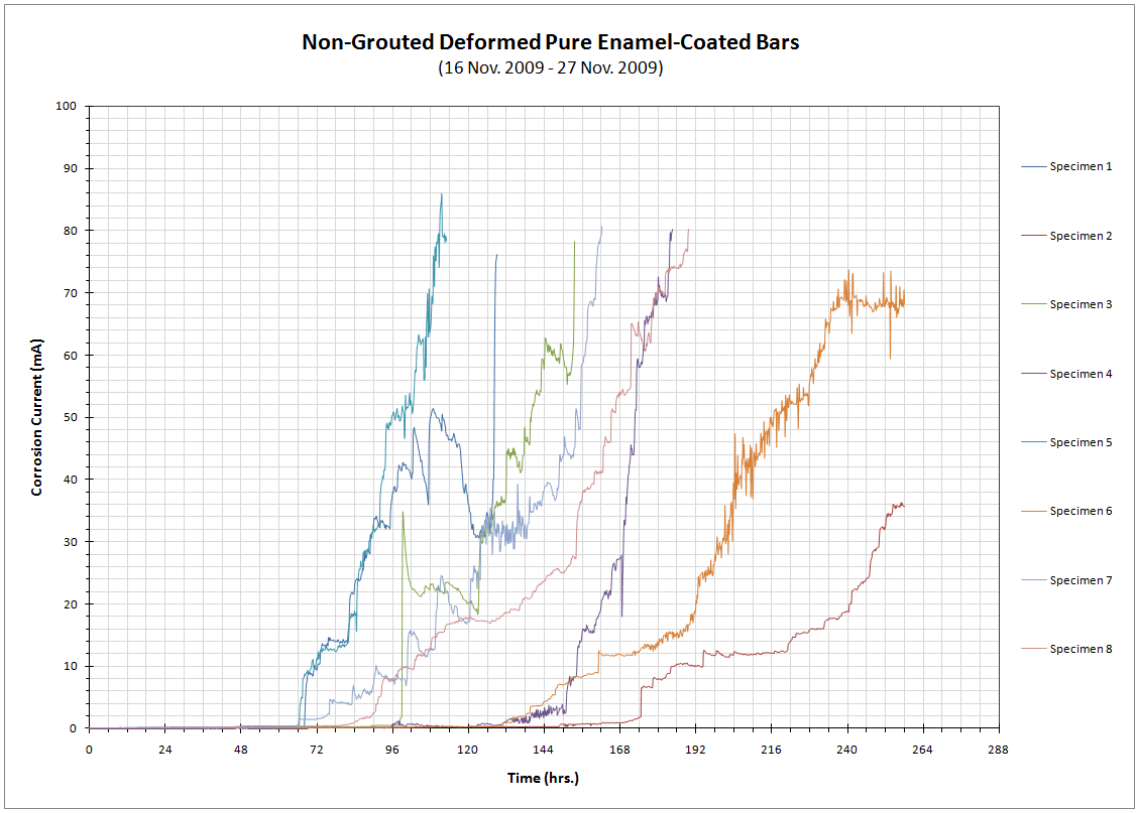

Figure B - 4: Corrosion current versus time plot for the non-grouted deformed pure enamel-coated ACT specimens.

Table B - 5: T_{corr} values for the non-grouted smooth double enamel-coated ACT specimens.

Specimen No.	t_{corr} (hrs.)
1	0
2	0
3	0
4	0
5	0
6	0
7	0
8	0
Average:	0
Standard Deviation:	0
Standard Error:	0
COV:	- - - - -

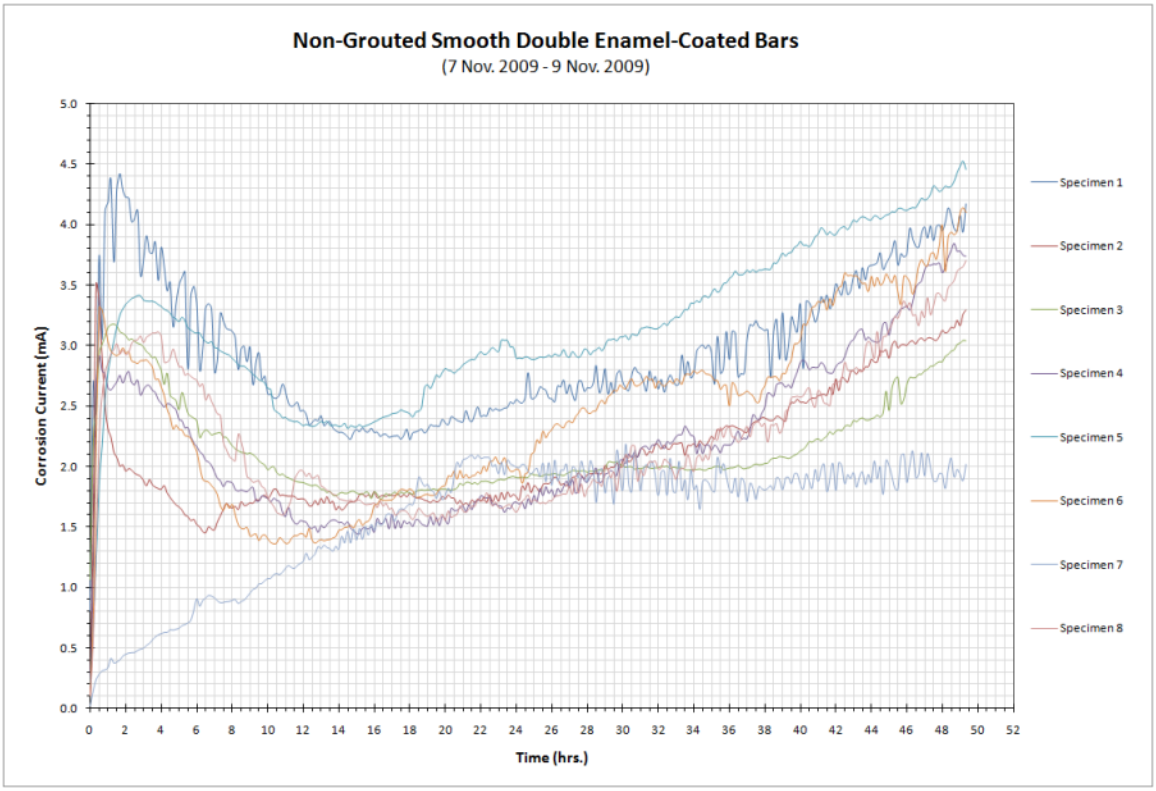

Figure B - 5: Corrosion current versus time plot for the non-grouted smooth double enamel-coated ACT specimens.

Table B - 6: t_{corr} values for the non-grouted deformed double enamel-coated ACT specimens.

Specimen No.	t_{corr} (hrs.)
1	0
2	0
3	0
4	0
5	0
6	0
7	0
8	0
Average:	0
Standard Deviation:	0
Standard Error:	0
COV:	- - - - -

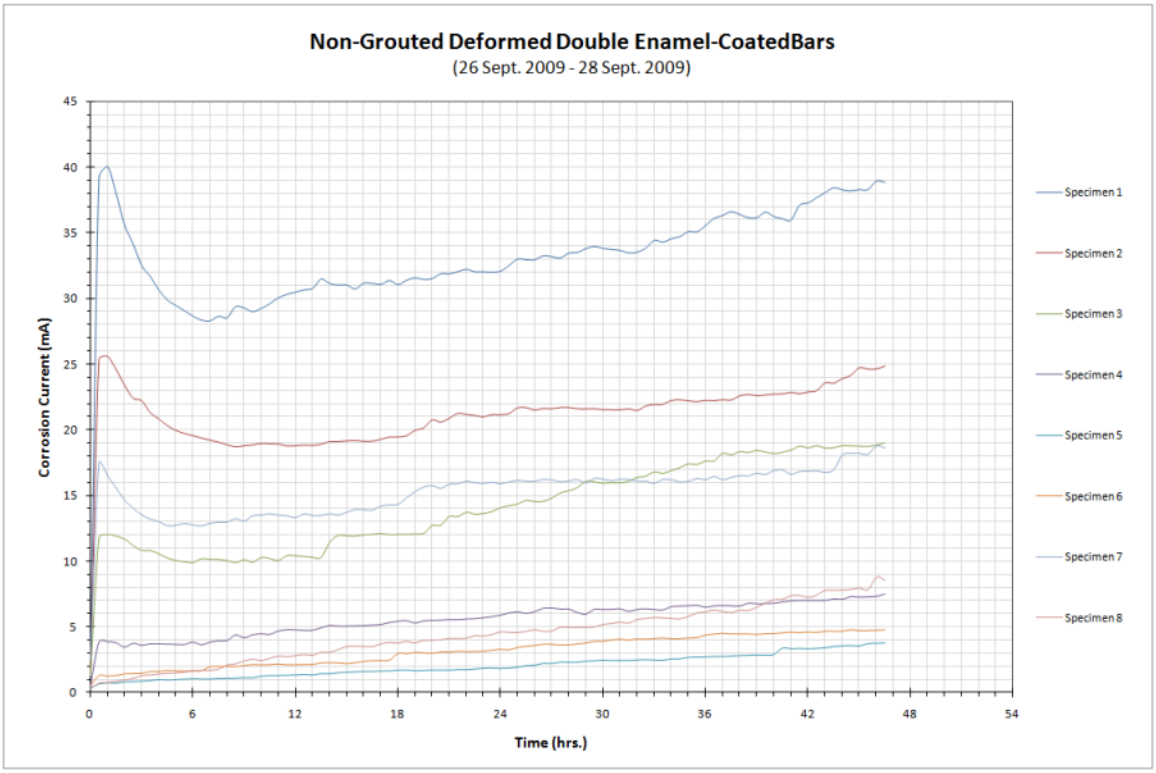

Figure B - 6: Corrosion current versus time plot for the non-grouted deformed double enamel-coated ACT specimens.

Table B - 7: T_{corr} values for the non-grouted smooth epoxy-coated ACT specimens.

Specimen No.	t_{corr} (hrs.)
1	> 668
2	> 668
3	> 668
4	> 668
5	> 668
6	> 668
7	> 668
8	> 668
Average:	> 668
Standard Deviation:	0
Standard Error:	0
COV:	- - - - -

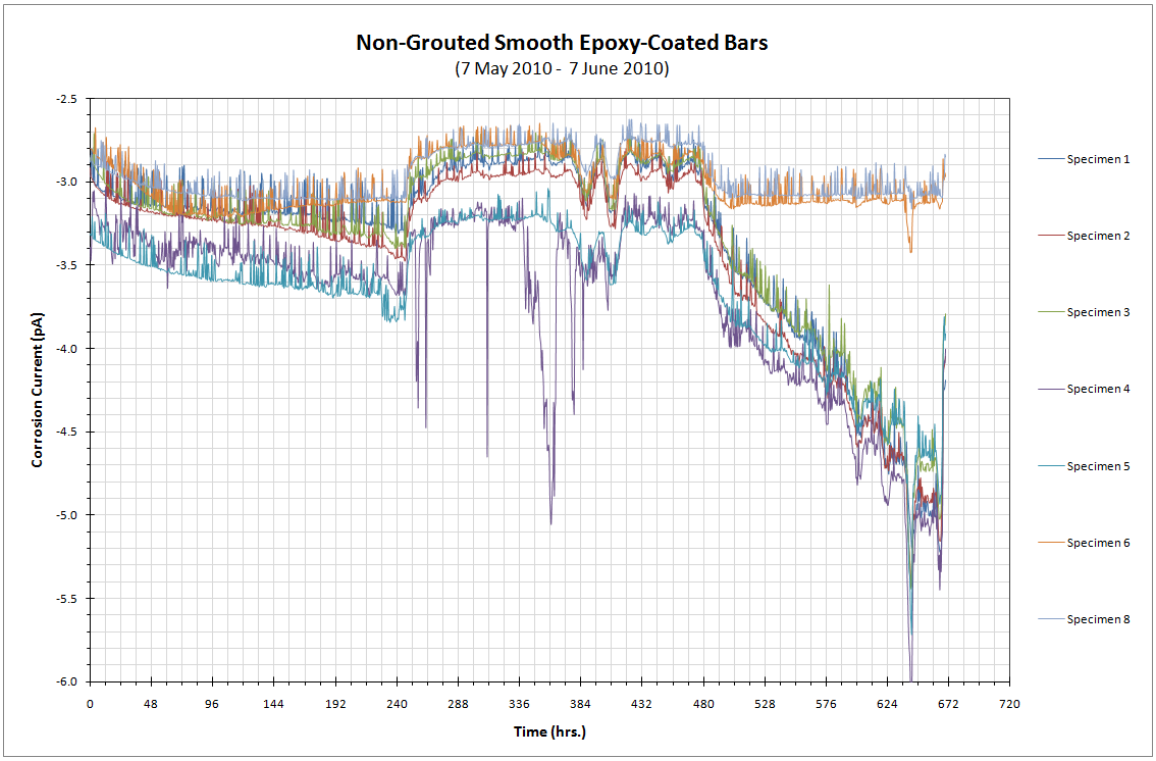

Figure B - 7: Corrosion current versus time plot for the non-grouted smooth epoxy-coated ACT specimens.

Table B - 8: T_{corr} values for the non-grouted deformed epoxy-coated ACT specimens.

Specimen No.	t_{corr} (hrs.)
1	> 746
2	> 746
3	> 746
4	> 746
5	> 746
6	> 746
7	> 746
8	> 746
Average:	> 746
Standard Deviation:	0
Standard Error:	0
COV:	- - - - -

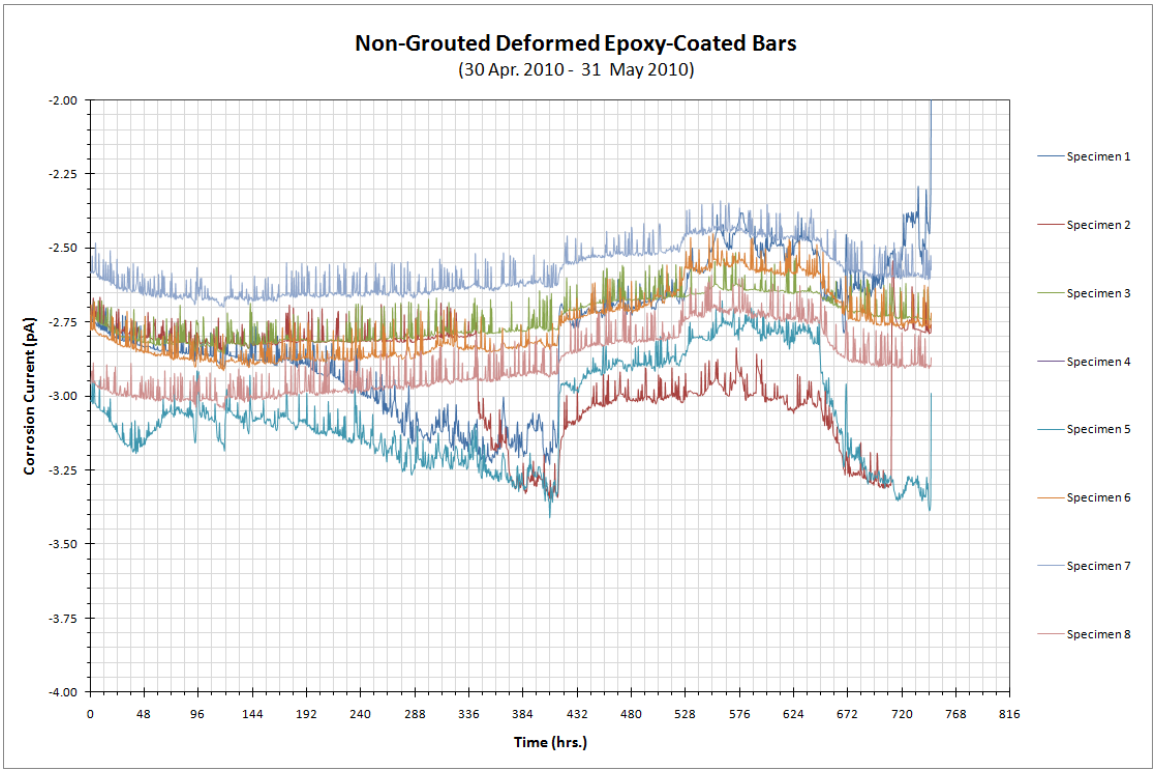

Figure B - 8: Corrosion current versus time plot for the non-grouted deformed epoxy-coated ACT specimens.

Table B - 9: T_{corr} values for the grouted smooth uncoated ACT specimens.

Specimen No.	t_{corr} (hrs.)
1	238
2	221
3	180
4	199
5	213
6	215
7	212
8	186
Average:	208
Standard Deviation:	19
Standard Error:	7
COV:	9.1%

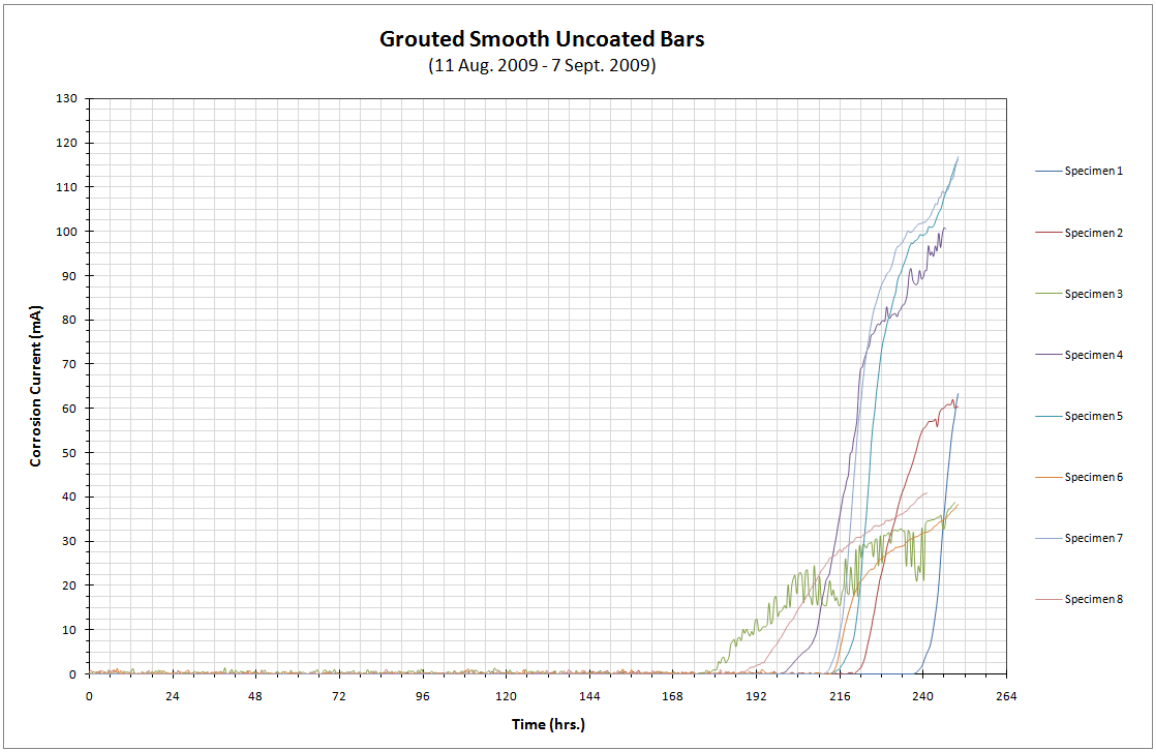

Figure B - 9: Corrosion current versus time plot for the grouted smooth uncoated ACT specimens.

Table B - 10: T_{corr} values for the grouted deformed uncoated ACT specimens.

Specimen No.	t_{corr} (hrs.)
1	198
2	148
3	195
4	168
5	196
6	128
7	187
8	OMITTED
Average:	174
Standard Deviation:	27
Standard Error:	10
COV:	15.7%

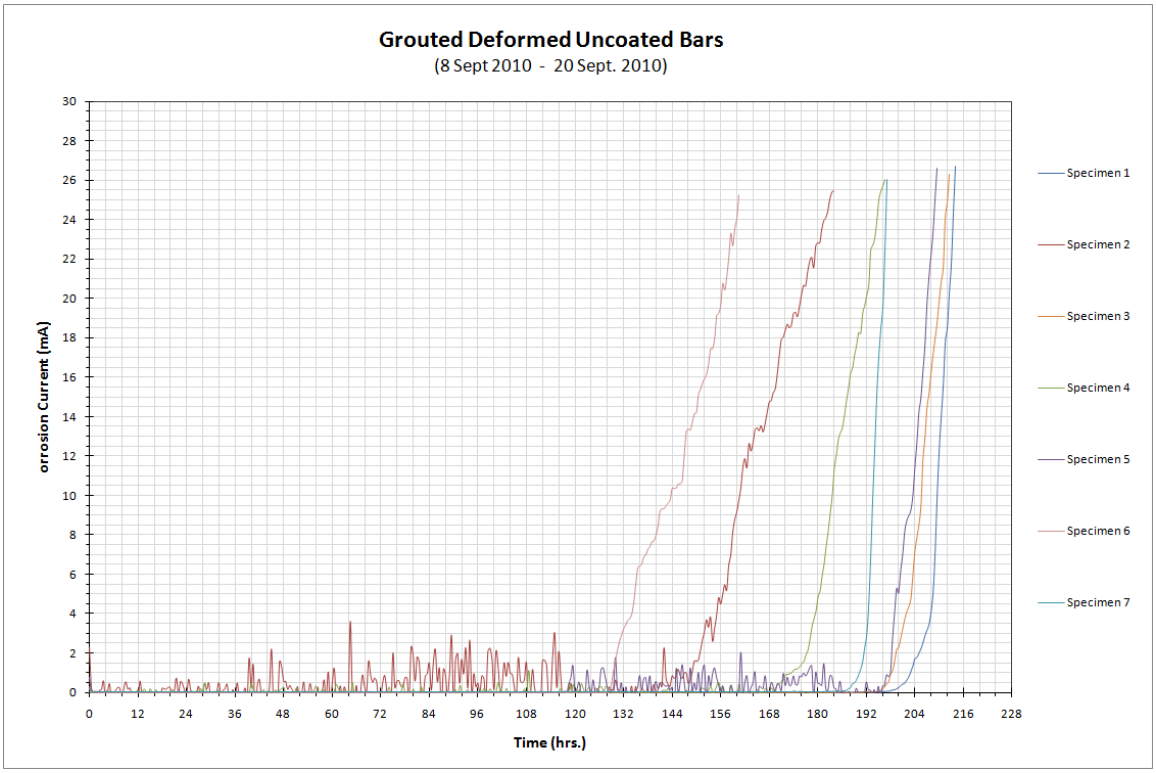

Figure B - 10: Corrosion current versus time plot for the grouted deformed uncoated ACT specimens.

Table B - 11: T_{corr} values for the grouted smooth 50/50 enamel-coated ACT specimens.

Specimen No.	t_{corr} (hrs.)
1	175
2	241
3	213
4	258
5	174
6	253
7	195
8	270
Average:	222
Standard Deviation:	38
Standard Error:	14
COV:	17.2%

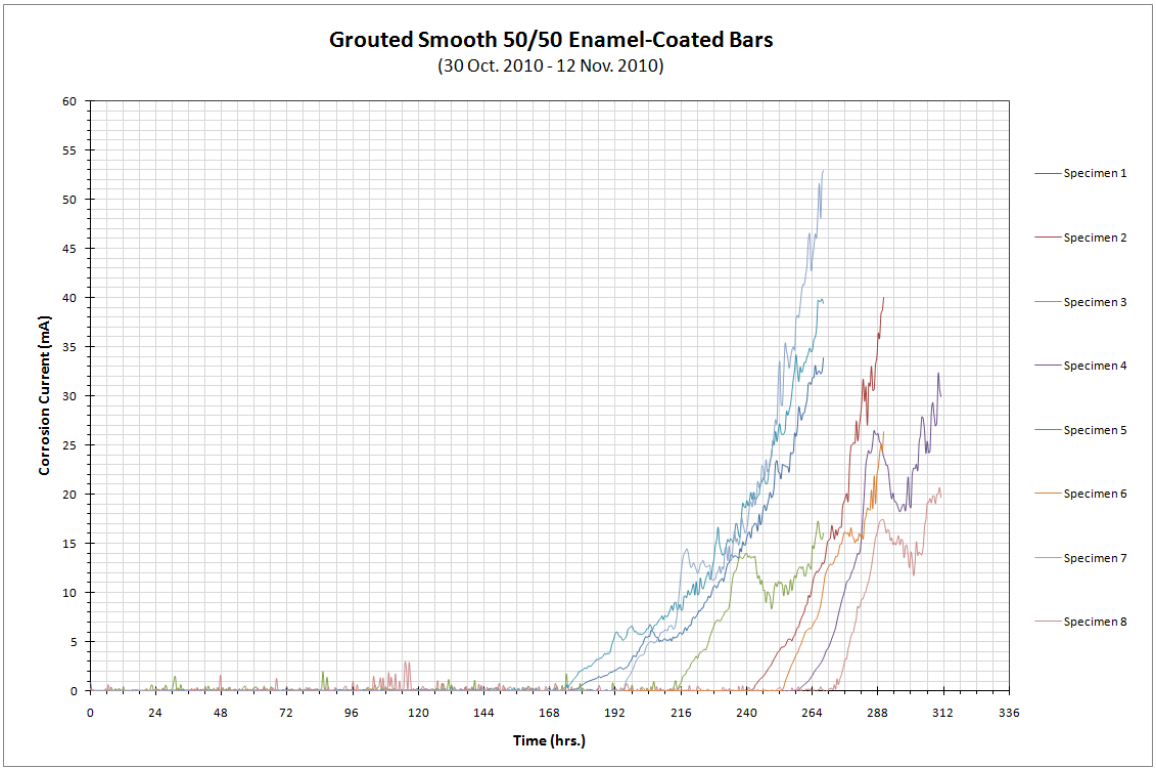

Figure B - 11: Corrosion current versus time plot for the grouted smooth 50/50 enamel-coated ACT specimens.

Table B - 12: T_{corr} values for the grouted deformed 50/50 enamel-coated ACT specimens.

Specimen No.	t_{corr} (hrs.)
1	228
2	216
3	102
4	252
5	198
6	204
7	126
8	OMITTED
Average:	189
Standard Deviation:	55
Standard Error:	21
COV:	29.0%

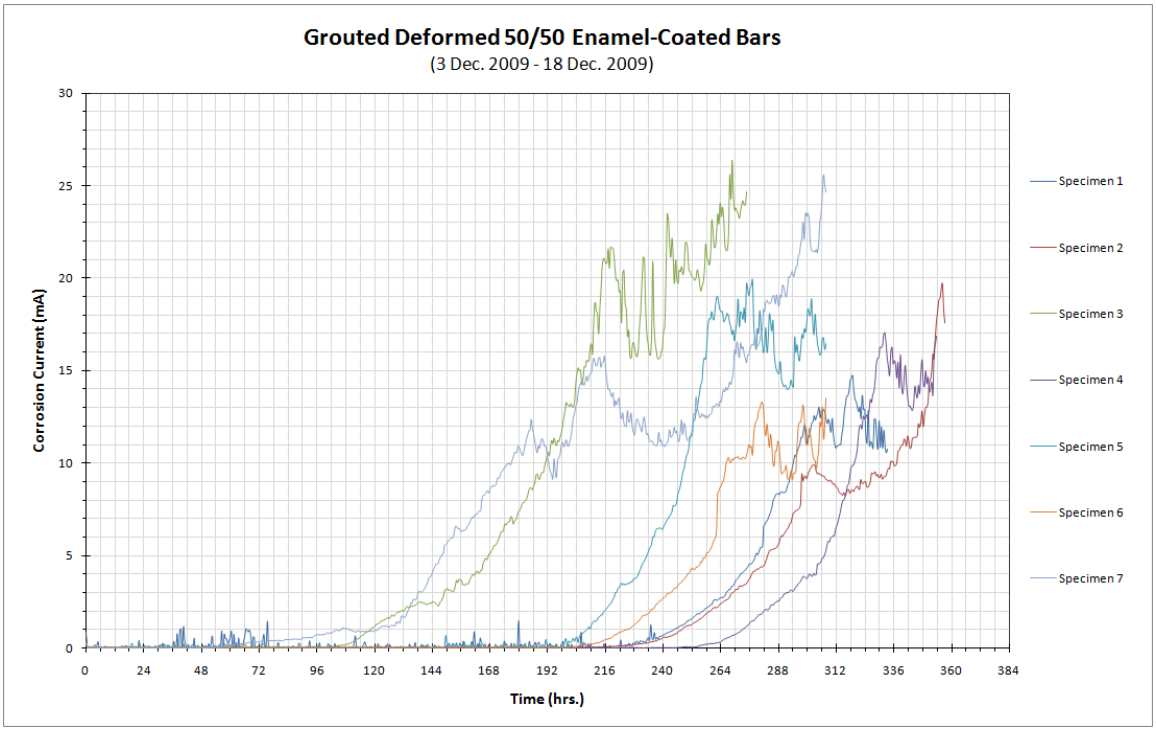

Figure B - 12: Corrosion current versus time plot for the grouted deformed 50/50 enamel-coated ACT specimens.

Table B - 13: T_{corr} values for the grouted smooth pure enamel-coated ACT specimens.

Specimen No.	t_{corr} (hrs.)
1	624
2	672
3	660
4	456
5	540
6	624
7	576
8	528
Average:	585
Standard Deviation:	74
Standard Error:	26
COV:	12.6%

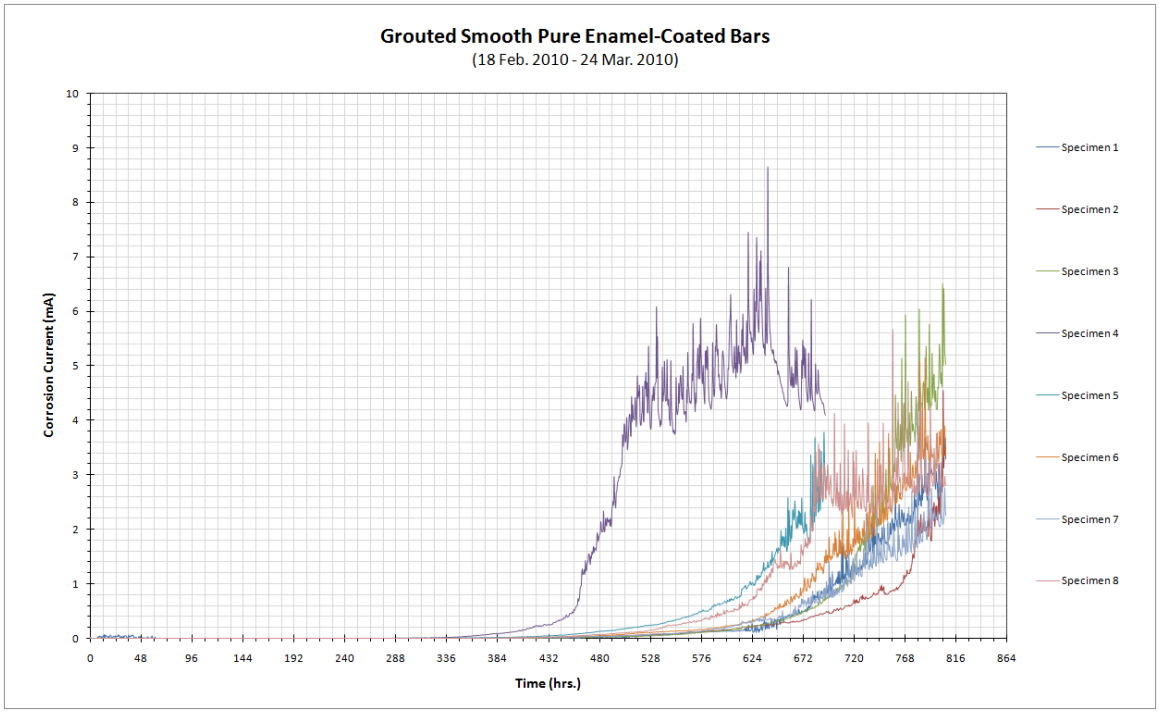

Figure B - 13: Corrosion current versus time plot for the grouted smooth pure enamel-coated ACT specimens.

Table B - 14: T_{corr} values for the grouted deformed pure enamel-coated ACT specimens.

Specimen No.	t_{corr} (hrs.)
1	588
2	439
3	408
4	412
5	620
6	260
7	238
8	303
Average:	409
Standard Deviation:	141
Standard Error:	50
COV:	34.6%

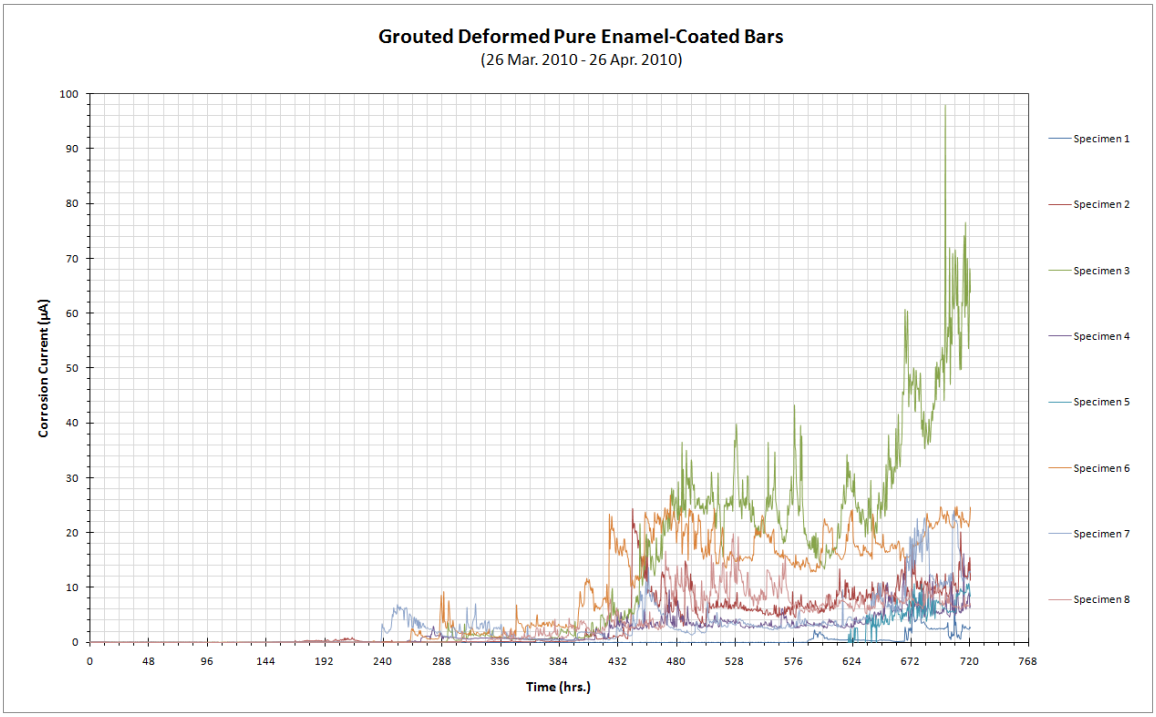

Figure B - 14: Corrosion current versus time plot for the grouted deformed pure enamel-coated ACT specimens.

Table B - 15: T_{corr} values for the grouted smooth double enamel-coated ACT specimens.

Specimen No.	t_{corr} (hrs.)
1	825
2	636
3	1080
4	912
5	694
6	1372
7	1154
8	1032
Average:	963
Standard Deviation:	246
Standard Error:	87
COV:	25.5%

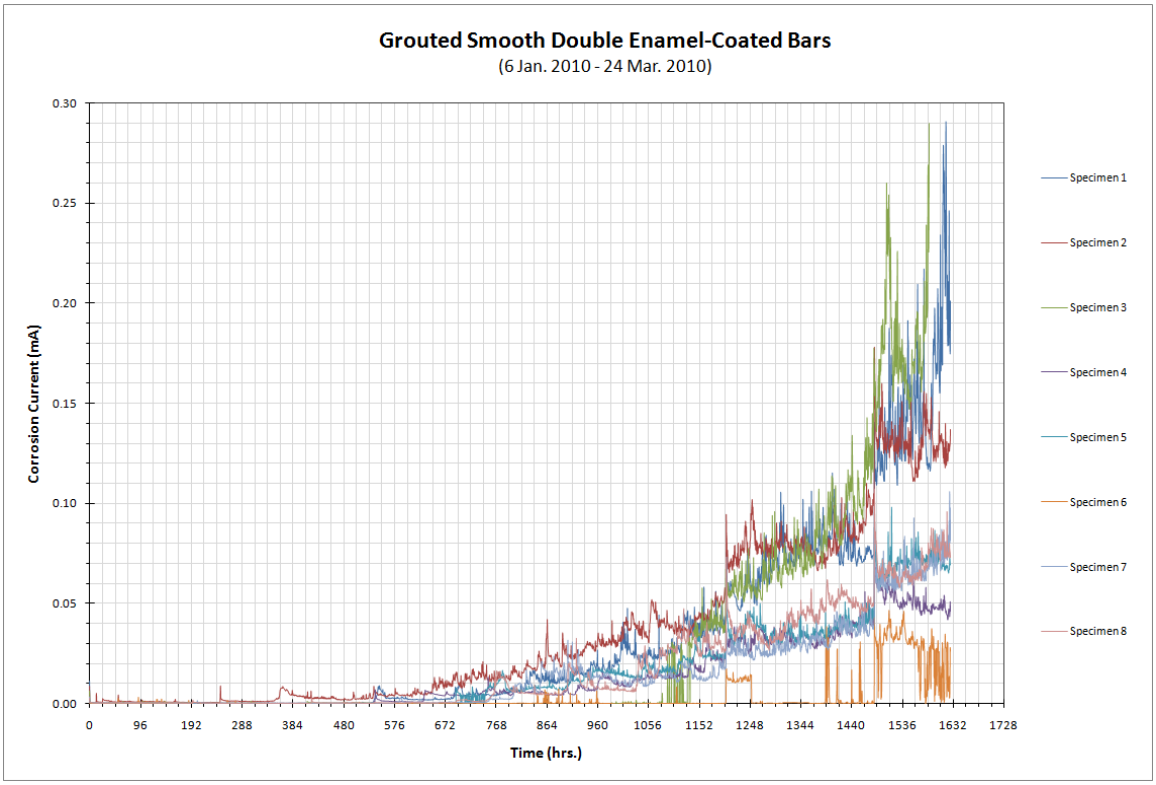

Figure B - 15: Corrosion current versus time plot for the grouted smooth double enamel-coated ACT specimens.

Table B - 16: T_{corr} values for the grouted deformed double enamel-coated ACT specimens.

Specimen No.	t_{corr} (hrs.)
1	824
2	720
3	624
4	594
5	471
6	648
7	738
8	690
Average:	664
Standard Deviation:	106
Standard Error:	38
COV:	16.0%

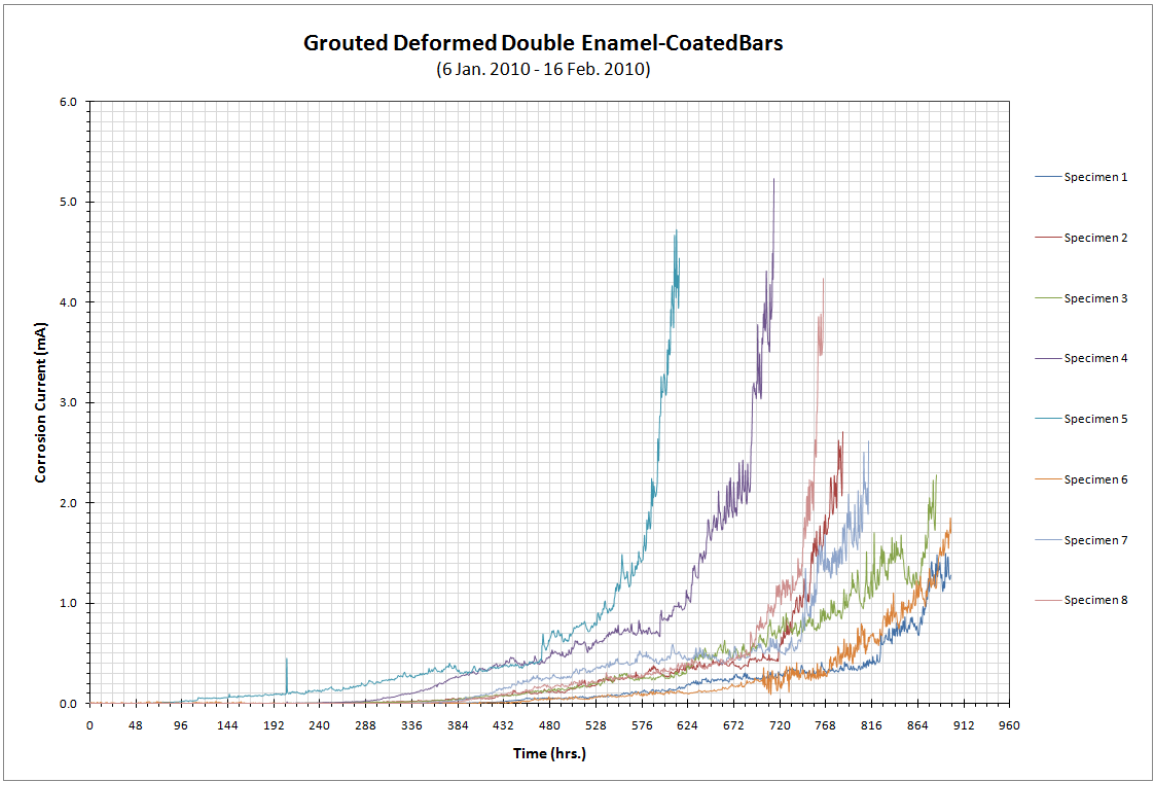

Figure B - 16: Corrosion current versus time plot for the grouted deformed double enamel-coated ACT specimens.

Table B - 17: T_{corr} values for the grouted smooth epoxy-coated ACT specimens.

Specimen No.	t_{corr} (hrs.)
1	> 1300
2	> 1300
3	> 1300
4	> 1300
5	> 1300
6	> 1300
7	> 1300
8	> 1300
Average:	> 1300
Standard Deviation:	0
Standard Error:	0
COV:	- - - - -

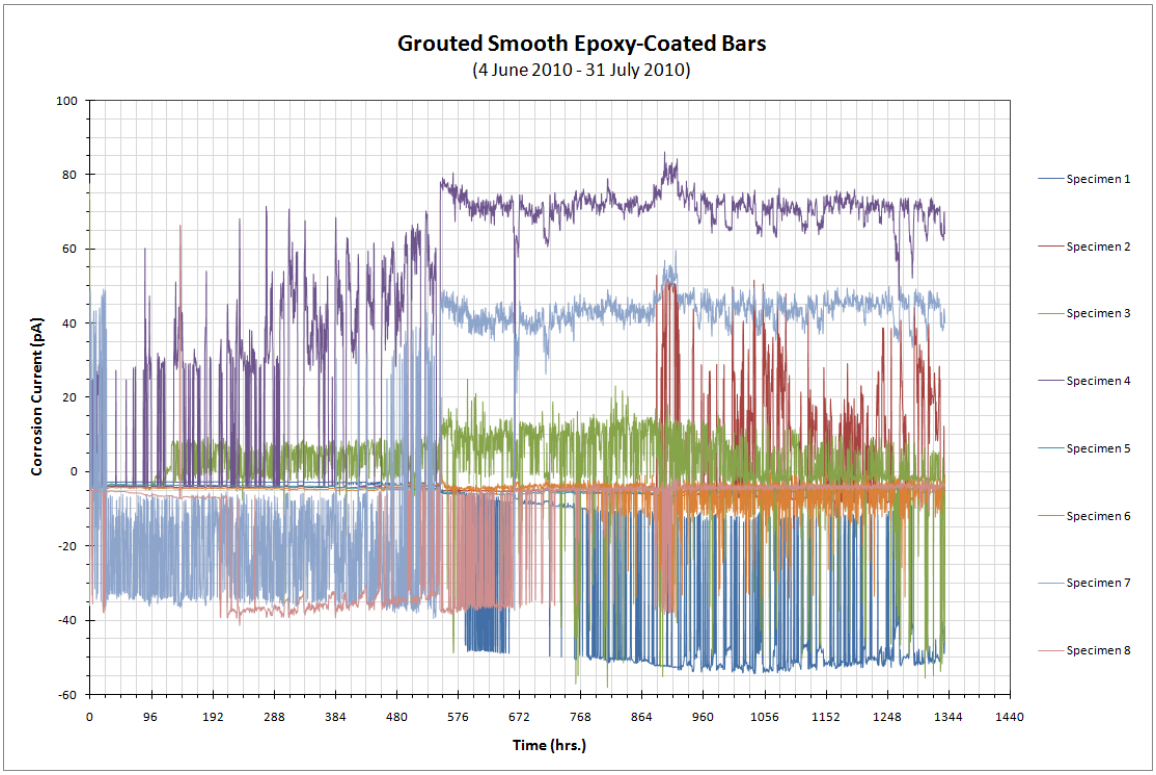

Figure B - 17: Corrosion current versus time plot for the grouted smooth epoxy-coated ACT specimens.

Table B - 18: T_{corr} values for the grouted deformed epoxy-coated ACT specimens.

Specimen No.	t_{corr} (hrs.)
1	> 1300
2	> 1300
3	> 1300
4	> 1300
5	> 1300
6	> 1300
7	> 1300
8	> 1300
Average:	> 1300
Standard Deviation:	0
Standard Error:	0
COV:	- - - - -

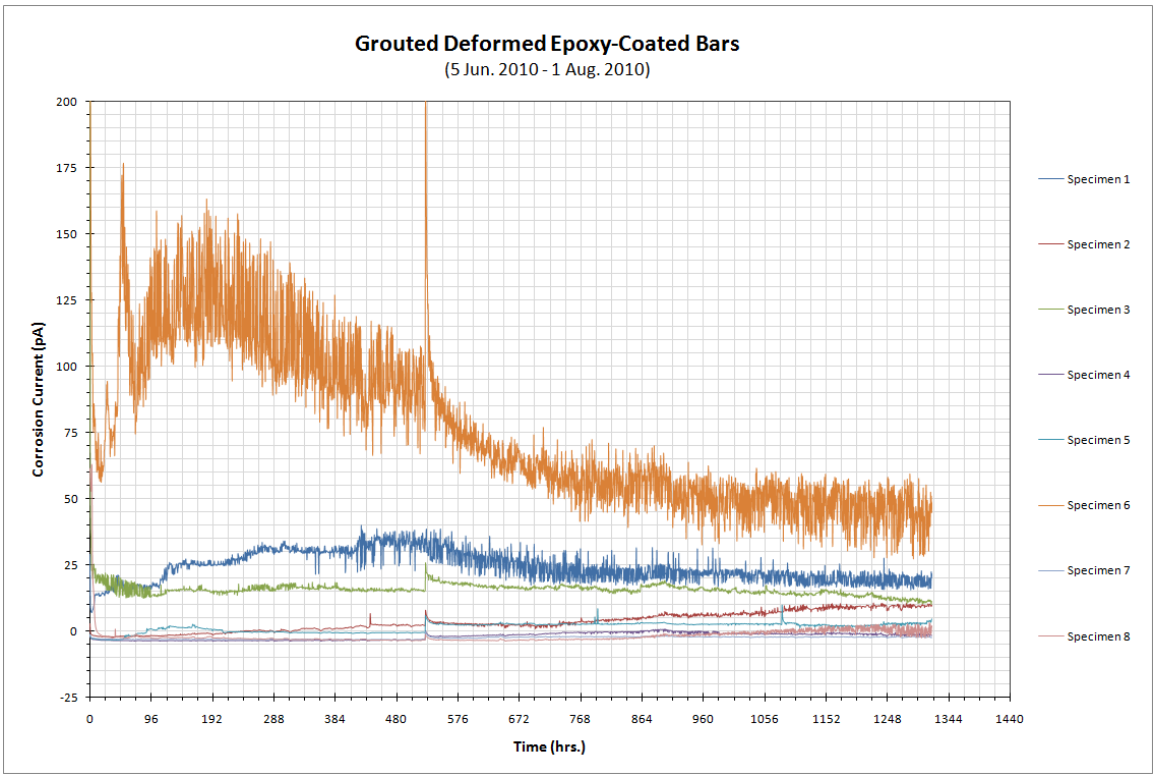

Figure B - 18: Corrosion current versus time plot for the grouted deformed epoxy-coated ACT specimens.

APPENDIX C: PONDING TEST

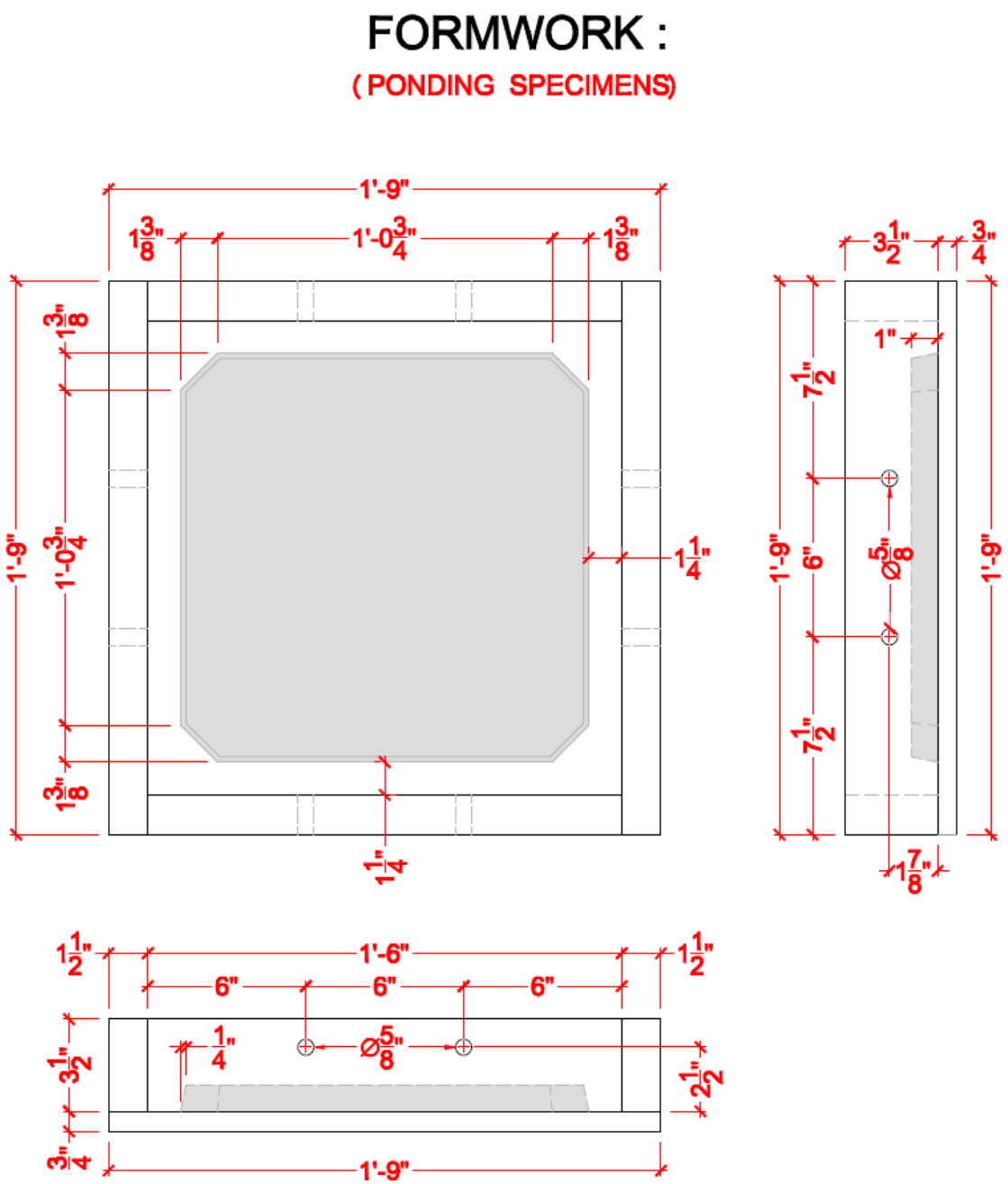

Figure C - 1: Typical ponding specimen form details and dimensions.

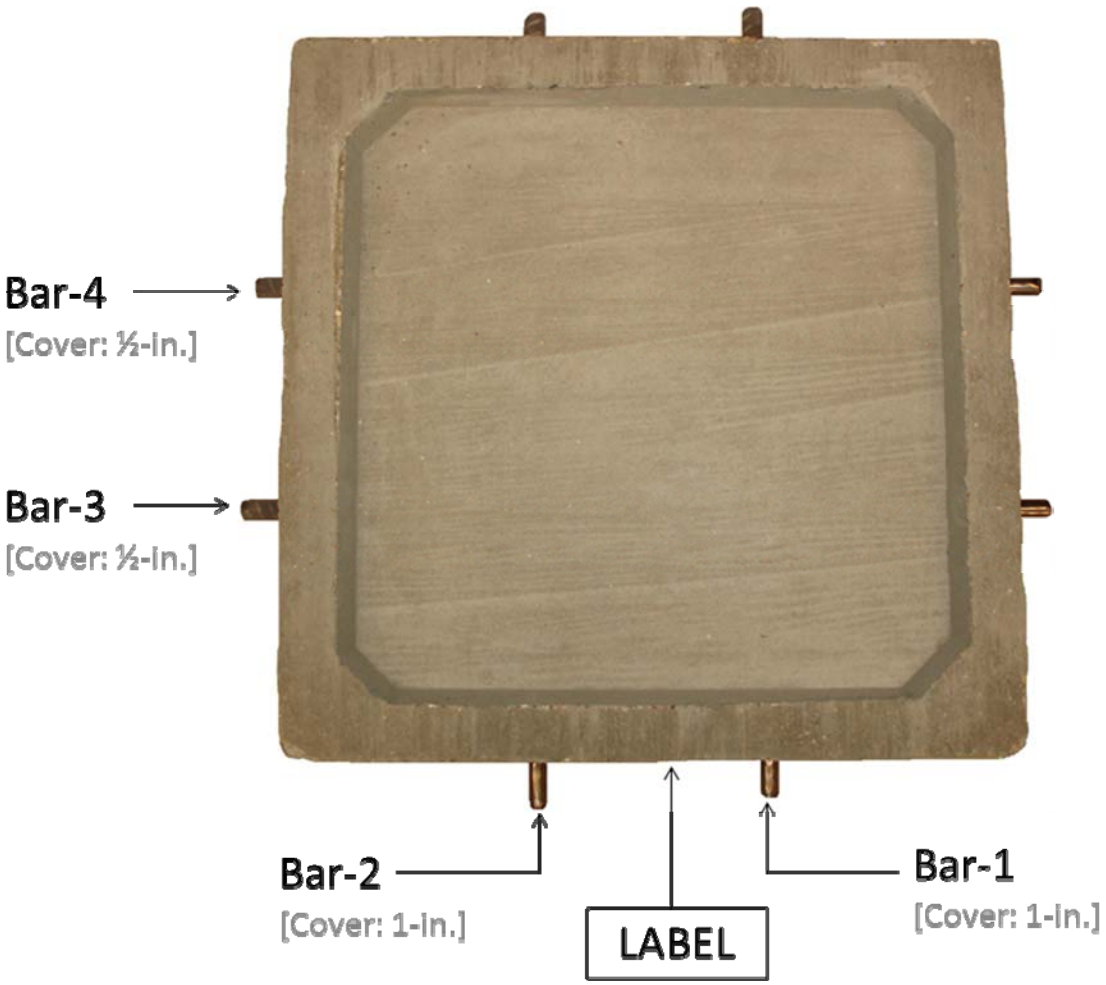

Figure C - 2: Labeling of bars embedded within a ponding specimen with respect to the specimen's label.

Table C - 1: Labels used for ponding specimens.

LABEL	COATING TYPE
M	Uncoated
EP	"Perfect" Epoxy
EP-D	Damaged Epoxy
EN	"Perfect" Enamel
EN-D	Damaged Enamel

MISSOURI S&T University of Science & Technology

Ponding Specimens: Impact Results

Standard: ASTM G14

Tup Wt. (lbs.): 2.0
Drop Height (in.): 36

ENAMEL-COATED (EN) REINFORCEMENT

	Bar	Location	Dimensions (in.)	
EN-D-1	1	1	1/2	1/4
		2	3/8	1/4
		3	1/2	1/2
	2	1	1/8	1/4
		2	3/4	1/2
		3	1/4	3/8
	3	1	3/8	3/4
		2	3/8	3/4
		3	1/2	5/8
	4	1	1/2	5/8
		2	1/8	5/8
		3	1/8	5/8
	Average:		0.38	0.51

	Bar	Location	Dimensions (in.)	
EN-D-2	1	1	1/4	1/2
		2	1/2	3/8
		3	1/2	5/8
	2	1	1 3/8	1/2
		2	1/8	1/2
		3	1/4	3/8
	3	1	1/8	1/8
		2	1/4	1/2
		3	1/8	3/8
	4	1	1/2	1
		2	1/4	1/4
		3	1/8	1/4
	Average:		0.36	0.45

	Bar	Location	Dimensions (in.)	
EN-D-3	1	1	1	3/4
		2	5/8	1/2
		3	13/16	1/2
	2	1	1	3/8
		2	3/16	5/16
		3	9/16	3/8
	3	1	1/2	13/16
		2	1/4	3/4
		3	1/8	1/2
	4	1	3/16	11/16
		2	7/16	9/16
		3	5/32	11/16
	Average:		0.49	0.57

	Bar	Location	Dimensions (in.)	
EN-D-4	1	1	3/16	1/4
		2	1/2	3/8
		3	11/16	3/8
	2	1	15/32	5/8
		2	1/8	3/8
		3	1/32	3/16
	3	1	3/8	5/8
		2	1/4	11/16
		3	3/16	1/4
	4	1	3/32	9/32
		2	1/16	5/32
		3	5/32	7/16
	Average:		0.26	0.39

Overall Average (in.):	0.37	0.48

EPOXY-COATED (EP) REINFORCEMENT

	Bar	Location	Dimensions (in.)	
EP-D-1	1	1	0	0
		2	1/32	1/8
		3	1/64	1/16
	2	1	1/16	3/16
		2	1/16	3/16
		3	1/16	3/16
	3	1	1/32	1/16
		2	1/16	1/8
		3	1/32	5/32
	4	1	1/16	3/16
		2	1/16	3/16
		3	1/32	5/32
	Average:		0.04	0.14

	Bar	Location	Dimensions (in.)	
EP-D-2	1	1	1/16	7/32
		2	1/32	3/16
		3	0	0
	2	1	1/32	5/32
		2	1/16	1/8
		3	1/32	7/32
	3	1	1/32	1/8
		2	1/32	1/8
		3	1/16	3/16
	4	1	1/32	3/16
		2	1/8	1/8
		3	3/32	5/32
	Average:		0.05	0.15

	Bar	Location	Dimensions (in.)	
EP-D-3	1	1	1/16	1/8
		2	1/32	3/16
		3	3/32	5/32
	2	1	1/32	3/16
		2	1/16	3/16
		3	1/32	1/8
	3	1	1/16	3/16
		2	1/16	3/16
		3	1/16	5/32
	4	1	1/16	3/16
		2	1/32	1/8
		3	1/32	1/8
	Average:		0.05	0.16

	Bar	Location	Dimensions (in.)	
EP-D-4	1	1	3/32	7/32
		2	1/16	1/8
		3	1/32	5/32
	2	1	1/32	1/8
		2	1/16	7/32
		3	1/16	1/8
	3	1	1/32	5/32
		2	1/16	7/32
		3	1/16	3/16
	4	1	1/16	1/4
		2	3/32	1/8
		3	1/16	3/16
	Average:		0.06	0.17

Overall Average (in.):	0.05	0.16

Figure C - 3: Dimensions of intentionally damaged areas along both epoxy and 50/50 enamel-coated bars embedded within the ponding specimens.

(a)

(b)

Figure C - 4: The locations of the (a) resistivity and (b) corrosion potential measurements with respect to a ponding specimen's label.

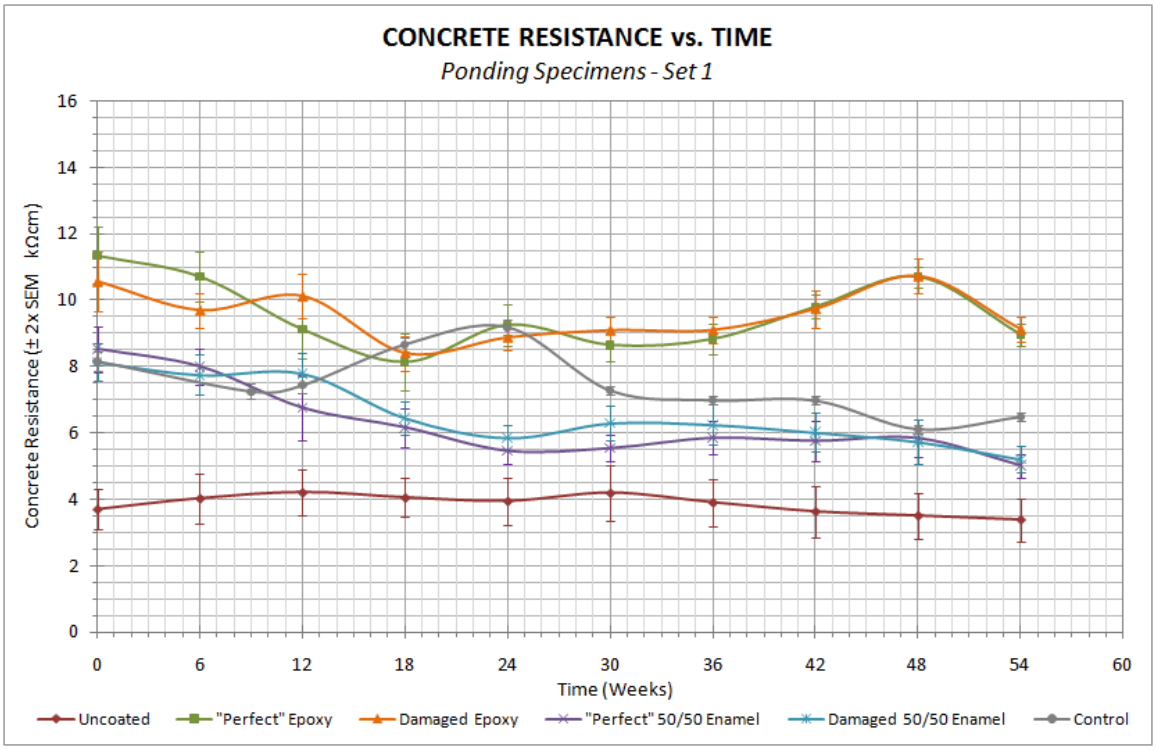

(a)

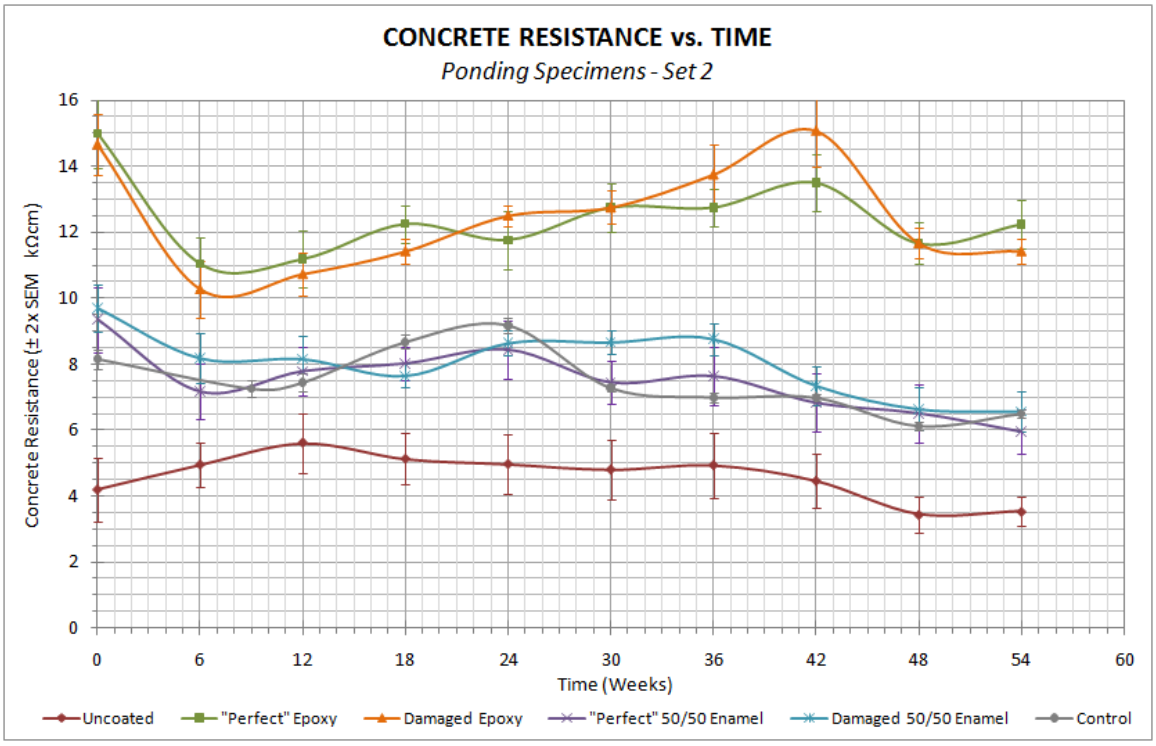

(b)

Figure C - 5: Average concrete resistance for (a) the first and second ponding specimen within each specimen group; (b) third and fourth ponding specimen within each specimen group.

Table C - 2: Resistivity measurements for the first and second uncoated ponding specimen.

Specimen:	Location:	Resistivity Measurements (kΩcm) vs. Time (weeks): 0	6	12	18	24	30	36	42	48	54
M-1	1	4.9	4.8	5.7	5.6	5.5	6.2	5.5	5.3	5.0	4.7
	2	4.9	4.8	4.6	5.4	5.5	5.4	5.4	4.6	4.9	4.7
	3	4.9	5.7	6.4	3.8	5.5	6.3	5.5	5.6	4.7	4.8
	4	3.5	3.9	3.8	3.8	3.8	3.8	2.9	3.3	3.0	3.1
	5	2.9	4.8	3.8	3.2	3.8	3.8	3.8	3.1	2.9	2.9
	6	2.8	3.2	3.2	3.0	3.0	2.9	2.9	2.5	2.4	2.3
M-2	1	5.0	5.6	5.6	5.0	4.6	5.1	4.8	5.6	5.5	5.1
	2	3.9	4.1	3.8	4.6	3.9	3.8	3.8	3.5	3.6	3.1
	3	3.9	5.0	4.6	5.1	4.7	5.4	4.5	3.6	3.4	3.3
	4	3.0	2.3	2.9	3.0	2.1	2.7	2.7	2.7	2.3	2.2
	5	2.3	2.0	2.4	3.0	2.1	2.1	2.2	1.7	2.1	2.1
	6	2.3	2.1	3.7	3.1	2.8	2.8	2.8	2.0	2.2	2.2
M-1 Average:		4.0	4.5	4.6	4.1	4.5	4.7	4.3	4.1	3.8	3.8
M-2 Average:		3.4	3.5	3.8	4.0	3.4	3.7	3.5	3.2	3.2	3.0
Overall Average:		3.69	4.03	4.21	4.05	3.94	4.19	3.90	3.63	3.50	3.38
Standard Dev.:		1.04	1.33	1.21	1.03	1.25	1.44	1.21	1.36	1.23	1.15
SEM:		0.30	0.38	0.35	0.30	0.36	0.42	0.35	0.39	0.35	0.33
Maximum:		5.0	5.7	6.4	5.6	5.5	6.3	5.5	5.6	5.5	5.1
Minimum:		2.3	2.0	2.4	3.0	2.1	2.1	2.2	1.7	2.1	2.1

Table C - 3: Resistivity measurements for the third and fourth uncoated ponding specimen.

Specimen:	Location:	Resistivity Measurements (kΩcm) vs. Time (weeks): 0	6	12	18	24	30	36	42	48	54
M-3	1	5.5	6.4	6.3	6.6	6.8	7.2	6.8	5.6	3.7	3.7
	2	4.6	4.5	6.4	6.3	6.0	5.5	5.4	4.8	3.7	3.8
	3	4.9	5.6	7.5	6.4	6.5	6.3	6.3	5.6	3.8	4.1
	4	3.1	4.0	4.6	4.6	4.0	3.8	3.7	3.1	2.3	3.0
	5	2.1	3.8	3.9	3.8	4.1	3.8	3.8	3.1	2.8	2.5
	6	2.1	3.8	3.8	3.8	3.2	2.9	3.0	3.1	2.5	2.4
M-4	1	6.4	6.9	7.3	7.4	7.4	7.1	8.1	7.4	5.4	4.7
	2	5.8	5.6	8.2	5.6	4.6	4.9	5.5	4.8	4.1	4.1
	3	6.8	6.4	6.4	5.5	6.4	5.9	6.3	5.6	4.6	4.7
	4	3.4	3.8	4.3	3.9	3.8	3.6	3.7	3.8	2.9	3.5
	5	3.2	3.8	4.7	3.8	3.8	3.7	3.7	3.7	2.8	3.0
	6	2.5	4.8	3.9	3.8	3.0	2.9	2.9	2.9	2.7	2.9
M-3 Average:		3.7	4.7	5.4	5.3	5.1	4.9	4.8	4.2	3.1	3.3
M-4 Average:		4.7	5.2	5.8	5.0	4.8	4.7	5.0	4.7	3.8	3.8
Overall Average:		4.20	4.95	5.61	5.13	4.97	4.80	4.93	4.46	3.44	3.53
Standard Dev.:		1.68	1.18	1.58	1.33	1.55	1.56	1.69	1.41	0.94	0.79
SEM:		0.49	0.34	0.46	0.38	0.45	0.45	0.49	0.41	0.27	0.23
Maximum:		6.8	6.9	8.2	7.4	7.4	7.2	8.1	7.4	5.4	4.7
Minimum:		2.1	3.8	3.8	3.8	3.0	2.9	2.9	2.9	2.3	2.4

Table C - 4: Resistivity measurements for the first and second "perfect" epoxy-coated ponding specimen.

Specimen:	Location:	Resistivity Measurements (kΩcm) vs. Time (weeks): 0	6	12	18	24	30	36	42	48	54
EP-1	1	13.0	11.0	7.6	9.0	9.8	9.8	9.8	9.7	9.9	9.0
	2	9.9	9.8	8.4	8.6	11.0	9.8	9.8	9.7	11.0	9.1
	3	12.0	11.0	7.1	5.5	9.4	8.1	9.0	9.8	9.6	8.0
	4	11.0	13.0	12.0	9.0	9.8	8.9	9.1	9.8	11.0	9.1
	5	9.2	9.8	11.0	9.0	10.0	9.0	9.8	11.0	11.0	9.8
	6	12.0	12.0	11.0	11.0	11.0	9.6	9.8	11.0	11.0	9.8
EP-2	1	13.0	9.9	9.0	7.5	8.3	7.3	8.0	9.0	11.0	8.6
	2	9.9	9.8	7.3	8.2	8.7	8.1	8.0	9.4	11.0	9.0
	3	13.0	12.0	9.1	5.6	8.1	8.1	8.2	9.1	11.0	9.0
	4	11.0	11.0	8.9	8.1	8.5	8.8	8.1	9.8	11.0	9.1
	5	9.0	8.1	8.9	7.9	8.3	8.1	8.2	9.7	11.0	9.0
	6	13.0	11.0	9.0	8.1	8.1	8.1	8.1	9.6	9.9	8.0
EP-1 Average:		11.2	11.1	9.5	8.7	10.2	9.2	9.6	10.2	10.6	9.1
EP-2 Average:		11.5	10.3	8.7	7.6	8.3	8.1	8.1	9.4	10.8	8.8
Overall Average:		11.33	10.70	9.11	8.13	9.25	8.64	8.83	9.80	10.70	8.96
Standard Dev.:		1.55	1.31	1.53	1.49	1.07	0.80	0.80	0.62	0.55	0.56
SEM:		0.45	0.38	0.44	0.43	0.31	0.23	0.23	0.18	0.16	0.16
Maximum:		13.0	13.0	12.0	11.0	11.0	9.8	9.8	11.0	11.0	9.8
Minimum:		9.0	8.1	7.1	5.5	8.1	7.3	8.0	9.0	9.6	8.0

Table C - 5: Resistivity measurements for the third and fourth "perfect" epoxy-coated ponding specimen.

Specimen:	Location:	Resistivity Measurements (kΩcm) vs. Time (weeks): 0	6	12	18	24	30	36	42	48	54
EP-3	1	15.0	11.0	12.0	12.0	12.0	12.0	12.0	14.0	12.0	12.0
	2	13.0	9.8	12.0	12.0	12.0	13.0	12.0	14.0	11.0	11.0
	3	18.0	12.0	12.0	13.0	14.0	14.0	12.0	14.0	9.9	9.9
	4	17.0	12.0	13.0	13.0	12.0	12.0	13.0	14.0	11.0	12.0
	5	14.0	11.0	12.0	13.0	12.0	14.0	13.0	15.0	11.0	11.0
	6	16.0	13.0	13.0	14.0	14.0	14.0	13.0	16.0	12.0	13.0
EP-4	1	16.0	11.0	10.0	12.0	12.0	12.0	13.0	13.0	12.0	13.0
	2	12.0	8.9	9.1	11.0	9.2	11.0	12.0	11.0	11.0	12.0
	3	16.0	12.0	12.0	12.0	10.0	13.0	14.0	12.0	13.0	13.0
	4	14.0	9.7	9.1	11.0	11.0	12.0	12.0	12.0	12.0	13.0
	5	13.0	9.1	9.0	11.0	10.0	11.0	12.0	12.0	11.0	12.0
	6	16.0	13.0	11.0	13.0	13.0	15.0	15.0	15.0	14.0	15.0
EP-3 Average:		15.5	11.5	12.3	12.8	12.7	13.2	12.5	14.5	11.2	11.5
EP-4 Average:		14.5	10.6	10.0	11.7	10.9	12.3	13.0	12.5	12.2	13.0
Overall Average:		15.00	11.04	11.18	12.25	11.77	12.75	12.75	13.50	11.66	12.24
Standard Dev.:		1.81	1.42	1.50	0.97	1.51	1.29	0.97	1.51	1.09	1.30
SEM:		0.52	0.41	0.43	0.28	0.44	0.37	0.28	0.44	0.31	0.38
Maximum:		18.0	13.0	13.0	14.0	14.0	15.0	15.0	16.0	14.0	15.0
Minimum:		12.0	8.9	9.0	11.0	9.2	11.0	12.0	11.0	9.9	9.9

Table C - 6: Resistivity measurements for the first and second damaged epoxy-coated ponding specimen.

Specimen:	Location:	Resistivity Measurements (kΩcm) vs. Time (weeks): 0	6	12	18	24	30	36	42	48	54
EP-D-1	1	12.0	11.0	9.8	8.1	9.0	9.8	9.7	11.0	11.0	9.1
	2	7.3	9.2	8.1	8.1	8.7	10.0	9.8	11.0	11.0	9.2
	3	11.0	9.8	9.0	9.0	8.1	8.9	9.8	9.6	10.0	9.0
	4	9.1	9.3	9.9	8.1	8.4	9.1	9.0	11.0	11.0	9.9
	5	9.1	8.9	9.8	8.3	9.1	8.9	9.2	10.0	11.0	9.1
	6	12.0	9.9	11.0	8.0	7.3	7.5	7.4	7.9	9.0	7.5
EP-D-2	1	12.0	8.7	9.9	8.9	9.0	8.2	8.6	8.4	9.8	8.9
	2	9.3	8.9	9.0	8.1	9.0	9.0	8.8	9.4	11.0	9.0
	3	12.0	11.0	11.0	6.4	9.1	9.6	9.0	10.0	12.0	9.8
	4	11.0	10.0	12.0	9.8	9.5	9.8	9.7	10.0	12.0	9.9
	5	10.0	8.7	10.0	8.2	9.5	8.7	8.9	9.3	11.0	9.0
	6	12.0	11.0	12.0	9.8	9.8	9.6	9.3	9.3	10.0	9.1
EP-D-1 Average:		10.1	9.7	9.6	8.3	8.4	9.0	9.2	10.1	10.5	9.0
EP-D-2 Average:		11.1	9.7	10.7	8.5	9.3	9.2	9.1	9.4	11.0	9.3
Overall Average:		10.57	9.70	10.13	8.40	8.88	9.09	9.10	9.74	10.73	9.13
Standard Dev.:		1.58	0.90	1.19	0.91	0.68	0.73	0.68	0.98	0.88	0.63
SEM:		0.46	0.26	0.34	0.26	0.20	0.21	0.20	0.28	0.26	0.18
Maximum:		12.0	11.0	12.0	9.8	9.8	10.0	9.8	11.0	12.0	9.9
Minimum:		7.3	8.7	8.1	6.4	7.3	7.5	7.4	7.9	9.0	7.5

Table C - 7: Resistivity measurements for the third and fourth damaged epoxy-coated ponding specimen.

Specimen:	Location:	Resistivity Measurements (kΩcm) vs. Time (weeks): 0	6	12	18	24	30	36	42	48	54
EP-D-3	1	14.0	12.0	11.0	11.0	12.0	12.0	13.0	14.0	11.0	12.0
	2	13.0	9.8	11.0	11.0	12.0	13.0	16.0	18.0	12.0	12.0
	3	18.0	11.0	12.0	11.0	13.0	13.0	14.0	14.0	12.0	12.0
	4	16.0	11.0	11.0	12.0	13.0	14.0	15.0	17.0	12.0	12.0
	5	14.0	11.0	12.0	11.0	12.0	14.0	16.0	17.0	13.0	12.0
	6	17.0	12.0	12.0	11.0	13.0	14.0	16.0	18.0	13.0	12.0
EP-D-4	1	15.0	9.9	10.0	13.0	13.0	12.0	13.0	15.0	12.0	11.0
	2	13.0	8.4	9.8	11.0	13.0	12.0	12.0	14.0	11.0	11.0
	3	14.0	7.1	8.1	11.0	12.0	12.0	12.0	13.0	11.0	11.0
	4	15.0	11.0	11.0	12.0	13.0	13.0	13.0	15.0	11.0	11.0
	5	13.0	9.0	9.8	11.0	12.0	12.0	13.0	13.0	11.0	10.0
	6	14.0	11.0	11.0	12.0	12.0	12.0	12.0	13.0	11.0	11.0
EP-D-3 Average:		15.3	11.1	11.5	11.2	12.5	13.3	15.0	16.3	12.2	12.0
EP-D-4 Average:		14.0	9.4	10.0	11.7	12.5	12.2	12.5	13.8	11.2	10.8
Overall Average:		14.67	10.27	10.73	11.42	12.50	12.75	13.75	15.08	11.67	11.42
Standard Dev.:		1.61	1.48	1.14	0.67	0.52	0.87	1.60	1.93	0.78	0.67
SEM:		0.47	0.43	0.33	0.19	0.15	0.25	0.46	0.56	0.22	0.19
Maximum:		18.0	12.0	12.0	13.0	13.0	14.0	16.0	18.0	13.0	12.0
Minimum:		13.0	7.1	8.1	11.0	12.0	12.0	12.0	13.0	11.0	10.0

Table C - 8: Resistivity measurements for the first and second "perfect" 50/50 enamel-coated ponding specimen.

Specimen:	Location:	Resistivity Measurements (kΩcm) vs. Time (weeks): 0	6	12	18	24	30	36	42	48	54
EN-1	1	9.0	6.3	9.8	7.3	6.3	6.3	6.0	5.8	6.3	4.8
	2	7.6	8.5	5.6	6.4	5.5	5.6	6.3	5.8	6.4	5.5
	3	9.4	9.2	7.2	4.7	4.9	4.7	5.4	5.9	6.3	5.4
	4	9.4	7.9	7.9	5.6	4.5	4.7	5.3	4.7	4.7	4.6
	5	7.4	7.1	3.7	7.3	4.7	4.7	4.7	4.4	4.5	4.2
	6	9.0	7.9	6.3	5.5	4.7	4.6	4.6	4.5	4.4	3.8
EN-2	1	9.3	9.1	4.7	4.7	5.5	6.4	7.3	7.8	7.1	5.6
	2	7.0	7.3	5.5	6.4	6.4	6.4	6.3	6.4	6.4	5.6
	3	11.0	8.8	9.0	8.0	6.4	5.9	7.2	7.1	7.2	5.7
	4	8.5	9.1	7.3	6.2	5.5	5.5	5.2	5.1	4.8	4.7
	5	7.4	7.3	6.9	5.5	5.5	5.6	5.6	5.4	5.6	4.9
	6	7.4	7.5	7.2	6.4	5.6	6.1	6.3	6.2	6.4	5.4
EN-1 Average:		8.6	7.8	6.8	6.1	5.1	5.1	5.4	5.2	5.4	4.7
EN-2 Average:		8.4	8.2	6.8	6.2	5.8	6.0	6.3	6.3	6.3	5.3
Overall Average:		8.53	8.00	6.76	6.17	5.46	5.54	5.85	5.76	5.84	5.02
Standard Dev.:		1.19	0.94	1.73	1.03	0.67	0.71	0.88	1.03	1.00	0.61
SEM:		0.34	0.27	0.50	0.30	0.19	0.20	0.25	0.30	0.29	0.18
Maximum:		11.0	9.2	9.8	8.0	6.4	6.4	7.3	7.8	7.2	5.7
Minimum:		7.0	6.3	3.7	4.7	4.5	4.6	4.6	4.4	4.4	3.8

Table C - 9: Resistivity measurements for the third and fourth "perfect" 50/50 enamel-coated ponding specimen.

Specimen:	Location:	Resistivity Measurements (kΩcm) vs. Time (weeks): 0	6	12	18	24	30	36	42	48	54
EN-3	1	9.9	6.3	7.3	7.3	6.8	6.4	6.4	5.5	5.3	4.7
	2	7.4	6.3	7.4	8.2	7.8	7.5	8.1	7.2	7.3	6.4
	3	9.3	8.0	7.4	9.0	9.5	9.0	11.0	9.3	9.8	8.2
	4	9.2	7.3	7.2	7.1	6.8	6.3	6.4	5.6	5.5	5.2
	5	7.5	7.2	6.4	7.1	6.7	5.6	5.6	5.5	5.2	4.8
	6	9.1	8.0	5.8	7.3	7.6	6.9	7.2	5.8	5.4	5.5
EN-4	1	13.0	3.7	8.8	9.0	9.4	8.9	8.9	8.9	7.3	7.3
	2	7.5	7.2	9.8	8.1	9.3	7.4	8.1	8.0	7.3	6.4
	3	12.0	10.0	10.0	9.8	12.0	9.0	9.1	8.9	8.5	7.3
	4	8.3	7.3	7.1	7.3	8.4	7.2	6.4	5.6	5.5	5.2
	5	9.1	7.2	8.1	8.1	8.5	7.9	7.2	5.7	5.5	4.9
	6	9.9	7.5	8.1	7.9	8.4	7.2	7.2	5.9	5.5	5.5
EN-3 Average:		8.7	7.2	6.9	7.7	7.5	7.0	7.5	6.5	6.4	5.8
EN-4 Average:		10.0	7.2	8.7	8.4	9.3	7.9	7.8	7.2	6.6	6.1
Overall Average:		9.35	7.17	7.78	8.02	8.43	7.44	7.63	6.83	6.51	5.95
Standard Dev.:		1.73	1.45	1.26	0.87	1.51	1.10	1.50	1.54	1.51	1.15
SEM:		0.50	0.42	0.36	0.25	0.44	0.32	0.43	0.44	0.44	0.33
Maximum:		13.0	10.0	10.0	9.8	12.0	9.0	11.0	9.3	9.8	8.2
Minimum:		7.4	3.7	5.8	7.1	6.7	5.6	5.6	5.5	5.2	4.7

Table C - 10: Resistivity measurements for the first and second damaged 50/50 enamel-coated ponding specimen.

Specimen:	Location:	Resistivity Measurements (kΩcm) vs. Time (weeks): 0	6	12	18	24	30	36	42	48	54
EN-D-1	1	9.0	7.9	8.9	7.3	5.6	6.4	6.4	6.3	5.7	5.6
	2	7.3	7.4	7.2	6.4	5.5	6.3	6.3	5.6	5.5	5.5
	3	9.4	9.1	8.1	6.8	6.4	7.2	6.9	7.4	6.4	5.8
	4	7.1	7.3	6.3	4.8	4.8	5.4	4.6	4.8	4.7	4.7
	5	8.2	6.6	6.3	5.6	5.5	4.9	4.9	4.3	4.7	4.8
	6	9.4	8.2	7.4	6.5	6.2	6.3	5.5	5.3	5.1	4.8
EN-D-2	1	8.5	9.1	8.9	8.1	7.3	8.0	8.1	7.2	8.0	6.5
	2	7.6	7.3	7.2	6.4	5.6	6.4	6.5	6.5	6.4	5.5
	3	9.3	9.1	9.8	7.3	6.5	7.7	7.6	7.3	7.2	5.7
	4	6.7	7.3	7.2	5.5	5.4	5.6	5.7	5.6	5.0	4.7
	5	7.5	5.7	8.1	6.4	5.9	5.6	5.7	5.3	4.0	4.0
	6	7.6	8.0	8.1	6.3	5.6	5.8	6.8	6.6	6.1	4.9
EN-D-1 Average:		8.4	7.8	7.4	6.2	5.7	6.1	5.8	5.6	5.4	5.2
EN-D-2 Average:		7.9	7.8	8.2	6.7	6.1	6.5	6.7	6.4	6.1	5.2
Overall Average:		8.13	7.75	7.79	6.45	5.86	6.30	6.25	6.02	5.73	5.21
Standard Dev.:		0.97	1.04	1.06	0.89	0.65	0.94	1.03	1.02	1.15	0.67
SEM:		0.28	0.30	0.31	0.26	0.19	0.27	0.30	0.29	0.33	0.19
Maximum:		9.4	9.1	9.8	8.1	7.3	8.0	8.1	7.4	8.0	6.5
Minimum:		6.7	5.7	6.3	4.8	4.8	4.9	4.6	4.3	4.0	4.0

Table C - 11: Resistivity measurements for the third and fourth damaged 50/50 enamel-coated ponding specimen.

Specimen:	Location:	Resistivity Measurements (kΩcm) vs. Time (weeks): 0	6	12	18	24	30	36	42	48	54
EN-D-3	1	9.9	9.8	9.0	8.1	9.2	8.9	10.0	9.0	8.5	6.4
	2	9.2	7.4	8.1	8.1	9.3	9.0	9.1	7.4	7.3	6.5
	3	11.0	9.2	8.8	8.1	9.6	8.9	9.5	7.8	6.4	6.6
	4	8.1	4.7	4.7	7.3	8.4	8.2	7.9	5.5	5.4	5.5
	5	7.6	8.0	8.1	7.2	8.6	8.9	8.9	6.5	5.6	5.5
	6	9.9	9.0	9.0	8.1	8.6	8.5	8.9	7.3	5.5	5.6
EN-D-4	1	11.0	8.1	7.9	7.9	8.4	8.5	9.1	8.9	8.7	8.1
	2	9.8	7.3	9.0	7.5	8.5	9.0	8.9	8.1	7.2	8.1
	3	12.0	9.0	9.0	8.1	9.5	9.9	9.7	7.2	7.2	8.2
	4	9.2	8.6	8.2	7.3	7.5	7.2	7.2	6.3	5.5	5.6
	5	9.1	8.1	8.1	8.1	8.5	8.9	8.0	7.4	6.2	6.4
	6	9.7	9.0	8.0	6.0	7.6	8.1	8.0	6.8	6.2	6.3
EN-D-3 Average:		9.3	8.0	8.0	7.8	9.0	8.7	9.1	7.3	6.5	6.0
EN-D-4 Average:		10.1	8.4	8.4	7.5	8.3	8.6	8.5	7.5	6.8	7.1
Overall Average:		9.71	8.18	8.16	7.65	8.64	8.67	8.77	7.35	6.64	6.57
Standard Dev.:		1.23	1.33	1.18	0.64	0.67	0.65	0.83	1.02	1.15	1.03
SEM:		0.35	0.38	0.34	0.18	0.19	0.19	0.24	0.29	0.33	0.30
Maximum:		12.0	9.8	9.0	8.1	9.6	9.9	10.0	9.0	8.7	8.2
Minimum:		7.6	4.7	4.7	6.0	7.5	7.2	7.2	5.5	5.4	5.5

Table C - 12: Resistivity measurements for the five non-reinforced ponding specimens.

Specimen:	Location:	Resistivity Measurements (kΩcm) vs. Time (weeks): 0	9	12	18	24	30	36	42	48	54
C-1	1	9.1	7.4	7.4	8.5	9.2	7.2	7.3	7.0	6.0	6.3
	2	8.1	7.3	7.4	8.7	8.8	7.2	6.4	6.6	6.5	6.4
	3	9.0	8.4	9.0	9.7	9.6	8.0	7.3	7.9	6.6	7.3
	4	9.2	8.4	9.0	9.8	9.9	8.0	7.7	7.9	6.4	7.2
	5	8.3	6.8	6.8	8.2	8.2	7.3	6.6	7.0	6.2	6.4
	6	9.2	7.6	7.5	8.9	9.0	7.2	6.5	7.0	5.7	6.5
C-2	1	8.4	7.5	7.1	7.8	8.5	6.6	6.4	6.8	5.5	6.1
	2	7.5	8.3	8.2	9.0	9.1	7.2	7.2	7.0	6.2	7.1
	3	8.3	7.5	7.1	8.1	9.0	7.3	7.3	7.0	6.2	6.9
	4	9.3	7.8	8.0	9.7	9.8	7.3	7.3	7.0	6.2	6.4
	5	7.8	7.5	7.2	8.5	9.1	7.3	7.2	7.0	6.2	6.4
	6	8.3	7.7	8.1	9.1	9.0	7.3	6.7	6.9	5.6	6.2
C-3	1	8.5	6.8	7.7	9.0	9.0	7.2	7.3	7.1	6.2	6.4
	2	7.5	6.8	8.1	9.0	9.7	7.3	7.3	7.0	6.3	6.4
	3	7.4	7.2	7.4	8.5	8.9	7.1	7.0	7.0	5.5	6.3
	4	8.0	7.4	8.1	9.6	9.9	7.5	7.3	7.1	6.3	6.4
	5	7.0	6.8	8.1	9.1	9.7	7.4	7.2	7.0	6.2	6.7
	6	7.6	7.5	8.0	9.0	8.4	7.3	7.1	7.1	5.4	6.3
C-4	1	8.5	6.8	7.2	8.2	9.7	7.3	7.3	7.0	6.3	6.3
	2	7.1	7.5	7.0	8.1	9.1	7.3	6.6	6.6	6.2	6.4
	3	7.6	8.3	8.0	9.0	11.0	7.3	7.4	7.0	6.8	7.3
	4	9.9	7.4	7.2	9.1	10.0	7.2	7.2	7.0	6.1	5.9
	5	7.4	7.4	7.3	8.2	9.8	7.4	7.3	7.0	6.3	6.4
	6	9.3	7.4	7.3	8.2	9.0	7.3	6.7	7.1	6.2	6.4
C-5	1	7.8	6.2	6.3	8.1	8.1	7.2	6.5	6.3	6.2	6.4
	2	7.0	6.2	6.3	8.1	8.2	6.8	6.6	6.7	6.2	6.4
	3	7.9	6.8	6.7	8.9	9.8	8.1	7.3	6.9	6.2	6.4
	4	8.8	5.9	6.3	8.0	8.5	6.8	6.5	7.0	6.2	6.5
	5	7.0	6.0	6.3	8.1	8.5	7.3	6.8	6.9	6.2	6.4
	6	7.9	7.0	7.2	7.9	8.8	6.6	6.4	6.5	5.5	6.3
C-1 Average:		8.8	7.7	7.9	9.0	9.1	7.5	7.0	7.2	6.2	6.7
C-2 Average:		8.3	7.7	7.6	8.7	9.1	7.2	7.0	7.0	6.0	6.5
C-3 Average:		7.7	7.1	7.9	9.0	9.3	7.3	7.2	7.1	6.0	6.4
C-4 Average:		8.3	7.5	7.3	8.5	9.8	7.3	7.1	7.0	6.3	6.5
C-5 Average:		7.7	6.4	6.5	8.2	8.7	7.1	6.7	6.7	6.1	6.4
Overall Average:		8.16	7.25	7.44	8.67	9.18	7.28	6.99	6.98	6.12	6.49
Standard Dev.:		0.94	0.73	0.61	0.42	0.63	0.29	0.31	0.29	0.23	0.20
SEM:		0.15	0.12	0.13	0.11	0.12	0.06	0.07	0.06	0.06	0.06
Maximum:		9.9	8.3	8.0	9.1	11.0	8.1	7.4	7.1	6.8	7.3
Minimum:		7.0	5.9	6.3	7.9	8.1	6.6	6.4	6.3	5.5	5.9

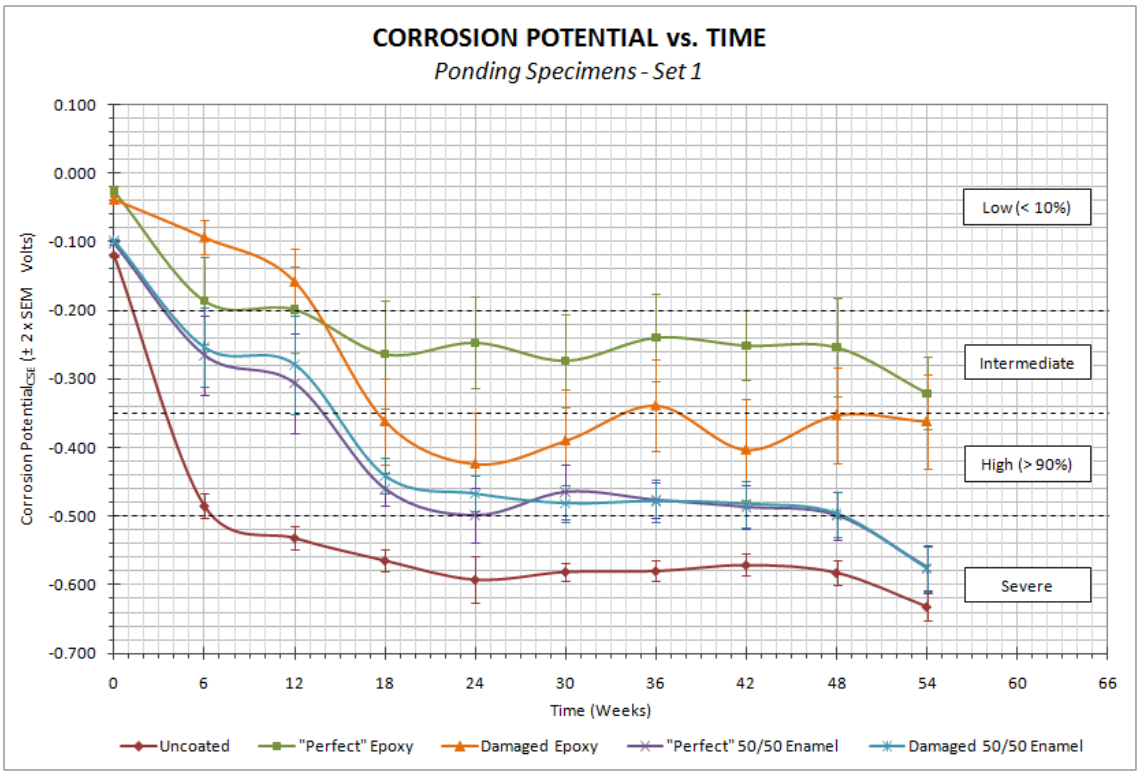

(a)

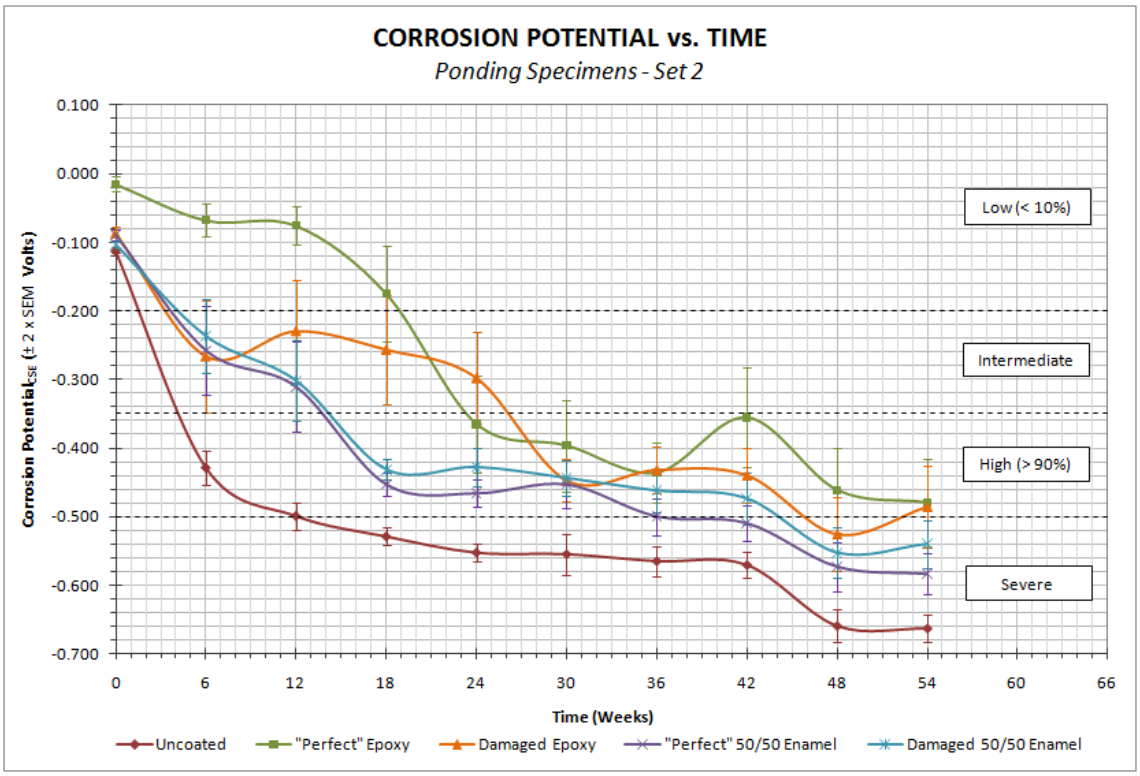

(b)

Figure C - 6: Average corrosion potential for (a) the first and second ponding specimen within each specimen group; (b) third and fourth ponding specimen within each specimen group.

Table C - 13: Corrosion potential measurements for the first and second uncoated ponding specimen.

Specimen:	Location:	Half-Cell Measurements (mV) vs. Time (weeks): 0	6	12	18	24	30	36	42	48	54
M-1	1.1	-128	-440	-511	-535	-554	-575	-564	-542	-556	-600
	1.2	-123	-464	-514	-547	-559	-582	-573	-560	-561	-604
	1.3	-118	-451	-499	-530	-562	-578	-573	-560	-557	-595
	2.1	-124	-457	-533	-568	-516	-537	-519	-504	-513	-583
	2.2	-119	-446	-514	-539	-484	-523	-517	-526	-532	-583
	2.3	-122	-437	-485	-516	-495	-524	-511	-523	-528	-565
	3.1	-121	-490	-569	-606	-629	-617	-599	-581	-595	-627
	3.2	-122	-462	-512	-559	-599	-594	-580	-565	-584	-621
	3.3	-118	-488	-559	-591	-616	-612	-589	-579	-600	-632
	4.1	-115	-425	-485	-504	-558	-576	-562	-549	-550	-594
	4.2	-122	-460	-481	-529	-571	-583	-576	-549	-552	-601
	4.3	-120	-494	-586	-609	-610	-619	-603	-577	-571	-611
M-2	1.1	-119	-456	-491	-535	-563	-534	-529	-511	-537	-585
	1.2	-125	-501	-525	-552	-572	-542	-549	-547	-560	-604
	1.3	-122	-537	-531	-546	-568	-547	-554	-549	-567	-617
	2.1	-116	-462	-500	-540	-546	-573	-585	-580	-618	-676
	2.2	-118	-508	-520	-554	-557	-588	-604	-607	-640	-703
	2.3	-118	-541	-523	-554	-556	-589	-608	-611	-639	-715
	3.1	-119	-485	-523	-563	-592	-617	-613	-597	-584	-632
	3.2	-118	-470	-531	-582	-593	-617	-603	-586	-579	-624
	3.3	-125	-470	-500	-539	-558	-601	-592	-580	-570	-620
	4.1	-124	-575	-619	-654	-796	-618	-639	-643	-662	-722
	4.2	-121	-533	-613	-639	-778	-589	-631	-636	-659	-721
	4.3	-121	-588	-632	-653	-776	-601	-635	-636	-657	-720
M-1 Average:		-121	-460	-521	-553	-563	-577	-564	-551	-558	-601
M-2 Average:		-121	-511	-542	-576	-621	-585	-595	-590	-606	-662
Average:		-121	-485	-532	-564	-592	-581	-580	-571	-582	-631
Standard Dev.:		3	43	43	41	81	31	36	38	43	50
SEM:		1	9	9	8	17	6	7	8	9	10
Maximum:		-115	-425	-481	-504	-484	-523	-511	-504	-513	-565
Minimum:		-128	-588	-632	-654	-796	-619	-639	-643	-662	-722

Table C - 14: Corrosion potential measurements for the third and fourth uncoated ponding specimen.

Specimen:	Location:	Half-Cell Measurements (mV) vs. Time (weeks): 0	6	12	18	24	30	36	42	48	54
M-3	1.1	-111	-438	-525	-505	-503	-449	-472	-497	-608	-632
	1.2	-117	-442	-512	-513	-534	-465	-500	-523	-660	-677
	1.3	-117	-424	-471	-504	-544	-480	-515	-530	-664	-667
	2.1	-116	-415	-492	-514	-509	-464	-509	-516	-587	-614
	2.2	-117	-416	-488	-509	-536	-484	-536	-546	-622	-635
	2.3	-110	-391	-461	-518	-556	-503	-554	-561	-624	-623
	3.1	-113	-436	-491	-532	-547	-573	-591	-622	-714	-695
	3.2	-110	-490	-575	-576	-570	-572	-568	-606	-712	-701
	3.3	-115	-435	-550	-571	-582	-591	-592	-622	-712	-697
	4.1	-109	-402	-467	-513	-582	-702	-670	-659	-674	-679
	4.2	-103	-409	-471	-528	-563	-707	-665	-662	-683	-701
	4.3	-114	-408	-448	-518	-576	-696	-662	-654	-674	-682
M-4	1.1	-117	-464	-502	-517	-520	-529	-545	-540	-567	-590
	1.2	-115	-454	-513	-528	-544	-552	-561	-563	-570	-592
	1.3	-113	-455	-510	-528	-552	-552	-565	-566	-557	-589
	2.1	-122	-294	-395	-453	-469	-464	-473	-490	-616	-629
	2.2	-115	-357	-469	-524	-548	-540	-548	-539	-638	-649
	2.3	-109	-367	-472	-518	-539	-530	-539	-545	-617	-621
	3.1	-120	-410	-456	-512	-536	-539	-552	-578	-699	-647
	3.2	-116	-379	-449	-499	-547	-544	-553	-586	-707	-655
	3.3	-110	-419	-532	-575	-592	-586	-584	-601	-704	-654
	4.1	-106	-617	-616	-607	-614	-603	-611	-564	-736	-758
	4.2	-109	-500	-556	-564	-590	-587	-593	-569	-737	-761
	4.3	-107	-463	-553	-564	-600	-597	-595	-548	-740	-763
M-3 Average:		-113	-426	-496	-525	-550	-557	-570	-583	-661	-667
M-4 Average:		-113	-432	-502	-532	-554	-552	-560	-557	-657	-659
Average:		-113	-429	-499	-529	-552	-555	-565	-570	-659	-663
Standard Dev.:		5	60	49	33	33	73	53	48	57	51
SEM:		1	12	10	7	7	15	11	10	12	10
Maximum:		-103	-294	-395	-453	-469	-449	-472	-490	-557	-589
Minimum:		-122	-617	-616	-607	-614	-707	-670	-662	-740	-763

Table C - 15: Corrosion potential measurements for the first and second "perfect" epoxy-coated ponding specimen.

Specimen:	Location:	Half-Cell Measurements (mV) vs. Time (weeks): 0	6	12	18	24	30	36	42	48	54
EP-1	1.1	-38	-75	-62	-43	-77	-127	-101	-335	-350	-354
	1.2	-40	-70	-54	-42	-74	-121	-97	-327	-344	-354
	1.3	-39	-74	-56	-40	-74	-119	-98	-329	-344	-355
	2.1	-13	-21	-62	-19	-104	-105	-107	-255	-94	-149
	2.2	-15	-20	-58	-14	-95	-103	-103	-258	-86	-146
	2.3	-12	-23	-52	-9	-92	-103	-101	-257	-85	-148
	3.1	-29	-474	-360	-405	-298	-399	-326	-320	-298	-358
	3.2	-31	-474	-364	-405	-297	-402	-325	-320	-300	-361
	3.3	-22	-477	-370	-410	-295	-403	-327	-322	-297	-361
	4.1	-47	-227	-231	-324	-380	-319	-415	-327	-345	-444
	4.2	-42	-232	-228	-318	-383	-319	-417	-329	-347	-443
	4.3	-41	-228	-224	-320	-385	-323	-418	-328	-346	-445
EP-2	1.1	-40	-73	-75	-513	-243	-431	-193	-134	-111	-326
	1.2	-37	-75	-78	-502	-239	-429	-185	-117	-103	-314
	1.3	-35	-76	-75	-504	-241	-430	-187	-119	-108	-314
	2.1	14	-77	-40	-36	-34	-21	-5	1	-3	-108
	2.2	15	-73	-37	-29	-20	-14	3	7	1	-93
	2.3	12	-75	-38	-28	-23	-16	1	6	1	-92
	3.1	-47	-388	-420	-397	-343	-288	-341	-270	-277	-355
	3.2	-42	-384	-420	-394	-336	-287	-336	-265	-275	-357
	3.3	-47	-374	-419	-394	-332	-287	-335	-261	-274	-349
	4.1	-29	-162	-351	-397	-528	-505	-448	-395	-576	-496
	4.2	-20	-156	-351	-395	-518	-500	-445	-390	-572	-493
	4.3	-18	-162	-350	-398	-517	-506	-445	-387	-567	-490
EP-1 Average:		-31	-200	-177	-196	-213	-237	-236	-309	-270	-327
EP-2 Average:		-23	-173	-221	-332	-281	-310	-243	-194	-239	-316
Average:		-27	-186	-199	-264	-247	-273	-240	-251	-254	-321
Standard Dev.:		19	157	154	192	164	167	157	124	175	129
SEM:		4	32	31	39	33	34	32	25	36	26
Maximum:		15	-20	-37	-9	-20	-14	3	7	1	-92
Minimum:		-47	-477	-420	-513	-528	-506	-448	-395	-576	-496

Table C - 16: Corrosion potential measurements for the third and fourth "perfect" epoxy-coated ponding specimen.

Specimen:	Location:	Half-Cell Measurements (mV) vs. Time (weeks): 0	6	12	18	24	30	36	42	48	54
EP-3	1.1	21	5	25	21	-160	-462	-578	-560	-535	-547
	1.2	15	10	30	33	-158	-456	-566	-529	-508	-543
	1.3	30	9	28	37	-158	-461	-579	-537	-515	-543
	2.1	-3	-46	-50	-164	-450	-509	-453	-306	-513	-572
	2.2	-42	-43	-49	-156	-448	-499	-433	-289	-492	-548
	2.3	3	-43	-50	-156	-452	-501	-435	-292	-500	-546
	3.1	20	-124	-143	-385	-455	-543	-559	-582	-655	-662
	3.2	-5	-124	-143	-387	-453	-543	-552	-581	-651	-652
	3.3	-32	-124	-145	-382	-456	-545	-552	-565	-648	-655
	4.1	-2	-63	-63	-58	-52	-76	-350	-87	-427	-582
	4.2	-1	-60	-57	-56	-56	-72	-341	-82	-421	-577
	4.3	0	-65	-56	-54	-46	-71	-342	-78	-419	-572
EP-4	1.1	-22	-46	-68	-104	-603	-580	-571	-569	-632	-618
	1.2	-23	-43	-65	-94	-595	-569	-565	-558	-622	-615
	1.3	-25	-34	-65	-97	-594	-568	-567	-553	-618	-610
	2.1	-2	-2	-13	-30	-499	-444	-346	-331	-483	-378
	2.2	-3	-2	-10	-17	-491	-434	-335	-317	-470	-365
	2.3	-5	-1	-9	-18	-491	-436	-337	-317	-479	-368
	3.1	-34	-171	-194	-466	-385	-227	-346	-187	-177	-193
	3.2	-30	-172	-192	-465	-383	-226	-341	-185	-171	-191
	3.3	-36	-163	-191	-469	-383	-226	-341	-179	-171	-186
	4.1	-65	-120	-117	-242	-331	-358	-329	-285	-327	-335
	4.2	-61	-110	-113	-245	-329	-352	-324	-283	-322	-331
	4.3	-59	-96	-108	-246	-328	-356	-322	-280	-320	-327
EP-3 Average:		0	-56	-56	-142	-279	-395	-478	-374	-524	-583
EP-4 Average:		-30	-80	-95	-208	-451	-398	-394	-337	-399	-376
Average:		-15	-68	-76	-175	-365	-396	-436	-356	-462	-480
Standard Dev.:		26	59	68	169	173	164	108	177	150	156
SEM:		5	12	14	35	35	33	22	36	31	32
Maximum:		30	10	30	37	-46	-71	-322	-78	-171	-186
Minimum:		-65	-172	-194	-469	-603	-580	-579	-582	-655	-662

Table C - 17: Corrosion potential measurements for the first and second damaged epoxy-coated ponding specimen.

Specimen:	Location:	Half-Cell Measurements (mV) vs. Time (weeks): 0	6	12	18	24	30	36	42	48	54
EP-D-1	1.1	-25	-24	-65	-61	-30	-26	-17	-8	-9	-60
	1.2	-26	-23	-59	-58	-21	-17	-5	-2	-3	-26
	1.3	-30	-20	-56	-54	-19	-15	-7	-2	-3	-21
	2.1	-42	-70	-68	-512	-578	-463	-460	-553	-475	-525
	2.2	-42	-70	-63	-512	-570	-463	-455	-549	-468	-527
	2.3	-38	-69	-63	-515	-571	-464	-452	-542	-462	-518
	3.1	-28	-77	-101	-325	-600	-516	-407	-544	-559	-349
	3.2	-34	-79	-96	-327	-597	-512	-402	-539	-559	-349
	3.3	-32	-78	-95	-325	-595	-512	-400	-541	-549	-343
	4.1	-52	-143	-243	-416	-514	-384	-411	-381	-349	-232
	4.2	-53	-143	-238	-412	-502	-377	-405	-378	-342	-228
	4.3	-49	-141	-237	-413	-505	-379	-406	-375	-339	-226
EP-D-2	1.1	-26	-40	-84	-429	-584	-586	-407	-498	-513	-545
	1.2	-24	-42	-87	-423	-578	-587	-402	-493	-510	-536
	1.3	-24	-42	-82	-421	-577	-588	-390	-490	-508	-531
	2.1	-23	-41	-80	-429	-404	-360	-316	-267	-203	-300
	2.2	-20	-46	-83	-423	-395	-358	-305	-259	-201	-297
	2.3	-15	-42	-76	-422	-401	-362	-305	-262	-193	-295
	3.1	-71	-164	-409	-527	-351	-238	-181	-480	-397	-527
	3.2	-74	-163	-408	-526	-345	-235	-182	-476	-400	-526
	3.3	-70	-160	-409	-534	-351	-235	-180	-476	-392	-524
	4.1	-46	-194	-237	-209	-363	-558	-546	-521	-347	-403
	4.2	-45	-190	-233	-206	-358	-555	-543	-518	-342	-396
	4.3	-41	-193	-232	-206	-357	-558	-543	-515	-340	-397
EP-D-1 Average:		-38	-78	-115	-328	-425	-344	-319	-368	-343	-284
EP-D-2 Average:		-40	-110	-202	-396	-422	-435	-358	-438	-362	-440
Average:		-39	-94	-159	-362	-424	-390	-339	-403	-353	-362
Standard Dev.:		16	60	119	153	182	180	163	179	172	167
SEM:		3	12	24	31	37	37	33	37	35	34
Maximum:		-15	-20	-56	-54	-19	-15	-5	-2	-3	-21
Minimum:		-74	-194	-409	-534	-600	-588	-546	-553	-559	-545

Table C - 18: Corrosion potential measurements for the third and fourth damaged epoxy-coated ponding specimen.

Specimen:	Location:	Half-Cell Measurements (mV) vs. Time (weeks): 0	6	12	18	24	30	36	42	48	54
EP-D-3	1.1	-114	-136	-133	-111	-416	-422	-289	-318	-585	-301
	1.2	-125	-128	-122	-102	-412	-415	-280	-313	-582	-298
	1.3	-114	-129	-125	-104	-415	-415	-280	-300	-571	-291
	2.1	-61	-131	-106	-89	-81	-472	-437	-348	-239	-224
	2.2	-53	-129	-95	-85	-76	-472	-430	-333	-246	-224
	2.3	-52	-125	-98	-80	-73	-473	-430	-328	-239	-219
	3.1	-110	-129	-144	-93	-75	-444	-449	-449	-591	-621
	3.2	-108	-126	-134	-92	-71	-432	-441	-450	-583	-619
	3.3	-104	-125	-137	-92	-67	-430	-434	-434	-576	-607
	4.1	-76	-570	-633	-556	-521	-546	-572	-539	-650	-630
	4.2	-64	-562	-627	-549	-520	-536	-555	-530	-639	-627
	4.3	-62	-562	-631	-547	-515	-532	-551	-517	-631	-618
EP-D-4	1.1	-96	-81	-75	-88	-190	-403	-466	-485	-389	-418
	1.2	-92	-80	-66	-77	-183	-397	-456	-478	-381	-414
	1.3	-81	-78	-64	-78	-183	-398	-452	-475	-378	-413
	2.1	-103	-121	-115	-569	-454	-588	-533	-561	-568	-550
	2.2	-91	-112	-104	-556	-450	-582	-525	-544	-556	-548
	2.3	-83	-111	-98	-557	-451	-582	-526	-544	-556	-552
	3.1	-118	-445	-321	-269	-375	-386	-376	-543	-598	-579
	3.2	-108	-441	-321	-270	-373	-381	-375	-535	-580	-577
	3.3	-97	-442	-323	-268	-373	-382	-373	-549	-581	-578
	4.1	-75	-543	-350	-311	-292	-348	-380	-331	-638	-579
	4.2	-74	-542	-347	-310	-292	-348	-377	-320	-629	-582
	4.3	-46	-543	-348	-312	-295	-346	-378	-326	-626	-581
EP-D-3 Average:		-87	-238	-249	-208	-270	-466	-429	-405	-511	-440
EP-D-4 Average:		-89	-295	-211	-305	-326	-428	-435	-474	-540	-531
Average:		-88	-266	-230	-257	-298	-447	-432	-440	-526	-485
Standard Dev.:		23	201	184	195	163	77	85	98	134	148
SEM:		5	41	38	40	33	16	17	20	27	30
Maximum:		-46	-78	-64	-77	-67	-346	-280	-300	-239	-219
Minimum:		-125	-570	-633	-569	-521	-588	-572	-561	-650	-630

Table C - 19: Corrosion potential measurements for the first and second "perfect" 50/50 enamel-coated ponding specimen.

Specimen:	Location:	Half-Cell Measurements (mV) vs. Time (weeks): 0	6	12	18	24	30	36	42	48	54
EN-1	1.1	-106	-125	-210	-390	-416	-438	-430	-411	-430	-517
	1.2	-104	-133	-219	-408	-398	-406	-401	-402	-431	-511
	1.3	-95	-133	-227	-457	-451	-443	-426	-450	-488	-567
	2.1	-96	-124	-114	-383	-460	-435	-466	-423	-430	-515
	2.2	-101	-114	-101	-376	-424	-399	-400	-391	-405	-487
	2.3	-92	-116	-104	-403	-447	-446	-417	-409	-419	-499
	3.1	-112	-412	-491	-534	-534	-541	-548	-583	-569	-632
	3.2	-111	-404	-482	-525	-527	-542	-561	-585	-562	-623
	3.3	-112	-423	-530	-541	-550	-560	-566	-589	-549	-619
	4.1	-106	-366	-430	-477	-717	-590	-499	-530	-629	-696
	4.2	-101	-387	-451	-487	-714	-578	-502	-550	-637	-701
	4.3	-104	-436	-546	-543	-719	-604	-560	-575	-635	-706
EN-2	1.1	-106	-126	-114	-423	-436	-264	-409	-413	-398	-458
	1.2	-106	-126	-108	-407	-409	-251	-389	-388	-385	-469
	1.3	-101	-133	-112	-446	-447	-288	-424	-406	-399	-487
	2.1	-108	-132	-111	-397	-424	-414	-420	-430	-434	-484
	2.2	-104	-128	-108	-386	-396	-395	-405	-406	-425	-497
	2.3	-94	-127	-106	-413	-429	-426	-436	-418	-443	-525
	3.1	-96	-409	-485	-551	-555	-570	-582	-560	-538	-615
	3.2	-97	-374	-441	-492	-507	-528	-536	-537	-517	-604
	3.3	-103	-364	-420	-481	-510	-533	-539	-535	-520	-599
	4.1	-97	-435	-498	-545	-520	-509	-533	-577	-588	-665
	4.2	-97	-411	-471	-497	-493	-505	-502	-564	-585	-667
	4.3	-99	-428	-475	-495	-494	-490	-489	-556	-568	-658
EN-1 Average:		-103	-264	-325	-460	-530	-499	-481	-492	-515	-589
EN-2 Average:		-101	-266	-287	-461	-468	-431	-472	-483	-483	-561
Average:		-102	-265	-306	-461	-499	-465	-477	-487	-499	-575
Standard Dev.:		6	143	179	60	97	100	65	79	84	82
SEM:		1	29	37	12	20	20	13	16	17	17
Maximum:		-92	-114	-101	-376	-396	-251	-389	-388	-385	-458
Minimum:		-112	-436	-546	-551	-719	-604	-582	-589	-637	-706

Table C - 20: Corrosion potential measurements for the third and fourth "perfect" 50/50 enamel-coated ponding specimen.

Specimen:	Location:	Half-Cell Measurements (mV) vs. Time (weeks): 0	6	12	18	24	30	36	42	48	54
EN-3	1.1	-98	-101	-379	-456	-489	-507	-515	-530	-575	-572
	1.2	-104	-105	-377	-413	-424	-427	-430	-459	-515	-526
	1.3	-99	-91	-387	-420	-418	-410	-422	-430	-480	-475
	2.1	-108	-98	-86	-450	-477	-339	-507	-546	-498	-576
	2.2	-108	-103	-94	-412	-445	-268	-446	-478	-420	-513
	2.3	-106	-113	-119	-435	-443	-268	-425	-456	-401	-478
	3.1	-95	-392	-435	-499	-530	-543	-577	-594	-678	-671
	3.2	-99	-433	-517	-532	-563	-557	-564	-585	-672	-669
	3.3	-94	-425	-489	-520	-514	-509	-528	-566	-676	-671
	4.1	-107	-352	-432	-475	-529	-559	-632	-582	-659	-649
	4.2	-109	-354	-437	-463	-494	-542	-609	-566	-654	-651
	4.3	-97	-349	-410	-457	-470	-485	-544	-536	-656	-650
EN-4	1.1	-66	-120	-110	-445	-433	-448	-459	-423	-492	-500
	1.2	-70	-104	-96	-388	-393	-412	-419	-387	-471	-482
	1.3	-86	-95	-91	-388	-408	-447	-455	-402	-493	-496
	2.1	-111	-112	-135	-448	-420	-384	-428	-489	-553	-568
	2.2	-110	-114	-137	-405	-398	-346	-405	-457	-514	-509
	2.3	-103	-133	-150	-432	-442	-387	-449	-463	-543	-524
	3.1	-65	-403	-408	-474	-477	-505	-542	-543	-638	-648
	3.2	-71	-397	-408	-461	-471	-513	-551	-557	-641	-650
	3.3	-61	-447	-482	-553	-550	-557	-559	-562	-636	-645
	4.1	-63	-517	-473	-491	-511	-515	-545	-563	-639	-632
	4.2	-58	-408	-398	-414	-432	-464	-499	-535	-625	-626
	4.3	-59	-414	-405	-438	-451	-480	-482	-516	-618	-622
EN-3 Average:		-102	-243	-347	-461	-483	-451	-517	-527	-574	-592
EN-4 Average:		-77	-272	-274	-445	-449	-455	-483	-491	-572	-575
Average:		-89	-258	-311	-453	-466	-453	-500	-509	-573	-583
Standard Dev.:		19	157	160	43	48	87	66	62	87	72
SEM:		4	32	33	9	10	18	13	13	18	15
Maximum:		-58	-91	-86	-388	-393	-268	-405	-387	-401	-475
Minimum:		-111	-517	-517	-553	-563	-559	-632	-594	-678	-671

Table C - 21: Corrosion potential measurements for the first and second damaged 50/50 enamel-coated ponding specimen.

Specimen:	Location:	Half-Cell Measurements (mV) vs. Time (weeks): 0	6	12	18	24	30	36	42	48	54
EN-D-1	1.1	-97	-110	-104	-385	-434	-488	-421	-404	-399	-463
	1.2	-92	-115	-96	-375	-400	-437	-393	-380	-394	-467
	1.3	-86	-116	-103	-402	-421	-438	-410	-409	-423	-502
	2.1	-95	-111	-107	-414	-454	-462	-453	-432	-443	-539
	2.2	-103	-123	-104	-392	-425	-425	-429	-429	-465	-564
	2.3	-98	-124	-103	-401	-437	-416	-418	-445	-460	-554
	3.1	-99	-481	-484	-531	-537	-569	-573	-590	-578	-644
	3.2	-97	-409	-436	-475	-492	-519	-524	-572	-568	-636
	3.3	-96	-387	-420	-464	-495	-500	-490	-567	-563	-626
	4.1	-97	-450	-511	-569	-602	-610	-614	-607	-590	-653
	4.2	-103	-388	-455	-512	-549	-569	-584	-584	-583	-654
	4.3	-102	-374	-451	-510	-545	-555	-559	-575	-571	-646
EN-D-2	1.1	-102	-123	-114	-380	-410	-427	-383	-400	-411	-465
	1.2	-101	-123	-112	-377	-394	-415	-376	-380	-395	-461
	1.3	-109	-127	-121	-404	-420	-457	-431	-426	-429	-510
	2.1	-104	-123	-108	-361	-389	-394	-404	-387	-410	-483
	2.2	-97	-124	-109	-362	-377	-376	-394	-378	-404	-513
	2.3	-96	-123	-113	-379	-399	-393	-429	-402	-420	-541
	3.1	-104	-419	-490	-541	-562	-572	-573	-556	-593	-674
	3.2	-102	-374	-422	-455	-483	-496	-507	-522	-590	-672
	3.3	-105	-368	-411	-452	-491	-487	-473	-461	-525	-669
	4.1	-85	-351	-457	-516	-532	-542	-571	-578	-583	-646
	4.2	-87	-330	-453	-478	-494	-516	-548	-560	-576	-641
	4.3	-92	-319	-412	-465	-479	-494	-521	-533	-548	-627
EN-D-1 Average:		-97	-266	-281	-453	-483	-499	-489	-500	-503	-579
EN-D-2 Average:		-99	-242	-277	-431	-453	-464	-468	-465	-490	-575
Average:		-98	-254	-279	-442	-468	-482	-478	-482	-497	-577
Standard Dev.:		6	140	176	64	63	66	76	84	80	79
SEM:		1	29	36	13	13	13	15	17	16	16
Maximum:		-85	-110	-96	-361	-377	-376	-376	-378	-394	-461
Minimum:		-109	-481	-511	-569	-602	-610	-614	-607	-593	-674

Table C - 22: Corrosion potential measurements for the third and fourth damaged 50/50 enamel-coated ponding specimen.

Specimen:	Location:	Half-Cell Measurements (mV) vs. Time (weeks): 0	6	12	18	24	30	36	42	48	54
EN-D-3	1.1	-111	-102	-84	-369	-341	-404	-333	-374	-490	-477
	1.2	-109	-110	-93	-387	-358	-387	-339	-363	-507	-495
	1.3	-107	-111	-109	-443	-402	-403	-354	-366	-556	-561
	2.1	-115	-120	-194	-370	-310	-408	-427	-376	-524	-513
	2.2	-121	-115	-183	-373	-297	-368	-396	-346	-545	-540
	2.3	-117	-114	-183	-411	-323	-370	-390	-331	-532	-512
	3.1	-104	-320	-447	-470	-449	-488	-526	-563	-630	-634
	3.2	-103	-316	-408	-422	-420	-426	-455	-527	-607	-609
	3.3	-105	-326	-406	-423	-441	-433	-452	-493	-594	-594
	4.1	-101	-355	-416	-482	-492	-522	-522	-570	-622	-613
	4.2	-108	-360	-411	-444	-470	-499	-531	-573	-637	-620
	4.3	-98	-395	-470	-488	-525	-541	-545	-571	-634	-618
EN-D-4	1.1	-101	-96	-312	-415	-408	-377	-427	-409	-414	-416
	1.2	-88	-107	-325	-417	-399	-374	-394	-397	-394	-401
	1.3	-96	-104	-343	-451	-440	-415	-416	-399	-404	-408
	2.1	-97	-113	-110	-421	-434	-407	-449	-455	-481	-448
	2.2	-99	-107	-102	-398	-407	-385	-425	-443	-469	-443
	2.3	-101	-102	-99	-422	-428	-397	-451	-436	-469	-435
	3.1	-104	-433	-471	-509	-566	-566	-559	-559	-597	-590
	3.2	-107	-381	-410	-426	-476	-481	-486	-500	-555	-554
	3.3	-105	-370	-400	-424	-474	-481	-487	-481	-526	-523
	4.1	-88	-382	-425	-465	-477	-499	-581	-624	-706	-662
	4.2	-99	-377	-428	-462	-458	-488	-565	-606	-693	-651
	4.3	-95	-364	-416	-459	-472	-532	-583	-607	-681	-644
EN-D-3 Average:		-108	-229	-284	-424	-402	-437	-439	-454	-573	-566
EN-D-4 Average:		-98	-245	-320	-439	-453	-450	-485	-493	-532	-515
Average:		-103	-237	-302	-431	-428	-444	-462	-474	-553	-540
Standard Dev.:		8	133	144	37	67	62	76	94	90	85
SEM:		2	27	29	8	14	13	16	19	18	17
Maximum:		-88	-96	-84	-369	-297	-368	-333	-331	-394	-401
Minimum:		-121	-433	-471	-509	-566	-566	-583	-624	-706	-662

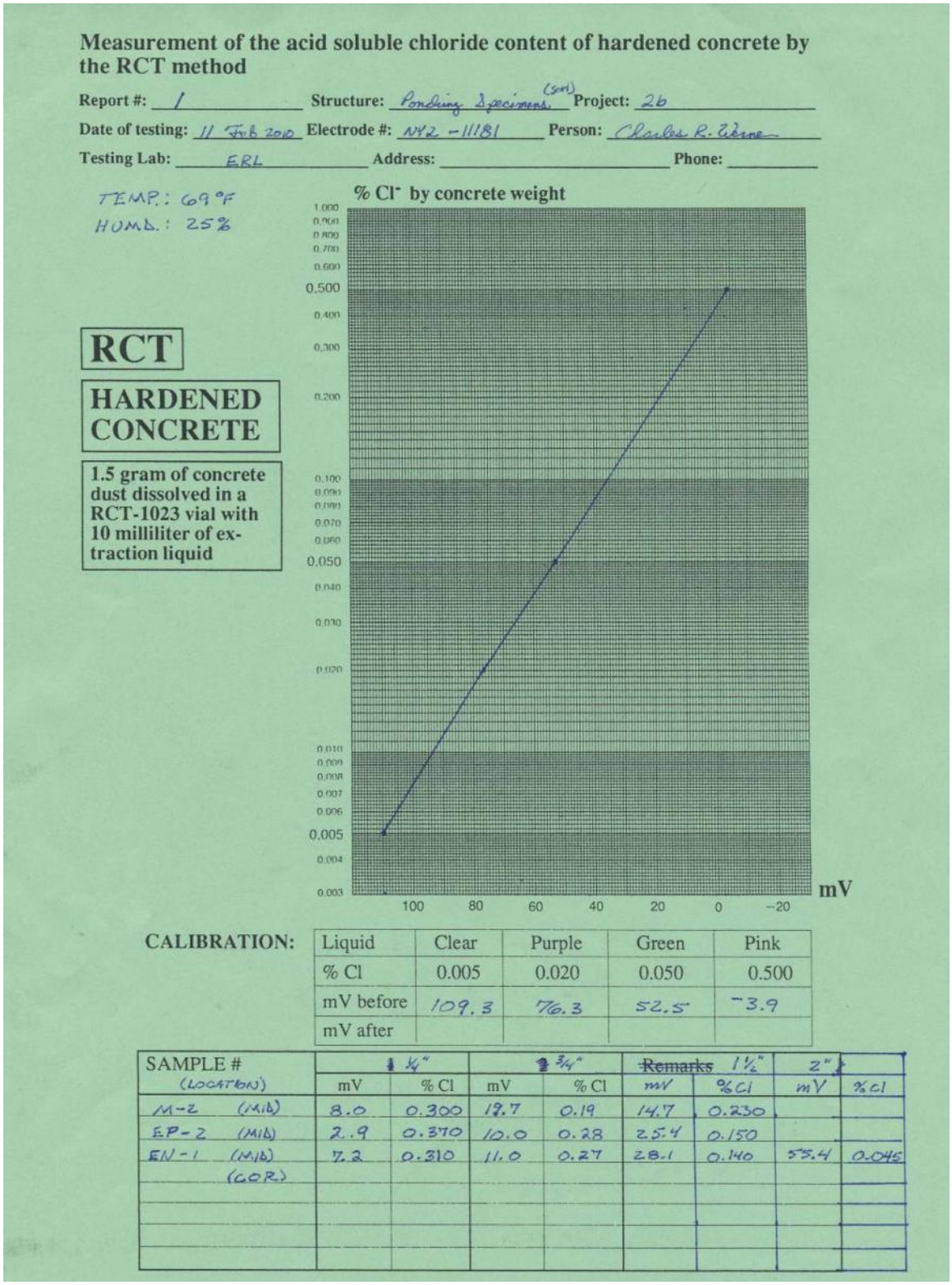

Figure C - 7: Typical data sheet used while conducting a chloride analysis upon a set of ponding specimens.

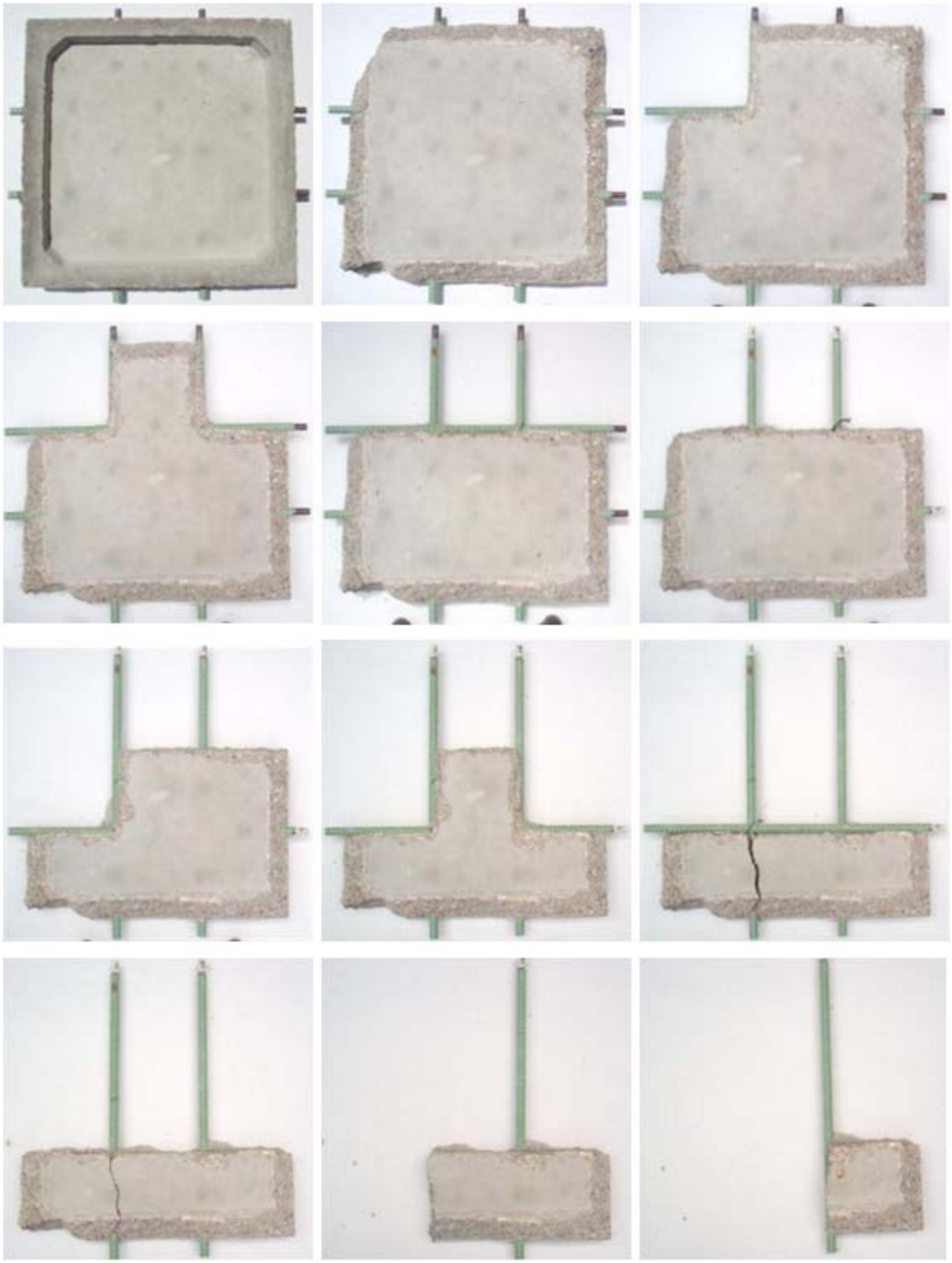

Figure C - 8: A series of images showing the progression of the removal of a ponding specimen's reinforcement.

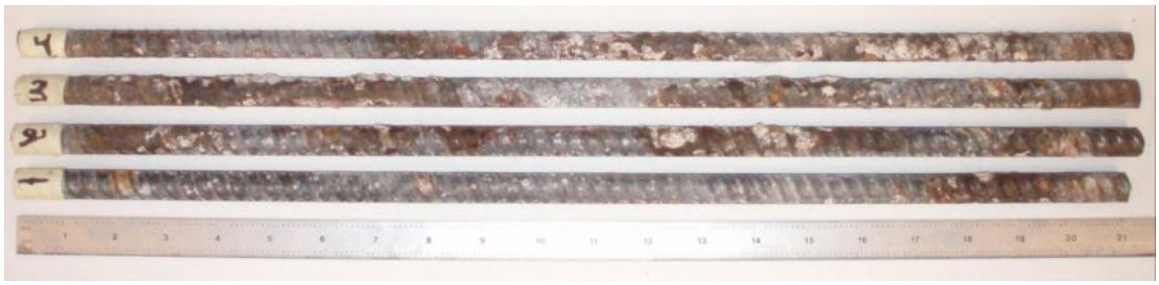

(a)

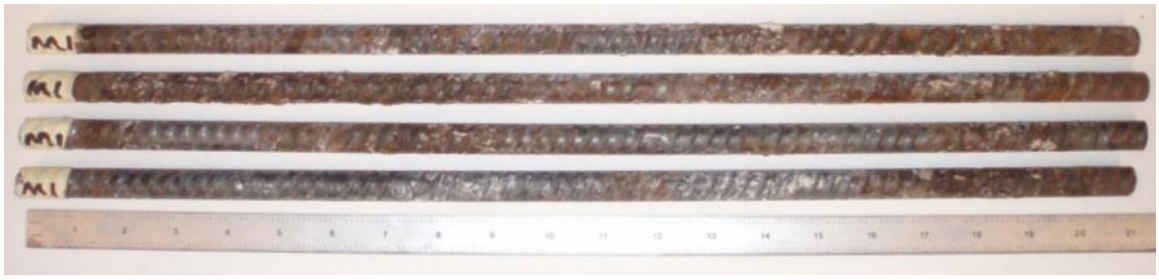

(b)

Figure C - 9: The (a) front and (b) back view of the four bars that were embedded within the first uncoated ponding specimen (M-1) which reported a final corrosion potential of -601 mV and an overall resistance of 4.2 kΩcm.

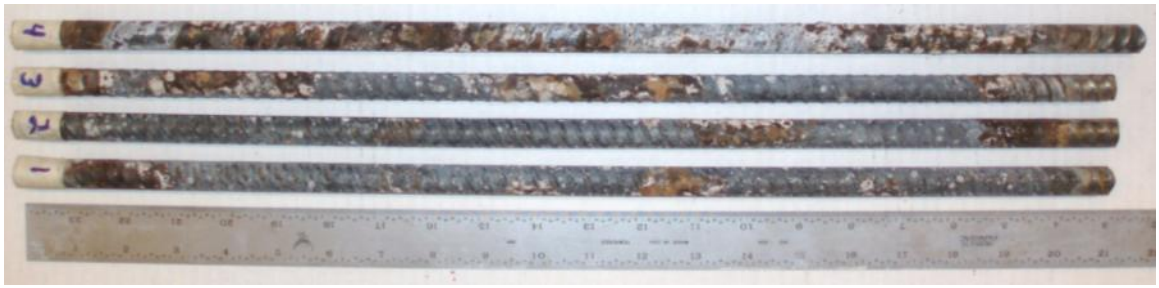

(a)

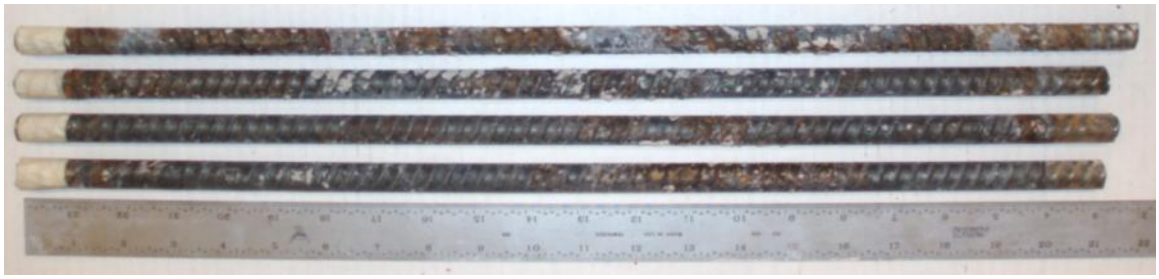

(b)

Figure C - 10: The (a) front and (b) back view of the four bars that were embedded within the second uncoated ponding specimen (M-2) which reported a final corrosion potential of -662 mV and an overall resistance of 3.5 kΩcm.

(a)

(b)

Figure C - 11: The (a) front and (b) back view of the four bars that were embedded within the third uncoated ponding specimen (M-3) which reported a final corrosion potential of -667 mV and an overall resistance of 4.5 kΩcm.

(a)

(b)

Figure C - 12: The (a) front and (b) back view of the four bars that were embedded within the fourth uncoated ponding specimen (M-4) which reported a final corrosion potential of -659 mV and an overall resistance of 4.8 kΩcm.

(a)

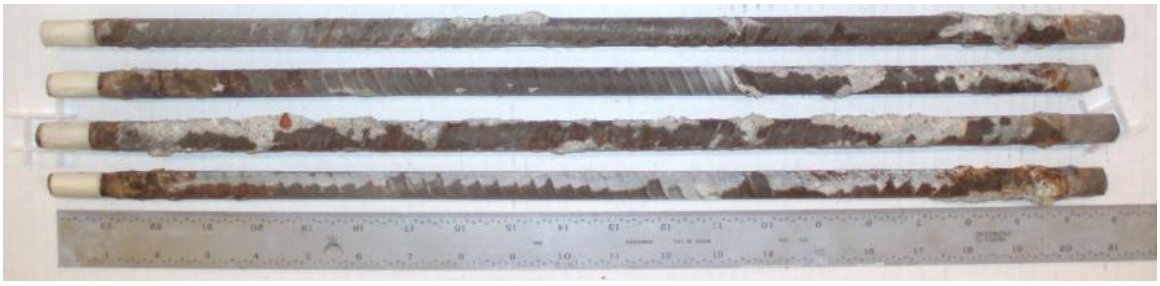

(b)

Figure C - 13: The (a) front and (b) back view of the four bars that were embedded within the first "perfect" 50/50 enamel-coated ponding specimen (EN-1) which reported a final corrosion potential of -589 mV and an overall resistance of 6.0 kΩcm.

(a)

(b)

Figure C - 14: The (a) front and (b) back view of the four bars that were embedded within the second "perfect" 50/50 enamel-coated ponding specimen (EN-2) which reported a final corrosion potential of -561 mV and an overall resistance of 6.6 kΩcm.

(a)

(b)

Figure C - 15: The (a) front and (b) back view of the four bars that were embedded within the third "perfect" 50/50 enamel-coated ponding specimen (EN-3) which reported a final corrosion potential of -592 mV and an overall resistance of 7.1 kΩcm.

(a)

(b)

Figure C - 16: The (a) front and (b) back view of the four bars that were embedded within the fourth "perfect" 50/50 enamel-coated ponding specimen (EN-4) which reported a final corrosion potential of -575 mV and an overall resistance of 7.9 kΩcm.

(a)

(b)

Figure C - 17: The (a) front and (b) back view of the four bars that were embedded within the first damaged 50/50 enamel-coated ponding specimen (EN-D-1) which reported a final corrosion potential of -579 mV and an overall resistance of 6.3 kΩcm.

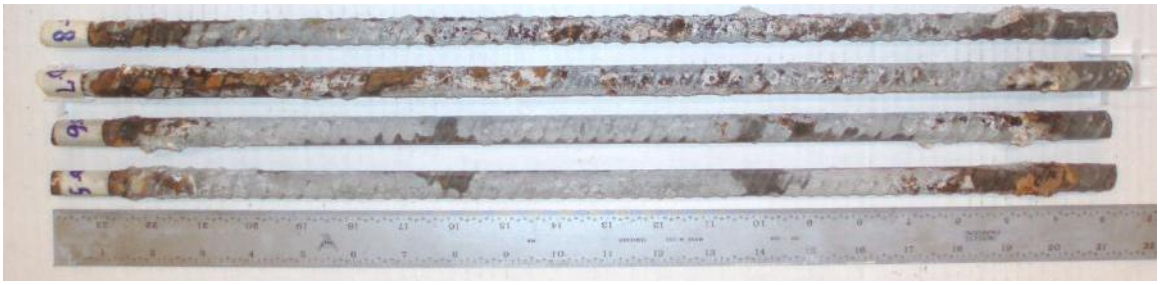

(a)

(b)

Figure C - 18: The (a) front and (b) back view of the four bars that were embedded within the second damaged 50/50 enamel-coated ponding specimen (EN-D-2) which reported a final corrosion potential of -575 mV and an overall resistance of 6.8 kΩcm.

(a)

(b)

Figure C - 19: The (a) front and (b) back view of the four bars that were embedded within the third damaged 50/50 enamel-coated ponding specimen (EN-D-3) which reported a final corrosion potential of -555 mV and an overall resistance of 4.8 kΩcm.

(a)

(b)

Figure C - 20: The (a) front and (b) back view of the four bars that were embedded within the fourth damaged 50/50 enamel-coated ponding specimen (EN-D-4) which reported a final corrosion potential of -555 mV and an overall resistance of 4.8 kΩcm.

(a)

(b)

Figure C - 21: The (a) front and (b) back view of the four bars that were embedded within the first "perfect" epoxy-coated ponding specimen (EP-1) which reported a final corrosion potential of -327 mV and an overall resistance of 9.9 kΩcm.

(a)

(b)

Figure C - 22: The (a) front and (b) back view of the four bars that were embedded within the second "perfect" epoxy-coated ponding specimen (EP-2) which reported a final corrosion potential of -316 mV and an overall resistance of 9.2 kΩcm.

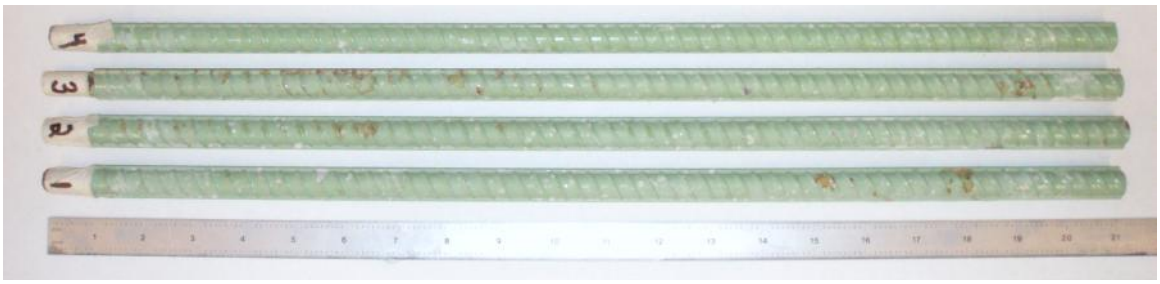

(a)

(b)

Figure C - 23: The (a) front and (b) back view of the four bars that were embedded within the third "perfect" epoxy-coated ponding specimen (EP-3) which reported a final corrosion potential of -583 mV and an overall resistance of 12.8 kΩcm.

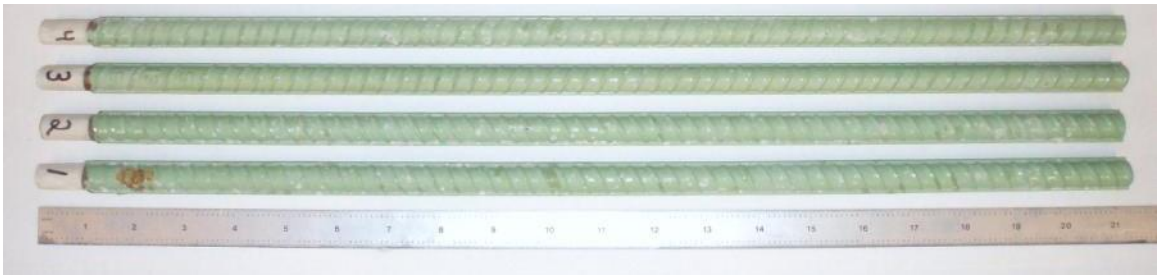

(a)

(b)

Figure C - 24: The (a) front and (b) back view of the four bars that were embedded within the fourth "perfect" epoxy-coated ponding specimen (EP-4) which reported a final corrosion potential of -376 mV and an overall resistance of 12.1 kΩcm.

(a)

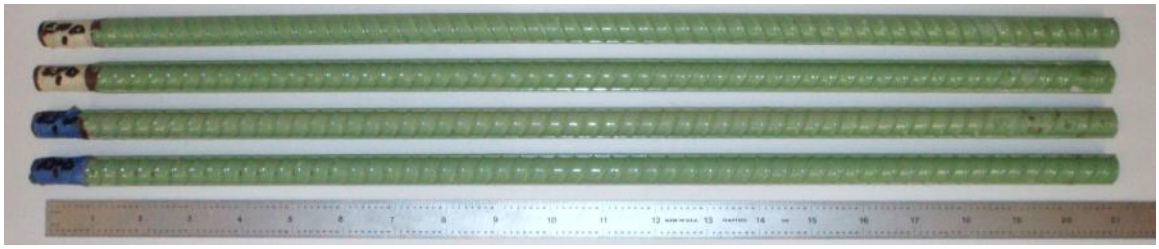

(b)

Figure C - 25: The (a) front and (b) back view of the four bars that were embedded within the first damaged epoxy-coated ponding specimen (EP-D-1) which reported a final corrosion potential of -284 mV and an overall resistance of 9.4 kΩcm.

(a)

(b)

Figure C - 26: The (a) front and (b) back view of the four bars that were embedded within the second damaged epoxy-coated ponding specimen (EP-D-2) which reported a final corrosion potential of -440 mV and an overall resistance of 9.7 kΩcm.

(a)

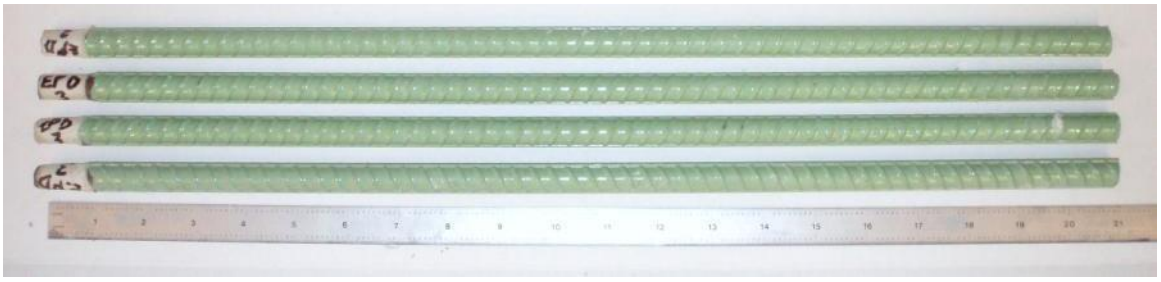

(b)

Figure C - 27: The (a) front and (b) back view of the four bars that were embedded within the third damaged epoxy-coated ponding specimen (EP-D-3) which reported a final corrosion potential of -440 mV and an overall resistance of 13.0 kΩcm.

(a)

(b)

Figure C - 28: The (a) front and (b) back view of the four bars that were embedded within the fourth damaged epoxy-coated ponding specimen (EP-D-4) which reported a final corrosion potential of -531 mV and an overall resistance of 11.8 kΩcm.

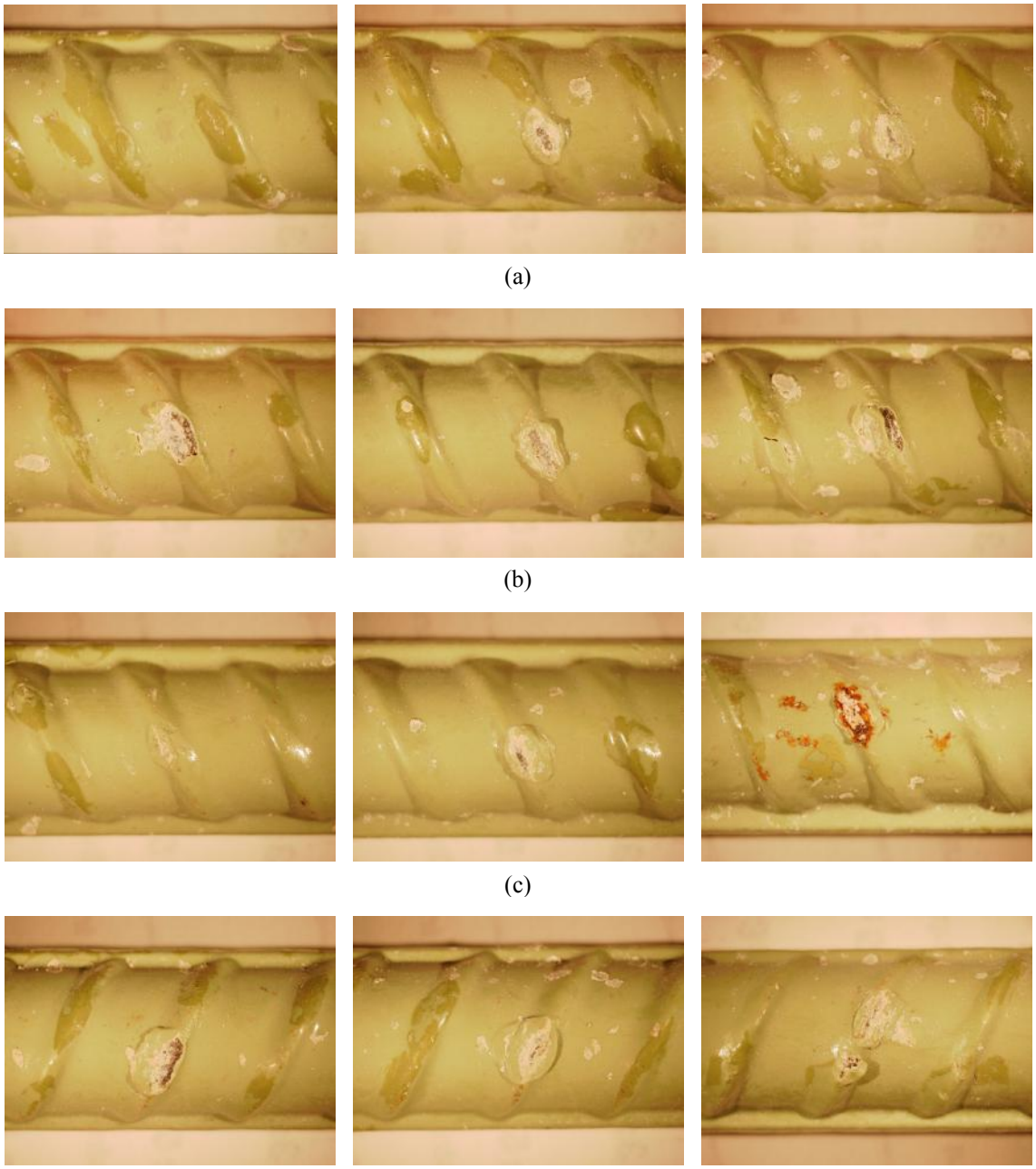

Figure C - 29: The three intentionally damaged areas along (a) bar-1; (b) bar-2; (c) bar-3; and (d) bar-4 of ponding specimen EP-D-1.

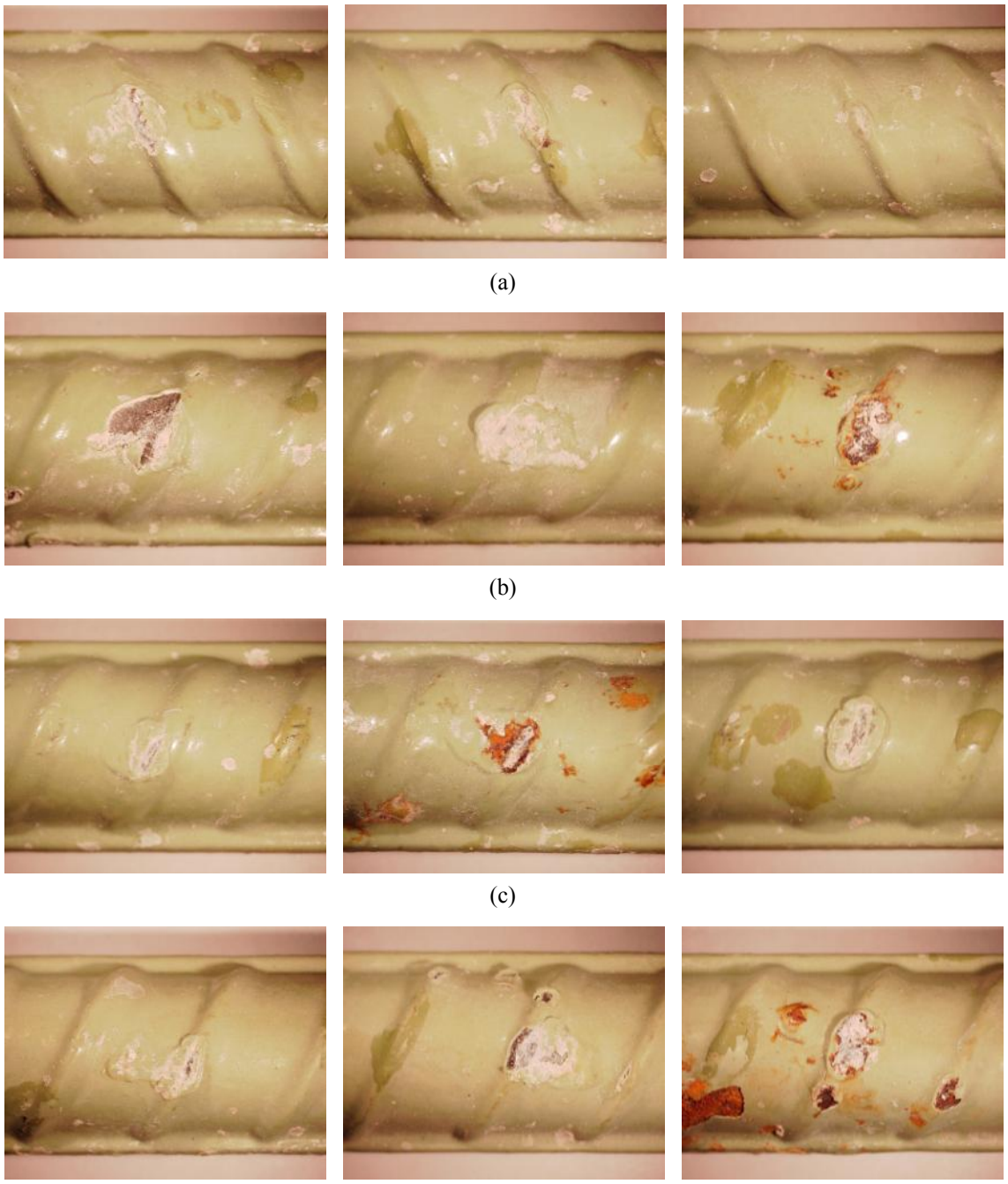

(a)

(b)

(c)

(d)

Figure C - 30: The three intentionally damaged areas along (a) bar-1; (b) bar-2; (c) bar-3; and (d) bar-4 of ponding specimen EP-D-2.

(a)

(b)

(c)

(d)

Figure C - 31: The three intentionally damaged areas along (a) bar-1; (b) bar-2; (c) bar-3; and (d) bar-4 of ponding specimen EP-D-3.

(a)

(b)

(c)

(d)

Figure C - 32: The three intentionally damaged areas along (a) bar-1; (b) bar-2; (c) bar-3; and (d) bar-4 of ponding specimen EP-D-4.

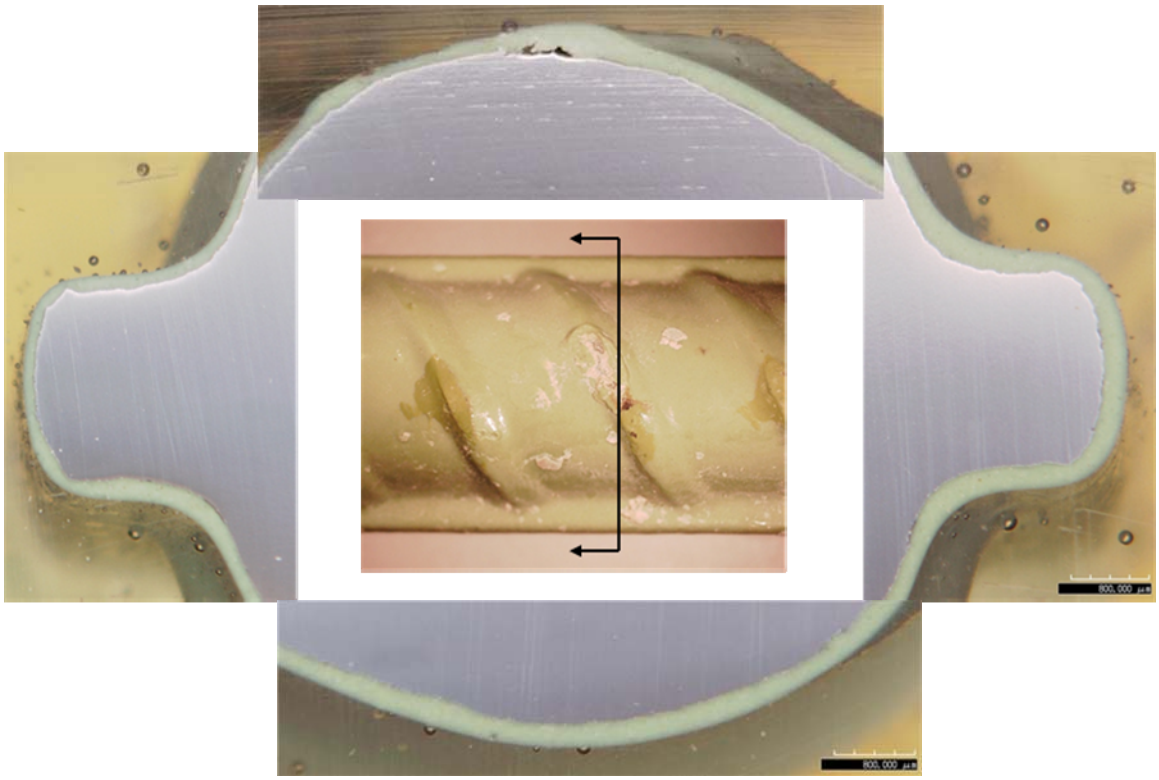

Figure C - 33: A cross-section through an intentionally damaged area along bar-1 of specimen EP-D-2.

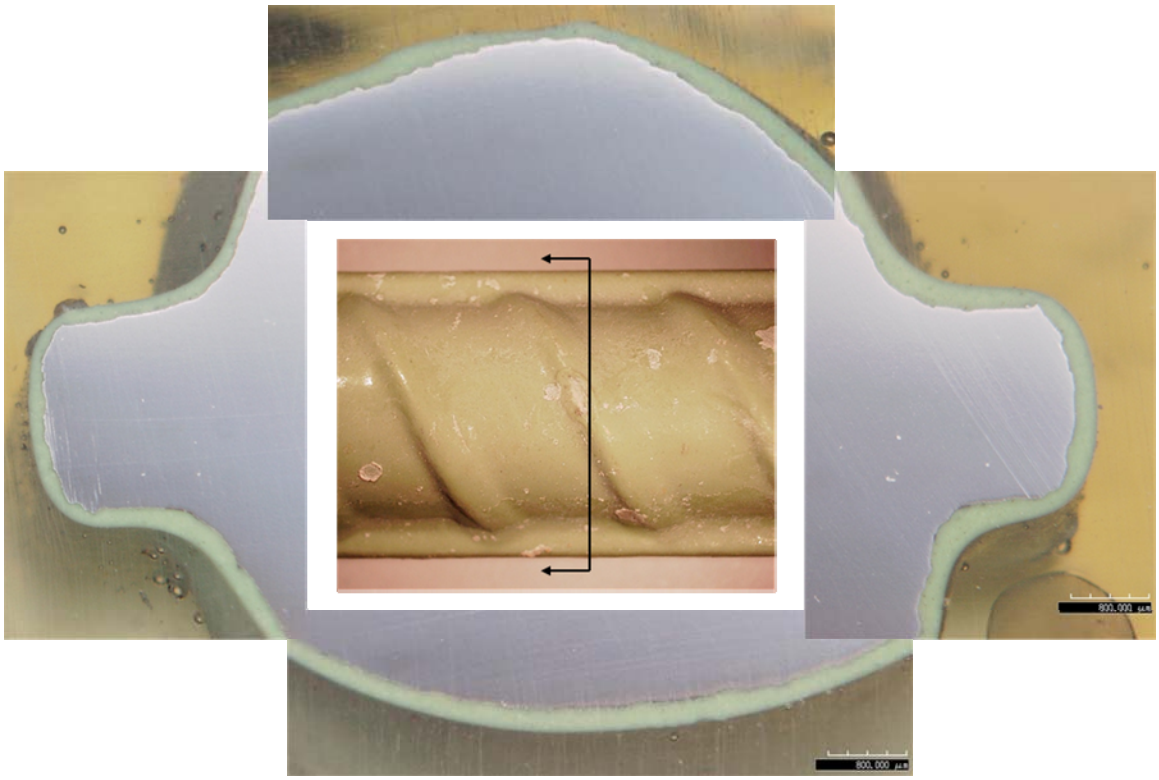

Figure C - 34: A cross-section through an intentionally damaged area along bar-1 of specimen EP-D-2.

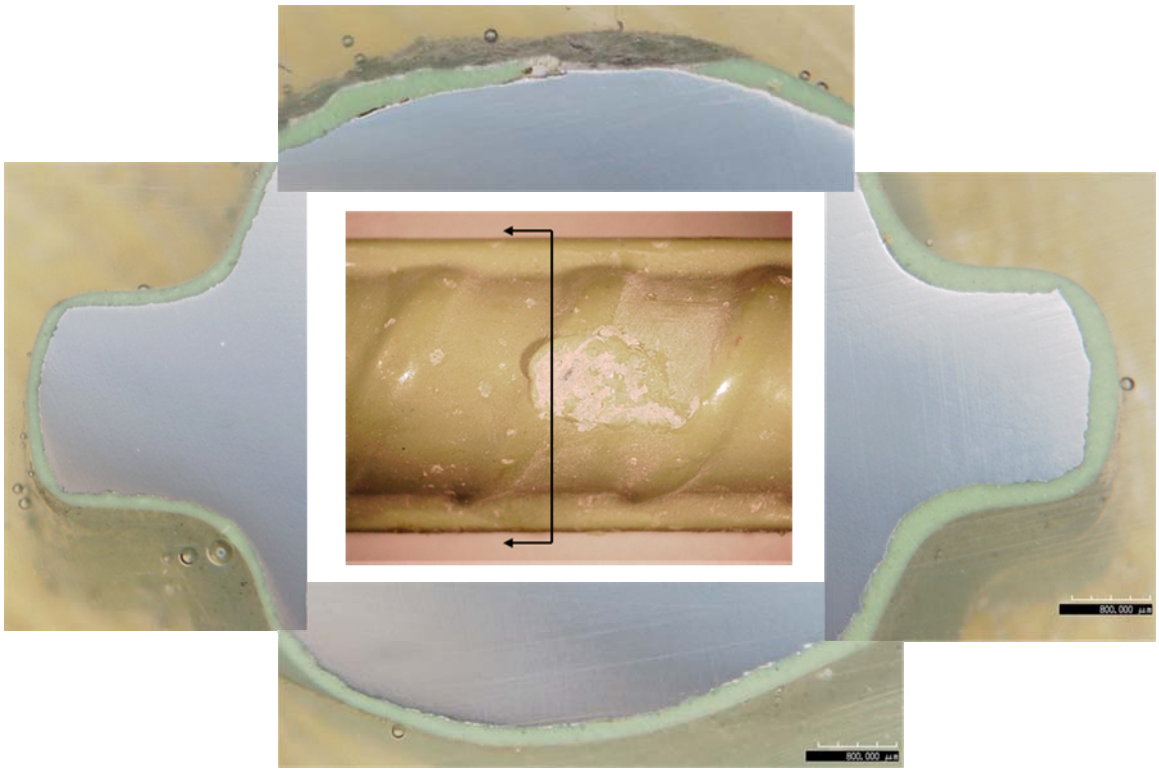

Figure C - 35: A cross-section through an intentionally damaged area along bar-2 of specimen EP-D-2.

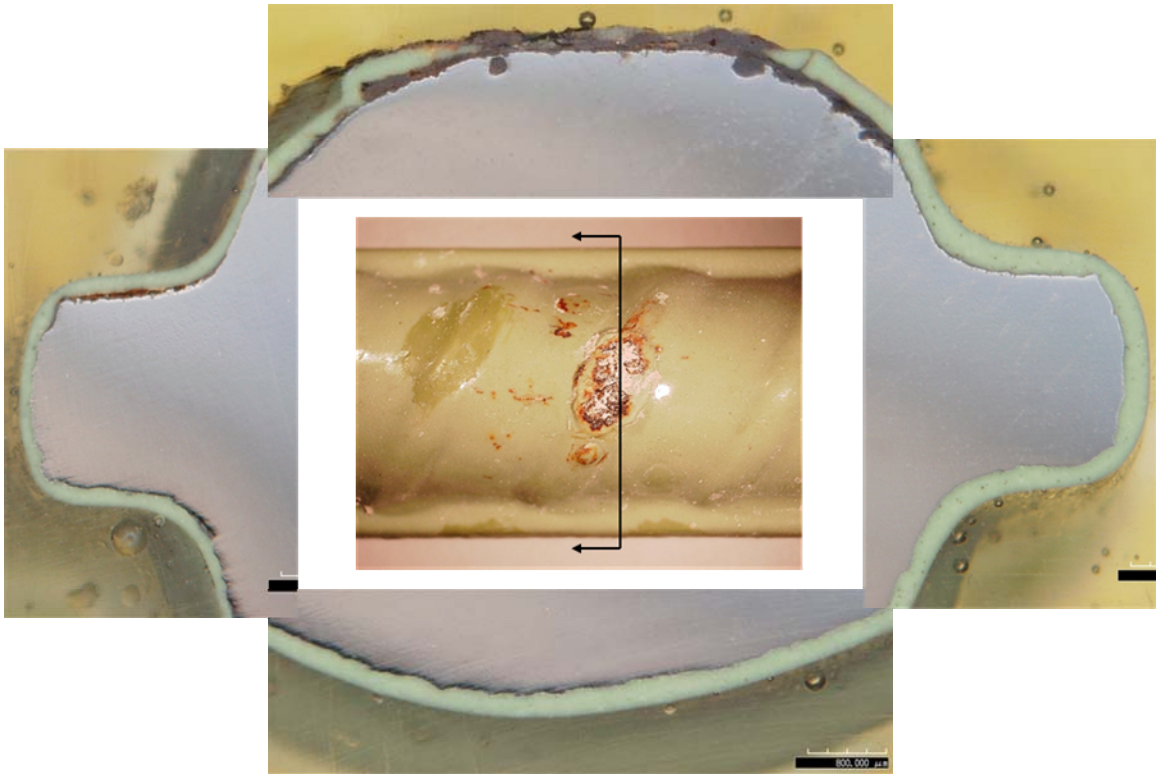

Figure C - 36: A cross-section through an intentionally damaged area along bar-2 of specimen EP-D-2.

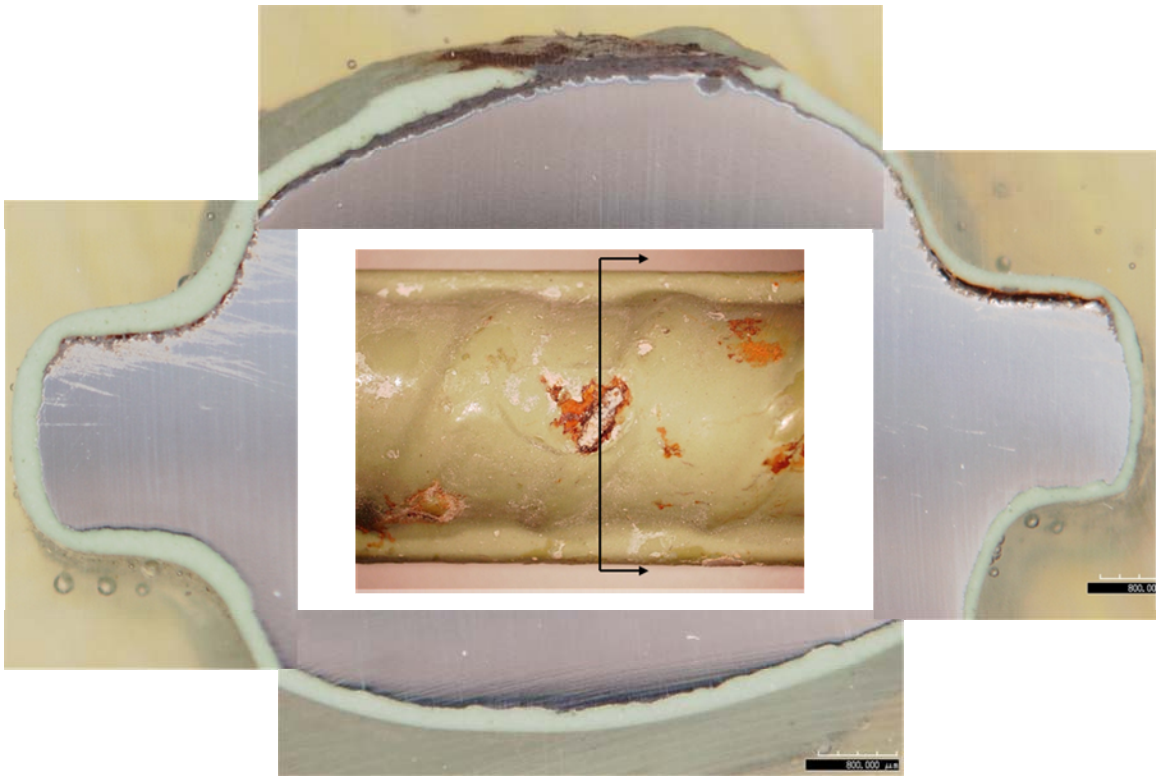

Figure C - 37: A cross-section through an intentionally damaged area along bar-3 of specimen EP-D-2.

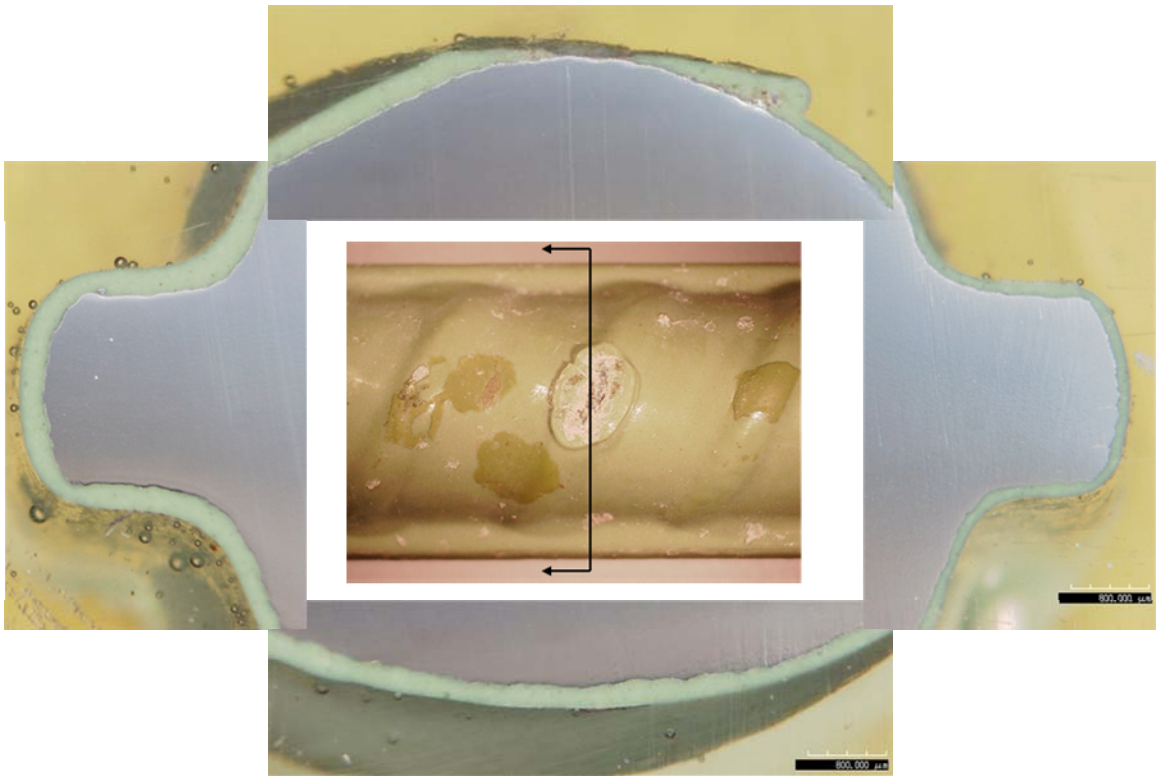

Figure C - 38: A cross-section through an intentionally damaged area along bar-3 of specimen EP-D-2.

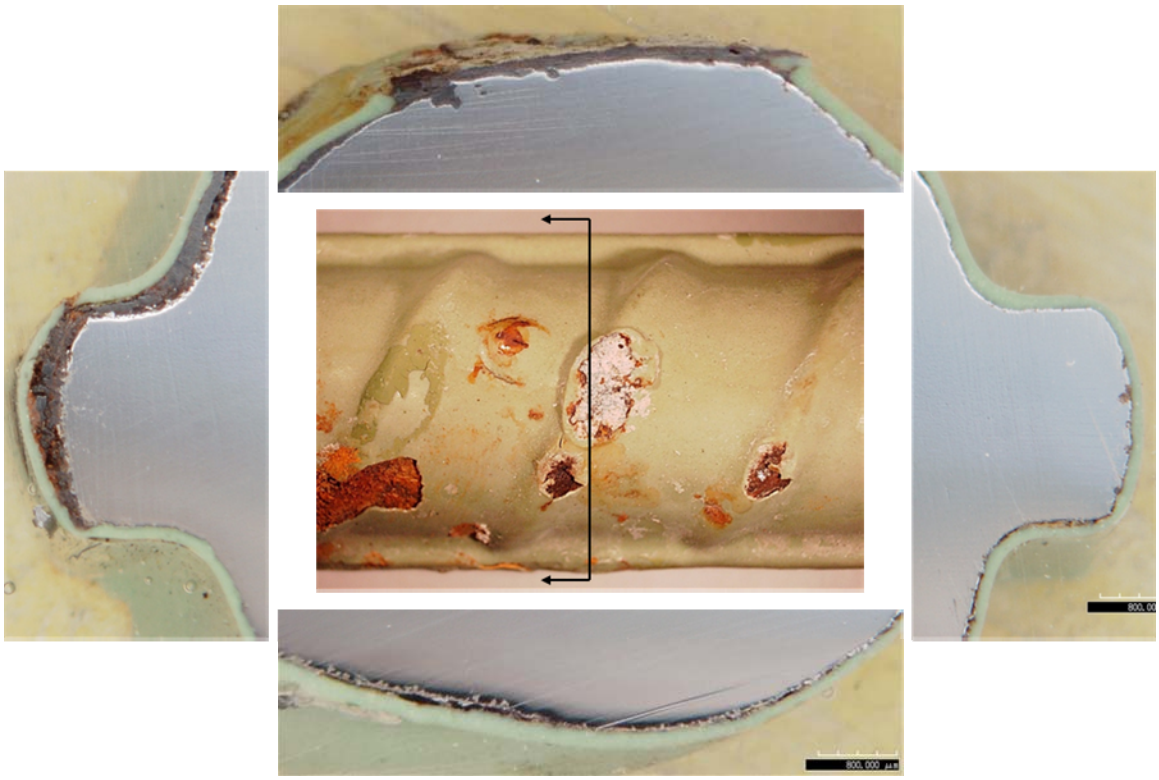

Figure C - 39: A cross-section through an intentionally damaged area along bar-4 of specimen EP-D-2.

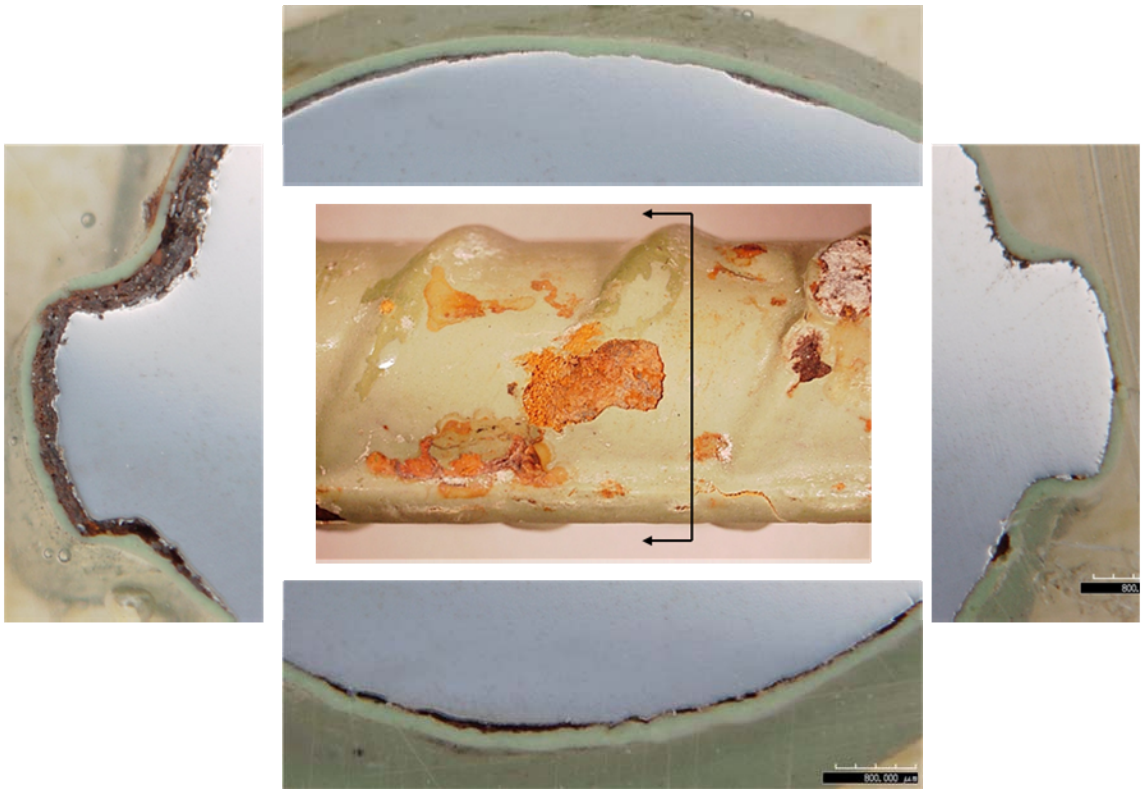

Figure C - 40: A cross-section through an unexplained area of damaged along bar-4 of specimen EP-D-2.

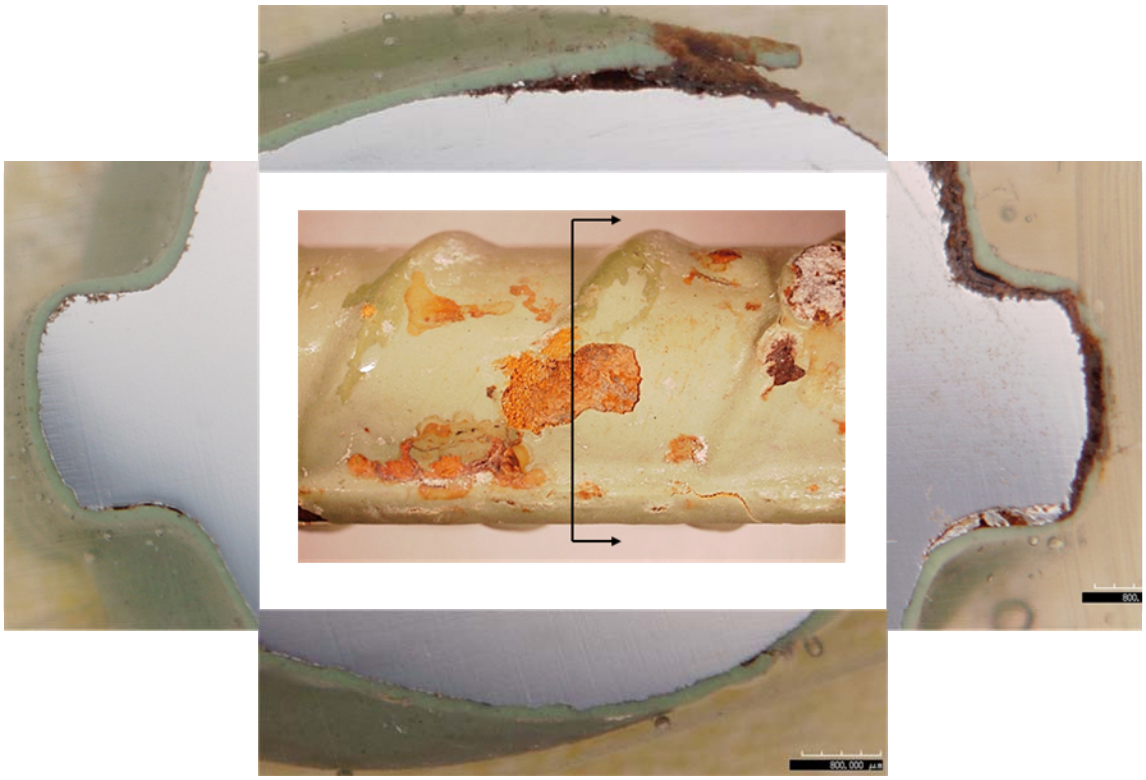

Figure C - 41: A cross-section through an unexplained area of damaged along bar-4 of specimen EP-D-2.

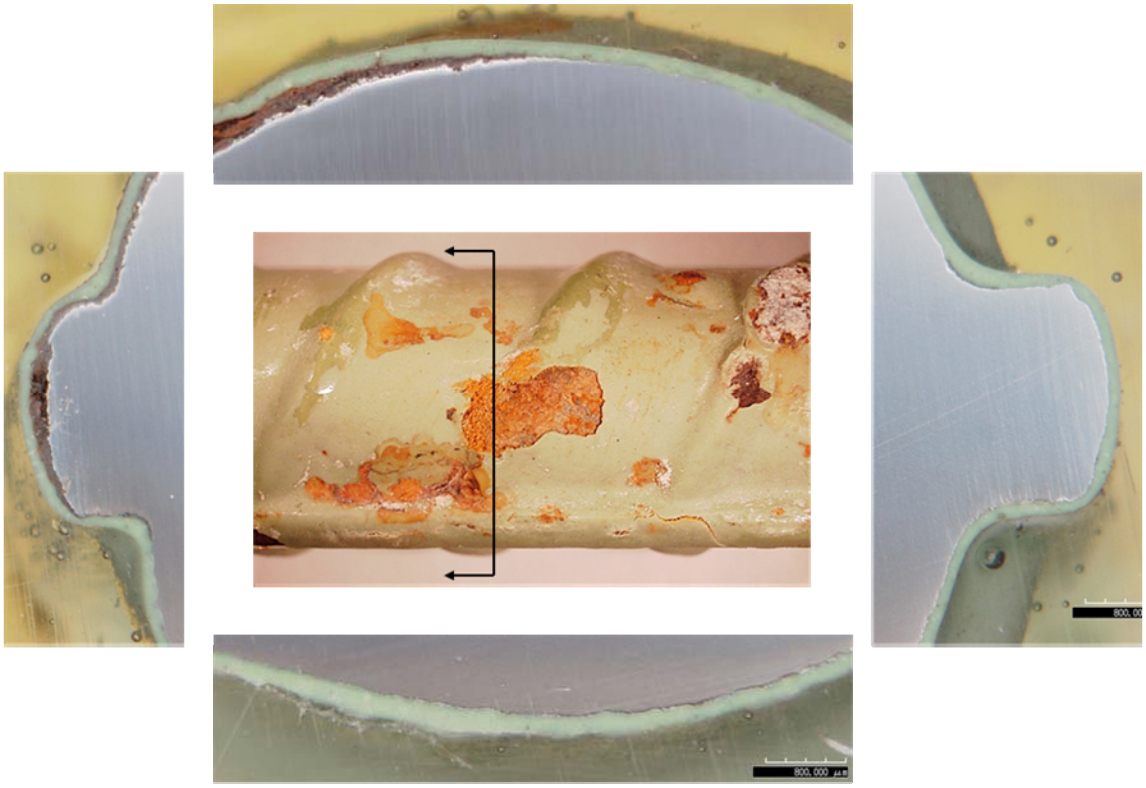

Figure C - 42: A cross-section through an unexplained area of damaged along bar-4 of specimen EP-D-2.